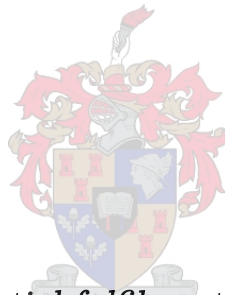


# Numerical modelling of wave-induced vertical ship motions at the Port of Richards Bay: calibration and computation of extreme values

by

Mogau Sebopa



*Thesis presented in partial fulfilment of the requirements for the degree of Master of Engineering (Civil) in the Faculty of Engineering at Stellenbosch University*

Supervisor: Dr. J.S. Schoonees

Co-supervisor: Mr. J. Moes

March 2020

# Declaration

By submitting this thesis electronically, I declare that the entirety of the work contained therein is my own, original work, that I am the sole author thereof (save to the extent explicitly otherwise stated), that reproduction and publication thereof by Stellenbosch University will not infringe any third party rights and that I have not previously in its entirety or in part submitted it for obtaining any qualification.

Date: March 2020

Copyright © 2020 Stellenbosch University  
All rights reserved.

# Abstract

## Numerical modelling of wave-induced vertical ship motions at the Port of Richards Bay: calibration and computation of extreme values

M. Sebopa

*Department of Civil Engineering,  
University of Stellenbosch,  
Private Bag X1, Matieland 7602, South Africa.*

Thesis: MEng (Civ)

March 2020

The CSIR conducted extensive scale model studies of wave-induced hull motion response of ships in shallow water. The aim of these studies was to produce a solid database that will, in future, assist South African ports with channel depth optimization. Physical model tests of a fully laden 150kt deadweight bulk carrier were carried out at a scale of 1:100. Physical model test results used to calibrate the Wavescat model and involved exciting the ship with waves from 90°, 135° and 180° with relation to the ship's bow at zero forward speed. Depth to draught ratio ( $d/D$ ) varied from 1.5, 1.4, 1.3 and 1.2 with a wave spectrum of significant wave heights of 3 m, 4 m and 5 m and a peak period of 10 s. Sensitivity tests for beam waves (90°) were conducted using  $d/D$  of 1.1, significant wave heights from 1m until bottom touching occurred and peak periods of 10 s and 12 s. The sensitivity tests were conducted to study the effects of wave heights on the hull motion response. Both wave spectrums and the response amplitude operators (RAOs) data were processed using a time-domain analysis to determine significant hull motion response in relation to angles of wave incidence and depth to draught ratios. The findings of the studies were that:

- The ratios of significant hull motion amplitudes to significant wave height ( $A_s/H_s$ ) for 135° and 180° have the same magnitude and are not sensitive to a reduction of depth to draught ratios up to about  $d/D$  of 1.5, where  $A_s/H_s$  starts decreasing with a further reduction of  $d/D$ .  $A_s/H_s$  values for 90° have the highest magnitude out of all the tested angles which appear to be directly proportional to  $d/D$  ratios as tested.

- The over-all pitch and heave significant hull motion amplitude ( $A_s$ ) values for  $135^\circ$  and  $180^\circ$  were 0.2 to 0.3 times  $H_s$ , while  $A_s$  for  $90^\circ$  was 0.75 times  $H_s$ .
- The Rayleigh probability distribution provided a good estimate of the most probable extreme motion amplitude in relation to the probability of occurrence of the numbers of motion amplitudes occurring in the given period of time.
- The relationship between the maximum individual hull motion amplitude ( $A_{max}$ ) and the significant hull motion amplitude ( $A_s$ ) for motions larger than 1.5m deviate from the initial linearity of this relationship.
- Significant hull motion increases linearly with an increase in wave height, from the wave height ranges tested for both physical and numerical models.

The objectives of the present studies is to use the Wavescat numerical model to test if it can accurately compute vertical keel point motions of a fully laden 150 kt deadweight coal carrier ship model with a draught of 17 m by :

- using results obtained from the fully laden 150 kt deadweight physical model, to calibrate the numerical model. Wave spectrums from Mike21BW and RAOs computed by the Wavescat model will be used to calculate vessel response spectrums, which will then help determine vertical keel point motions for different depths, wave heights and incident wave directions.
- converting the vessel response spectrums to time domain to obtain time-series for each selected depth, wave height and incident wave direction. Since the wave phase of the original timeseries is unknown, wave phases will randomly be chosen between  $-\pi$  and  $\pi$ .
- using the zero - crossing method to determine the ship motion amplitudes for each selected depth, wave height and incident wave direction. This exercise will be followed by grouping ship motion amplitudes of the same heights and incident wave direction which will then be fitted to non-linear probability distributions.
- For the latter purpose, the Rayleigh distribution, the Generalized Extreme Value distribution, the Generalized Pareto distribution and the Weibull distribution will be applied to determine which distribution best represents the non-linear relationship of maximum individual hull motion amplitudes for ship motion amplitude more than 1.5 m. These probability distributions will be fitted to ship motion amplitudes greater than 1.5



m because their non-linearity were not well represented by the Rayleigh distribution in the research previously conducted by the CSIR.

The calibrated Wavescat model will then be used to investigate the non-linear factors that affect the vertical keel point motions. These non-linear factors are speed, centre of roll rotation, small underkeel clearance and squat. The ship model's vertical keel point motions will be tested for storm conditions with wave heights of 3 m and 4 m and peak periods of 14 s 16 s and 18s.

# Uittreksel

## Numeriese modellering van golfgeïnduseerde vertikale skeepsbewegings by Hawe van Richardsbaai: yking en berekening van uiterste waardes

*(“Numerical modelling of wave-induced vertical ship motions at Richards Bay: calibration and computation of extreme values”)*

M. Sebopa

*Departement Siviele Ingenieurswese,  
Universiteit van Stellenbosch,  
Privaatsak X1, Matieland 7602, Suid Afrika.*

Tesis: MIng (Civ)

Maart 2020

Die WNNR het uitgebreide skaalmodelstudies van golfgeïnduseerde rompbeweging van skepe in vlak water gedoen. Die doel van die studies was om 'n omvattende databasis te produseer wat in die toekoms Suid-Afrikaanse hawens sal help met die optimalisering van kanaaldieptes. Fisiese modeltoetse van 'n volgelaide 150 kt dooiegewig grootmaatskip is op 'n skaal van 1: 100 uitgevoer. Die fisiese modelresultate is gebruik om die Wavescat-model te yk vir skeepsbeweging as gevolg van golwe van  $90^\circ$ ,  $135^\circ$  en  $180^\circ$  teen geen voorwaartse spoed. Diepte tot diepgangverhouding ( $d/D$ ) wissel van 1.2 tot 1.5 met 'n golfspektrum van maatgewende golfhoogtes van 3 m, 4 m, 5 m met 'n spitsperiode van 10 s. Sensitiwiteitstoetse is onderneem met 'n  $d/D$  van 1.1, maatgewende golfhoogtes vanaf 1 m totdat die bodem geraak word en vir spitsperiodes van 10 s en 12 s. Die sensitiwiteitstoetse is onderneem om die effek van golfhoogtes op die rompbeweging te bestudeer. Die data is toe verwerk met behulp van 'n tyddomein-ontleding om maatgewende rompbeweging te bepaal met betrekking tot golfvalhoeke en  $d/D$ -verhoudings. Die bevindings van die studies is soos volg:

- Die verhoudings van maatgewende rompbewegings tot maatgewende golfhoogte ( $A_s/H_s$ ) vir  $135^\circ$  en  $180^\circ$  is dieselfde grootte en is nie sensitief vir 'n vermindering van  $d/D$  tot ongeveer 1.5 nie. Daarna begin  $A_s/H_s$

afneem met 'n vermindering van  $d/D$ .  $A_s/H_s$ -waardes vir  $90^\circ$  is die grootste vir al die getoetste hoeke. Dit kom voor dat  $A_s/H_s$  toeneem soos  $d/D$  toeneem.

- Die amplitude van die maatgewende rompbewegings ( $A_s$ ) vir stamp en dein se waardes vir  $135^\circ$  en  $180^\circ$  is tussen 0.2 en 0.3 keer  $H_s$ , terwyl dit 0.75 keer  $H_s$  vir  $90^\circ$  is.
- Die Rayleigh-waarskynlikheidsverdeling verskaf 'n goeie skatting van die mees waarskynlike uiterste bewegingsamplitude in verhouding met die waarskynlikheid van voorkoms van die grootste waardes van die bewegingsamplitude in die gegewe tydperk.
- Die verband tussen die maksimum individuele rompbewegingsamplitude ( $A_{max}$ ) en die maatgewende rompbewegingsamplitude ( $A_s$ ) vir bewegings groter as 1.5 m wyk af van die aanvanklike lineêre verband.
- Maatgewende rompbeweging styg lineêr met 'n toename in golfhoogte vir die getoetste bereik vir beide fisiese en numeriese modelle.

Die doelwit van hierdie studie is om te toets of die wiskundige skeepsbewegingsmodel Wavescat vertikale kielpunte se bewegings akkuraat kan voorspel vir 'n volgelaaide 150 kt-dooiegewig grootmaatsteenkoolskip met 'n diepgang van 17 m. Dit word gedoen deur:

- Resultate wat in 'n fisiese modelstudie verkry is, vir yking van die wiskundige model te gebruik. Golfspektrums van Mike21BW en die berekende RAO's van die Wavescat-model is benut om die skeepsbewegingspektrums te bereken. Op sy beurt word hierdie spektrums dan gebruik om die vertikale kielpuntbewegings vir verskillende dieptes, golfhoogtes, en invallende golfrigtings te bepaal.
- Om die skeepsbewegingspektrums na die tyddomein oor te sit ten einde tydreeks vir elke gekose diepte, golfhoogte en invallende golfrigting te verkry. Omdat die golf fase van die oorspronklike tydreeks onbekend is, word lukrake golf fases tussen  $+\pi$  en  $-\pi$  gekies.
- Deur die nulkrusmetode te gebruik om die skeepsbewegingsamplitudes vir elke diepte, golfhoogte en invallende golfrigting te bepaal. Hierdie oefening word gevolg deur die groepering van skeepsbewegingsamplitudes vir dieselfde hoogtes en invallende golfrigting, wat dan teen nie-lineêre waarskynlikheidsverdelings gepas word.
- Vir laasgenoemde doelwit, is die Rayleigh-, Veralgemeende Uiterste waarde (GEV)-, die Algemene Pareto en die Weibullverdelings toegepas. So-doende kon bepaal word watter verdeling die nie-lineêre verwantskap

van die maksimum individuele rompbeweging se amplitudes vir skeepsbeweging van meer as 1.5 m die beste weergee. Hierdie waarskynlikheidsverdelings is vir skeepsbeweging van meer as 1.5 m gepas omdat die nie-lineêre aard nie goed deur die Rayleigh-verdeling in die WNNR se vorige toetse weergegee is nie.

Die geykte Wavescat-model is toe gebruik om die nie-lineêre faktore wat die vertikale kielpuntbewegings beïnvloed, te ondersoek. Hierdie nie-lineêre faktore is spoed, swaartepuntrotasie tydens skeepsrol, klein kielvryhoogtes en hurk. Die skeepsmodel se vertikale kielpuntbewegings is getoets vir stormtoestande met golfhoogtes van 3 m en 4 m, met spitperiodes van 14 s, 16 s en 18 s.

# Acknowledgements

I, the author would like to express my sincere gratitude towards the people who made the completion of this thesis possible namely;

- Professor Koos Schoonees for his insightful guidance of my thesis,
- Johan Kieviet and Sonwabiso Yoyo for assisting me with their insight on how to model and calibrate ships in a physical model,
- Dr Wim van Molen, Jatin Harribhai and Chris Troch for assisting me with the technicalities of setting up the Wavescat and Quaysim models,
- Sarel Haasbroek and Ursula von Saint Ange for furnishing me with Port of Richards Bay wave data,
- Jarryd Barnes for simulating the Delft 3D SWAN model,
- My family, for always cheering me on all the way,
- CSIR, for funding my studies,
- God, for my mere existence.

With special thanks to my co-supervisor, Mr Johannes Moes, for patiently walking me through this Coastal Engineering journey until the very end of the completion of this thesis.

# Dedications

*This thesis is dedicated to by beloved younger sister, Mahlatse Magdeline Sebopa who left us on the 13<sup>th</sup> of March 2017 and my beloved grandmother Matshelane Maria Rahlogo, who left us on the 26<sup>th</sup> of August 2017. You are in the warm hands of God now.*

# Contents

<b>Declaration</b>	<b>i</b>
<b>Abstract</b>	<b>ii</b>
<b>Uittreksel</b>	<b>v</b>
<b>Acknowledgements</b>	<b>viii</b>
<b>Dedications</b>	<b>ix</b>
<b>Contents</b>	<b>x</b>
<b>List of Figures</b>	<b>xii</b>
<b>List of Tables</b>	<b>xix</b>
<b>Nomenclature</b>	<b>xxiii</b>
<b>1 Introduction</b>	<b>1</b>
1.1 Problem Statement . . . . .	1
1.2 Objective . . . . .	5
1.3 Methodology . . . . .	6
<b>2 Richards Bay Wave Climate</b>	<b>7</b>
2.1 Description of the Port of Richards Bay . . . . .	7
2.2 Wave data . . . . .	9
2.3 Wave conditions . . . . .	9
<b>3 Ship Specifications</b>	<b>14</b>
3.1 Types of ships . . . . .	14
3.2 Future ships . . . . .	17
<b>4 Ship Motions Theory</b>	<b>19</b>
4.1 Coordinate systems . . . . .	19
4.2 Ship hydromechanics . . . . .	20
4.3 Mass spring system . . . . .	25

<i>CONTENTS</i>	xi
4.4 3D Panel method . . . . .	28
<b>5 Historic Model Tests</b>	<b>31</b>
5.1 Results of the calibrated 150kt deadweight bulk carrier . . . . .	34
<b>6 Calibration of Numerical Models</b>	<b>40</b>
6.1 Waves numerical modelling . . . . .	40
6.2 Numerical modelling of a 150kt DWT bulk carrier . . . . .	57
6.3 Keel points probabilistic investigations . . . . .	86
<b>7 Modelling of Ship in Storm Conditions</b>	<b>98</b>
7.1 Underkeel clearance for 4m/s ship speed . . . . .	98
<b>8 Discussion and Interpretation of Results</b>	<b>104</b>
8.1 General discussion . . . . .	104
8.2 Reliability of calibration test results . . . . .	108
<b>9 Conclusions and Recommendations</b>	<b>109</b>
<b>10 Application of the Wavescat model on storm conditions</b>	<b>112</b>
10.1 Mike21BW test conditions . . . . .	112
10.2 Underkeel clearance calculations . . . . .	112
<b>Appendices</b>	<b>114</b>
<b>A Computed Wave and Ship Motion Spectra</b>	<b>115</b>
<b>B LIST OF PROBABILITY DISTRIBUTIONS</b>	<b>127</b>
<b>C List of Figures</b>	<b>140</b>
C.1 Underkeel clearance sensitivity tests . . . . .	141
C.2 Underkeel clearance for $d/D = 1.5$ to $1.1$ , depth = 25m, 23m, 21m, 19m and 18m . . . . .	143
<b>D List of Tables</b>	<b>146</b>
D.1 Depth to draught ( $d/D$ ) test tables . . . . .	146
D.2 Underkeel clearance sensitivity test tables for $d/D = 1.1$ , $\alpha = 90^\circ$	148
D.3 Significant hull motion amplitudes for the underkeel clearance sensitivity tests ( $d/D = 1.1$ ), depth = 20m . . . . .	149
D.4 Significant hull motion amplitudes for MIKE21BW measure- ment points . . . . .	153
D.5 Significant hull motion amplitudes for values for Mike21BW measurement points . . . . .	156
D.6 Underkeel clearance values for Mike21BW measurement points .	159
<b>List of References</b>	<b>163</b>



# List of Figures

1.1	Ship departure route and storms wave direction (Google, 2019) . . . .	1
1.2	Keel points . . . . .	2
1.3	Centre of gravity . . . . .	2
1.4	Translation motions (Journee and Massie, 2001 <i>a</i> ) . . . . .	3
1.5	Rotation motions (Journee and Massie, 2001 <i>a</i> ) . . . . .	4
1.6	Richards Bay DMAX interface (Moes, 2007) . . . . .	5
2.1	Entrance to the Port of Richards Bay (Google, 2019) . . . . .	7
2.2	Port of Richards Bay berths (Transnet National Ports Authority, 2010) . . . . .	8
2.3	Comparison of the entire data set wave roses for (a) Durban Waverider (2007 to 2009), (b) Durban ADCP (2002 to 2006) and (c) Richards Bay Waverider (1997 to 2009) (Corbella and Stretch, 2012)	10
2.4	KwaZulu-Natal Wave Rose (1997-2009) (Corbella and Stretch, 2012)	10
2.5	Richards Bay CSIR Wave height (H <sub>m0</sub> ) vs wave direction rose (2003-2017) (CSIR, 2017) . . . . .	11
2.6	Richards Bay wave period histogram (2003-2017) (CSIR, 2017) . . . .	12
2.7	Richards Bay current speed rose presenting speed vs direction (2017-2018) (CSIR, 2017) . . . . .	13
3.1	Cape America Dimensions (Marine Traffic, 2018 <i>a</i> ) . . . . .	14
3.2	Ocean Prometheus Coal Carrier Dimensions (Marine Traffic, 2018 <i>d</i> )	15
3.3	Clipper Quito LPG Tanker Dimensions (Marine Traffic, 2018 <i>b</i> ) . . . .	16
3.4	Leading Glory Dimensions, (Marine Traffic, 2018 <i>c</i> ) . . . . .	16
4.1	Coordinate systems . . . . .	20
4.2	Relationship of waves and motions . . . . .	21
4.3	Harmonic displacement, velocity and acceleration of a timeseries . . .	21
4.4	Ship direction relative to wave directions (Journee and Massie, 2001 <i>a</i> )	23
4.5	Harmonic wave and roll signal (Journee and Massie, 2001 <i>a</i> ) . . . .	24
4.6	Damped mass spring system (Naaijen, 2013) . . . . .	25
4.7	Stages of damping (United States Naval Academy, 2018) . . . . .	26
4.8	Ship mass spring system for heave (Naaijen, 2013) . . . . .	26
4.9	Ship roll (United States Naval Academy, 2018) . . . . .	27

4.10	Pitching ship ((National Program on Technology Enhanced Learning, 2011)) . . . . .	28
4.11	3D Panel figure of a crude oil hull form . . . . .	29
5.1	Depth to draught results . . . . .	37
5.2	Maximum versus significant hull motion amplitudes . . . . .	38
5.3	Influence of wave height on hull motion amplitudes . . . . .	39
6.1	Richards Bay Swan bathymetry (Rautenbach <i>et al.</i> , 2015) . . . . .	41
6.2	Swan nested medium and fine grid (Rautenbach <i>et al.</i> , 2015) . . . . .	42
6.3	Swan fine grid (Rautenbach <i>et al.</i> , 2015) . . . . .	42
6.4	Port of Richards Bay Mike 21BW layout . . . . .	47
6.5	Mike21BW Setup Planner (DHI, 2017) . . . . .	52
6.6	Porosity reflection coefficients (DHI, 2017) . . . . .	53
6.7	Porosity plot . . . . .	54
6.8	Sponge plot . . . . .	55
6.9	Mike21BW surface elevation plot for $H_s = 1\text{m}$ , $T_p = 10\text{s}$ and $\alpha = 90^\circ$ . . . . .	56
6.10	Mike21BW surface elevation plot for $H_s = 1\text{m}$ , $T_p = 10\text{s}$ and $\alpha = 135^\circ$ . . . . .	56
6.11	Mike21BW surface elevation plot for $H_s = 1\text{m}$ , $T_p = 10\text{s}$ and $\alpha = 180^\circ$ . . . . .	57
6.12	150k DWT hullform mesh (4402 panels) . . . . .	58
6.13	150k DWT hullform body plan . . . . .	59
6.14	Physical model vertical hull motion measurement system (Jonker <i>et al.</i> , 1991) . . . . .	61
6.15	Physical model ship fixed orientation system and earth fixed orientation system (Jonker <i>et al.</i> , 1991) . . . . .	62
6.16	Wavescat ship heading direction . . . . .	63
6.17	Effects of viscous roll damping on roll response . . . . .	64
6.18	Comparison of physical model and Wavescat model for $d/D = 1.5$ . . . . .	66
6.19	Comparison of physical model and Wavescat model for $d/D = 1.4$ . . . . .	67
6.20	Comparison of physical model and Wavescat model for $d/D = 1.3$ . . . . .	68
6.21	Comparison of physical model and Wavescat model for $d/D = 1.2$ . . . . .	69
6.22	Comparison of physical model and Wavescat model for $d/D = 1.1$ . . . . .	70
6.23	Physical model versus Wavescat model for $d/D = 1.5$ . . . . .	71
6.24	Physical model versus Wavescat model for $d/D = 1.4$ . . . . .	71
6.25	Physical model versus Wavescat model for $d/D = 1.3$ . . . . .	71
6.26	Physical model versus Wavescat model for $d/D = 1.2$ . . . . .	71
6.27	Physical model versus Wavescat model for $d/D = 1.1$ . . . . .	72
6.28	Effect of water depth on significant hull motion response . . . . .	73
6.29	RAOs for 25.2m, $90^\circ$ . . . . .	75
6.30	RAOs for 25.2m, $135^\circ$ . . . . .	75
6.31	RAOs for 25.2m, $180^\circ$ . . . . .	75
6.32	RAOs for 23.4m, $90^\circ$ . . . . .	75
6.33	RAOs for 23.4m, $135^\circ$ . . . . .	75
6.34	RAOs for 23.4m, $180^\circ$ . . . . .	75

6.35	RAOs for 21.6m, 90°	76
6.36	RAOs for 21.6m, 135°	76
6.37	RAOs for 21.6m, 180°	76
6.38	RAOs for 19.8m, 90°	76
6.39	RAOs for 19.8m, 135°	76
6.40	RAOs for 19.8m, 180°	76
6.41	RAOs for 18.7m, 90°	77
6.42	RAOs for 18.7m, 135°	77
6.43	RAOs for 18.7m, 180°	77
6.44	Vessel response spectrum for $H_s = 3\text{m}$ , Direction = 90°	77
6.45	Vessel response spectrum for $H_s = 4\text{m}$ , Direction = 90°	78
6.46	Vessel response spectrum for $H_s = 5\text{m}$ , Direction = 90°	78
6.47	Vessel response spectrum for $H_s = 3\text{m}$ , Direction = 135°	78
6.48	Vessel response spectrum for $H_s = 4\text{m}$ , Direction = 135°	78
6.49	Vessel response spectrum for $H_s = 5\text{m}$ , Direction = 135°	79
6.50	Vessel response spectrum for $H_s = 3\text{m}$ , Direction = 180°	79
6.51	Vessel response spectrum for $H_s = 4\text{m}$ , Direction = 180°	79
6.52	Vessel response spectrum for $H_s = 5\text{m}$ , Direction = 180°	79
6.53	Factors affecting underkeel clearance	81
6.54	Underkeel clearance for $H_s = 1\text{m}$ , $T_p = 10\text{s}$	83
6.55	Underkeel clearance for $H_s = 1\text{m}$ , $T_p = 12\text{s}$	83
6.56	Underkeel clearance for $H_s = 2\text{m}$ , $T_p = 10\text{s}$	83
6.57	Underkeel clearance for $H_s = 2\text{m}$ , $T_p = 12\text{s}$	83
6.58	Underkeel clearance for $H_s = 3\text{m}$ , $T_p = 10\text{s}$	83
6.59	Underkeel clearance for $H_s = 3\text{m}$ , $T_p = 12\text{s}$	83
6.60	Underkeel clearance for $H_s = 4\text{m}$ , $T_p = 10\text{s}$	84
6.61	Underkeel clearance for $H_s = 4\text{m}$ , $T_p = 12\text{s}$	84
6.62	Underkeel clearance for $H_s = 5\text{m}$ , $T_p = 10\text{s}$	84
6.63	Underkeel clearance for $H_s = 5\text{m}$ , $T_p = 12\text{s}$	84
6.64	Underkeel clearance for $H_s = 5.5\text{m}$ , $T_p = 10\text{s}$	84
6.65	Underkeel clearance for $H_s = 5.5\text{m}$ , $T_p = 12\text{s}$	84
6.66	Underkeel clearance for $H_s = 6\text{m}$ , $T_p = 10\text{s}$	85
6.67	Underkeel clearance for $H_s = 6\text{m}$ , $T_p = 12\text{s}$	85
6.68	Influence of wave height on hull motion amplitudes for $T_p = 10\text{s}$	85
6.69	Influence of wave height on hull motion amplitudes for $T_p = 12\text{s}$	86
6.70	Rayleigh distribution density function and probability plot for ship motion amplitudes with $H_s = 3\text{m}$	90
6.71	Rayleigh distribution density function and probability plot for ship motion amplitudes with $H_s = 4\text{m}$	91
6.72	Rayleigh distribution density function and probability plot for ship motion amplitudes with $H_s = 5\text{m}$	91
6.73	Weibull distribution density function and probability plot for ship motion amplitudes with $H_s = 3\text{m}$	92

6.74	Weibull distribution density function and probability plot for ship motion amplitudes with $H_s = 4\text{m}$ . . . . .	93
6.75	Weibull distribution density function and probability plot for ship motion amplitudes with $H_s = 5\text{m}$ . . . . .	93
6.76	Generalized Extreme Value distribution density function and probability plot for ship motion amplitudes with $H_s = 3\text{m}$ . . . . .	94
6.77	Generalized Extreme Value distribution density function and probability plot for ship motion amplitudes with $H_s = 4\text{m}$ . . . . .	95
6.78	Generalized Extreme Value distribution density function and probability plot for ship motion amplitudes with $H_s = 5\text{m}$ . . . . .	95
6.79	Generalized Pareto distribution density function and probability plot for ship motion amplitudes with $H_s = 3\text{m}$ . . . . .	96
6.80	Generalized Pareto distribution density function and probability plot for ship motion amplitudes with $H_s = 4\text{m}$ . . . . .	97
6.81	Generalized Pareto distribution density function and probability plot for ship motion amplitudes with $H_s = 5\text{m}$ . . . . .	97
7.1	Squat for varying water depths . . . . .	99
7.2	Underkeel clearance for $H_s = 3\text{m}$ , $T_p = 14\text{s}$ . . . . .	100
7.3	Underkeel clearance for $H_s = 4\text{m}$ , $T_p = 14\text{s}$ . . . . .	100
7.4	Underkeel clearance for $H_s = 3\text{m}$ , $T_p = 16\text{s}$ . . . . .	100
7.5	Underkeel clearance for $H_s = 4\text{m}$ , $T_p = 16\text{s}$ . . . . .	100
7.6	Underkeel clearance for $H_s = 3\text{m}$ , $T_p = 18\text{s}$ . . . . .	101
7.7	Underkeel clearance for $H_s = 4\text{m}$ , $T_p = 18\text{s}$ . . . . .	101
7.8	Underkeel clearance for $H_s = 3\text{m}$ , $T_p = 14\text{s}$ . . . . .	101
7.9	Underkeel clearance for $H_s = 4\text{m}$ , $T_p = 14\text{s}$ . . . . .	101
7.10	Underkeel clearance for $H_s = 3\text{m}$ , $T_p = 16\text{s}$ . . . . .	101
7.11	Underkeel clearance for $H_s = 4\text{m}$ , $T_p = 16\text{s}$ . . . . .	101
7.12	Underkeel clearance for $H_s = 3\text{m}$ , $T_p = 18\text{s}$ . . . . .	102
7.13	Underkeel clearance for $H_s = 4\text{m}$ , $T_p = 18\text{s}$ . . . . .	102
8.1	Comparison of effects of water depth on significant hull motion response between physical and Wavescat model . . . . .	105
A.1	Vessel response spectrum for $H_s = 3\text{m}$ , Direction = $90^\circ$ . . . . .	115
A.2	Vessel response spectrum for $H_s = 4\text{m}$ , Direction = $90^\circ$ . . . . .	115
A.3	Vessel response spectrum for $H_s = 5\text{m}$ , Direction = $90^\circ$ . . . . .	116
A.4	Vessel response spectrum for $H_s = 3\text{m}$ , Direction = $90^\circ$ . . . . .	116
A.5	Vessel response spectrum for $H_s = 4\text{m}$ , Direction = $90^\circ$ . . . . .	116
A.6	Vessel response spectrum for $H_s = 5\text{m}$ , Direction = $90^\circ$ . . . . .	116
A.7	Vessel response spectrum for $H_s = 3\text{m}$ , Direction = $90^\circ$ . . . . .	117
A.8	Vessel response spectrum for $H_s = 4\text{m}$ , Direction = $90^\circ$ . . . . .	117
A.9	Vessel response spectrum for $H_s = 5\text{m}$ , Direction = $90^\circ$ . . . . .	117
A.10	Vessel response spectrum for $H_s = 1\text{m}$ , Direction = $90^\circ$ . . . . .	117

A.11 Vessel response spectrum for $H_s = 2\text{m}$ , Direction = $90^\circ$ . . . . .	118
A.12 Vessel response spectrum for $H_s = 3\text{m}$ , Direction = $90^\circ$ . . . . .	118
A.13 Vessel response spectrum for $H_s = 4\text{m}$ , Direction = $90^\circ$ . . . . .	118
A.14 Vessel response spectrum for $H_s = 5\text{m}$ , Direction = $90^\circ$ . . . . .	118
A.15 Vessel response spectrum for $H_s = 3\text{m}$ , Direction = $135^\circ$ . . . . .	119
A.16 Vessel response spectrum for $H_s = 4\text{m}$ , Direction = $135^\circ$ . . . . .	119
A.17 Vessel response spectrum for $H_s = 5\text{m}$ , Direction = $135^\circ$ . . . . .	119
A.18 Vessel response spectrum for $H_s = 3\text{m}$ , Direction = $135^\circ$ . . . . .	119
A.19 Vessel response spectrum for $H_s = 4\text{m}$ , Direction = $135^\circ$ . . . . .	120
A.20 Vessel response spectrum for $H_s = 5\text{m}$ , Direction = $135^\circ$ . . . . .	120
A.21 Vessel response spectrum for $H_s = 3\text{m}$ , Direction = $135^\circ$ . . . . .	120
A.22 Vessel response spectrum for $H_s = 4\text{m}$ , Direction = $135^\circ$ . . . . .	120
A.23 Vessel response spectrum for $H_s = 5\text{m}$ , Direction = $135^\circ$ . . . . .	121
A.24 Vessel response spectrum for $H_s = 3\text{m}$ , Direction = $135^\circ$ . . . . .	121
A.25 Vessel response spectrum for $H_s = 4\text{m}$ , Direction = $135^\circ$ . . . . .	121
A.26 Vessel response spectrum for $H_s = 5\text{m}$ , Direction = $135^\circ$ . . . . .	121
A.27 Vessel response spectrum for $H_s = 3\text{m}$ , Direction = $135^\circ$ . . . . .	122
A.28 Vessel response spectrum for $H_s = 4\text{m}$ , Direction = $135^\circ$ . . . . .	122
A.29 Vessel response spectrum for $H_s = 5\text{m}$ , Direction = $135^\circ$ . . . . .	122
A.30 Vessel response spectrum for $H_s = 3\text{m}$ , Direction = $180^\circ$ . . . . .	122
A.31 Vessel response spectrum for $H_s = 4\text{m}$ , Direction = $180^\circ$ . . . . .	123
A.32 Vessel response spectrum for $H_s = 5\text{m}$ , Direction = $180^\circ$ . . . . .	123
A.33 Vessel response spectrum for $H_s = 3\text{m}$ , Direction = $180^\circ$ . . . . .	123
A.34 Vessel response spectrum for $H_s = 4\text{m}$ , Direction = $180^\circ$ . . . . .	123
A.35 Vessel response spectrum for $H_s = 5\text{m}$ , Direction = $180^\circ$ . . . . .	124
A.36 Vessel response spectrum for $H_s = 3\text{m}$ , Direction = $180^\circ$ . . . . .	124
A.37 Vessel response spectrum for $H_s = 4\text{m}$ , Direction = $180^\circ$ . . . . .	124
A.38 Vessel response spectrum for $H_s = 5\text{m}$ , Direction = $180^\circ$ . . . . .	124
A.39 Vessel response spectrum for $H_s = 3\text{m}$ , Direction = $180^\circ$ . . . . .	125
A.40 Vessel response spectrum for $H_s = 4\text{m}$ , Direction = $180^\circ$ . . . . .	125
A.41 Vessel response spectrum for $H_s = 5\text{m}$ , Direction = $180^\circ$ . . . . .	125
A.42 Vessel response spectrum for $H_s = 3\text{m}$ , Direction = $180^\circ$ . . . . .	125
A.43 Vessel response spectrum for $H_s = 4\text{m}$ , Direction = $180^\circ$ . . . . .	126
A.44 Vessel response spectrum for $H_s = 5\text{m}$ , Direction = $180^\circ$ . . . . .	126
B.1 Rayleigh distribution density function and probability plot for ship motion amplitudes with $H_s = 3\text{m}$ . . . . .	127
B.2 Rayleigh distribution density function and probability plot for ship motion amplitudes with $H_s = 4\text{m}$ . . . . .	128
B.3 Rayleigh distribution density function and probability plot for ship motion amplitudes with $H_s = 5\text{m}$ . . . . .	128
B.4 Rayleigh distribution density function and probability plot for ship motion amplitudes with $H_s = 3\text{m}$ . . . . .	129

B.5	Rayleigh distribution density function and probability plot for ship motion amplitudes with $H_s = 4\text{m}$ . . . . .	129
B.6	Rayleigh distribution density function and probability plot for ship motion amplitudes with $H_s = 5\text{m}$ . . . . .	130
B.7	Weibull distribution density function and probability plot for ship motion amplitudes with $H_s = 3\text{m}$ . . . . .	130
B.8	Weibull distribution density function and probability plot for ship motion amplitudes with $H_s = 4\text{m}$ . . . . .	131
B.9	Weibull distribution density function and probability plot for ship motion amplitudes with $H_s = 5\text{m}$ . . . . .	131
B.10	Weibull distribution density function and probability plot for ship motion amplitudes with $H_s = 3\text{m}$ . . . . .	132
B.11	Weibull distribution density function and probability plot for ship motion amplitudes with $H_s = 4\text{m}$ . . . . .	132
B.12	Weibull distribution density function and probability plot for ship motion amplitudes with $H_s = 5\text{m}$ . . . . .	133
B.13	Generalized Extreme Value distribution density function and probability plot for ship motion amplitudes with $H_s = 3\text{m}$ . . . . .	133
B.14	Generalized Extreme Value distribution density function and probability plot for ship motion amplitudes with $H_s = 4\text{m}$ . . . . .	134
B.15	Generalized Extreme Value distribution density function and probability plot for ship motion amplitudes with $H_s = 5\text{m}$ . . . . .	134
B.16	Generalized Extreme Value distribution density function and probability plot for ship motion amplitudes with $H_s = 3\text{m}$ . . . . .	135
B.17	Generalized Extreme Value distribution density function and probability plot for ship motion amplitudes with $H_s = 5\text{m}$ . . . . .	135
B.18	Generalized Extreme Value distribution density function and probability plot for ship motion amplitudes with $H_s = 4\text{m}$ . . . . .	136
B.19	Generalized Pareto distribution density function and probability plot for ship motion amplitudes with $H_s = 3\text{m}$ . . . . .	136
B.20	Generalized Pareto distribution density function and probability plot for ship motion amplitudes with $H_s = 4\text{m}$ . . . . .	137
B.21	Generalized Pareto distribution density function and probability plot for ship motion amplitudes with $H_s = 5\text{m}$ . . . . .	137
B.22	Generalized Pareto distribution density function and probability plot for ship motion amplitudes with $H_s = 3\text{m}$ . . . . .	138
B.23	Generalized Pareto distribution density function and probability plot for ship motion amplitudes with $H_s = 4\text{m}$ . . . . .	138
B.24	Generalized Pareto distribution density function and probability plot for ship motion amplitudes with $H_s = 5\text{m}$ . . . . .	139
C.1	Underkeel clearance for $H_s = 3\text{m}$ , $T_p = 10\text{s}$ . . . . .	141
C.2	Underkeel clearance for $H_s = 4\text{m}$ , $T_p = 10\text{s}$ . . . . .	141
C.3	Underkeel clearance for $H_s = 5\text{m}$ , $T_p = 10\text{s}$ . . . . .	141



C.4	Underkeel clearance for $H_s = 3\text{m}$ , $T_p = 10\text{s}$	142
C.5	Underkeel clearance for $H_s = 4\text{m}$ , $T_p = 10\text{s}$	142
C.6	Underkeel clearance for $H_s = 5\text{m}$ , $T_p = 10\text{s}$	142
C.7	Underkeel clearance for $H_s = 3\text{m}$ , $T_p = 10\text{s}$	143
C.8	Underkeel clearance for $H_s = 4\text{m}$ , $T_p = 10\text{s}$	143
C.9	Underkeel clearance for $H_s = 5\text{m}$ , $T_p = 10\text{s}$	143
C.10	Underkeel clearance for $H_s = 3\text{m}$ , $T_p = 10\text{s}$	144
C.11	Underkeel clearance for $H_s = 4\text{m}$ , $T_p = 10\text{s}$	144
C.12	Underkeel clearance for $H_s = 5\text{m}$ , $T_p = 10\text{s}$	144
C.13	Underkeel clearance for $H_s = 3\text{m}$ , $T_p = 10\text{s}$	145
C.14	Underkeel clearance for $H_s = 4\text{m}$ , $T_p = 10\text{s}$	145
C.15	Underkeel clearance for $H_s = 5\text{m}$ , $T_p = 10\text{s}$	145

# List of Tables

2.1	Port of Richards Bay berth information . . . . .	8
2.2	Richards Bay Chart Datum Levels (SANHO, 2019) . . . . .	9
3.1	Brazillian Pride Dimensions . . . . .	15
3.2	Ship sizes and their dimensions, (TNPA, 2016) . . . . .	17
3.3	Ship sizes and their dimensions, (PIANC, 2014) . . . . .	18
5.1	1989 Historical test conditions (Jonker <i>et al.</i> , 1991) . . . . .	33
5.2	Ratios of $(A_s/H_s)$ for depth to draught ratio $(d/D) = 1.5$ . . . . .	34
5.3	Ratios of $(A_s/H_s)$ for depth to draught ratio $(d/D) = 1.4$ (Jonker <i>et al.</i> , 1991) . . . . .	35
5.4	Ratios of $(A_s/H_s)$ for depth to draught ratio $(d/D) = 1.3$ (Jonker <i>et al.</i> , 1991) . . . . .	35
5.5	Ratios of $(A_s/H_s)$ for depth to draught ratio $(d/D) = 1.2$ . . . . .	36
5.6	Ratios of $(A_s/H_s)$ for depth to draught ratio $(d/D) = 1.1$ (Jonker <i>et al.</i> , 1991) . . . . .	36
6.1	Summer wave heights versus wave direction occurrence . . . . .	43
6.2	Autumn wave heights versus wave direction occurrence . . . . .	43
6.3	Winter wave heights versus wave direction occurrence . . . . .	43
6.4	Winter wave heights versus wave direction occurrence . . . . .	44
6.5	Overall wave heights versus wave direction occurrence . . . . .	44
6.6	Summer wave heights versus peak periods occurrence . . . . .	45
6.7	Autumn wave heights versus peak periods occurrence . . . . .	45
6.8	Winter wave heights versus peak periods occurrence . . . . .	45
6.9	Winter wave heights versus peak periods occurrence . . . . .	46
6.10	Overall wave heights versus peak periods occurrence . . . . .	46
6.11	Ship model's fixed orientation systems and waves' earth bound ori- entation system . . . . .	48
6.12	Waverider and ADCP calibration wave conditions . . . . .	49
6.13	Mike21BW Waverider and ADCP calibration wave conditions results	49
6.14	Accuracy percentage table for measured and simulated Mike21BW wave conditions . . . . .	50
6.15	Mike 21BW input conditions . . . . .	51
6.16	150kt DWT Bulk vessel dimensions . . . . .	59



6.17	Water depth in the physical model and Wavescat/Mike21BW model	60
6.18	Test conditions for 150kt DWT bulk carrier with 0 m/s . . . . .	60
6.19	Viscous damping coefficients for 90° . . . . .	64
6.20	Viscous damping coefficients for 135° . . . . .	65
6.21	Viscous damping coefficients for 180° . . . . .	65
6.22	Wavescat under prediction percentages for 90° . . . . .	72
6.23	Wavescat under prediction percentages for 135° . . . . .	73
6.24	Wavescat under prediction percentages for 180° . . . . .	73
6.25	Underkeel sensitivity test conditions . . . . .	82
6.26	Hull keel points . . . . .	82
6.27	Rayleigh distribution's estimated maximum value for PQT/PSH, incident wave angle 90° . . . . .	89
6.28	Rayleigh distribution's estimated maximum value for PQT/PSH, incident wave angle 135° . . . . .	89
6.29	Rayleigh distribution's estimated maximum value for PQT/PSH, incident wave angle 180° . . . . .	89
7.1	Squat for ship speed of 4m/s . . . . .	99
7.2	Underkeel clearance for $H_s = 3\text{m}$ , $T_p = 14\text{s}$ . . . . .	102
7.3	Underkeel clearance for $H_s = 3\text{m}$ , $T_p = 14\text{s}$ . . . . .	102
7.4	Underkeel clearance for $H_s = 3\text{m}$ , $T_p = 16\text{s}$ . . . . .	102
7.5	Underkeel clearance for $H_s = 3\text{m}$ , $T_p = 16\text{s}$ . . . . .	102
7.6	Underkeel clearance for $H_s = 3\text{m}$ , $T_p = 18\text{s}$ . . . . .	102
7.7	Underkeel clearance for $H_s = 3\text{m}$ , $T_p = 18\text{s}$ . . . . .	102
7.8	Underkeel clearance for $H_s = 3\text{m}$ , $T_p = 14\text{s}$ . . . . .	103
7.9	Underkeel clearance for $H_s = 3\text{m}$ , $T_p = 14\text{s}$ . . . . .	103
7.10	Underkeel clearance for $H_s = 3\text{m}$ , $T_p = 16\text{s}$ . . . . .	103
7.11	Underkeel clearance for $H_s = 3\text{m}$ , $T_p = 16\text{s}$ . . . . .	103
7.12	Underkeel clearance for $H_s = 3\text{m}$ , $T_p = 18\text{s}$ . . . . .	103
7.13	Underkeel clearance for $H_s = 3\text{m}$ , $T_p = 18\text{s}$ . . . . .	103
8.1	Averaged differences between the physical and the Wavescat model for 90°, 135° and 180° . . . . .	105
10.1	Mike 21BW input conditions . . . . .	112
C.1	Channel probe locations, water depths and $d/D$ ratios . . . . .	140
D.1	Physical and Wavescat model results for depth to draught ratio ( $d/D$ ) = 1.5 . . . . .	146
D.2	Physical and Wavescat model results for depth to draught ratio ( $d/D$ ) = 1.4 . . . . .	147
D.3	Physical and Wavescat model results for depth to draught ratio ( $d/D$ ) = 1.3 . . . . .	147

D.4	Physical and Wavescat model results for depth to draught ratio (d/D) = 1.2 . . . . .	147
D.5	Physical and Wavescat model results for depth to draught ratio (d/D) = 1.1 . . . . .	148
D.6	As versus Hs results for Tp =10s . . . . .	148
D.7	As versus Hs results for Tp =12s . . . . .	148
D.8	As for Hs = 1m, Tp =10s and $\alpha = 90^\circ$ . . . . .	149
D.9	As for Hs = 1m, Tp =12s and $\alpha = 90^\circ$ . . . . .	149
D.10	As for Hs = 2m, Tp =10s and $\alpha = 90^\circ$ . . . . .	149
D.11	As for Hs = 2m, Tp =12s and $\alpha = 90^\circ$ . . . . .	150
D.12	As for Hs = 3m, Tp =10s and $\alpha = 90^\circ$ . . . . .	150
D.13	As for Hs = 3m, Tp =12s and $\alpha = 90^\circ$ . . . . .	150
D.14	As for Hs = 4m, Tp =10s and $\alpha = 90^\circ$ . . . . .	151
D.15	As for Hs = 4m, Tp =12s and $\alpha = 90^\circ$ . . . . .	151
D.16	As for Hs = 5m, Tp =10s and $\alpha = 90^\circ$ . . . . .	151
D.17	As for Hs = 5m, Tp =12s and $\alpha = 90^\circ$ . . . . .	152
D.18	As for Hs = 5.5m, Tp =10s and $\alpha = 90^\circ$ . . . . .	152
D.19	As for Hs = 5.5m, Tp =12s and $\alpha = 90^\circ$ . . . . .	152
D.20	As for Hs = 6m, Tp =10s and $\alpha = 90^\circ$ . . . . .	153
D.21	As for Hs = 6m, Tp =12s and $\alpha = 90^\circ$ . . . . .	153
D.22	As for Hs = 3m, Tp =10s and $\alpha = 90^\circ$ . . . . .	153
D.23	As for Hs = 4m, Tp =10s and $\alpha = 90^\circ$ . . . . .	154
D.24	As for Hs = 5m, Tp =10s and $\alpha = 90^\circ$ . . . . .	154
D.25	As for Hs = 3m, Tp =10s and $\alpha = 135^\circ$ . . . . .	154
D.26	As for Hs = 4m, Tp =10s and $\alpha = 135^\circ$ . . . . .	155
D.27	As for Hs = 5m, Tp =10s and $\alpha = 135^\circ$ . . . . .	155
D.28	As for Hs = 3m, Tp =10s and $\alpha = 180^\circ$ . . . . .	155
D.29	As for Hs = 4m, Tp =10s and $\alpha = 180^\circ$ . . . . .	156
D.30	As for Hs = 5m, Tp =10s and $\alpha = 180^\circ$ . . . . .	156
D.31	As for Hs = 3m, Tp =14s . . . . .	156
D.32	As for Hs = 4m, Tp =14s . . . . .	157
D.33	As for Hs = 3m, Tp =16s . . . . .	157
D.34	As for Hs = 4m, Tp =16s . . . . .	157
D.35	As for Hs = 3m, Tp =18s . . . . .	157
D.36	As for Hs = 4m, Tp =18s . . . . .	158
D.37	As for Hs = 3m, Tp =14s . . . . .	158
D.38	As for Hs = 4m, Tp =14s . . . . .	158
D.39	As for Hs = 3m, Tp =16s . . . . .	158
D.40	As for Hs = 4m, Tp =16s . . . . .	159
D.41	As for Hs = 3m, Tp =18s . . . . .	159
D.42	As for Hs = 4m, Tp =18s . . . . .	159
D.43	UKC for Hs = 3m, Tp =10s and $\alpha = 90^\circ$ . . . . .	159
D.44	UKC for Hs = 4m, Tp =10s and $\alpha = 90^\circ$ . . . . .	160
D.45	UKC for Hs = 5m, Tp =10s and $\alpha = 90^\circ$ . . . . .	160

D.46 UKC for $H_s = 3\text{m}$ , $T_p = 10\text{s}$ and $\alpha = 135^\circ$ . . . . .	160
D.47 UKC for $H_s = 4\text{m}$ , $T_p = 10\text{s}$ and $\alpha = 135^\circ$ . . . . .	161
D.48 UKC for $H_s = 5\text{m}$ , $T_p = 10\text{s}$ and $\alpha = 135^\circ$ . . . . .	161
D.49 UKC for $H_s = 3\text{m}$ , $T_p = 10\text{s}$ and $\alpha = 180^\circ$ . . . . .	161
D.50 UKC for $H_s = 4\text{m}$ , $T_p = 10\text{s}$ and $\alpha = 180^\circ$ . . . . .	162
D.51 UKC for $H_s = 5\text{m}$ , $T_p = 10\text{s}$ and $\alpha = 180^\circ$ . . . . .	162

# Nomenclature

## Symbols and definitions

$\alpha$	dimensionless JONSWAP spectrum for fetch-limited seas	[–]
$\alpha$	probability scale . . . . .	[–]
$\sigma$	scale parameter . . . . .	[–]
$\alpha_x, \alpha_z$	fluid particle acceleration . . . . .	[m/s <sup>2</sup> ]
$\beta$	resistance coefficient for turbulent flow in porous media	[–]
$\gamma_b$	breaker index . . . . .	[–]
$\Delta p$	difference in pressure at a point . . . . .	[N/m <sup>2</sup> ]
$\epsilon$	perturbation expansion parameter . . . . .	[–]
$\epsilon$	wave steepness=H/L . . . . .	[–]
$\varepsilon$	phase . . . . .	[deg]
$\kappa$	shape parameter . . . . .	[–]
$\mu$	location parameter . . . . .	[–]
$\Gamma$	gamma . . . . .	[–]
$\zeta$	vertical displacement of the water particle from mean position	[ m ]
$\xi$	horizontal displacement of the water particle from mean position	[ m ]

$\xi$	shape parameter . . . . .	[–]
$\eta$	water surface relative to the SWL . . . . .	[m]
$\eta_{envelope}$	envelope wave form of two or more superimposed wave trains	[m]
$\theta$	wave direction . . . . .	[deg]
$\theta$	angle . . . . .	[deg]
$\theta$	pitch . . . . .	[deg]
$\phi$	roll angle . . . . .	[deg]
$\rho$	water density . . . . .	[kg/m <sup>3</sup> ]
$\Phi$	velocity potential . . . . .	[m <sup>2</sup> /s]
$\Psi$	stream function . . . . .	[–]
$\Psi$	yaw . . . . .	[deg]
$\omega$	wave angular or radian frequency = $2\pi/T$ . . . . .	[s <sup>-1</sup> ]
$A_s$	Significant hull motion amplitude . . . . .	[m]
$B$	Boussinesq dispersion factor . . . . .	[–]
$c_g$	wave group velocity . . . . .	[m/s]
$C$	chezy resistance number . . . . .	[m <sup>0.5</sup> /s]
$c_{bow}$	bow sinkage coefficient . . . . .	[–]
$c_{stern}$	stern sinkage coefficient . . . . .	[–]
$D$	Draught . . . . .	[m]
$d$	water depth . . . . .	[m]

$E$	total wave energy in one wavelength per unit crest width [m <sup>2</sup> ]
$\bar{E}_k$	kinetic energy per unit length of wave crest for a linear wave [m – N/m <sup>2</sup> ]
$\bar{E}_p$	potential energy per unit length of wave crest for a linear wave [m – N/m <sup>2</sup> ]
$F_x$	Horizontal stress term in x-direction . . . . . [–]
$F_h$	depth based Froude number . . . . . [–]
$F_y$	Horizontal stress term in y-direction . . . . . [–]
$g$	gravitational acceleration . . . . . [m/s <sup>2</sup> ]
$h$	total water depth . . . . . [m]
$H$	wave height . . . . . [m]
$H_{rms}$	root mean square . . . . . [m]
$H_s$	significant wave height . . . . . [m]
$k$	wave number . . . . . [m <sup>-1</sup> ]
$k$	modulus of the elliptic integrals . . . . . [–]
$k$	number of lags between waves in a sequence in a record [–]
$L$	wave length . . . . . [m]
$n$	porosity . . . . . [–]
$N_z$	number of zero upcrossing and crests in a wave record . [–]
$p$	pressure . . . . . [N/m <sup>2</sup> ]
$p'$	absolute subsurface pressure . . . . . [N/m <sup>2</sup> ]
$P$	flux density in the x-direction . . . . . [m <sup>3</sup> /m/s]

$Q$	flux density in the y-direction . . . . .	[m <sup>3</sup> /m/s]
$t - T$	period . . . . .	[s]
$T_r$	wave record length . . . . .	[s]
$T_z$	zero crossing period . . . . .	[s]
$T_p$	peak period . . . . .	[s]
$u$	fluid velocity in the x direction . . . . .	[m/s]
$U_R$	ursell number . . . . .	[–]
$w$	fluid velocity in the z direction . . . . .	[m/s]
$y_c$	vertical distance from seabed to wave crest . . . . .	[m]
$y_s$	vertical distance from seabed to water surface . . . . .	[m]
$y_t$	vertical distance from seabed to wave trough . . . . .	[m]
$z$	water depth below SWL . . . . .	[m]
$\nabla$	Ship's displacement volume . . . . .	[m <sup>3</sup> ]

# Chapter 1

## Introduction

### 1.1 Problem Statement

The Port of Richards Bay is a major coal export harbour in South Africa. For efficiency, departing coal carriers should be loaded up to their maximum safe draught. Port of Richards Bay's storm conditions peak periods are in the ranges of 14s to 18s and wave directions relative to the vector bow direction of the departing laden ship which is  $225^\circ$  as shown in Figure 1.1 .



Figure 1.1: Ship departure route and storms wave direction (Google, 2019)

During these storms, large vertical ship motions of more than 1.5 m occur. These large ship motions pose as a risk for fully laden coal carriers with large



draught, especially when the incident wave direction is  $90^\circ$  or  $270^\circ$  because it is from these angles that large movements of the ship's hull occur. These large movements affect the underkeel clearance safety limits of the Port's channel. Six keel points in relation to the centre of gravity were used to test vertical ship motions for different peak periods and wave directions during the CSIR's physical modelling tests as shown in Figure 1.2 and 1.3.

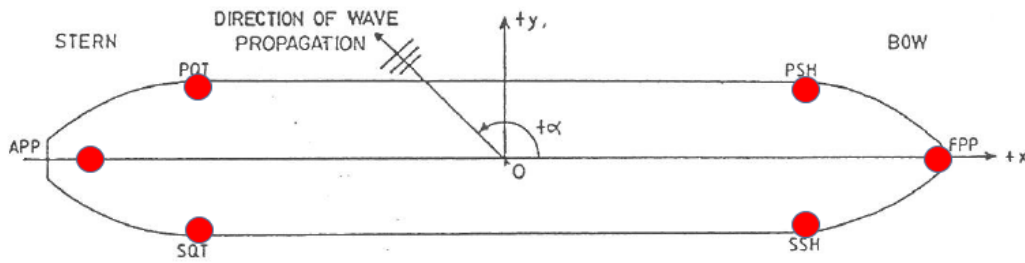


Figure 1.2: Keel points

where:

APP = aft perpendicular

PQT = port quarter

SQT = starboard quarter

PSH = port shoulder

SSH = starboard shoulder

FPP = forward perpendicular

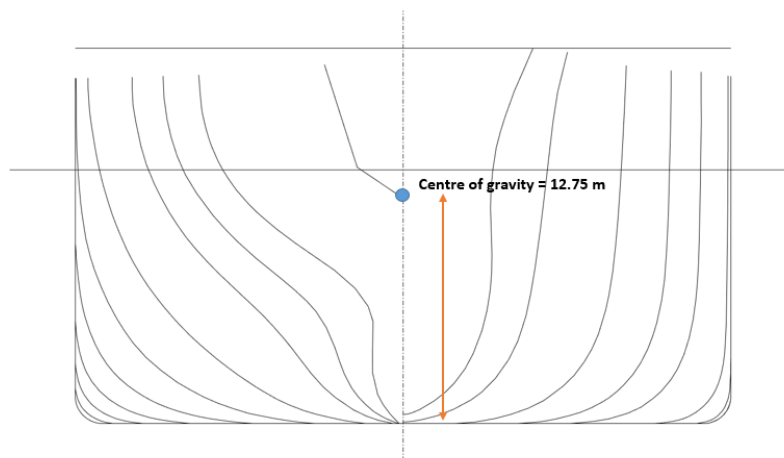
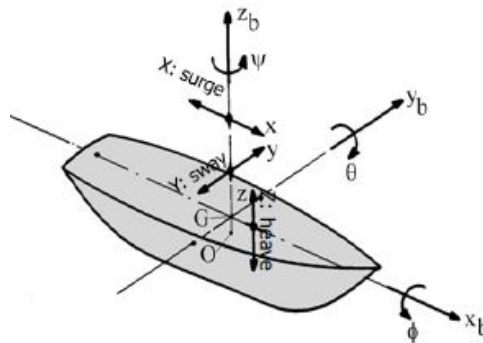


Figure 1.3: Centre of gravity

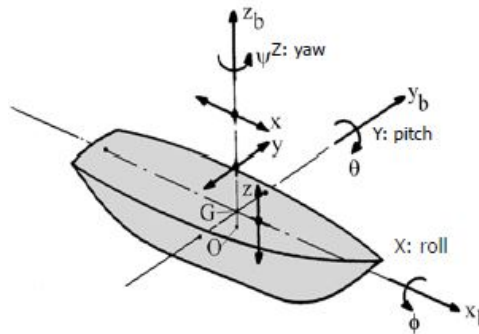
The probability of exceedance for maximum hull motion amplitudes less than 1.5 m can be approximated using the Rayleigh distribution. The physical test results show that ship motion amplitudes more than 1.5 m for incident wave angles  $90^\circ/270^\circ$  no longer seem to follow the linear trend, which means that ship motion amplitudes greater than 1.5 m need to further be tested, to estimate the exceedance of these maximum vertical hull motion amplitudes using non-linear probability distributions namely Weibull, Extreme Generalized Value and Generalized Pareto.

Six ship degrees of freedom are defined. Figures 1.4 and 1.5 show the three translation and the three rotation motions respectively.



Translation motions	Description
Surge (x)	Linear longitudinal ship movement in the x direction
Sway (y)	Linear lateral ship movement in the y direction
Heave (z)	Linear vertical ship movement in the z direction

Figure 1.4: Translation motions (Journee and Massie, 2001a)



Rotation motions	Description
Roll ( $\phi$ )	Side to side tilting ship movement on its x-axis
Pitch ( $\theta$ )	Up and down tilting ship movement on its y-axis
Yaw ( $\Psi$ )	Turning vertical ship movement on its z-axis

Figure 1.5: Rotation motions (Journee and Massie, 2001a)

Factors that lead to wave-induced vertical keel point motions are heave, roll and pitch. These motions are accepted to be linearly proportional to wave heights (by frequency-dependent Response Amplitude Operators or RAOs). RAOs are transfer functions used to predict the behaviour of a ship under different wave conditions.

The wave heights in a sea state are accepted to be Rayleigh distributed and therefore also the heave, roll and pitch motions as well as their combined motion, are accepted to be Rayleigh distributed. If the wave conditions are linear, the resulting ship motions will also be linear. Nonlinear aspects that play a role are the location of the centre of gravity of the vessel, assumed to be centre of roll rotation, the viscous roll damping, small-underkeel clearance damping and squat. These factors have an impact on the significant vertical keel point motion ( $A_s$ ) as well as on the ratio of  $A_{max}/A_s$ , where  $A_{max}$  is the maximum expected vertical keel point motion.

The aim of the present research study is to investigate whether maximum vertical keel point motions of coal carriers can be computed accurately on the basis of predicted wave and tide conditions. Their probability of exceedance should also be determined so that acceptable risk factors can be chosen. This process will require a calibrated numerical model and forecasting of environmental conditions. If this would be possible, the maximum safe draught of coal carriers could be predicted for future departing conditions, as function of time, and the optimum time of departure can be established, through the use of a CSIR underkeel clearance program called the DMAX given by Figure 1.6.

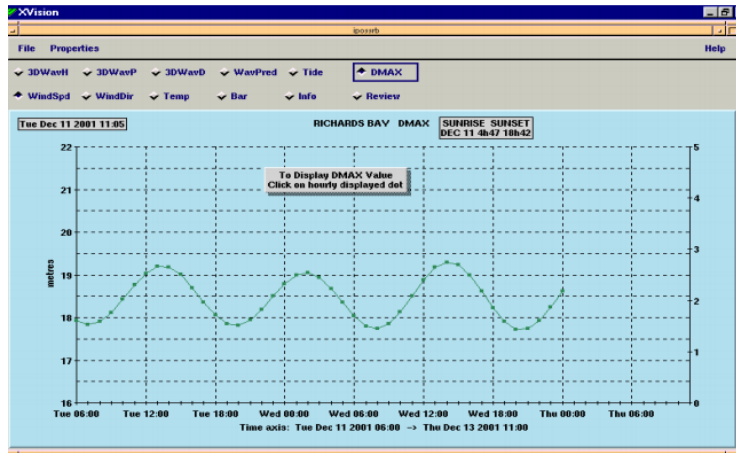


Figure 1.6: Richards Bay DMAX interface (Moes, 2007)

This would form the basis for port operational procedures for the departure of laden deep-draught coal carriers.

## 1.2 Objective

Assuming that linear wave theory is valid, the specific objectives of the present study are to:

- calibrate the Wavescat numerical model, using data obtained from the fully laden 150 kt deadweight physical model studies, to compute ship motions for wave heights of 3 m, 4 m and 5 m. The wave heights will be increased from  $A_{max}$  until the ship touches the bottom of the Port of Richards Bay entrance channel
- determine maximum ship motions in relation to their corresponding wave heights, peak periods and directions with much focus on beam waves
- determine the probability of exceedance of maximum hull motions, for significant motions greater than 1.5 m, by using non-linear quantile probability distributions namely the Generalized Extreme Value distribution (GEV), Generalized Pareto distribution (GP) and Weibull distribution with the purpose to find out which one best represent the non-linear relationship of maximum individual hull motion amplitudes for significant ship motions more than 1.5 m. The maximum ship motions will contribute towards improving the accuracy of an underkeel clearance model software called DMAX given by Figure 1.6, which helps determine safe ship draught limits for ship manoeuvring in the Richards Bay entrance channel.

- determine the effects that speed has on the underkeel clearance of a 150kt DWT bulk carrier moving at 4 m/s speed in storm conditions through the use of the Wavescat model.

### 1.3 Methodology

The objectives will be achieved by:

- using the National Centers for Environmental Prediction (NCEP) wave data to model Port of Richards Bay's offshore wave conditions. The NCEP wave data will be used to calibrate DELFT 3D-Swan by selecting certain storm conditions. The Delft3D-Swan will be used to calibrate Mike21BW by bring offshore wave data to nearshore. Boundary conditions will be tested in Delft3D-Swan and used as input to calibrate Mike21BW.
- using Mike21BW to model wave heights in the Port for selected peak periods and incident wave angles, on a more refined grid
- creating a 3D mesh of a 150 kt deadweight vessel with a draught of 17m and computing RAOs of each of the six keel points for each selected wave condition and calibrating the ship with the physical model test results. Vessel response spectra will be obtained by computing and multiplying wave spectra by the square of the RAOs for each wave period and waves incidence angles
- converting the vessel response spectrum to vessel motions timeseries for each selected wave condition using Mike21BW
- fitting each timeseries to the GEV, Weibull and GP probability densities to estimate the maximum probabilities of exceedance.

## Chapter 2

# Richards Bay Wave Climate

### 2.1 Description of the Port of Richards Bay

The Port of Richards Bay is located along the eastern coastline of South Africa at latitude  $28^{\circ}46'50.53''\text{S}$  and longitude  $32^{\circ}2'17.83''\text{E}$  as shown on Figure 2.1. The port's entrance channel has a bed width of 300m, with channel depths varying from 19.5m to 22m within the harbour, and water depth of  $\pm 24\text{m}$  that extends 4km beyond the breakwaters (depths referenced to Chart Datum).



Figure 2.1: Entrance to the Port of Richards Bay (Google, 2019)



The Port has 23 berths and their cargo types, depths and quay lengths are shown in Figure 2.2 and summarised in Table 2.1.

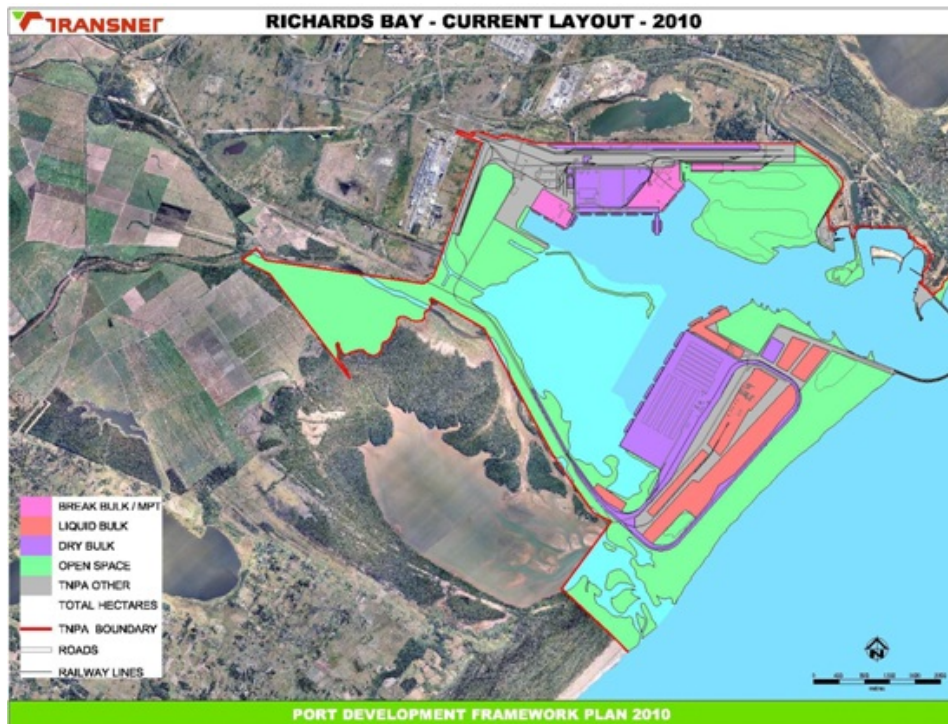


Figure 2.2: Port of Richards Bay berths (Transnet National Ports Authority, 2010)

Vessel type	No. of berths	Depth (CD) (m)	Quay lengths (m)
Bulk liquid	2	14	250, 300
Coal	6	19	184, 280, 350
General cargo	7	14.5, 14.7, 19	200, 204, 220, 280
Dry Liquid	7	14.5, 19	240, 260, 300
Repair berth	1	8	300

Table 2.1: Port of Richards Bay berth information

The approximate maximum tidal levels at Port of Richards Bay are shown in Table 2.2. The values of Lowest Astronomical Tide (LAT) and Highest Astronomical Tide (HAT) are computed from 19 years predictions and the Mean Levels are computed from the predictions of a recent year when the moon's average maximum declination was  $23.5^\circ$  SANHO (2019).

PLACE	LAT	MLWS	MLWN	ML	MHWN	MHWS	HAT
Richards Bay	0	0.27	0.97	1.2	1.48	2.11	2.47

Table 2.2: Richards Bay Chart Datum Levels (SANHO, 2019)

## 2.2 Wave data

Datawell Waveriders are floating moored wave recording buoys, which are exclusive to Durban and Richards Bay. Durban has two waveriders, one that belongs to TNPA, positioned at a depth of 30m off the Bluff, about 1.7km from the shore and one that belongs to eThekweni Municipality, positioned off the mouth of the Umgeni River in 15m water depth, about 1.5km from the shore. The significance of the Richards Bay waverider for this particular study is to calibrate the Mike21BW numerical model to ensure that all wave actions of importance in the Port are well represented.

The TNPA Datawell Waverider at Richards Bay is positioned at a depth of 22m, about 1.4km off the point of the southern breakwater as seen in Figure 2.1. The TNPA Waverider at Richards Bay records data continuously in real time, and is used for port operational purposes. The data is processed on board and transmitted to shore station every half an hour. The analysed data is downloaded in near real-time to the CSIR-Stellenbosch offices where it is also stored in a database.

An Acoustic Doppler Current Profiler (ADCP) is another wave measurement tool placed on the inside of the Port on the bed of the entrance channel (Figure 2.1), at water depth of  $\pm 21$ m CD. The ADCP records wave conditions at two hours intervals.

Data obtained from TNPA's Richards Bay Waverider and from CSIR's ADCP instrument was used in this study. The two wave recording tools are selected because of the ease of access to information from the CSIR database.

## 2.3 Wave conditions

Since the Port of Richards Bay is located in the KwaZulu-Natal Province, an overview of the Province's wave climate gives a general idea of the coastal wave conditions, before detailed wave data of the Port of Richards Bay is reviewed. Based on data obtained from the Durban and Richards Bay Waveriders, a study by Corbella and Stretch (2012) reveal that KwaZulu-Natal coast's aver-



age mean wave direction is  $130^\circ$  true north (TN), with an average wave period 10 s 20 s and an average mean significant wave height of 1.65m.

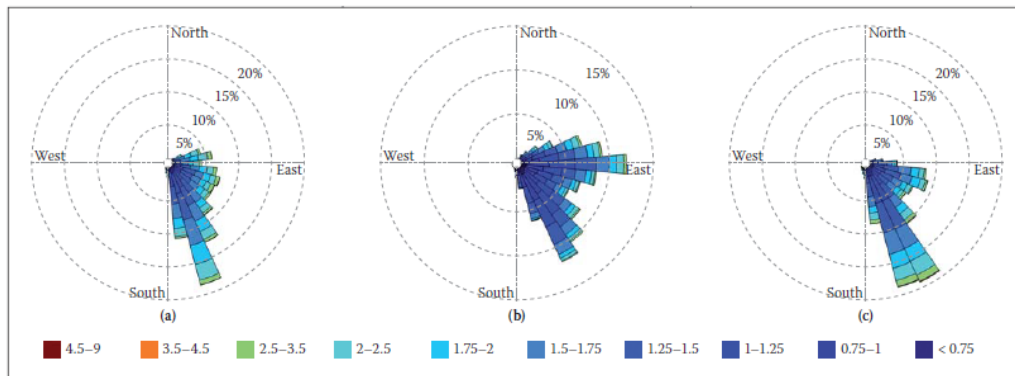


Figure 2.3: Comparison of the entire data set wave roses for (a) Durban Waverider (2007 to 2009), (b) Durban ADCP (2002 to 2006) and (c) Richards Bay Waverider (1997 to 2009) (Corbella and Stretch, 2012)

The 12 years of data also reveals that the most frequent and largest wave events occur in summer and autumn as shown in Figure 2.4.

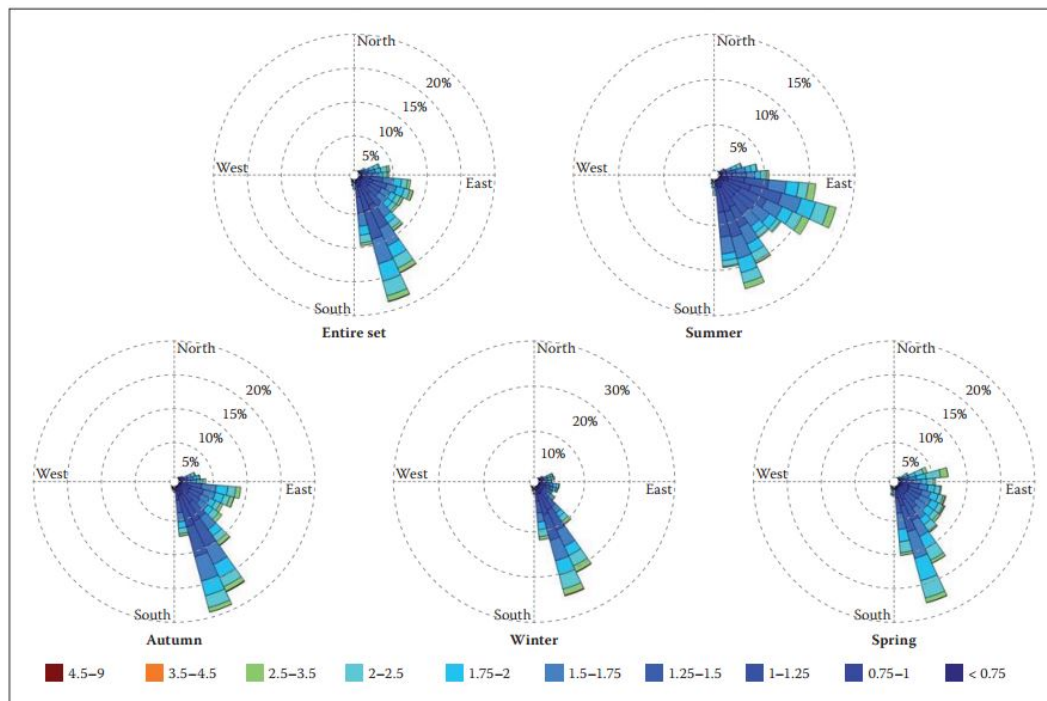


Figure 2.4: KwaZulu-Natal Wave Rose (1997-2009) (Corbella and Stretch, 2012)

The CSIR wave data dates back to 1979 but due some unavailable wave parameters, this study will use wave data from 2003 to 2017 obtained from CSIR/Transnet Wavenet IPOSS annual reports. They reveal that over the past 14 years, the season with the highest frequency of wave events is winter with the average wave direction of around 157.5° TN as shown in Figure 2.5.

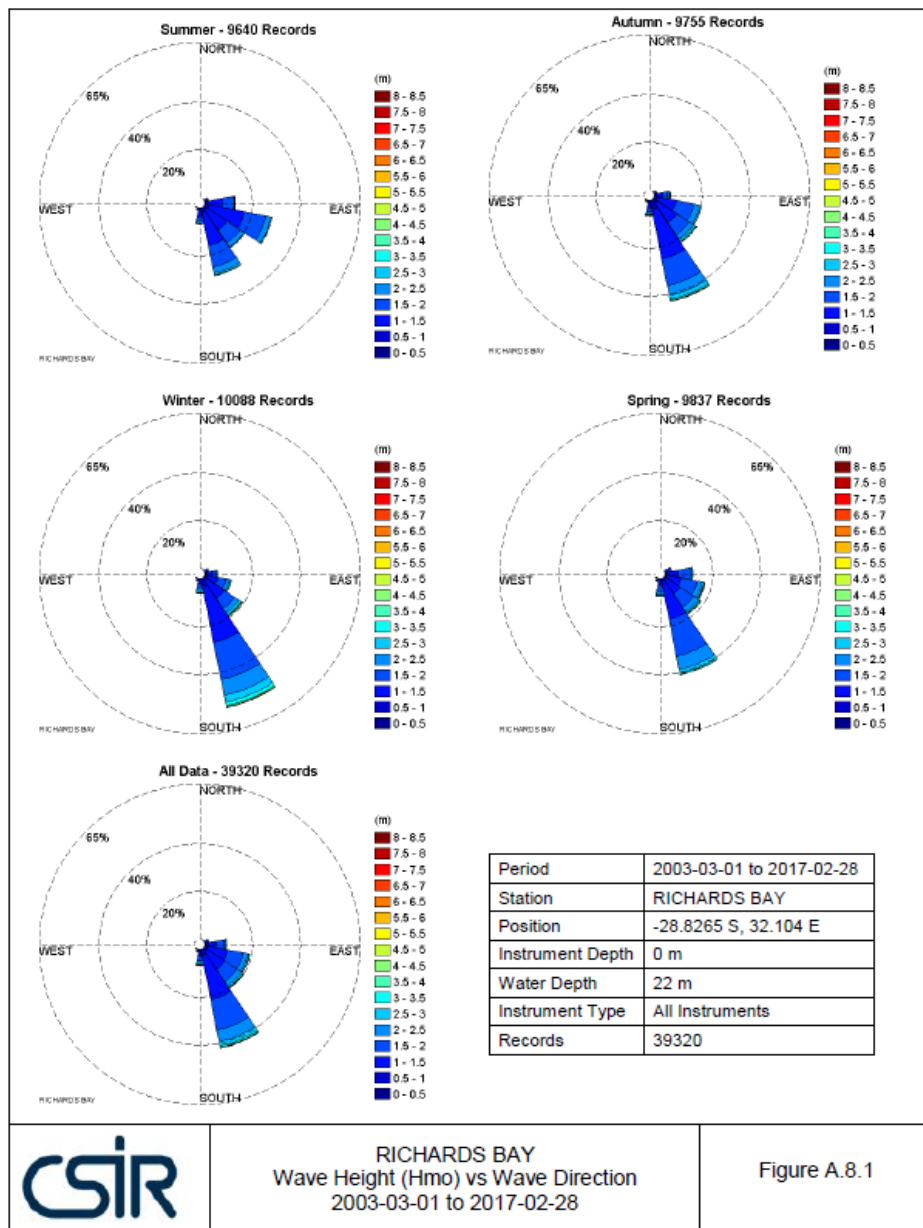


Figure 2.5: Richards Bay CSIR Wave height (Hmo) vs wave direction rose (2003-2017) (CSIR, 2017)

Figure 2.6 also shows a 14 years wave period histogram from 2003 to 2017.

The Figure shows that Richards Bay’s overall periods range from 4 s to 20 s with period of 12 s having the most percentage of occurrence.

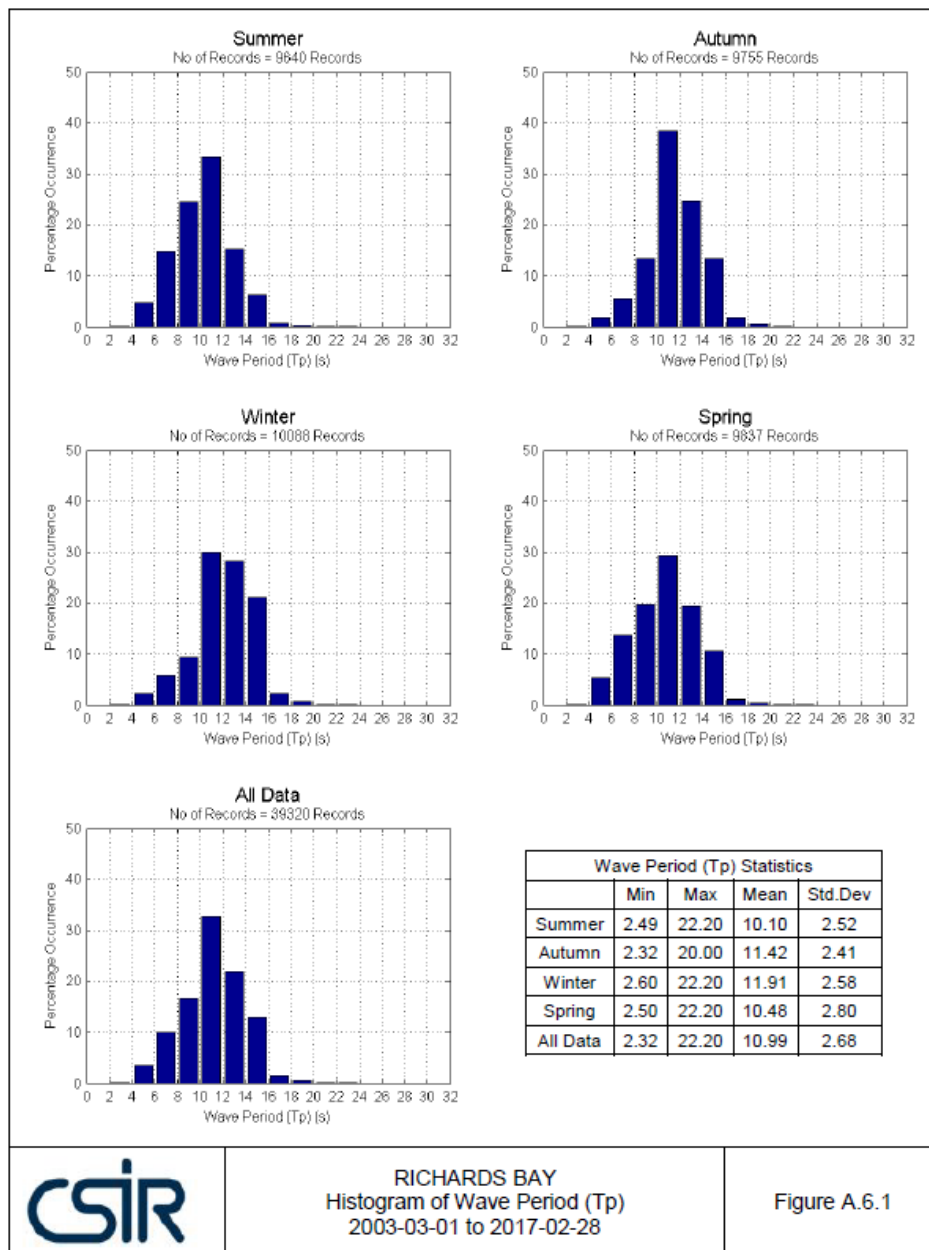


Figure 2.6: Richards Bay wave period histogram (2003-2017) (CSIR, 2017)

Figure 2.7 shows the Port of Richards Bay Waverider’s latest current speed plotted against current direction from 2017 to 2018. It can be seen from the roses that the most dominant current directions are South West and North East.

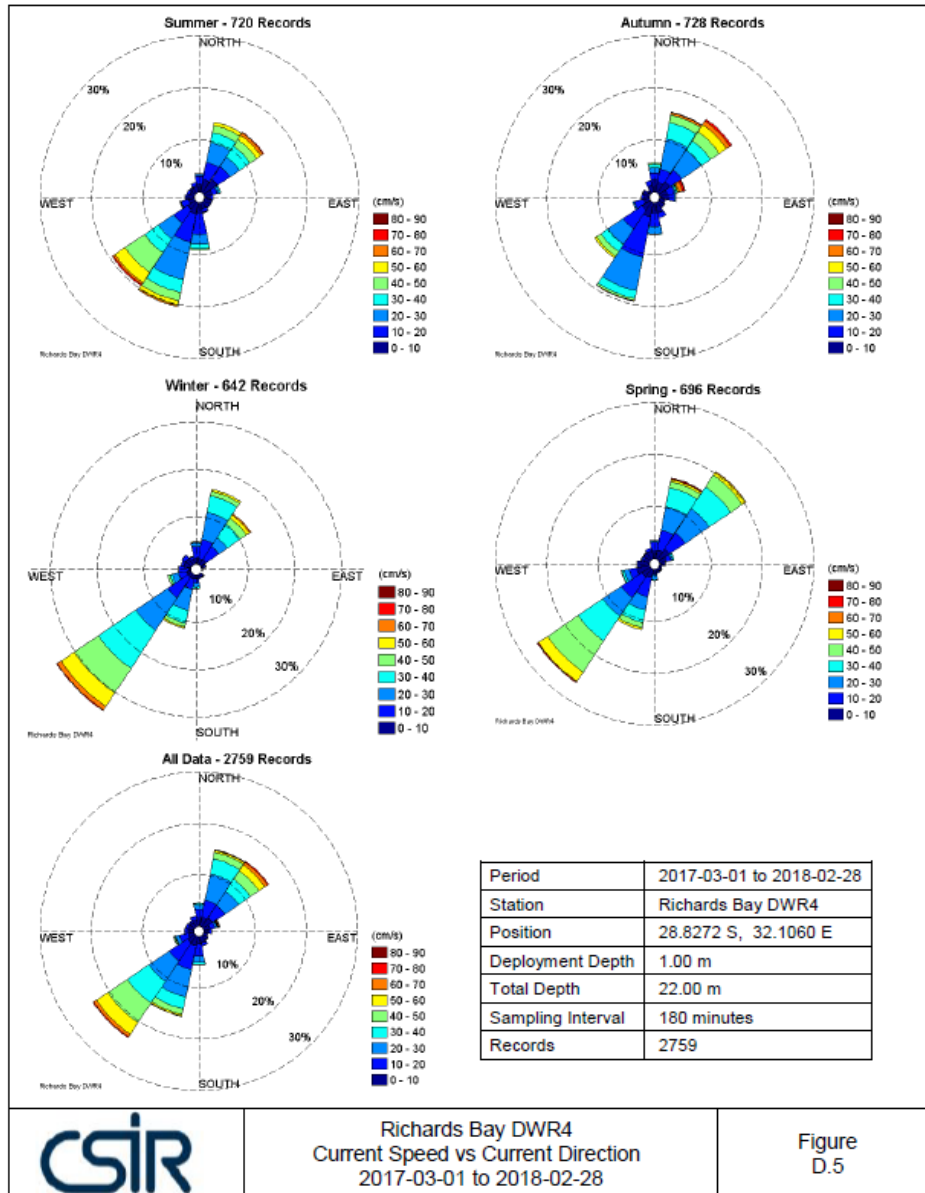


Figure 2.7: Richards Bay current speed rose presenting speed vs direction (2017-2018) (CSIR, 2017)

Only annual current speed plots can be obtained from the CSIR/Transnet Port of Richards Bay Wavenet IPOSS annual reports. The annual current speed plot for other years can be obtained from the same CSIR/Transnet reports.

# Chapter 3

## Ship Specifications

### 3.1 Types of ships

The Port of Richards Bay is one of the largest coal export harbours in the world. Besides coal bulk carriers, the port also receives ships carrying liquefied petroleum gas (LPG), bulk liquids, general cargo as well as bulk carriers for wood pulp. Although coal carriers are the main focus of this research, this chapter gives a general idea of other types of vessels expected and accommodated at Richards Bay as well as their dimensions. The vessel data used was provided by Transnet (TNPA) and is data from 29 February 2016 up until 23 March 2017.

#### 3.1.1 Bulk carrier

The largest general bulk carrier to be handled at the port between 2016 and 2017 is the Cape America shown on Figure 3.1 registered in Singapore with the following dimensions where:

LOA = Length overall (m)

B = Beam (m)

DWT = Deadweight tonnage (kt)

GRT = Gross register tonnage ( $m^3$ )



Max design draught	17.5 m
LOA	299.84 m
B	47.56 m
DWT	186300 t
GRT	99195 $m^3$

Figure 3.1: Cape America Dimensions (Marine Traffic, 2018a)

The largest partially loaded coal carrier to be ever be handled at Port of Richards Bay is the Pride registered in Brazil, with dimensions presented in Table 3.1:

Max design draught	21.8 m
LOA	363.7 m
B	63.4 m
DWT	372200 m <sup>3</sup>

Table 3.1: Brazillian Pride Dimensions

The largest coal carrier to be handled at the Port between 2016 and 2017 is the Ocean Prometheus registered in Liberia with the following dimensions:



Max design draught	17.2 m
LOA	300 m
B	50 m
DWT	203200 t
GRT	101953 m <sup>3</sup>

Figure 3.2: Ocean Prometheus Coal Carrier Dimensions (Marine Traffic, 2018*d*)

### 3.1.2 Bulk liquids

The largest LPG tanker handled at the port between 2016 and 2017 is the Clipper Quito registered in Norway (see Figure 3.3) with the following dimensions as above:





Max design draught	12.01 m
LOA	225 m
B	36.6 m
DWT	55047 t
GRT	48051 m <sup>3</sup>

Figure 3.3: Clipper Quito LPG Tanker Dimensions (Marine Traffic, 2018*b*)

### 3.1.3 General cargo

The largest general cargo ship handled at the port between 2016 and 2017 is the Leading Glory registered in China, with the following dimensions:



Max design draught	14 m
LOA	235 m
B	38 m
DWT	93729 t
GRT	52735 m <sup>3</sup>

Figure 3.4: Leading Glory Dimensions, (Marine Traffic, 2018*c*)

Table 3.2 gives an idea of the types of ships that visited the Port of Richards Bay from March 2016 to March 2017. The ship information was provided by TNPA Port of Richards Bay Harbour Master.

Vessel	Flag	Reason	Port Limits	Cubic	GRT	DWT	LOA	Fwd	Aft	Breakwater	Berth 1	First Line	Last Line	Berth 2	Pilot 1 Duration	Tug 1
AGRIA	MALTA	Bulk Cargo	17-Mar-2016 15:30	93515	33044	56805	190	4.2	6.5	27-Mar-2016 20:20	701	27-Mar-2016 19:12	27-Mar-2016 19:48	701	1:50	RBS - Uzavulo
JIN FAN	CHINA	Bulk Cargo	14-Mar-2016 03:45	144698	51130	93069	229	14.4	14.6	26-Mar-2016 01:30	801	26-Mar-2016 00:48	26-Mar-2016 00:54	801	0:57	RBS - Indlazi
BULK CHINA	MALTA	Bulk Cargo	19-Mar-2016 16:00	250911	88661	176274	289	11.0	14.1	20-Mar-2016 13:35	702	30-Mar-2016 01:24	30-Mar-2016 02:24	702	1:58	RBS - Uzavulo
FPMC P GLORY	LIBERIA	Bunkers Only	28-Mar-2016 05:12	119822	42340	74788	228	12.3	12.3	29-Mar-2016 00:12					3:06	2:15
FPMC P GLORY	LIBERIA	Bunkers Only	28-Mar-2016 05:12	119822	42340	74788	228	12.4	12.4	29-Mar-2016 16:30	306	29-Mar-2016 15:12	29-Mar-2016 15:42	306	1:52	RBS - Indlazi
THE WISE	PANAMA	Bunkers Only	29-Mar-2016 15:00	113834	40224	73594	225	13.2	13.2	30-Mar-2016 14:58					6:09	2:06
VISHVA PREETI	INDIA	Coal	17-Mar-2016 09:40	124540	44007	80250	229	14.3	14.4	26-Mar-2016 07:40	302	26-Mar-2016 07:00	26-Mar-2016 07:06	302	1:00	RBS - Indlazi
CORAL ISLAND	MALTA	Coal	22-Mar-2016 10:15	86836	30684	55699	190	10.3	10.3	26-Mar-2016 15:30	305	26-Mar-2016 14:36	26-Mar-2016 14:48	305	1:21	RBS - Indlazi
SPAR CORONA	NORWAY	Coal	19-Mar-2016 07:30	92934	32839	58000	190	12.0	12.1	26-Mar-2016 17:08	306	26-Mar-2016 16:12	26-Mar-2016 16:30	306	1:13	RBS - Indlazi
KOTA FAJAR	SINGAPORE	Container	14-Apr-2016 08:40	72157	25497	28879	194	5.3	6.8	14-Apr-2016 17:22					6:08	2:26
KOTA FAJAR	SINGAPORE	Container	14-Apr-2016 08:40	72157	25497	28879	194	7.2	8.2	17-Apr-2016 12:36	608	17-Apr-2016 11:56	17-Apr-2016 12:01	608	1:01	RBS - Uzavulo
KOTA ARIF	SINGAPORE	Container	09-May-2016 13:56	49955	17652	23849	183	7.1	7.6	10-May-2016 00:36					6:08	2:24
ISANDLWANA DREDGER	SOUTH AFRICA	Dredger	04-Oct-2015 05:06	13859	4897		85	5.0	6.0	12-Jun-2016 13:20	Repair					
ITALENI	SOUTH AFRICA	Dredger	06-May-2016 19:00	4412	1559	1415	62	4.0	4.5	06-May-2016 19:24						
ITALENI	SOUTH AFRICA	Dredger	06-May-2016 19:00	4412	1559	1415	62	2.0	4.2	11-Aug-2016 14:40	Repair					
FV ATU 5	SOUTH AFRICA	Fishing Vessel	08-Aug-2016 13:35	563	199	240	33	4.0	4.2	08-Aug-2016 14:50						Ice Plant
FV ATU 5	SOUTH AFRICA	Fishing Vessel	08-Aug-2016 13:35	563	199	240	33	4.0	4.2	14-Aug-2016 13:39						Ice Plant
FV ATU 5	SOUTH AFRICA	Fishing Vessel	22-Aug-2016 05:50	566	200		32	2.4	2.3	22-Aug-2016 07:50						Ice Plant
BLUE MARLIN 1	LIBERIA	General Cargo	19-Mar-2016 03:06	93268	32957	57078	190	11.8	11.8	27-Mar-2016 00:34	708	26-Mar-2016 23:15	26-Mar-2016 23:50	708	1:08	RBS - Uzavulo
AFRICAN WAGTAIL	BAHAMAS	General Cargo	20-Mar-2016 13:30	93936	33193	58340	197	4.1	6.3	26-Mar-2016 19:50	608	26-Mar-2016 18:25	26-Mar-2016 19:00	608	1:21	RBS - Uzavulo
YELLOWSTONE	SINGAPORE	General Cargo	15-Mar-2016 00:01	78784	27839	37541	188	9.0	10.0		607	27-Mar-2016 06:54	27-Mar-2016 07:00	708	1:35	RBS - Indlazi
DALBY VENTURE	UNITED KINGDOM	Lay By	07-Nov-2016 21:18	264	72		22	4.5	5.0	05-May-2016 06:00	TUZI GAD					TUZI GAD
IYS NARUO	PANAMA	Lay By	18-Apr-2016 14:36	97208	34349	60317	198	4.9	6.4	20-Apr-2016 17:06	703	23-Apr-2016 23:57	24-Apr-2016 00:20		1:40	RBS - Uzavulo
IYS NARUO	PANAMA	Lay By	18-Apr-2016 14:36	97208	34349	60317	198	8.3	8.3	24-Apr-2016 14:08	208	24-Apr-2016 13:24	24-Apr-2016 13:36	208	1:07	RBS - Uzavulo
HAMBURG	BAHAMAS	Passenger	08-Apr-2016 11:16	42640	15067	1474	144	4.9	5.4	08-Apr-2016 12:08						Repair
HAMBURG	BAHAMAS	Passenger	08-Apr-2016 11:16	42640	15067	1474	144	4.9	5.4	08-Apr-2016 21:18	Repair	08-Apr-2016 20:54	08-Apr-2016 21:00		0:31	RBS - Indlazi
LOGOS HOPE	MALTA	Passenger	02-May-2016 17:12	35375	12500	7921	132	5.1	5.3	02-May-2016 18:58						Repair
BERLIAN EKUATOR	PANAMA	Tanker	01-Sep-2016 18:48	62851	22209	26776	170	7.2	7.5	02-Sep-2016 23:15					2:09	1:25
FAIRCHEM YUKA	PANAMA	Tanker	25-Mar-2016 12:28	32984	11655	19950	146	8.5	8.5	28-Mar-2016 13:42					2:08	0:40
MAERSK BRIGIT	SINGAPORE	Tanker	26-Mar-2016 08:55	55915	19758	29016	175	8.8	8.8	26-Mar-2016 10:06					2:09	1:31
MAERSK BRIGIT	SINGAPORE	Tanker	26-Mar-2016 08:55	55915	19758	29016	175	7.9	7.8	27-Mar-2016 11:56	209	27-Mar-2016 11:18	27-Mar-2016 11:30	209	1:20	RBA - Lilane
BERLIAN EKUATOR	PANAMA	Tanker - LPG	21-Jun-2016 07:20	62851	22209	26776	170	8.2	8.7	23-Jun-2016 10:25					2:09	1:50
BERLIAN EKUATOR	PANAMA	Tanker - LPG	21-Jun-2016 07:20	62851	22209	26776	170	7.2	7.5	25-Jun-2016 01:15	209	25-Jun-2016 00:53	25-Jun-2016 00:54	209	0:37	RBS - Indlazi
BERLIAN EKUATOR	PANAMA	Tanker - LPG	25-Sep-2016 18:48	62851	22209	26776	170	6.8	7.6	29-Sep-2016 08:54					2:09	1:55
JO KASHI	SINGAPORE	Tanker - Products	05-Jun-2016 15:34	44983	15895	25148	159	6.6	8.0	06-Jun-2016 00:40					6:09	1:41
JO KASHI	SINGAPORE	Tanker - Products	05-Jun-2016 15:34	44983	15895	25148	159	6.7	10.2	06-Jun-2016 00:40	609	06-Jun-2016 14:48	06-Jun-2016 14:54	608	1:34	RBS - Indlazi
CELSUS MANHATTAN	MARSHALL ISLANDS	Tankers - Acid	05-Oct-2016 16:12	32870	11615	19806	141	4.7	6.8	10-Oct-2016 23:05					6:08	1:56
CELSUS MANHATTAN	MARSHALL ISLANDS	Tankers - Acid	05-Oct-2016 16:12	32870	11615	19806	141	9.0	10.4	13-Oct-2016 03:32	608	13-Oct-2016 02:50	13-Oct-2016 02:55	608	1:15	RBS - Indlazi

Table 3.2: Ship sizes and their dimensions, (TNPA, 2016)

## 3.2 Future ships

Maritime cargo transport in the world is continuously increasing, leading to a demand in the expansion of ship sizes. Table 3.3 shows the dimensions of different ship sizes to date.



Classification	Displacement (t)	Capacity	Length overall $L_{oa}$ (m)	Beam $B$ (m)	Draught $T_{FL}$ (m)
<b>Tankers</b>					
Panamax	90 000	70 000 DWT	245.0	32.2	12.0
Aframax	140 000	125 000 DWT	274.0	43.8	16.2
New Panamax	220 000	170 000 DWT	366.0	49.0	15.2
Suezmax	238 700	185 000 DWT	330.0	53.0	18.6
<b>Bulk Carriers</b>					
St Lawrence Seaway	35 000	25 000 DWT	226.0	24.0	8.0
Panamax	86 000	70 000 DWT	236.0	32.2	12.0
Capesize	192 000	150 000 DWT	294.0	45.9	17.5
New Panamax	220 000	180 000 DWT	366.0	49.0	15.2
Chinamax	450 000	400 000 DWT	365.0	65.0	22.0
<b>LNG Carriers</b>					
Spherical	107 000	145 000 m <sup>3</sup>	283.0	42.7	12.0
QFlex	141 000	218 000 m <sup>3</sup>	315.0	50.0	12.0
QMax	175 000	267 000 m <sup>3</sup>	345.0	55.0	12.0
<b>Container ships</b>					
Panamax	83 000	5 000 TEU	290.0	32.2	13.2
New Panamax	180 000	13 000 TEU	366.0	49.0	15.2
Suezmax	210 000	15 000 TEU	382.0	56.4	15.5
VLCS	260 000	18 000 TEU	400.0	59.0	18.0

Table 3.3: Ship sizes and their dimensions, (PIANC, 2014)

The expansion of ships lead to larger draughts which affects channel depths. To keep up with these expansions, Port of Richards Bay's channel depth optimization can be achieved by conducting further studies that will advise if the channel should be maintained or deepened to accomodate future vessels with larger draughts.

# Chapter 4

## Ship Motions Theory

### 4.1 Coordinate systems

This section is based on Offshore Hydromechanics by Journee and Massie (2001*a*).

In ship motions, three coordinate systems are often used. Firstly is the earth-bound coordinate system (S) where the  $X_0$  and  $Y_0$  axes lies at the still water surface and the positive  $Z_0$  points upwards. The positive  $X_0$  axis is in the direction of wave propagation which can be rotated at a horizontal angle  $\mu$  relative to the translating axis System O(x, y, z).

Secondly the body bound coordinate system (G) is connected to the ship and its origin is the centre of gravity where  $X_b$  is the longitudinal forward direction,  $Y_b$  is the lateral port side direction and  $Z_b$  points upwards.

Thirdly we have a steadily translating coordinate system (O) which moves forward with the ship at constant speed  $V$ . When the ship is stationery, G is at O and the directions (X,Y,Z) are the same as those of body-bound coordinate system. The X, Y plane lies in still water with it's origin at, under or above the time averaged position of the centre of gravity (Journee and Massie, 2001*b*).

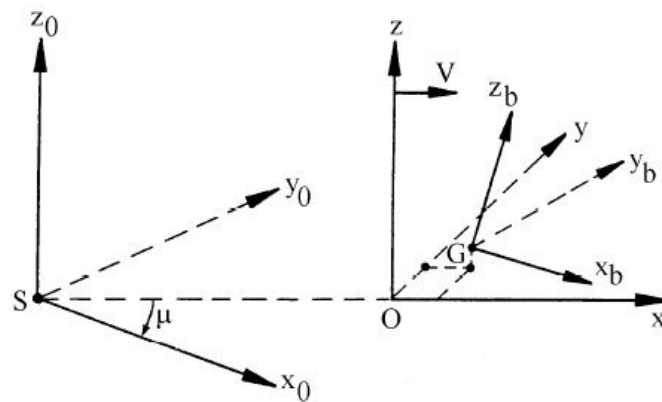


Figure 4.1: Coordinate systems

## 4.2 Ship hydromechanics

Ship hydromechanics is a division of ship studies that focuses on how ships behave in fluids that are in equilibrium and in motion. Ship hydromechanics has a subdivision called ship hydrodynamics which is the study of the behaviour of ships in fluids that are in motion and it defines how ships respond when fluids exert forces on them.

Ship hydromechanics can be understood by firstly understanding the relationship between waves and motions.

### 4.2.1 Relationship between waves and motion

When regular waves (unidirectional waves) are used as input into a computation model that has linear characteristics, the resulting motions will be regular. When irregular waves with known directional spectrum is used as input into the same computation model with linear characteristics, the resulting motions will be irregular (Journee and Massie, 2001a).

Since ship motions are usually linear in nature, the superposition of first harmonic of motions with their different ranges of frequencies and propagation directions can be computed realistically (Journee and Massie, 2001b). Figure 4.2 illustrates the relationship between a wave spectrum as input and the resulting output motion spectrum of a mathematical model (Journee and Massie, 2001a).

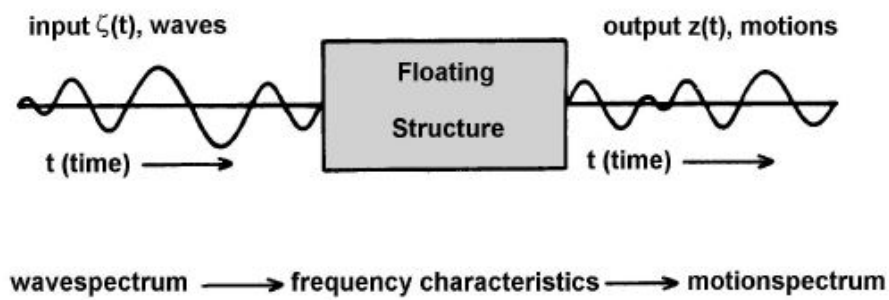


Figure 4.2: Relationship of waves and motions

Figure 4.3 shows harmonic angular displacement, velocity and acceleration of a timeseries.

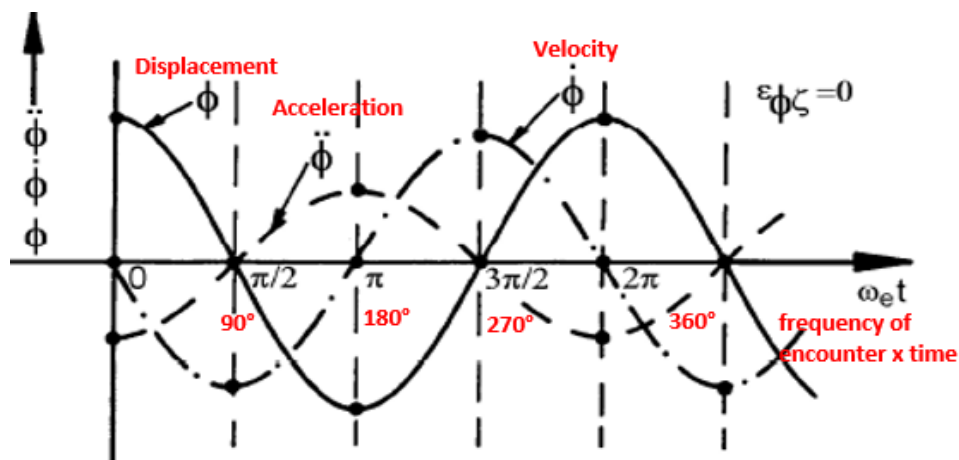


Figure 4.3: Harmonic displacement, velocity and acceleration of a timeseries

There are two types of motions superposition namely absolute motions and vertical relative motions. Absolute ship motions are in the steadily translating coordinate system  $O(x, y, z)$  and their angles of rotation are small and usually less than  $6^\circ$ . The vertical motions are made up of heave, roll and pitch. A matrix given by equation 4.1 is used to transform the body bound coordinate system to steadily translating coordinate system.

$$\begin{pmatrix} x \\ y \\ z \end{pmatrix} = \begin{pmatrix} 1 & -\psi & \theta \\ \phi & 1 & -\psi \\ -\theta & -\phi & 1 \end{pmatrix} = \begin{pmatrix} x_b \\ y_b \\ z_b \end{pmatrix} \quad (4.1)$$

where  $x, y, z, \phi, \theta, \psi$  are the motions of and about the centre of gravity.

$x$  = surge (-)

$y$  = sway (-)

$z$  = heave (-)  
 $\phi$  = roll motion (deg/m)  
 $\theta$  = pitch motion (deg/m)  
 $\psi$  = yaw motion (deg/m)

The transformation matrix makes it possible to determine absolute harmonic motions at any point of a ship using the following equations:

$$\begin{aligned}
 x_P &= x - y_b\psi + z_b\theta \\
 y_P &= y + x_b\psi + z_b\phi \\
 z_P &= z - x_b\theta + z_b\phi
 \end{aligned} \tag{4.2}$$

Vertical motion  $z_P$  in relation to any  $P(x_b, y_b, z_b)$  point on the floating ship is made up of heave roll and pitch motions which is made of linearly, superimposing three harmonic motions, ((Journee and Massie, 2001a)). The equation can be given by:

$$\begin{aligned}
 h(\omega_e, t) &= h_a \cos(\omega_e t + \varepsilon_{h\zeta}) \\
 &= (h_a \cos \varepsilon_{h\zeta}) \cdot \cos(\omega_e t) - (h_a \sin \varepsilon_{h\zeta}) \cdot \sin(\omega_e t)
 \end{aligned} \tag{4.3}$$

where  $h_a$  is the amplitude of the motion and  $\varepsilon_{h\zeta}$  is the phase lag.

Vertical velocity and acceleration of  $h$  in respect to time are given by:

$$\begin{aligned}
 \dot{h} &= -\omega_e h_a \sin(\omega_e t + \varepsilon_{h\zeta}) = (\omega_e h_a) \cdot \cos(\omega_e t + \varepsilon_{h\zeta} + \pi/2) \\
 \ddot{h} &= -\omega_e^2 h_a \cos(\omega_e t + \varepsilon_{h\zeta}) = (\omega_e^2 h_a) \cdot \cos(\omega_e t + \varepsilon_{h\zeta} + \pi)
 \end{aligned} \tag{4.4}$$

where  $\dot{h}$  is velocity and  $\ddot{h}$  is acceleration of the three super-imposed harmonic motions.

Vertical relative motions are the motions seen overboard a moving ship. These motions are usually large at the end of the ship. The largeness of the motions in shipping water occurs because of speed in head waves. When the ship is in still water, sinkage, trim and ship's wave system will effect geometric freeboard. Slamming of waves on a ship influences local pressures of the hull plating but does not influence vertical displacement as such.

## 4.2.2 Waves and ship motions encounter

The harmonic wave elevation equation based on linear wave theory for an earth bound coordinate system (S)(figure 4.1) is given by:

$$\zeta = \zeta_a \cos(\omega t - kx_0) \tag{4.5}$$

where  $\zeta$  = harmonic wave surface in the earth bound coordinate system (m)  
 $\zeta_a$  = wave amplitude (m)

$k = 2\pi/\lambda =$  wave number (rad/m)  
 $\lambda =$  wave length (m)  
 $\omega = \frac{2\pi}{T} =$  circular wave frequency (rad/s)  
 $\omega_e =$  frequency of encounter (rad/s)  
 $c =$  celerity (m/s)  
 $V =$  ship speed (m/s)  $t =$  time (s)

When a ship is moving at a particular forward speed, it encounters waves at the circular frequency of encounter ( $\omega_e$ ) and the period at which that encounter occurs is called period of encounter ( $T_e$ ) where  $T_e$  is given by:

$$T_e = \frac{\lambda}{c - V \cos \mu} \quad (4.6)$$

where  $\lambda$  is the wave length,  $V$  is the ship speed,  $\mu$  is the wave direction relative to ship's speed vector  $V$ . Frequency of encounter and wave frequency's relation is given by:

$$\omega_e = \omega - kV \cos \mu \quad (4.7)$$

where  $k$  is the wave number and  $\omega$  is the circular wave frequency ((Journee and Massie, 2001b)). Figure 4.4 shows a sketch of ship heading direction relative to wave direction.

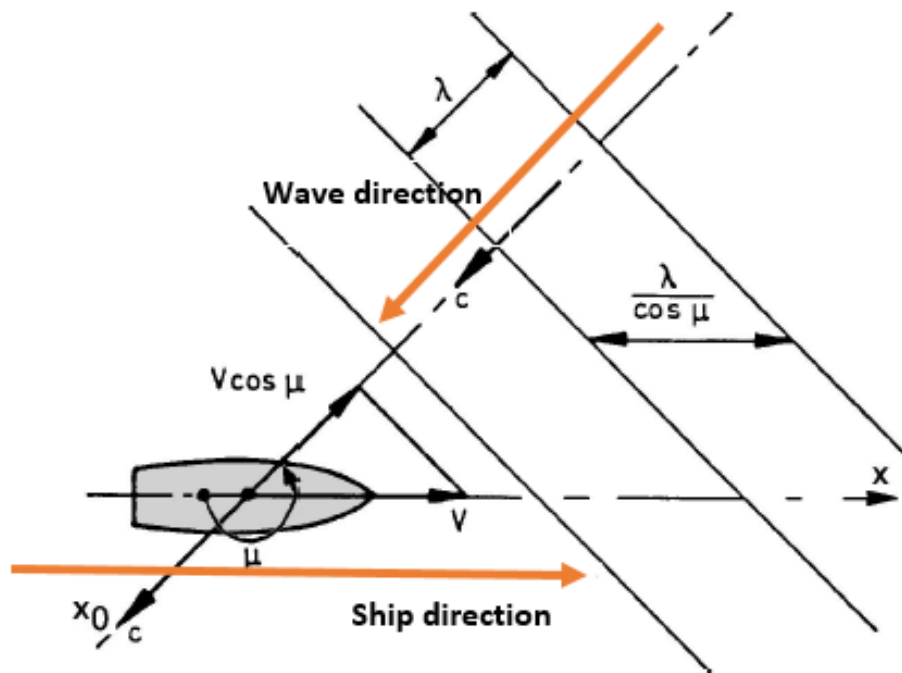


Figure 4.4: Ship direction relative to wave directions (Journee and Massie, 2001a)

### 4.2.3 Motions based on centre of gravity

The following are equations used to calculate the six degrees of freedom motions and are related to the translating coordinate system (O) in relation to the centre of gravity in the direction  $x_b$ ,  $y_b$  and  $z_b$ -axes (figure 4.1) ((Journee and Massie, 2001b)):

$$\begin{aligned}
 \text{Surge : } x &= x_a \cos(\omega_e t + \varepsilon_x \zeta) \\
 \text{Sway : } y &= y_a \cos(\omega_e t + \varepsilon_y \zeta) \\
 \text{Heave : } z &= z_a \cos(\omega_e t + \varepsilon_z \zeta) \\
 \text{Roll : } \phi &= \phi_a \cos(\omega_e t + \varepsilon_\phi \zeta) \\
 \text{Pitch : } \theta &= \theta_a \cos(\omega_e t + \varepsilon_\theta \zeta) \\
 \text{Yaw : } \psi &= \psi_a \cos(\omega_e t + \varepsilon_\psi \zeta)
 \end{aligned} \tag{4.8}$$

where  $\varepsilon\zeta$  is the harmonic wave surface phase angle between the wave and the resulting ship motion for each motion.

### 4.2.4 Roll displacement, velocity and acceleration

The following equations of motion are used to calculate roll displacement, velocity and acceleration:

$$\left. \begin{aligned}
 \text{Displacement: } \phi &= \phi_a \cos(\omega_e t + \varepsilon_\phi \zeta) \\
 \text{Velocity: } \dot{\phi} &= -\omega_e \phi_a \sin(\omega_e t + \varepsilon_\phi \zeta) = \omega_e \phi_a \cos(\omega_e t + \varepsilon_\phi \zeta + \frac{\pi}{2}) \\
 \text{Acceleration: } \ddot{\phi} &= -\omega_e^2 \phi_a \cos(\omega_e t + \varepsilon_\phi \zeta) = \omega_e^2 \phi_a \cos(\omega_e t + \varepsilon_\phi \zeta + \pi)
 \end{aligned} \right\} \tag{4.9}$$

where  $\varepsilon_\phi \zeta$  is the roll phase shift which is the space or distance between roll motion and wave crest or trough. This phase shift elevation should be considered positive when assumed that by the time wave elevation passes zero, roll motion had already passed zero under harmonic conditions, (Journee and Massie, 2001a). This is explained by Figure 4.5.

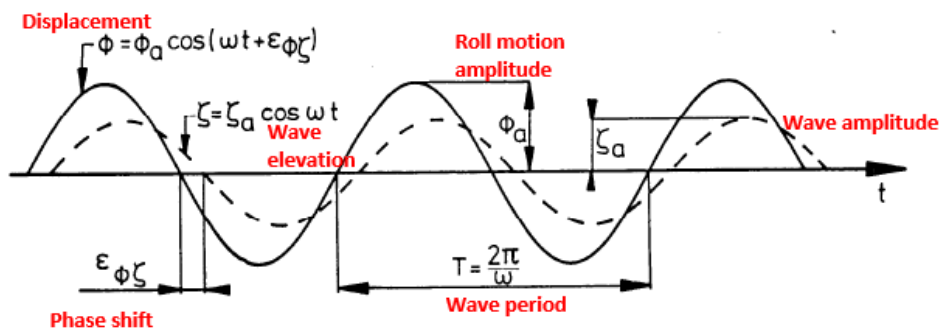


Figure 4.5: Harmonic wave and roll signal (Journee and Massie, 2001a)



### 4.3 Mass spring system

A mass spring system describes the ability of an oscillating body such as a ship, to restore itself in still water and in waves depending on whether it is restrained or not. The focal point here is a free moving ship in waves, represented by a vertical mass spring system. When only a linear restoring force acts on the system, it is a simple harmonic oscillating system but when damping is included, the system is called a damped oscillating system, as illustrated in Figure 4.6, where  $F$  is the force,  $m$  is the mass,  $c$  is the spring constant and  $b$  is the damping constant (Journee and Massie, 2001*b*).

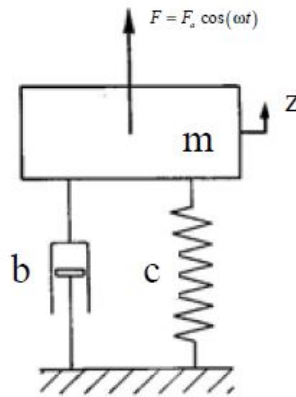


Figure 4.6: Damped mass spring system (Naaijen, 2013)

Damping allows restoration of a ship to its original position. An under damped ship oscillates for a certain period before returning to its original position, while a critically damped ship oscillates once before returning to its initial position. An over damped ship returns to its upright position very slowly. A ship needs to be critically damped, to allow for restoration of the ship to its initial position, in the shortest period. Figure 4.7 shows different types of damping.



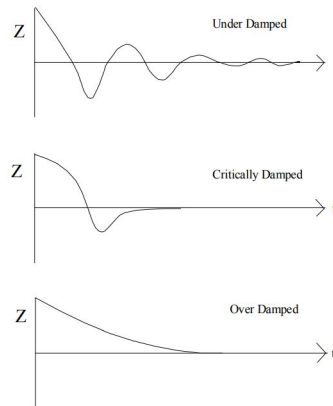


Figure 4.7: Stages of damping (United States Naval Academy, 2018)

Figure 4.8 depicts how the damped mass spring system works on a heaving ship in water.

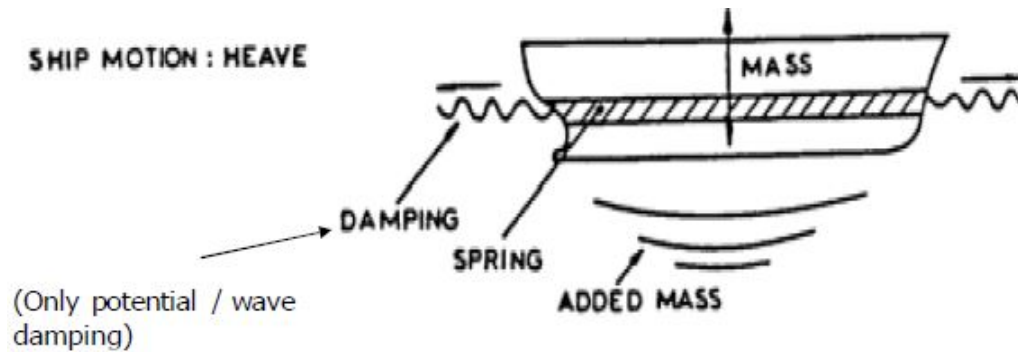


Figure 4.8: Ship mass spring system for heave (Naaijen, 2013)

Natural heave period can be obtained by using equation 4.10 (National Program on Technology Enhanced Learning, 2011):

$$\tau = 2\pi \sqrt{\frac{m + m_a}{\rho g A_{wp}}} \quad (4.10)$$

where  $m$  is the mass of the ship,  $g$  is gravity,  $\rho$  is the water density,  $m_a$  is the heave added mass and  $A_{wp}$  is the waterplane area.

When a ship's centre of buoyancy (B) shifts from the centre line while the centre of gravity (G) remains in the same position. The forces of both B and G are equal and act along parallel lines, in opposite directions, creating a rotation that returns the ship to where the forces of both B and G balance out.

The distance between B and G is the righting arm ( $Z$ ) of the ship (United States Naval Academy, 2018). The rolling of a ship in relation to its centre of gravity  $G$  creates righting moments depending on the level of displacement as shown in Figure 4.9.

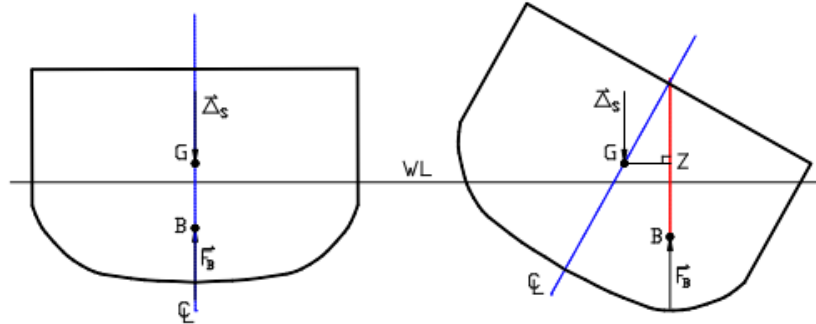


Figure 4.9: Ship roll (United States Naval Academy, 2018)

Its restoring moment can be given by a spring constant  $k = DGZ$ , where  $D$  is the displacement of the ship and  $GZ$  is the right arm curve. The natural roll frequency is given by equation 4.11

$$\omega_e = \frac{\sqrt{g\overline{GM}}}{r} \quad (4.11)$$

where  $\omega_e$  is the natural roll frequency,  $g$  is gravity,  $\overline{GM}$  is the transverse metacentric height and  $r$  is the gyration radius for roll. Roll period is given by:

$$T_r = 2\pi \sqrt{\frac{I + I_a r}{\rho g \nabla \overline{GM}_T}} \quad (4.12)$$

where  $I$  is the ship's inertia of roll rotation,  $I_a$  is the roll added inertia and  $\nabla$  is the submerged hull volume off ship displacement.

Pitching is caused by the change of the waterline and the alignment of the centre of buoyancy relative to the centre of gravity. The centre of buoyancy moves back or forth and the vessel either tilts up or down, as shown in Figure 4.10.

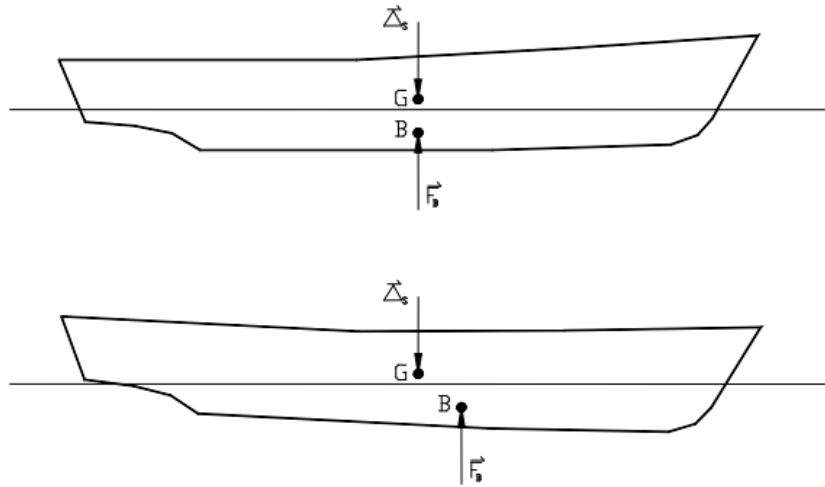


Figure 4.10: Pitching ship ((National Program on Technology Enhanced Learning, 2011))

The pitch's spring constant  $k = \nabla \overline{GM}_L$  and  $I_p$  is the inertia of pitch rotation and  $\overline{GM}_L$  is the longitudinal metacentric height. Ships usually with large  $\overline{GM}_L$  which will experience large pitching restoration moments, especially for bulbous vessels.

## 4.4 3D Panel method

3D panel method is based on the Green's integral method and is used to calculate potential flow around a body in water with zero mean forward speed. Green's theorem states the possibility of transforming a 3D linear homogeneous equation to a 2D integral equation where the Laplace equation is transformed to surface integral equation called Green's identity. The Wavescat model uses linear partial differential equations to solve the ship motion dynamics.

When numerically solving the integral equation, the surface of the ship is divided into a large number of panels as shown in figure 4.11. Certain parts of the ship shape are too small to be covered by panels and are therefore covered by N shaped type of mesh.

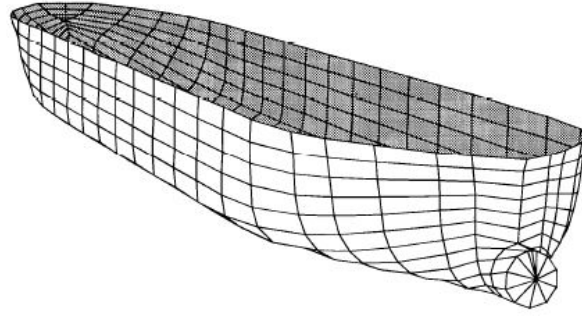


Figure 4.11: 3D Panel figure of a crude oil hull form

#### 4.4.1 Governing equations

According to Islam *et al.* (2004), when considering ship amplitude motions as well as the incident waves to be small and assuming the fluid to be ideal, the total velocity potential ( $\Phi$ ) with the effect of forward ship speed ( $V$ ) for steady conditions is given by:

$$\Phi(x, y, z, t) = [-Vx + \phi_s(x, y, z)] + \phi_T(x, y, z)e^{-i\omega t} \quad (4.13)$$

where  $V$  is the ship speed,  $\phi_s$  is the steady perturbation potential and  $\phi_T$  is the time dependant potential. The components of time dependant potential ( $\phi_T(x, y, z, t)$ ) are given by:

$$\begin{aligned} \text{incident wave potential} &: \phi_0(x, y, z, t) \\ \text{diffraction potential} &: \phi_\tau(x, y, z, t) \\ \text{radiation potential} &: \phi_j(x, y, z, t) \end{aligned} \quad (4.14)$$

and  $\phi_T$  is then given by:

$$\phi_T = \phi_0 + \phi_\tau + \sum_{i=1}^6 \zeta_i \phi_i \quad (4.15)$$

where  $\phi_i$  is the velocity potential of the  $i$ th mode of motion. One of the components of the time-dependant potential ( $\phi_T$ ), the incident wave potential ( $\phi_0$ ), can be expressed by equation 4.16 for small amplitude harmonic waves which have an infinite depth by (Islam. M.R.et.al.2003);

$$\phi_0 = \frac{-ig\zeta_a}{\omega} \frac{\cosh[k(z+h)]}{\cosh(kh)} e^{ik(x\cos\mu + y\sin\mu)} \quad (4.16)$$

where  $\zeta_a$  is the wave amplitude,  $\mu$  is the angle between incident waves and the vessel's heading direction and  $k$  is the wave number.

The incident wave potential should satisfy the Laplace equation as it then can be solved analytically (Islam *et al.*, 2004). However diffraction and radiation potentials are of nonlinear nature (Taylan M, 2000) and can be solved using numerical computations in a specified domain area.

All six degrees of freedom motions that occur, as a response to the steady contributions and the complex time dependant potentials, can be used to solve the forces, added mass and damping coefficients. This will allow the solution of the equation of motion give by equation 4.17:

$$\sum_{j=1}^6 (M_{kj} + A_{kj}) \ddot{X}_j + B_{kj} \dot{X}_j + C_{kj} X_j = F_k \quad (4.17)$$

where  $M_{kj}$  is body inertia matrix including moments of inertia for rotational modes,  $A_{kj}$  is the added mass coefficient matrix,  $X_j$  is the amplitude of periodic motions of the ship's displacement, velocity  $\dot{X}_j$  and acceleration  $\ddot{X}_j$ ,  $B_{kj}$  is the damping coefficient,  $C_{kj}$  is the restoring coefficient and  $F_k$  is the amplitudes of wave exciting forces and moments. (M.N Islam, Computation of Ship Responses in waves using panel method)

## Chapter 5

# Historic Model Tests

Extensive research has been undertaken by the CSIR on wave-induced vertical ship motions, particularly for the Port of Richards Bay. Small scale physical model tests were undertaken since 1970.

In 1988, CSIR undertook systematic scale model (physical modelling) studies to determine wave induced hull motion response on ships of 150kt and 270kt deadweight bulk carriers in shallow water. Model simulation studies were conducted to determine the responses of two models, the M150 (draught = 17 m) and the M270 (draught = 21 m), representing typical 150 and 270 kt deadweight bulk carriers. Their vertical hull motions resulting from heaving, pitching and rolling in waves from various directions and in different depths of water were measured (Jonker *et al.*, 1991).

The primary test conditions were selected to represent, in broad outline, the range of conditions most likely to influence ship behaviour at the major South African ports particularly Port of Richards Bay. The ship model responses to these conditions were determined by physical modelling to a 1:100 scale as well as by mathematical simulation using a 3-D source method. The hull geometries for the two 1-in-100 scale model ships were determined from line drawings of existing prototype vessels.

During testing each model was run along a straight course at the appropriate angle to the waves, covering a distance of about 20 m (2 km prototype). Each test condition was repeated between 20 and 30 times to obtain sufficient data for reliable statistical analysis. During a time-domain analysis the recorded motion time series were used to derive time series of roll, pitch and heave and these principal motions were then used to calculate the vertical motion time series at the keel perpendiculars, shoulders and quarters of the models for each individual run. An in-house built data Acquisition system consisting of a computer that can input 16 channel analog signal conditioning units was used. Through the use of a locally developed software, the following could

computed:

32 ADC input channels,  
adjustable sampling rates between 500 and 0.02 hertz per channel,  
a buffer capacity of 32 kByte,  
analog and digital outputs to control devices and recorders,  
a serial port to communicate with a personal computer.

These time series together with the recorded waves were spectrally analysed individually and averaged over the number of runs during the test. The averaged spectra were then used to calculate the significant wave height and significant keel motion amplitudes (defined as twice the standard deviation of the motion time series) for heave, roll and pitch and for the vertical motions at the six hull points (i.e. the perpendiculars, shoulders and quarters). The data were also reduced to response amplitude operators (RAOs) for the said principal and hull motions, using the encountered wave spectra derived from the incident wave spectra, average angle of wave incidence and average ship speed during the test. Only swells ranging from 1 m to 4 m in height and with spectral peak periods of 12 s to 16 s were considered. The angles of wave incidence relative to the models could, depending on their sailing directions, vary from following waves, through beam waves, to heading waves. Online processing was done on a M280 personal computer. A locally developed software was used to:

calibrate instrument in prototype units,  
analyse waves in time domain,  
store data.

A software was used to perform the following offline:

spectral analysis,  
cross-spectral analysis,  
various statistical calculations.

The 1988 test results were mentioned and discussed in the 1991 CSIR report ((Jonker *et al.*, 1991)) but no table of test conditions was available.

Subsequently, spectral shape, based on field measurements, was used to reconstruct a swell spectrum with a significant wave height of 3 m and a spectral peak period of 14 s. An appropriate ship speed of 4 m/s (8kn) was chosen to run the model ships in the specified swell conditions with the angles of wave incidence relative to the model to be incremented in steps of 15°. These tests were all done in a relative water-depth (depth-to-draught ratio) of 1.3. The influence of different relative water depths, ranging from 1,1 to 1,5 in steps of 0,1 was studied for the primary angles of wave incidence, that is, following ( $\alpha = 0^\circ$ ), heading ( $\alpha = 180^\circ$ ), beam ( $\alpha = 270^\circ$ ) and stern and bow quartering waves ( $\alpha = 315^\circ$  and  $135^\circ$ ). In addition to the primary tests, secondary test programmes were devised to serve both for checking the validity of the study and

for studying the influence of additional factors such as the absence/presence of bilge keels on the models, different loading conditions and different spectral shapes.

In 1989, CSIR undertook another systematic series of scale model test except this time, larger wave heights were modelled. The research involved carrying out physical and numerical model studies of the 150 kt deadweight bulk carrier ship model with zero forward speed. During the physical modelling study, six points on the hull of the ship were observed under the chosen angles of wave incidence which were from  $0^\circ$  to  $180^\circ$  at increments of  $45^\circ$ . Depth to draught ratios used for this study ranged from 2.1 to 1.2. The physical model which had a typical wave spectrum with significant wave height ( $H_s$ ) above 3m (3m to 7m) with spectral peak period of 10s was used as the base-line wave condition and  $T_p = 12s$  used for underkeel sensitivity tests. The results presented were limited to those obtained from the online, time domain analysis performed during the tests.

New tests consisting of two tests of each wave incidence angle was ran for comparison to calibrate the physical model with the prototype data. A wave spectrum with  $T_p = 10s$  is used for all the test conditions except test condition 10, which used a wave spectrum with  $T_p = 12s$ . Table 5.1 presents the wave conditions that were tested.

Test no. (-)	Depth (m)	depth to Draught ratio (-)	Wave incidence angle $\alpha$ ( $^\circ$ )	No. of test runs (-)
1	36.0	2.12	0, 45, 90, 135, 180	2 per $\alpha$
2	34.2	2.00	0, 45, 90, 135, 180	2 per $\alpha$
3	31.5	1.85	0, 45, 90, 135, 180	2 per $\alpha$
4	27.0	1.59	0, 45, 90, 135, 180	2 per $\alpha$
5	25.2	1.48	0, 45, 90, 135, 180	2 per $\alpha$
6	23.4	1.38	0, 45, 90, 135, 180	2 per $\alpha$
7	21.6	1.27	0, 45, 90, 135, 180	2 per $\alpha$
8	19.8	1.16	0, 45, 90, 135, 180	2 per $\alpha$
9	18.7	1.10	90	3 per $\alpha$
10	18.7	1.10	90	2 per $\alpha$

Table 5.1: 1989 Historical test conditions (Jonker *et al.*, 1991)

Test conditions number 9 and 10 are sensitivity tests, where wave heights were increased until bottom touching occurred, for  $T_p = 10s$  (test no. 9) and  $T_p = 12s$  (test no. 10).



## 5.1 Results of the calibrated 150kt deadweight bulk carrier

Four probes were used to record the results of each run. The significant motion amplitude ( $A_s$ ) and significant wave heights ( $H_s$ ) of the four probe points for each run were averaged and, their results are given in Table 5.2 to 5.6. The tested results were for  $d/D$  ratios of 2.0 to 1.1 but only significant motion amplitudes to significant wave height ( $A_s/H_s$ ) results will be limited to depth to draught ratios from 1.5 to 1.1, as their results are more relevant to these studies. The peak period for the  $A_s/H_s$  results is 10s.

Tp (s)	$\alpha$ (°)	Hs (m)	APP	PQT	SQT	PSH	SSH	FPP
10	0	3.92	0.14	0.03	0.04	0.10	0.11	0.16
10	0	4.14	0.16	0.03	0.05	0.10	0.12	0.18
10	45	4.05	0.17	0.11	0.13	0.23	0.12	0.20
10	45	4.23	0.19	0.18	0.14	0.26	0.12	0.22
10	90	2.90	0.38	0.60	0.27	0.58	0.33	0.34
10	90	2.87	0.28	0.63	0.27	0.66	0.30	0.32
10	135	3.97	0.24	0.21	0.09	0.15	0.15	0.17
10	135	4.01	0.27	0.21	0.09	0.15	0.18	0.22
10	180	3.49	0.20	0.05	0.03	0.07	0.11	0.16
10	180	4.14	0.24	0.06	0.06	0.10	0.08	0.18

Table 5.2: Ratios of ( $A_s/H_s$ ) for depth to draught ratio ( $d/D$ ) = 1.5

$T_p$ (s)	$\alpha(\circ)$	$H_s$ (m)	APP	PQT	SQT	PSH	SSH	FPP
10	0	3.96	0.08	0.04	0.04	0.10	0.12	0.18
10	0	4.01	0.08	0.04	0.03	0.09	0.11	0.17
10	45	4.15	0.17	0.16	0.10	0.23	0.13	0.20
10	45	4.13	0.16	0.15	0.08	0.22	0.14	0.19
10	90	3.06	0.32	0.63	0.29	0.63	0.33	0.29
10	90	3.04	0.37	0.65	0.29	0.63	0.36	0.28
10	135	4.07	0.25	0.20	0.08	0.13	0.14	0.18
	135	4.02	0.25	0.20	0.06	0.12	0.14	0.19
10	180	4.15	0.21	0.05	0.06	0.09	0.07	0.16
10	180	4.11	0.21	0.05	0.05	0.09	0.07	0.16

Table 5.3: Ratios of  $(A_s/H_s)$  for depth to draught ratio  $(d/D) = 1.4$  (Jonker *et al.*, 1991)

$T_p$ (s)	$\alpha(\circ)$	$H_s$ (m)	APP	PQT	SQT	PSH	SSH	FPP
10	0	3.89	0.07	0.03	0.03	0.08	0.09	0.14
10	0	3.93	0.07	0.03	0.03	0.08	0.09	0.15
10	45	4.08	0.15	0.14	0.09	0.19	0.11	0.16
10	45	4.13	0.15	0.08	0.10	0.20	0.10	0.17
10	90	3.11	0.28	0.50	0.14	0.47	0.23	0.16
10	90	3.11	0.25	0.49	0.22	0.49	0.26	0.22
10	135	3.99	0.23	0.18	0.05	0.13	0.13	0.17
10	135	4.03	0.21	0.17	0.06	0.13	0.12	0.15
10	180	4.05	0.20	0.05	0.06	0.08	0.07	0.16
10	180	3.93	0.19	0.05	0.05	0.08	0.06	0.15

Table 5.4: Ratios of  $(A_s/H_s)$  for depth to draught ratio  $(d/D) = 1.3$  (Jonker *et al.*, 1991)

Tp (s)	$\alpha(\circ)$	Hs (m)	APP	PQT	SQT	PSH	SSH	FPP
10	0	4.50	0.06	0.04	0.03	0.06	0.09	0.13
10	0	3.78	0.05	0.02	0.03	0.07	0.07	0.11
10	45	4.13	0.13	0.06	0.07	0.15	0.08	0.14
10	45	3.86	0.14	0.07	0.09	0.17	0.09	0.15
10	90	2.89	0.12	0.40	0.14	0.42	0.22	0.19
10	90	2.91	0.27	0.44	0.15	0.39	0.25	0.13
10	135	3.38	0.12	0.11	0.09	0.16	0.12	0.14
10	135	4.14	0.22	0.19	0.07	0.10	0.14	0.15
10	180	3.44	0.09	0.05	0.05	0.07	0.05	0.13
10	180	3.73	0.09	0.04	0.05	0.07	0.05	0.13

Table 5.5: Ratios of  $(A_s/H_s)$  for depth to draught ratio  $(d/D) = 1.2$ 

Tp (s)	$\alpha(\circ)$	Hs (m)	APP	PQT	SQT	PSH	SSH	FPP
10	0	3.40	0.06	0.02	0.03	0.06	0.06	0.10
10	0	3.36	0.06	0.02	0.03	0.06	0.06	0.10
10	45	3.56	0.05	0.04	0.08	0.13	0.07	0.12
10	45	3.52	0.10	0.05	0.09	0.14	0.05	0.13
10	90	2.62	0.14	0.35	0.17	0.32	0.21	0.11
10	90	2.61	0.12	0.34	0.16	0.34	0.21	0.12
10	135	3.43	0.10	0.07	0.06	0.10	0.08	0.12
10	135	2.55	0.09	0.08	0.07	0.11	0.09	0.11
10	180	3.49	0.07	0.03	0.04	0.06	0.04	0.10
10	180	3.42	0.08	0.03	0.04	0.06	0.04	0.10

Table 5.6: Ratios of  $(A_s/H_s)$  for depth to draught ratio  $(d/D) = 1.1$  (Jonker *et al.*, 1991)

The results of the primary tests reveal that  $A_s/H_s$  reduces with a reduction of the depth to draught  $(d/D)$  ratios. The  $A_s/H_s$  ratios for wave incident angles  $0^\circ$ ,  $45^\circ$ ,  $135^\circ$  and  $180^\circ$  seem to not be influenced much by a reduction of  $d/D$  above 1.5. It is only  $A_s/H_s$  that decrease gradually for  $d/D$  ratios from 1.5 to

1.1. As values that have high  $d/D$  ratios were 0.2 to 0.3 times the  $H_s$ .

$A_s/H_s$  for incident wave angle  $90^\circ/270^\circ$  had higher magnitude than all the other tested incident wave angles. The  $A_s$  values of these incident wave angles were about 0.75 times those of  $H_s$ .

### 5.1.1 Influence of depth to draught ratio

Severe motions were recorded at the quarters and shoulders for wave incident angles  $90^\circ/270^\circ$ , which means beam waves have the most extreme hull motions as given in Figure 5.1.

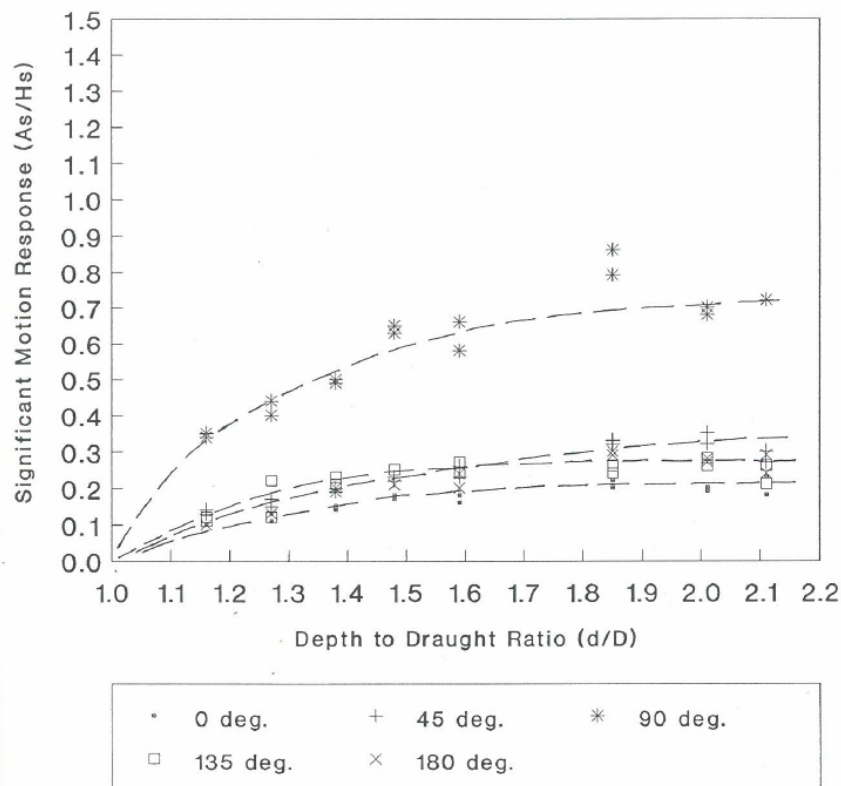


Figure 5.1: Depth to draught results

### 5.1.2 Relationship between significant and maximum hull motion amplitude

The most probable extreme value  $\mu(A_{max})$  is the extreme value that is most likely to occur during a certain number of oscillations of a ship. This probable extreme value is the modal value of the probability density function associated with extreme motion amplitudes. Test duration of 3000s and an average of

10s gave 300 number (N) of oscillations.

When Rayleigh probability distribution is used to determine hull motion amplitudes ( $\mu(A_{max}) = \frac{1}{\sqrt{2}}(\ln N)^{0.5} \cdot A_s$ ), the most probable extreme value = 1.69. The tested results for  $A_s$  less than 1.5 m agree with the theoretical relationship of  $A_{max}$  and  $A_s$  while the relationship deviates for  $A_s$  larger than 1.5 m.

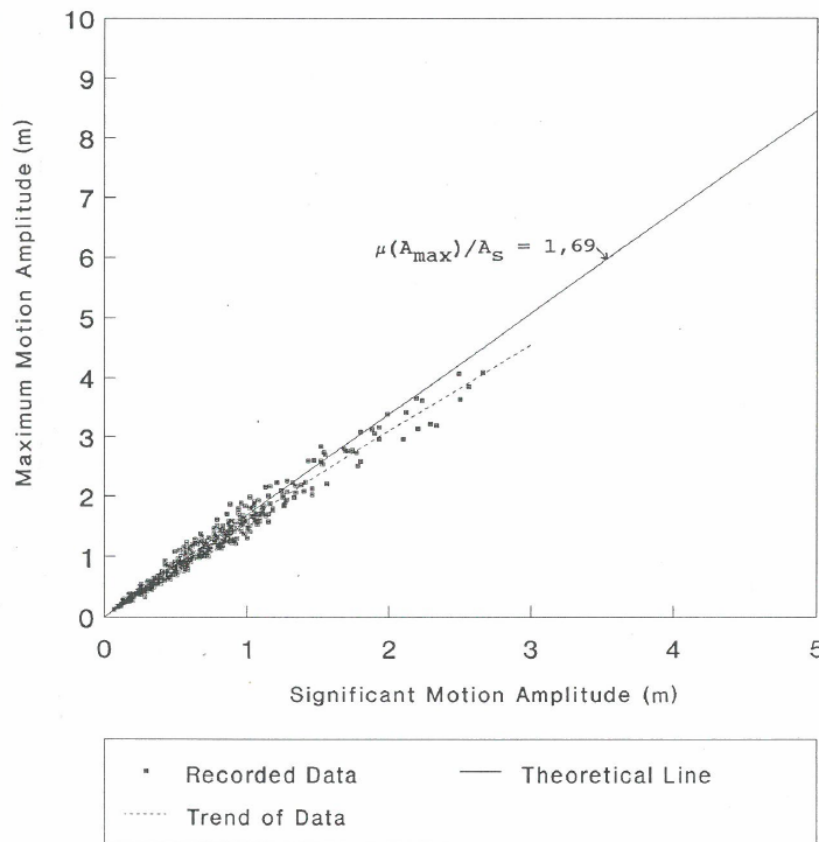


Figure 5.2: Maximum versus significant hull motion amplitudes

It will therefore be of interest to investigate the non-linearity of wave-induced vertical ship motions (especially roll) for larger wave heights and ship motions by understanding which probability distribution will best represent extreme significant motions for  $A_s$  above 1.5m. The accurate prediction of extreme ship motions is important for determining safe underkeel clearance limits at the Port.

### 5.1.3 Influence of wave height

The significant motion amplitudes showed an almost linear increase with increase in wave height for all test conditions except those in following waves ( $\alpha = 0^\circ$ ). During these latter conditions the maximum motions were recorded

at the aft perpendiculars of the models and would therefore have resulted from a combination of heaving and pitching. The results that focused on the influence of wave height on the significant hull motion amplitude revealed that the ratio of angle  $90^\circ$  and  $270^\circ$  (beam waves) were much higher than those for the other angles of wave incident ( $0^\circ$ ,  $45^\circ$ ,  $135^\circ$  and  $180^\circ$ ). Values of significant hull motion ( $A_s$ ) also appeared to strive to 0.75 times  $H_s$  with increase of depth (19.8m to 36m) over draught ratio (1.16 to 2.12). The influence of significant wave height  $H_s$  on hull motion response showed that significant hull amplitudes increase almost linearly with increase in wave height. However  $H_s$  of about 5m to 7m acting on the hull of the ship made it touch bottom (Figure 5.3) which makes the results rather suspect .

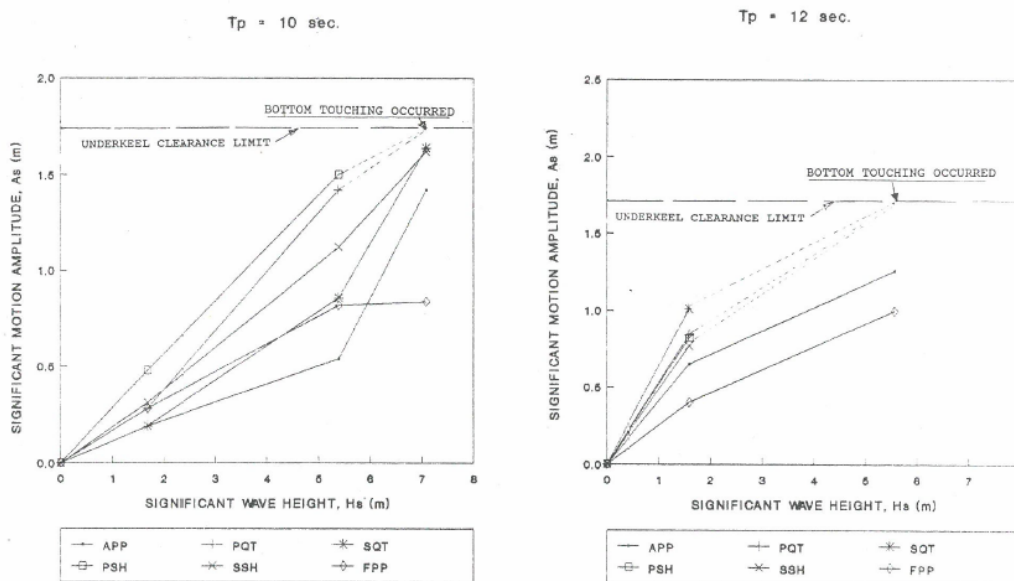


Figure 5.3: Influence of wave height on hull motion amplitudes

# Chapter 6

## Calibration of Numerical Models

Three simulation software packages namely Delft 3D-Swan, Mike 21BW and Wavescat are discussed. Delft3D-Swan and Mike21BW packages are used to simulate wave conditions and Wavescat simulates the interaction of the wave conditions in this case on a 150kt DWT bulk carrier.

### 6.1 Waves numerical modelling

#### 6.1.1 Delft 3D-Swan

Delft3D-Swan (Simulating wave nearshore) is a fully implicit scheme wave model which is based on a discrete spectral action balance equation which simulates random short crested wind generated waves. Delft3D-Swan model simulates wave mechanisms such as refraction over variable depth and/or a spatially varying current, depth and current induced shoaling, wind wave generation, dissipation by whitecapping, dissipation by depth-induced breaking, dissipation due to bottom friction, non-linear wave-wave interactions, wave blocking by flow and transmission through blockage by or reflection against obstacles. Delft3D-Swan does not model diffraction directly but does approximate it's effect, even in confined spaces such as harbours and ports.

In this study, offshore wave conditions selected from the National Centres for Environmental Predictions (NCEP) (2002/01/01 to 2018/10/31) are downloaded from the Wavewatch III model (Wavewatch3DG, 2019). Wavewatch III models the growth and decay of offshore mean current and water depth wave conditions, as a results of surface wind (WorldWinds Inc, 2019). Delft3D-Swan then simulates these offshore wave conditions to determine nearshore wave conditions. Tables of the frequency of occurrence of nearshore wave conditions are then created through a process called Intercoef. Intercoef is a CSIR computation process that averages wave conditions to determine their frequency. The Delft3D-Swan frequency of occurrence wave conditions are also used as bound-

ary input conditions for Mike21BW, to better simulate extreme wave actions such as reflection off walls, refraction and diffraction as waves propagate into the Port. The Delft3D-Swan was calibrated by simulating extreme wave conditions from the Wavewatch III data and comparing them with the measured Waverider data.

Below are plots of the Richards Bay Swan bathymetry as well as the two nested medium ( $1\text{km}\times 1\text{km}$ ) and fine ( $500\text{m}\times 500\text{m}$ ) grids that were used to create the bathymetry.

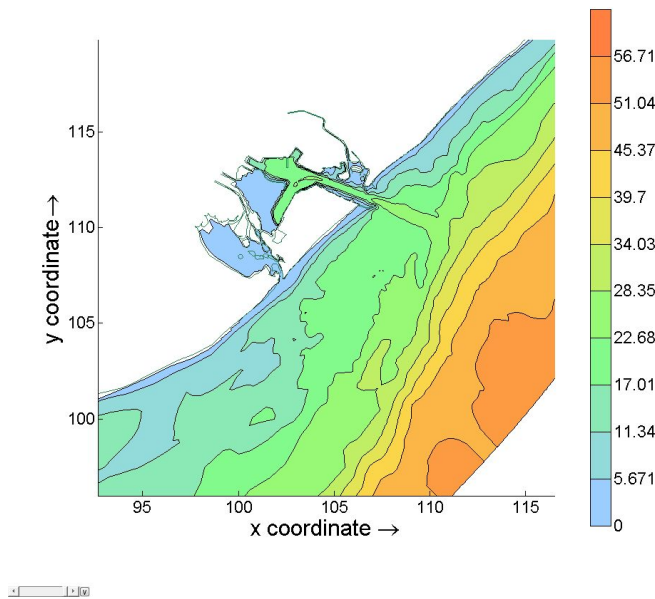


Figure 6.1: Richards Bay Swan bathymetry (Rautenbach *et al.*, 2015)



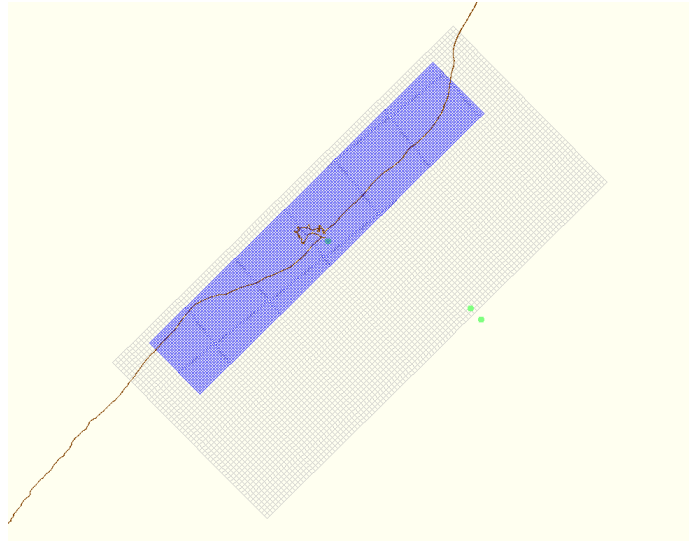


Figure 6.2: Swan nested medium and fine grid (Rautenbach *et al.*, 2015)

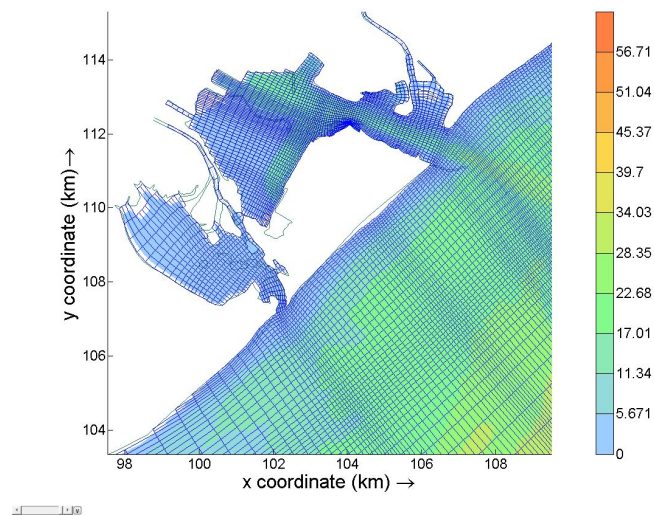


Figure 6.3: Swan fine grid (Rautenbach *et al.*, 2015)

The Swan simulation outputs are used to create occurrence tables which show the directions, periods ( $T_p$ ) and wave heights ( $H_{m0}$ ) conditions experienced at Richards Bay. These occurrence tables are categorized into five groups, four of which are summer, autumn, winter and spring and for all four seasons. Table 6.1 to 6.5 shows wave heights and wave direction occurrence tables.

Hmo (m)	Wave Direction (degrees TN)															Total	
	N	NNE	NE	ENE	E	ESE	SE	SSE	S	SSW	SW	WSW	W	WNW	NW		NNW
0.0 - 0.5						0.00		0.00									0.00
0.5 - 1.0				0.05	0.70	1.87	1.26	1.89	0.62	0.00	0.00						6.40
1.0 - 1.5	0.00	0.01	0.09	0.96	7.30	15.30	10.06	13.98	3.04	0.24	0.09	0.00					51.07
1.5 - 2.0	0.00		0.05	0.55	4.06	9.37	6.22	8.91	1.73	0.56	0.06						31.50
2.0 - 2.5				0.02	0.71	2.07	1.96	2.54	0.84	0.24	0.00						8.38
2.5 - 3.0					0.25	0.40	0.37	0.77	0.21	0.01							2.01
3.0 - 3.5					0.12	0.11	0.04	0.21	0.03	0.01							0.51
3.5 - 4.0					0.02	0.02	0.02	0.05	0.01								0.11
4.0 - 4.5						0.00		0.02									0.02
4.5 - 5.0																	0.00
5.0 - 5.5																	0.00
5.5 - 6.0																	0.00
6.0 - 6.5																	0.00
6.5 - 7.0																	0.00
7.0 - 7.5																	0.00
7.5 - 8.0																	0.00
8.0 - 8.5																	0.00
Total	0.00	0.01	0.14	1.59	13.15	29.13	19.93	28.37	6.48	1.05	0.15	0.00	0.00	0.00	0.00	0.00	100.

Table 6.1: Summer wave heights versus wave direction occurrence

Hmo (m)	Wave Direction (degrees TN)															Total	
	N	NNE	NE	ENE	E	ESE	SE	SSE	S	SSW	SW	WSW	W	WNW	NW		NNW
0.0 - 0.5						0.00	0.00	0.00									0.00
0.5 - 1.0			0.00	0.11	0.30	1.11	2.04	4.15	0.83	0.00	0.00						8.56
1.0 - 1.5				0.64	3.26	8.78	10.48	20.23	2.49	0.16	0.07						46.11
1.5 - 2.0			0.01	0.14	1.82	7.18	6.15	10.81	1.64	0.41	0.05			0.00			28.21
2.0 - 2.5			0.00	0.01	0.74	2.30	2.19	4.41	1.05	0.28	0.00						10.99
2.5 - 3.0				0.00	0.19	0.64	0.89	1.61	0.51	0.09							3.93
3.0 - 3.5					0.13	0.13	0.35	0.56	0.14	0.00							1.31
3.5 - 4.0					0.06	0.03	0.18	0.24	0.03								0.55
4.0 - 4.5					0.04	0.02	0.05	0.07	0.00								0.18
4.5 - 5.0					0.00		0.03	0.03	0.00								0.06
5.0 - 5.5							0.03	0.01									0.04
5.5 - 6.0							0.02	0.00									0.02
6.0 - 6.5							0.00	0.01									0.01
6.5 - 7.0								0.01									0.01
7.0 - 7.5								0.00									0.00
7.5 - 8.0						0.00	0.00	0.01									0.01
8.0 - 8.5							0.00	0.00									0.00
Total	0.00	0.00	0.01	0.91	6.54	20.19	22.42	42.14	6.70	0.95	0.12	0.00	0.00	0.00	0.00	0.00	100.

Table 6.2: Autumn wave heights versus wave direction occurrence

Hmo (m)	Wave Direction (degrees TN)															Total	
	N	NNE	NE	ENE	E	ESE	SE	SSE	S	SSW	SW	WSW	W	WNW	NW		NNW
0.0 - 0.5						0.00	0.00	0.00	0.00								0.01
0.5 - 1.0				0.09	0.26	0.49	1.66	3.61	0.18	0.00	0.00						6.29
1.0 - 1.5		0.02	0.01	1.16	3.23	5.13	8.45	24.55	1.94	0.16	0.08						44.74
1.5 - 2.0		0.00	0.01	0.54	1.67	3.34	5.12	15.40	1.78	0.49	0.06						28.41
2.0 - 2.5			0.01	0.02	0.25	1.26	2.02	6.62	1.12	0.37	0.01						11.68
2.5 - 3.0					0.05	0.52	0.96	2.81	0.81	0.15							5.31
3.0 - 3.5					0.02	0.12	0.46	1.37	0.27	0.00							2.25
3.5 - 4.0					0.00	0.07	0.20	0.50	0.06								0.83
4.0 - 4.5						0.01	0.10	0.15	0.01								0.27
4.5 - 5.0							0.09	0.04									0.13
5.0 - 5.5							0.05	0.02									0.07
5.5 - 6.0							0.01	0.01									0.02
6.0 - 6.5																	0.00
6.5 - 7.0																	0.00
7.0 - 7.5																	0.00
7.5 - 8.0																	0.00
8.0 - 8.5																	0.00
Total	0.00	0.03	0.03	1.81	5.49	10.95	19.12	55.09	6.17	1.18	0.15	0.00	0.00	0.00	0.00	0.00	100.

Table 6.3: Winterwave heights versus wave direction occurrence

Hmo (m)	Wave Direction (degrees TN)																Total
	N	NNE	NE	ENE	E	ESE	SE	SSE	S	SSW	SW	WSW	W	WNW	NW	NNW	
0.0 - 0.5							0.00									0.00	0.00
0.5 - 1.0				0.03	0.27	0.49	0.71	0.78	0.10	0.00							2.38
1.0 - 1.5			0.00	1.48	5.25	6.62	7.36	16.70	2.52	0.19	0.15						40.28
1.5 - 2.0			0.00	1.41	4.87	6.53	6.79	14.97	2.48	0.73	0.17						37.95
2.0 - 2.5				0.07	0.85	1.99	2.62	5.67	1.37	0.34	0.01						12.92
2.5 - 3.0					0.10	0.59	0.75	1.67	0.59	0.07							3.77
3.0 - 3.5					0.02	0.21	0.48	0.54	0.21	0.02							1.48
3.5 - 4.0					0.01	0.21	0.32	0.21	0.05								0.80
4.0 - 4.5						0.12	0.15	0.09	0.01								0.37
4.5 - 5.0						0.01	0.02	0.03									0.05
5.0 - 5.5								0.00									0.00
5.5 - 6.0																	0.00
6.0 - 6.5																	0.00
6.5 - 7.0																	0.00
7.0 - 7.5																	0.00
7.5 - 8.0																	0.00
8.0 - 8.5																	0.00
Total	0.00	0.00	0.00	2.99	11.37	16.76	19.20	40.66	7.33	1.35	0.33	0.00	0.00	0.00	0.00	0.00	100.

Table 6.4: Winter wave heights versus wave direction occurrence

Hmo (m)	Wave Direction (degrees TN)																Total
	N	NNE	NE	ENE	E	ESE	SE	SSE	S	SSW	SW	WSW	W	WNW	NW	NNW	
0.0 - 0.5						0.00	0.00	0.00	0.00							0.00	0.00
0.5 - 1.0				0.00	0.07	0.38	0.98	1.42	2.62	0.43	0.00	0.00					5.91
1.0 - 1.5	0.00	0.01	0.03	1.06	4.74	8.91	9.08	18.92	2.49	0.19	0.10	0.00					45.52
1.5 - 2.0	0.00	0.00	0.02	0.66	3.09	6.58	6.07	12.55	1.91	0.55	0.08			0.00			31.50
2.0 - 2.5				0.00	0.03	0.64	1.90	2.20	4.83	1.10	0.31	0.01					11.01
2.5 - 3.0					0.00	0.15	0.54	0.74	1.73	0.53	0.08						3.77
3.0 - 3.5						0.07	0.14	0.33	0.67	0.16	0.01						1.39
3.5 - 4.0						0.02	0.08	0.18	0.25	0.04							0.58
4.0 - 4.5						0.01	0.04	0.08	0.08	0.00							0.21
4.5 - 5.0						0.00	0.00	0.03	0.02	0.00							0.06
5.0 - 5.5								0.02	0.01								0.03
5.5 - 6.0								0.01	0.00								0.01
6.0 - 6.5								0.00	0.00								0.00
6.5 - 7.0									0.00								0.00
7.0 - 7.5								0.00									0.00
7.5 - 8.0							0.00	0.00	0.00								0.00
8.0 - 8.5								0.00	0.00								0.00
Total	0.00	0.01	0.05	1.82	9.10	19.18	20.17	41.68	6.67	1.13	0.19	0.00	0.00	0.00	0.00	0.00	100.

Table 6.5: Overall wave heights versus wave direction occurrence

Table 6.6 to 6.10 shows wave heights and period occurrence .

Hmo (m)	Period (Tp) (s)																Total
	0-2	2-4	4-6	6-8	8-10	10-12	12-14	14-16	16-18	18-20	20-22	22-24	24-26	26-28	28-30	30-32	
0.0 - 0.5						0.00					0.00						0.00
0.5 - 1.0		0.01	0.26	1.19	1.71	2.17	0.83	0.23	0.02	0.00							6.41
1.0 - 1.5		0.11	2.83	8.51	13.00	16.16	7.66	2.38	0.29	0.11	0.02	0.00				0.00	51.09
1.5 - 2.0		0.02	1.53	3.72	7.81	10.76	4.92	2.28	0.29	0.10	0.03			0.00			31.47
2.0 - 2.5			0.16	0.97	1.84	3.15	1.30	0.85	0.07	0.03	0.00						8.37
2.5 - 3.0			0.00	0.14	0.40	0.63	0.55	0.24	0.04	0.01	0.00						2.01
3.0 - 3.5				0.01	0.04	0.09	0.24	0.12	0.01	0.00							0.51
3.5 - 4.0					0.01	0.06	0.05										0.11
4.0 - 4.5					0.00	0.01	0.01										0.02
4.5 - 5.0																	0.00
5.0 - 5.5																	0.00
5.5 - 6.0																	0.00
6.0 - 6.5																	0.00
6.5 - 7.0																	0.00
7.0 - 7.5																	0.00
7.5 - 8.0																	0.00
8.0 - 8.5																	0.00
Total	0.00	0.13	4.78	14.54	24.80	32.97	15.57	6.16	0.72	0.26	0.06	0.00	0.00	0.00	0.00	0.00	100.

Table 6.6: Summer wave heights versus peak periods occurrence

Hmo (m)	Period (Tp) (s)																Total
	0-2	2-4	4-6	6-8	8-10	10-12	12-14	14-16	16-18	18-20	20-22	22-24	24-26	26-28	28-30	30-32	
0.0 - 0.5					0.00	0.00											0.00
0.5 - 1.0		0.01	0.11	0.43	0.82	3.56	2.62	0.88	0.07	0.03	0.01						8.54
1.0 - 1.5		0.06	0.96	2.75	7.27	15.46	12.18	6.27	0.85	0.30	0.05	0.01					46.16
1.5 - 2.0		0.04	0.65	1.28	4.86	10.75	5.73	4.03	0.68	0.14	0.02	0.00					28.19
2.0 - 2.5		0.00	0.18	0.82	1.61	4.28	2.27	1.53	0.21	0.09	0.00	0.00					10.98
2.5 - 3.0			0.02	0.27	0.58	1.58	0.99	0.44	0.04	0.02	0.01						3.93
3.0 - 3.5				0.04	0.12	0.50	0.36	0.26	0.03	0.01							1.31
3.5 - 4.0					0.03	0.27	0.12	0.10	0.01	0.00							0.55
4.0 - 4.5					0.00	0.06	0.09	0.03	0.00								0.18
4.5 - 5.0						0.02	0.02										0.06
5.0 - 5.5						0.01		0.02	0.01								0.04
5.5 - 6.0								0.01	0.01	0.00							0.02
6.0 - 6.5								0.01	0.00								0.01
6.5 - 7.0								0.00	0.01								0.01
7.0 - 7.5									0.00	0.00							0.00
7.5 - 8.0									0.00	0.01							0.01
8.0 - 8.5										0.00							0.00
Total	0.00	0.11	1.93	5.58	15.29	36.49	24.37	13.60	1.94	0.60	0.09	0.01	0.00	0.00	0.00	0.00	100.

Table 6.7: Autumn wave heights versus peak periods occurrence

Hmo (m)	Period (Tp) (s)																Total
	0-2	2-4	4-6	6-8	8-10	10-12	12-14	14-16	16-18	18-20	20-22	22-24	24-26	26-28	28-30	30-32	
0.0 - 0.5					0.00	0.00											0.01
0.5 - 1.0			0.06	0.24	0.47	2.55	1.95	0.84	0.15	0.03	0.00						6.28
1.0 - 1.5		0.06	1.20	2.45	4.95	12.82	13.26	8.89	0.73	0.28	0.06	0.01					44.72
1.5 - 2.0		0.01	0.99	1.64	2.90	7.48	7.56	6.73	0.82	0.26	0.01	0.00					28.41
2.0 - 2.5	0.00	0.03	0.22	0.95	1.16	3.12	2.66	2.89	0.48	0.13	0.02						11.67
2.5 - 3.0			0.01	0.51	0.55	1.38	1.38	1.15	0.22	0.10	0.02						5.32
3.0 - 3.5				0.05	0.18	0.59	0.62	0.62	0.11	0.08	0.01						2.25
3.5 - 4.0				0.00	0.06	0.23	0.21	0.26	0.03	0.05	0.00						0.84
4.0 - 4.5					0.01	0.07	0.05	0.10	0.02	0.02							0.27
4.5 - 5.0					0.00	0.03	0.02	0.05	0.01	0.01							0.13
5.0 - 5.5					0.00	0.03	0.01	0.02	0.00	0.01							0.07
5.5 - 6.0						0.02	0.00		0.00	0.00							0.02
6.0 - 6.5																	0.00
6.5 - 7.0																	0.00
7.0 - 7.5																	0.00
7.5 - 8.0																	0.00
8.0 - 8.5																	0.00
Total	0.00	0.11	2.49	5.84	10.28	28.31	27.73	21.55	2.58	0.97	0.13	0.01	0.00	0.00	0.00	0.00	100.

Table 6.8: Winter wave heights versus peak periods occurrence

Hmo (m)	Period (Tp) (s)															Total	
	0-2	2-4	4-6	6-8	8-10	10-12	12-14	14-16	16-18	18-20	20-22	22-24	24-26	26-28	28-30		30-32
0.0 - 0.5			0.00														0.00
0.5 - 1.0		0.01	0.08	0.29	0.51	1.09	0.31	0.09	0.01	0.00							2.38
1.0 - 1.5		0.02	2.37	5.75	7.85	11.96	8.24	3.64	0.31	0.10	0.03	0.00					40.27
1.5 - 2.0			2.61	5.24	7.95	10.21	6.78	4.39	0.48	0.22	0.07	0.01					37.95
2.0 - 2.5			0.32	1.68	2.71	3.90	2.13	1.79	0.27	0.08	0.02	0.00					12.90
2.5 - 3.0			0.02	0.42	0.79	1.08	0.73	0.57	0.08	0.05	0.01	0.00					3.77
3.0 - 3.5				0.07	0.19	0.47	0.48	0.22	0.04	0.02	0.00						1.48
3.5 - 4.0				0.00	0.03	0.34	0.30	0.13	0.00	0.00							0.81
4.0 - 4.5					0.00	0.11	0.18	0.08	0.00								0.37
4.5 - 5.0						0.01	0.03	0.01									0.05
5.0 - 5.5						0.00	0.00										0.01
5.5 - 6.0																	0.00
6.0 - 6.5																	0.00
6.5 - 7.0																	0.00
7.0 - 7.5																	0.00
7.5 - 8.0																	0.00
8.0 - 8.5																	0.00
Total	0.00	0.03	5.40	13.47	20.02	29.17	19.17	10.91	1.20	0.46	0.14	0.02	0.00	0.00	0.00	0.00	100.

Table 6.9: Winter wave heights versus peak periods occurrence

Hmo (m)	Period (Tp) (s)															Total	
	0-2	2-4	4-6	6-8	8-10	10-12	12-14	14-16	16-18	18-20	20-22	22-24	24-26	26-28	28-30		30-32
0.0 - 0.5			0.00		0.00	0.00	0.00				0.00						0.00
0.5 - 1.0		0.01	0.13	0.53	0.87	2.35	1.44	0.51	0.06	0.02	0.00						5.91
1.0 - 1.5		0.06	1.83	4.83	8.22	14.09	10.37	5.33	0.55	0.20	0.04	0.01				0.00	45.53
1.5 - 2.0		0.02	1.44	2.96	5.85	9.78	6.26	4.38	0.57	0.18	0.03	0.00		0.00			31.48
2.0 - 2.5	0.00	0.01	0.22	1.10	1.83	3.62	2.10	1.77	0.26	0.08	0.01	0.00					11.00
2.5 - 3.0			0.02	0.33	0.58	1.17	0.92	0.60	0.10	0.05	0.01	0.00					3.78
3.0 - 3.5				0.04	0.13	0.41	0.42	0.31	0.05	0.03	0.00						1.40
3.5 - 4.0				0.00	0.03	0.21	0.17	0.14	0.01	0.01	0.00						0.58
4.0 - 4.5					0.00	0.06	0.08	0.06	0.01	0.01							0.21
4.5 - 5.0					0.00	0.02	0.02	0.02	0.00	0.00							0.06
5.0 - 5.5					0.00	0.01	0.00	0.01	0.00	0.00							0.03
5.5 - 6.0						0.00	0.00	0.00	0.00	0.00							0.01
6.0 - 6.5							0.00	0.00									0.00
6.5 - 7.0								0.00									0.00
7.0 - 7.5									0.00	0.00							0.00
7.5 - 8.0									0.00	0.00							0.00
8.0 - 8.5										0.00							0.00
Total	0.00	0.09	3.63	9.80	17.51	31.72	21.78	13.14	1.62	0.58	0.11	0.01	0.00	0.00	0.00	0.00	100.

Table 6.10: Overall wave heights versus peak periods occurrence

Wave conditions are selected from the occurrence tables and simulated in Mike21BW, on a more refined grid.

### 6.1.2 Mike21BW

Mike21BW is a time-domain numerical model that uses Boussinesq equations to solve a number of wave propagation phenomena in and around a port or harbour. The Boussinesq equation takes into account the non-linearity of waves as well as frequency dispersion. Frequency dispersion is expressed in momentum equations and it takes into account the effects of vertical accelerations on the pressure distribution. Mike21BW is depth limited and the maximum depth to deep water wave length is  $h/L_0 \approx 0.5$  and the maximum depth to deep water wave length for classical Boussinesq equation should be  $h/L_0 \approx 0.22$ .

Mike21BW is used in this study, to capture refraction, diffraction, partial reflection and transmission, non-linear wave-wave interaction, frequency spreading and directional spreading (DHI, 2017).

Six output points are selected along the Port's entrance channel. Figure 6.4 shows the layout of the Port as well as the positions of the output points in the Mike21BW, model where point 0 is the Waverider.

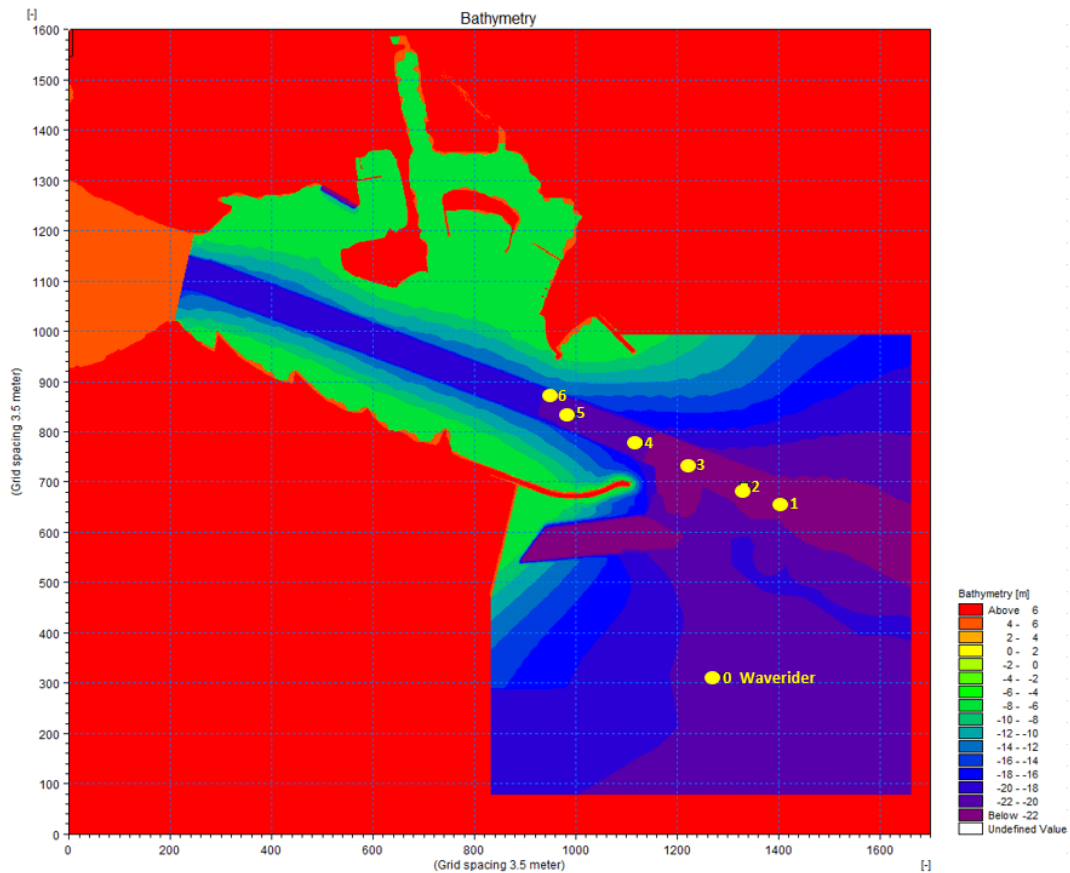


Figure 6.4: Port of Richards Bay Mike 21BW layout

### 6.1.3 Ship and waves orientation

Wave directions  $90^\circ$ ,  $135^\circ$  and  $180^\circ$  in the earth fixed orientation are simulated using wave generators placed on the east and south edges of the Mike 21BW model. Figure 6.11 presents the ship model fixed orientation and the waves earth fixed orientation.



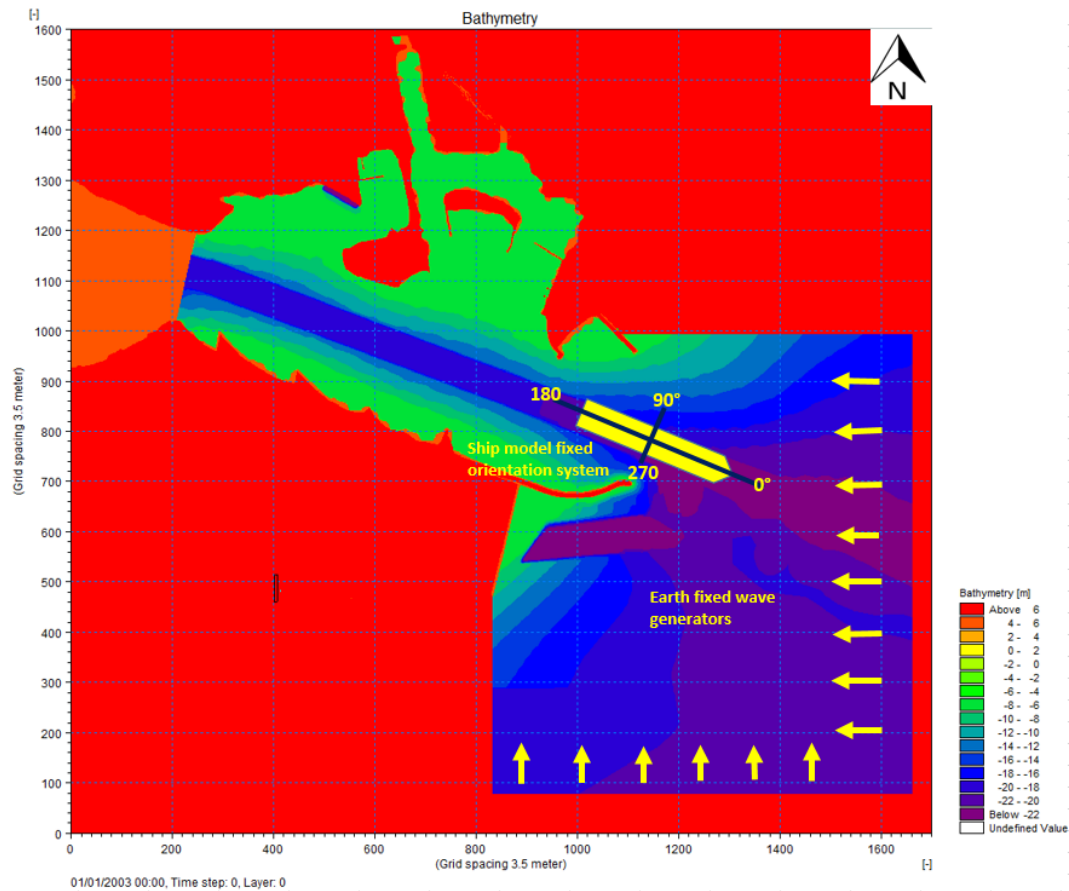


Table 6.11: Ship model's fixed orientation systems and waves' earth bound orientation system

### 6.1.3.1 Calibration of the Mike 21BW model

The Richards Bay Waverider and the Acoustic Doppler Current Profiler (ADCP), are used to calibrate the Mike21BW wave model. Two Waverider wave conditions from 90°, 135° and 180°, are simulated and compared to the ADCP recorded wave conditions. The results of the simulated wave conditions are compared to the exact dates and time of the ADCP wave conditions. The Waverider records every 30 minutes and the ADCP records every 2 hours. The calibration wave conditions are given in Table 6.12.



Waverider			ADCP		
Hmo (m)	Tp (s)	Direction (°)	Hmo (m)	Tp (s)	Direction (°)
1.21	7.41	96.62	0.56	5.40	114.0
1.88	6.06	91.52	0.59	5.03	133.0
1.40	12.50	133.10	0.46	12.10	138.00
2.14	12.50	135.12	0.55	13.40	139.00
1.28	14.29	181.63	0.52	14.90	139.00
1.69	12.15	179.87	0.59	14.90	108.00

Table 6.12: Waverider and ADCP calibration wave conditions

Mike21BW runs the selected calibration wave conditions for 30 minutes. Table 6.13 gives the results of the simulated wave conditions used to calibrate Mike21BW.

Waverider			ADCP		
Hmo (m)	Tp (s)	Direction (°)	Hmo (m)	Tp (s)	Direction (°)
1.09	7.68	92.10	0.57	7.37	105.30
1.52	6.04	92.00	0.90	6.06	100.50
1.40	12.29	130.50	0.90	12.29	120.80
2.05	13.17	137.40	0.80	13.70	120.00
1.29	14.18	182.00	0.46	15.36	135.60
1.55	11.52	188.00	0.70	12.70	135.00

Table 6.13: Mike21BW Waverider and ADCP calibration wave conditions results

Table 6.14 gives the accuracy percentages of the wave conditions measured versus those obtained from the simulation.

Waverider			ADCP		
Hmo	Tp	Direction	Hmo	Tp	Direction
90%	96%	95%	98%	73%	92%
81%	99%	99%	65%	83%	75%
100%	98%	98%	51%	98%	87%
96%	95%	98%	66%	98%	86%
99%	99%	99%	88%	97%	97%
92%	95%	95%	84%	85%	80%

Table 6.14: Accuracy percentage table for measured and simulated Mike21BW wave conditions

Table 6.13 shows that the Mike21BW wave heights from wave incidence angle  $135^\circ$ , are significantly higher than those measured by the ADCP. Given that Mike 21BW uses two generation lines to generate wave heights from  $135^\circ$ , it can be expected that more energy enters into the channel. The Mike21BW results may lead to higher ship motions in the Wavescat model for wave incidence  $135^\circ$ .

### 6.1.3.2 Mike 21BW test conditions

The Richards Bay physical model study done by the CSIR in March 1991, comprised primary tests for wave heights of above 3m and  $T_p$  of 10s. The primary tests were used to determine the angles of wave incidence relative to the model ship.  $T_p$  of 12s is used to run sensitivity tests to study the effect of wave period on the hull motion response. The Port of Richards Bay entrance channel orientation is  $111^\circ$  True North. Table 6.15 lists all the input conditions used to setup the Mike21BW model run conditions. The list is obtained from the occurrence tables created from the Delft3D-Swan:

Direction (°)	Hmo (m)	Tp = 10s	Tp = 12s	Tp = 14s	Tp = 16s	Tp = 18s
90	1	x	x			
	1.5	x	x			
	2	x	x			
	3	x	x	x	x	x
	4	x	x	x	x	x
	5	x	x			
135	6	x	x			
	1	x				
	2	x				
	3	x	x	x	x	x
	4	x	x	x	x	x
180	5	x				
	1	x				
	2	x				
	3	x				
	4	x				
	5	x				

Table 6.15: Mike 21BW input conditions

#### 6.1.4 Mike 21BW setup

Mike 21 BW's bathymetry has computation limitations, therefore Mike 21BW Model Setup Planner is used to determine simulation time, minimum wave period, maximum spatial resolution, maximum time, estimated CPU time in hours and courant number amongst other variables for classical and enhanced equations. The courant number is a number that ensures the model's calculation stability. Figure 6.5 shows the Setup Planner used for these studies.

MIKE 21 BW Model Setup Planner



Define your model

SI units for lengths (m)  
 US units for length (ft)

Max. water depth:   
 Min. water depth:   
 Model extent in X-direction:   
 Model extent in Y-direction:   
 Percentage of water points (%):   
 Max. distance for waves to propagate:   
 Time required for calculation of statistics (minutes prototype time):   
 Computational points per CPU second <sup>2)</sup>:   
 Spectral peak period (s):

Exclude wave breaking/moving shoreline  
 Include wave breaking/moving shoreline

Calculate simulation period

**A: Total simulation time**

Total time required for simulation (minutes prototype time) <sup>3)</sup>

**Reset and clear all**

**Legend:** OK Not OK

- Notes:**
- 1) The MIKE 21 BW Model Setup Planner is based on the step-by-step procedure shown [here](#).
  - 2) The computational points per CPU second can be found at the end of the run log file.
  - 3) Includes the travel time of the first wave and the time required for calculation of wave statistics.
  - 4) The spatial resolution may be OK in case of wave breaking/moving shoreline. Make sure the ratio  $L/dx$  is 20-40 for  $T_p$  (see check/evaluation box).

Calculate and check/evaluate  $T_{min}$ ,  $dx$  and  $dt$  <sup>1)</sup>

**B: Calculate default upper limits**

Upper limits	Classical eq.	Enhanced eq.
Min. wave period, $T_{min}$ (s)	8.53	5.66
Max. spatial resolution, $dx$	8.14	5.07
Max. time step, $dt$ (s)	0.519	0.161

**C: Update upper limits using  $T_{min}$  and check/evaluation**

**Own suggestion**

Min. wave period, $T_{min}$ (s)	8.53	5.66
Spatial resolution <sup>4)</sup> , $dx$	8.14	5.07
Time step, $dt$ (s)	0.519	0.161

**Check/evaluation of selected  $T_{min}$ ,  $dx$  and  $dt$**

Max. ratio $h/L_0$ for $T_{min}$	0.2198	0.4993
Max. ratio $h/L_0$ for $T_p$	0.0319	0.0319
Min. ratio $L/dx$ for $T_{min}$	7.0036	7.0011
Min. ratio $L/dx$ for $T_p$	8.3191	13.356
Ratio $T/dt$ for $T_{min}$	16.435	35.155
Ratio $T/dt$ for $T_p$	19.267	62.111
Max. Courant Number	0.9990	0.4975
Estimated CPU time (hours)	0.1540	1.2751
Estimated RAM (MB)	9.7311	15.582

Figure 6.5: Mike21BW Setup Planner (DHI, 2017)

Porosity determines how much reflection or transmission is allowed through porous structures depending on the slope and the structure or type of armour . Porosity can be determined from Mike21 toolbox, under Waves - Calculation of Reflection Coefficients. Figure 6.6 can also be used to approximate porosity coefficient.

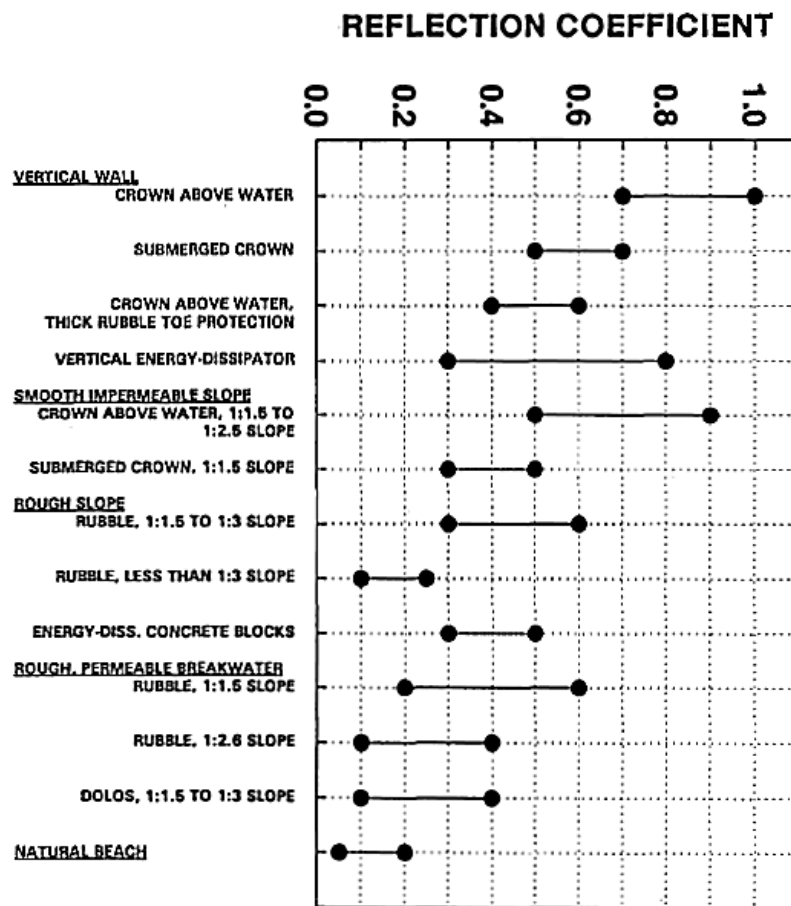


Figure 6.6: Porosity reflection coefficients (DHI, 2017)

Porosity of 0.4 is used for Port of Richards Bay's permeable breakwater dolos. Figure 6.7 shows Port of Richards Bay breakwaters porosity plot.

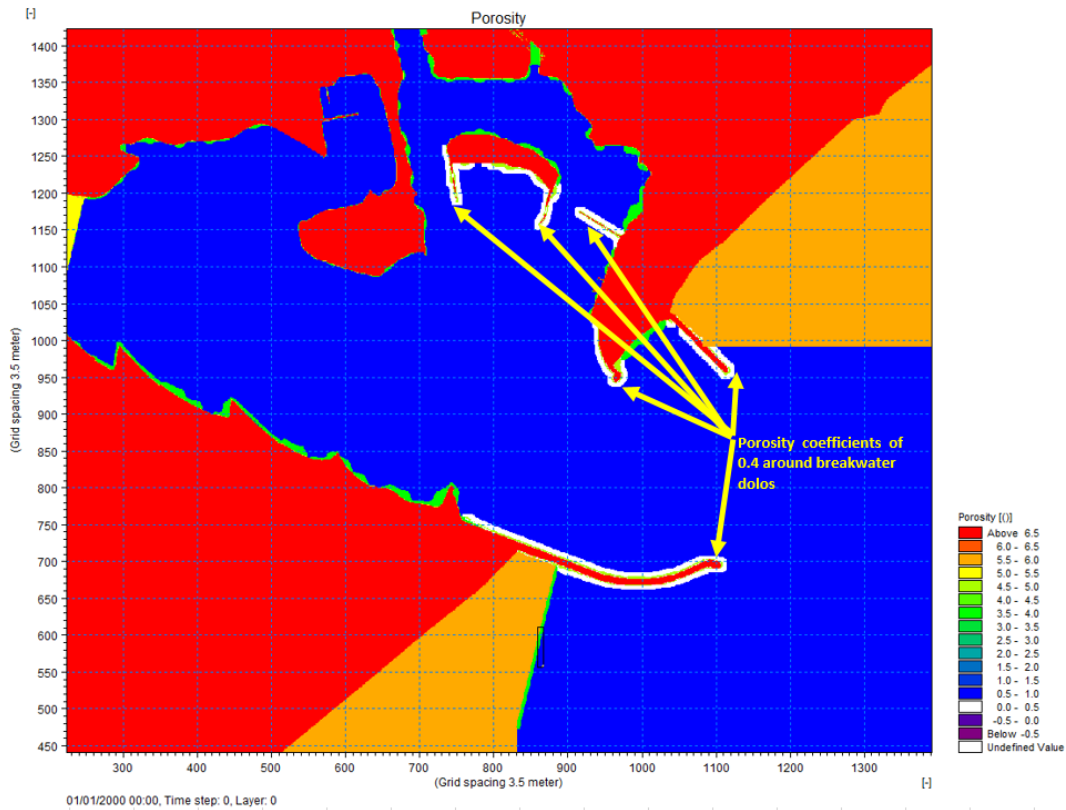


Figure 6.7: Porosity plot

A sponge is an input into a bathymetry that absorbs unwanted energy from returning back into the model. In this study, sponge layers are put around the east and south edges of the bathymetry domain as well as on the inside of the bathymetry. Sponge layers are placed behind generation lines. Two generation lines are used in this study. The eastern generation line is used to generate waves from wave direction  $45^\circ$ , both the east and south generation lines are used to generate waves from wave direction  $135^\circ$  and the south generation line is used to generate waves from wave direction  $180^\circ$ . Figure 6.8 shows the sponge layers and generation lines positions in the bathymetry.

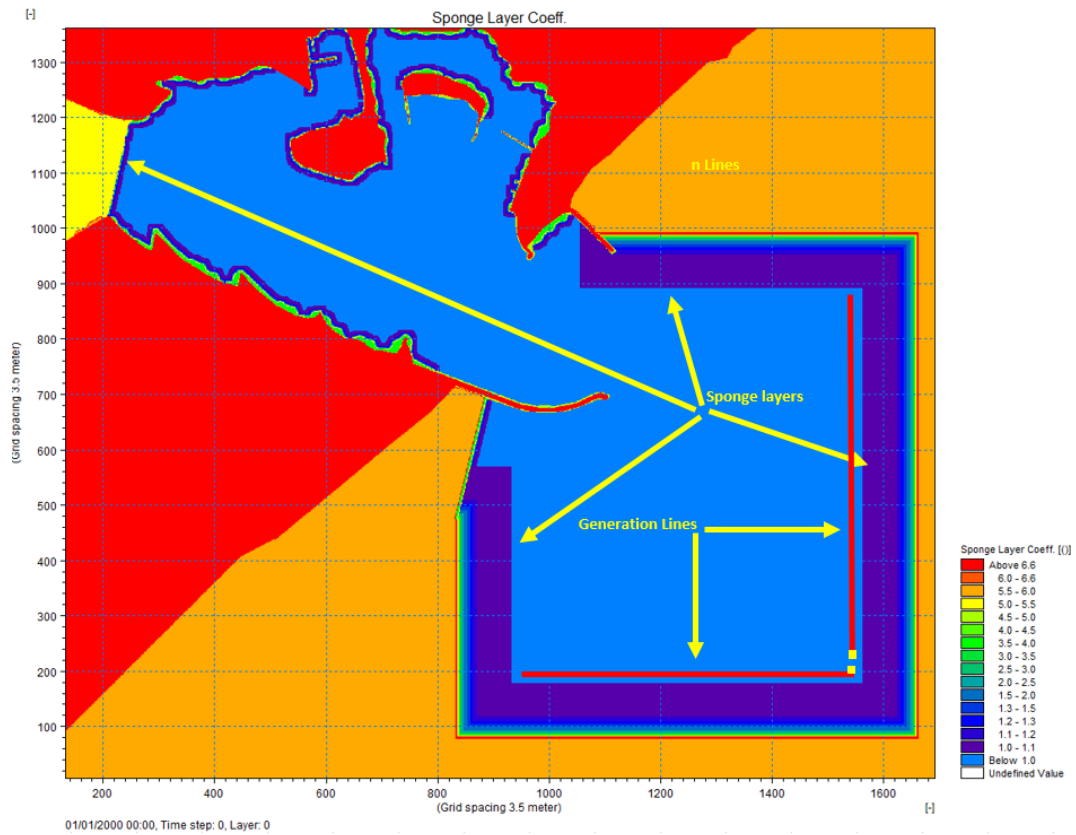


Figure 6.8: Sponge plot

Figures 6.9, 6.10 and 6.11 presents the three directions simulated in Mike 21BW. Each wave condition is ran for 30 minutes at a time step of 0.09 seconds, using a grid size of 3.5m  $\times$  3.5m.



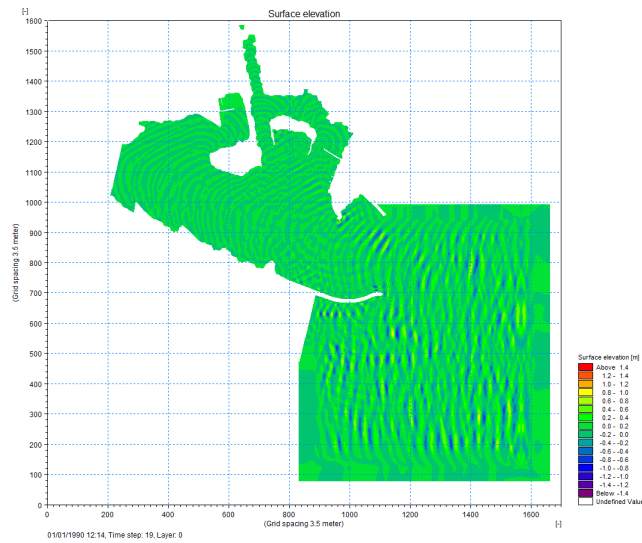


Figure 6.9: Mike21BW surface elevation plot for  $H_s = 1\text{m}$ ,  $T_p = 10\text{s}$  and  $\alpha = 90^\circ$

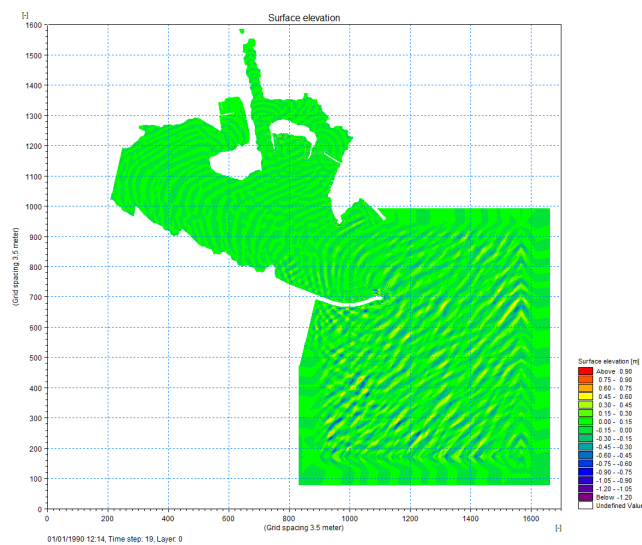


Figure 6.10: Mike21BW surface elevation plot for  $H_s = 1\text{m}$ ,  $T_p = 10\text{s}$  and  $\alpha = 135^\circ$

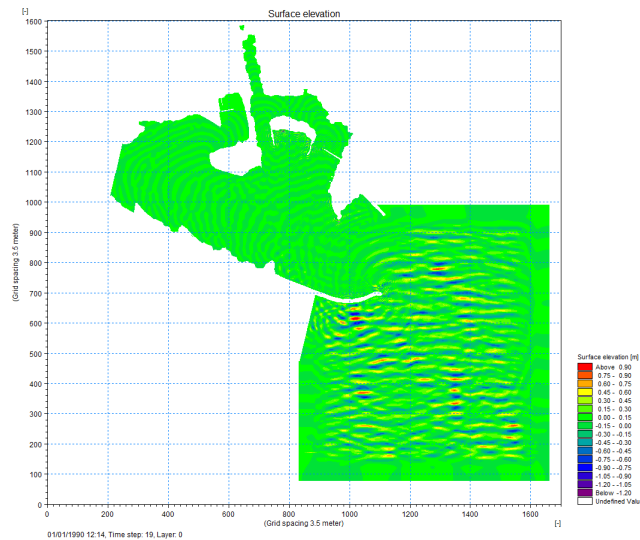


Figure 6.11: Mike21BW surface elevation plot for  $H_s = 1\text{m}$ ,  $T_p = 10\text{s}$  and  $\alpha = 180^\circ$

## 6.2 Numerical modelling of a 150kt DWT bulk carrier

### 6.2.1 Wavescat model

The Wavescat program models wave forces acting on a floating body like a ship, as well as its response due to regular waves. The program is a 3D panel numerical model that uses the Rankine Green function to solve the potential velocity values on each wetted submerged hull panel for specific set of wave heights and wave directions.

The model has two ascii input files namely the setup file and the mesh file. The mesh file contains the hull mesh dimensions such as number of nodes, planes, lines and transverse radii of gyration. The mesh file is an input into the main file. The main file is where the following are specified:

$g$  = acceleration of gravity ( $m/s^2$ )

$\rho$  = fluid density ( $kg/m^3$ )

$h$  = water depth (m)

viscous roll damping coefficients (-)

nondimensional viscous roll damping coefficients (-)

wave height (m)

number of ships

mesh file

number of ships, their X and Y positions (m), heading direction ( $^\circ$ ), forward

speed (m/s)  
number of wave directions (-)  
wave directions ( $^{\circ}$ )  
quay wall (0 for no quay wall and 1 for quay wall)  
drift force option

The model outputs a response amplitude operators (.rao) file and hydrodynamic (.hyd) file for different wave directions. (Dr Wim van der Molen, 2011).

### 6.2.2 Ship mesh

A 150k DWT bulk carrier is selected as the design vessel of this study, following the CSIR (1990) Richards Bay report that contains sufficient physical model wave-ship interaction data for comparison with the output of the numerical model study. The hull comprises of 4402 panels, 4396 nodes and 160 lines.

Figure 6.12 presents a hull mesh file with a lid at the water level as a representation of the submerged body of the ship. Figure 6.13 presents the hull's body plan and Table 6.16 shows the main dimensions of the ship.

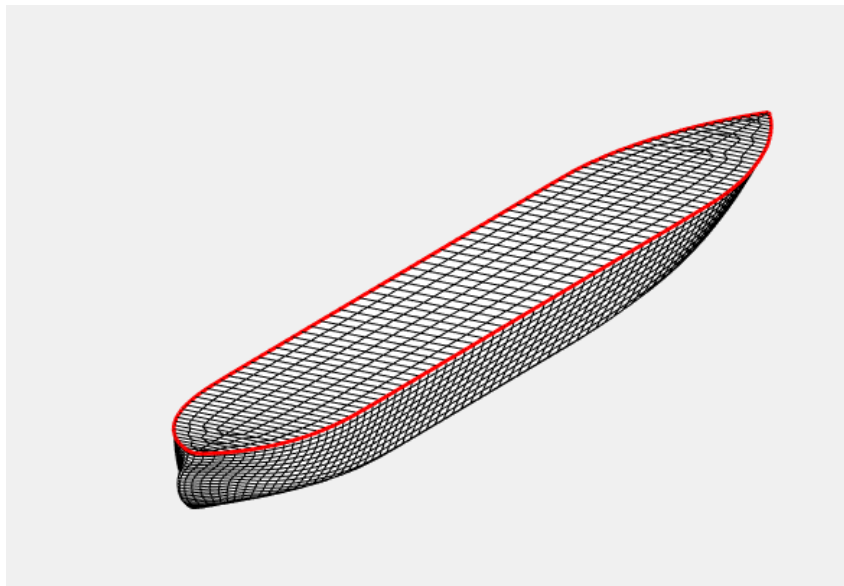


Figure 6.12: 150k DWT hullform mesh (4402 panels)

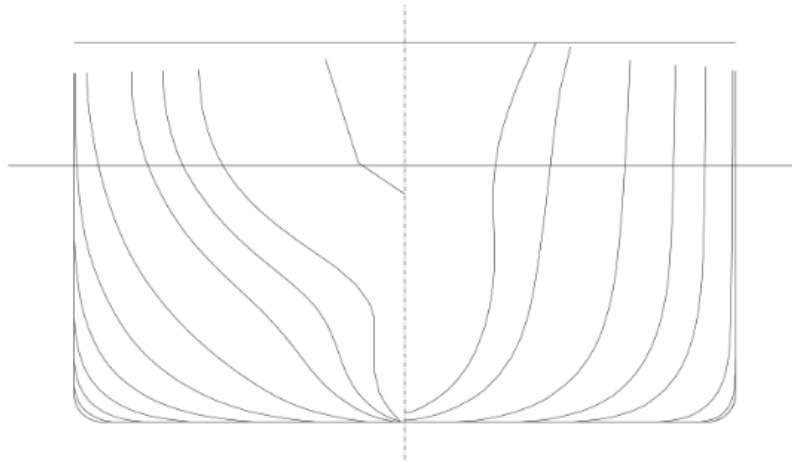


Figure 6.13: 150k DWT hullform body plan

Parameter	Symbol	Value
Length between perpendiculars	Lpp	295m
Breadth	B	44m
Draught	D	17m
Displacement volume	V	182 729.65m <sup>3</sup>
Block coefficient	Cb	0.828
Centre of buoyancy forward of midship	LCB	8m
Centre of gravity above keel	KG	12.75m
Transverse radius of gyration	Kxx	13.2m (=0.30×B)
Transverse metacentric height	$\overline{GM}_T$	9.41m
Longitudinal radius of gyration	Kyy	73.75m(=0.25×Lpp)
Longitudinal metacentric height	$\overline{GM}_L$	390.38m

Table 6.16: 150kt DWT Bulk vessel dimensions

### 6.2.3 Validation of the Wavescat model

A wave spectrum with  $H_s$  of 3m and  $T_p$  of 10s is selected as a baseline for the Wavescat model, following the physical model studies, which had the same wave conditions.  $H_s$  is increased gradually, from 3m to 5m. The results are then, compared to those of the physical model. Table 6.17 shows the water depths in the Wavescat and Mike21BW models.

d/D ratio(-)	Physical model depth (m)	Mike21BW depth (m)	Mike21BW probe number
1.5	25.2	25	1
1.4	23.4	24	2
1.3	21.6	22	4
1.2	19.8	20	6
1.1	18.7	20	6

Table 6.17: Water depth in the physical model and Wavescat/Mike21BW model

Table 6.18 shows a list of the physical model test conditions that are used to validate the Wavescat model. The ship model was stationary during the tests (0 m/s speed).

Test number	d(m)	d/D	Wave angles( °)	Tp(s)	Speed(m/s)
1	25.2	1.5	90, 135, 180	10	0
2	23.4	1.4	90, 135, 180	10	0
3	21.6	1.3	90, 135, 180	10	0
4	19.8	1.2	90, 135, 180	10	0
5	18.7	1.1	90, 135, 180	10, 12	0

Table 6.18: Test conditions for 150kt DWT bulk carrier with 0 m/s

During the physical model tests, the ship was held in place by two thin piano wires attached to the bow and stern with the ship's X defining (0°) straight ahead in the bow direction and Y (90°) on the port side defining the body-bound coordinate system. Figure 6.14 shows vertical hull motion measurement system used during the physical model tests.

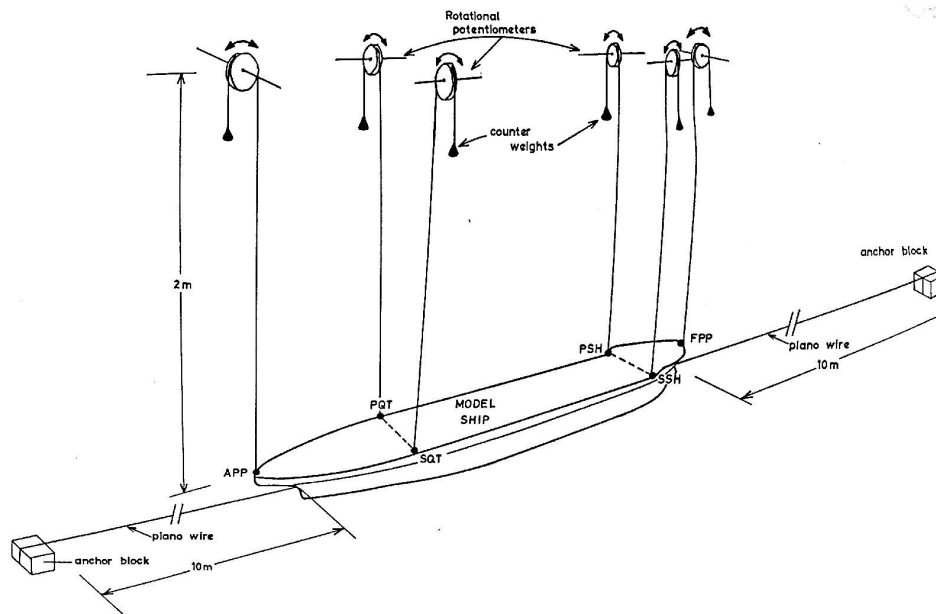


Figure 6.14: Physical model vertical hull motion measurement system (Jonker *et al.*, 1991)

The ship's heading degree was  $135^\circ$  in the global coordinate system. The ship was exposed to waves from  $0^\circ$ ,  $45^\circ$ ,  $90^\circ$ ,  $135^\circ$  and  $180^\circ$  in the global coordinate system. Figure 6.15 shows the ship model's fixed orientation system and earth fixed orientation systems used in the physical model.

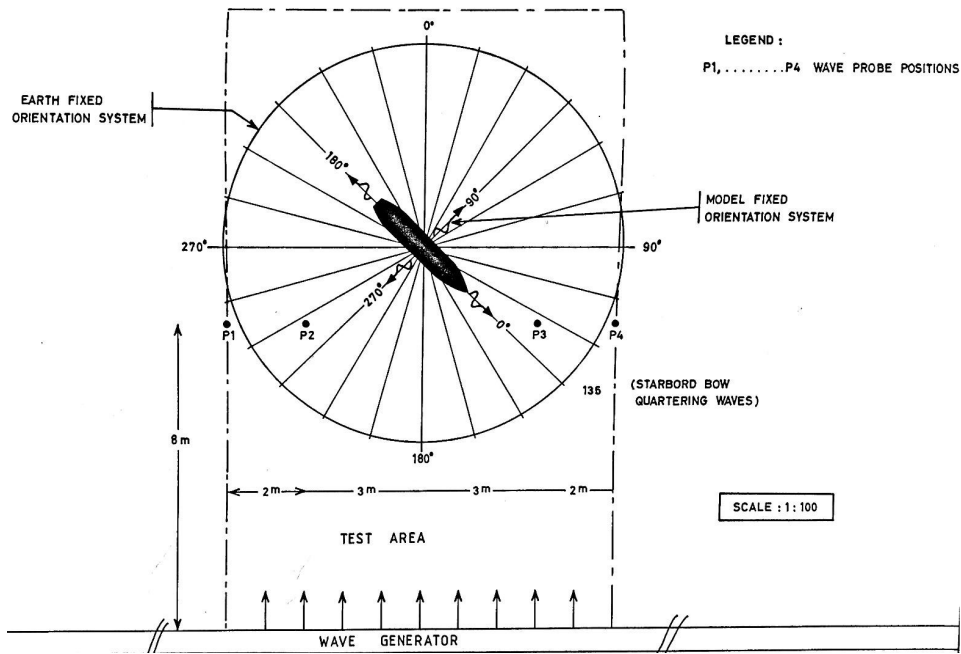


Figure 6.15: Physical model ship fixed orientation system and earth fixed orientation system (Jonker *et al.*, 1991)

In order to match the body bound coordinate system with the earth bound coordinate system, the ship model's (body bound coordinate system) heading direction in the Wavescat model is  $0^\circ$  True North which is the same as the earth bound's  $0^\circ$  True North direction. This way the wave directions will be the same as wave incident angles. Figure 6.16 presents ship heading direction in the Wavescat model.

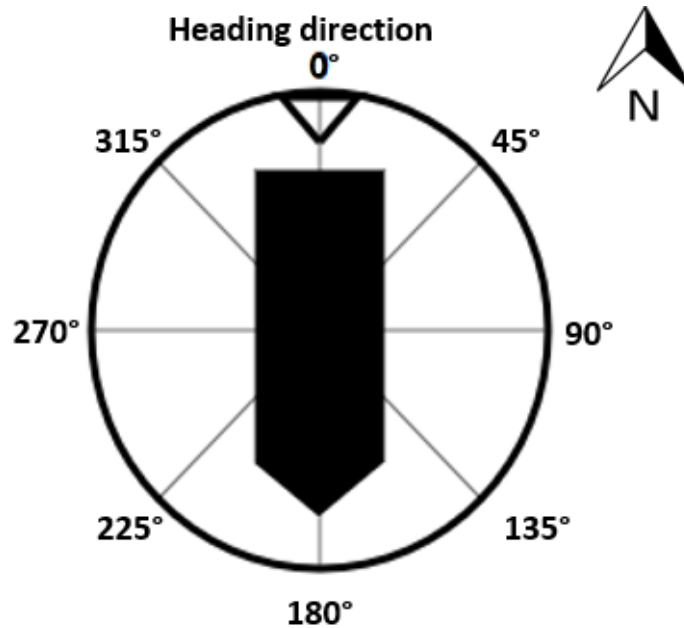


Figure 6.16: Wavescat ship heading direction

### 6.2.3.1 Viscous roll damping

Viscous roll damping is the dissipation of energy of a vessel in motion, in a body of water, which is directly proportional to the velocity (Hosch, 2006). Viscous roll damping coefficients are numerical representations of the viscous roll damping that occurs in real life, and are used to apply damping of the vessel when using models to compute ship motions.

In the Wavescat model, the viscous roll damping coefficient is related to the roll motion squared. The viscous damping is however, linearized in the equation of motion, which results in varying coefficients for different roll amplitudes. These varying viscous damping coefficients are estimated through iteration (Molen and Ligteringen, 2005).

According to the International Maritime Organization (2008), the angle of heel for bulk carriers exposed to steady winds should not exceed  $16^\circ$ . Figure 6.17 shows roll RAOs for different viscous damping coefficients, for varying water depths of 25.2m, 23.4m, 21.6m, 19.8m and 18.7m. The figure also shows that large roll response is associated with large viscous damping and that significant damping occurs for roll response angles of more than 10 degrees with a damping coefficient of 0.0001 to 0.0045 for the 150kt DWT bulk carrier. Small viscous roll damping leads to large roll motions and large viscous roll damping leads to small roll motions.



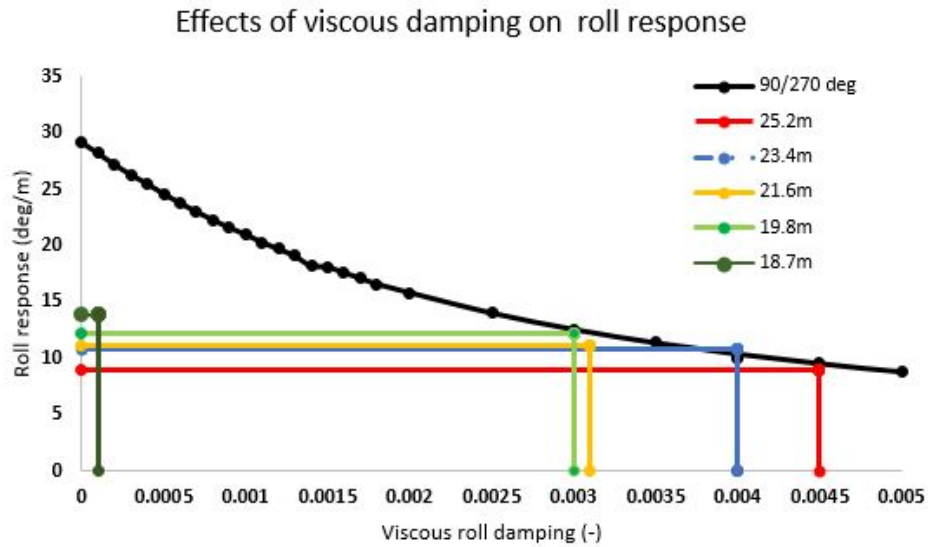


Figure 6.17: Effects of viscous roll damping on roll response

Table 6.19 shows the damping coefficients that were found to give the best results in comparison to the results obtained from the physical model studies for wave incident angle  $90^\circ$ .

Wavescat damping coefficient (-)	Water depth (m)
0.0045	25.2
0.004	23.4
0.0031	21.6
0.003	19.8
0.0001	18.7

Table 6.19: Viscous damping coefficients for  $90^\circ$ 

Table 6.20 shows the damping coefficients that were found to give the best results in comparison to the results obtained from the physical model studies for wave incident angle  $135^\circ$ .

Wavescat damping coefficient (-)	Water depth (m)
0.1	25.2
0.02	23.4
0.005	21.
0.002	19.8
0.001	18.7

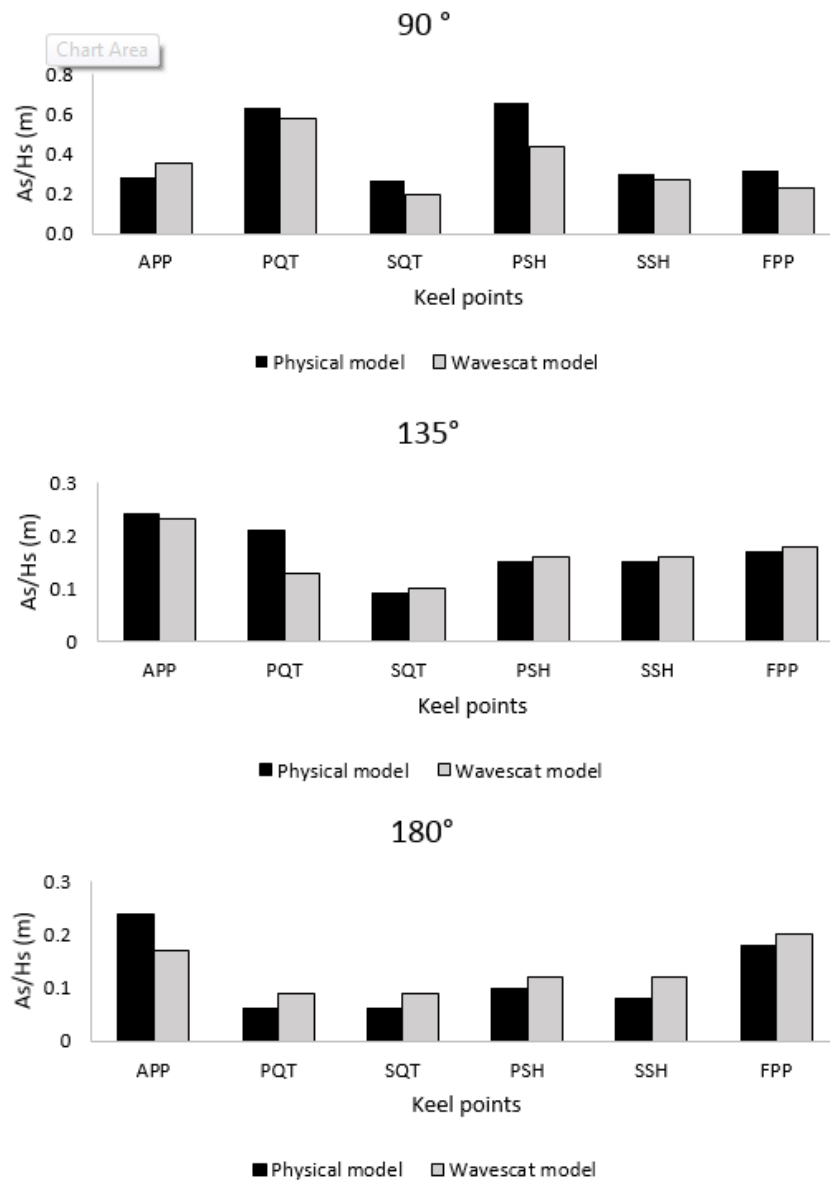
Table 6.20: Viscous damping coefficients for 135°

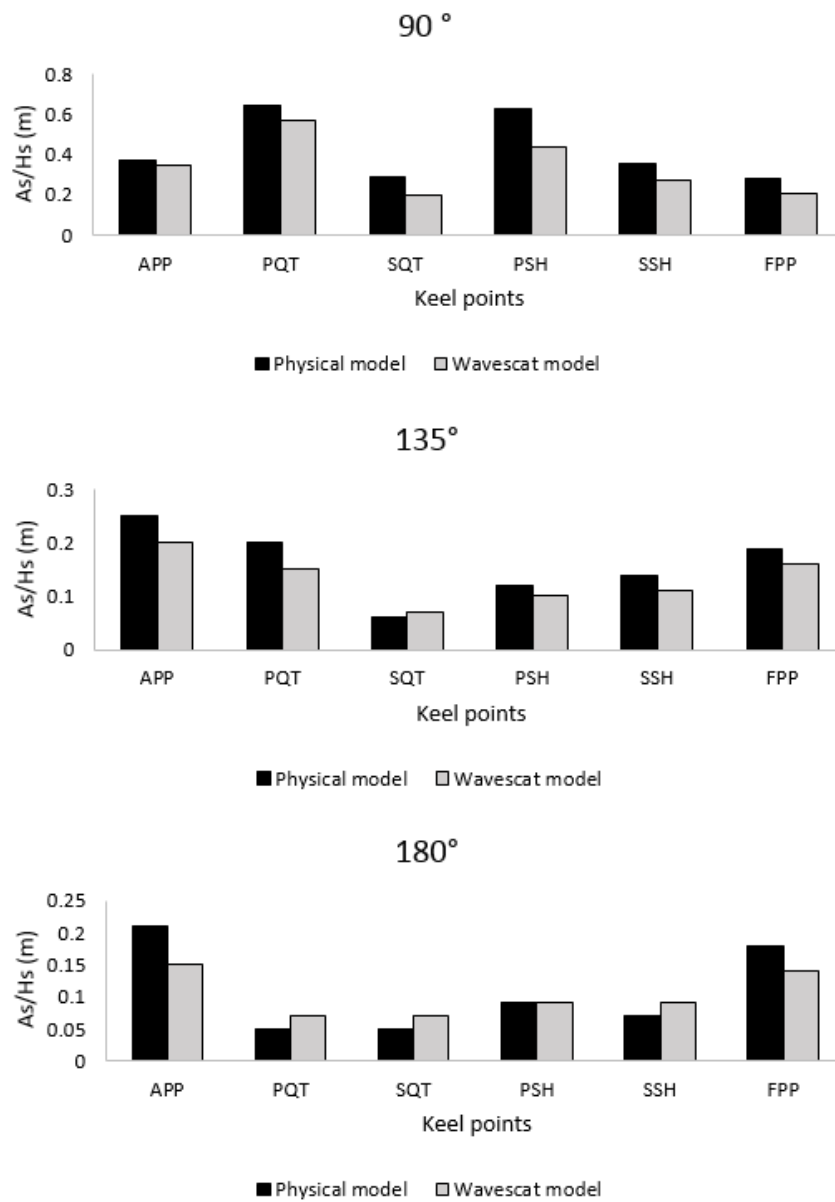
Table 6.21 shows the damping coefficients that were found to give the best results in comparison to the results obtained from the physical model studies for wave incident angle 180°.

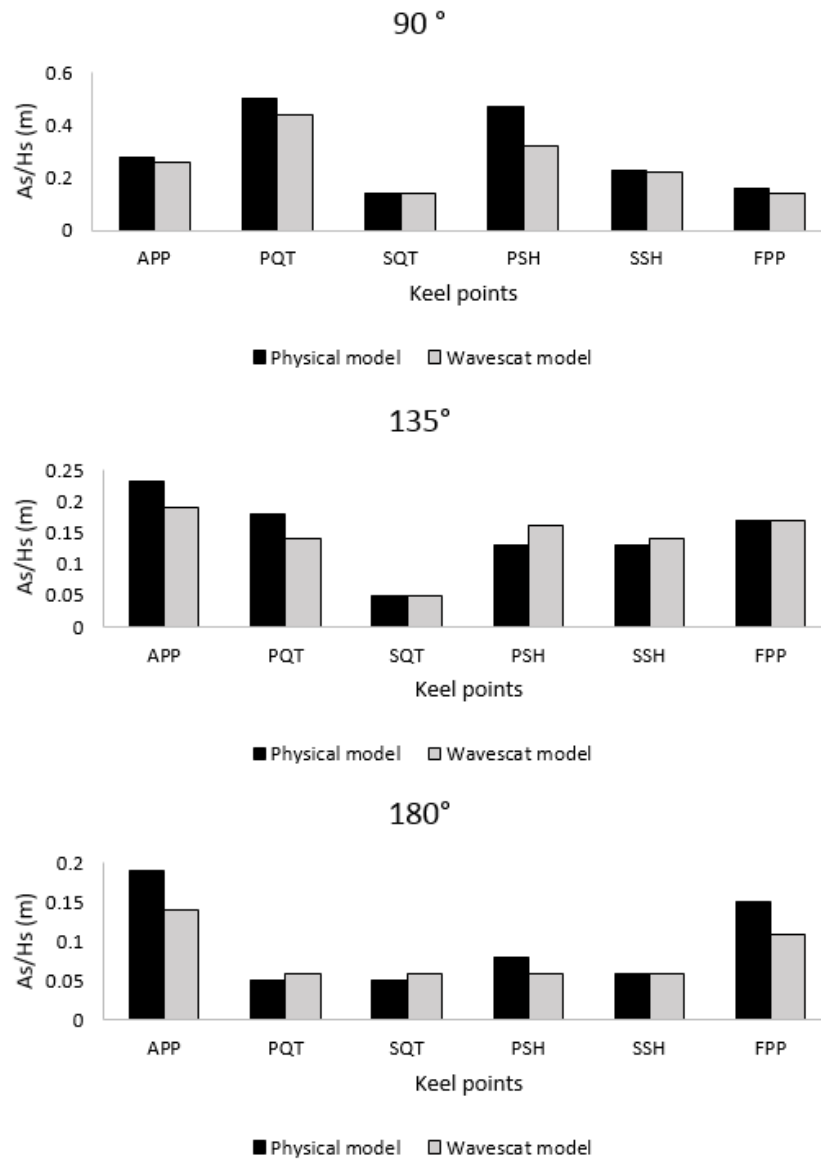
Wavescat damping coefficient (-)	Water depth (m)
0.5	25.2
0.1	23.4
0.05	21.6
0.02	19.8
0.01	18.7

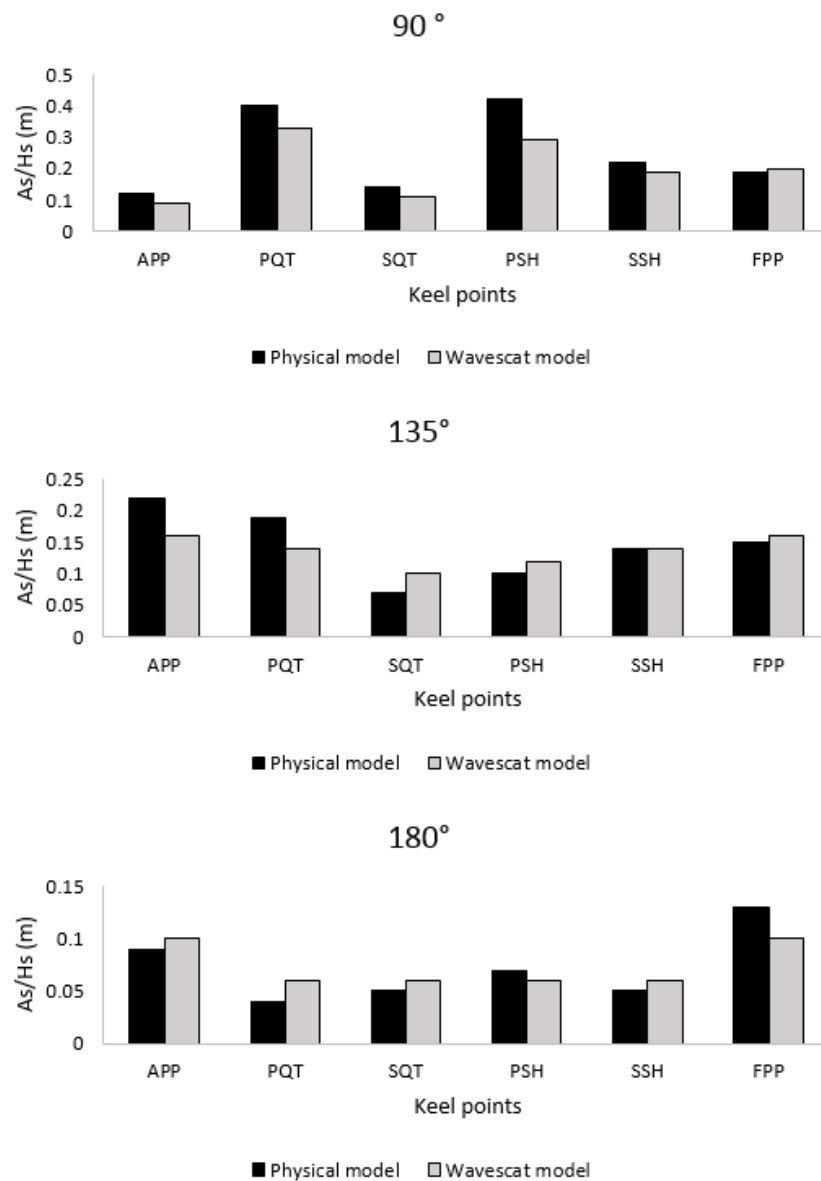
Table 6.21: Viscous damping coefficients for 180°

Figures 6.18 to 6.22 show the comparison of both the results of the physical model and the Wavescat model for depth/draught ratio of 1.5, 1.4 1.3, 1.2 and 1.1, wave incident angle 90°.

Figure 6.18: Comparison of physical model and Wavescat model for  $d/D = 1.5$

Figure 6.19: Comparison of physical model and Wavescat model for  $d/D = 1.4$

Figure 6.20: Comparison of physical model and Wavescat model for  $d/D = 1.3$

Figure 6.21: Comparison of physical model and Wavescat model for  $d/D = 1.2$

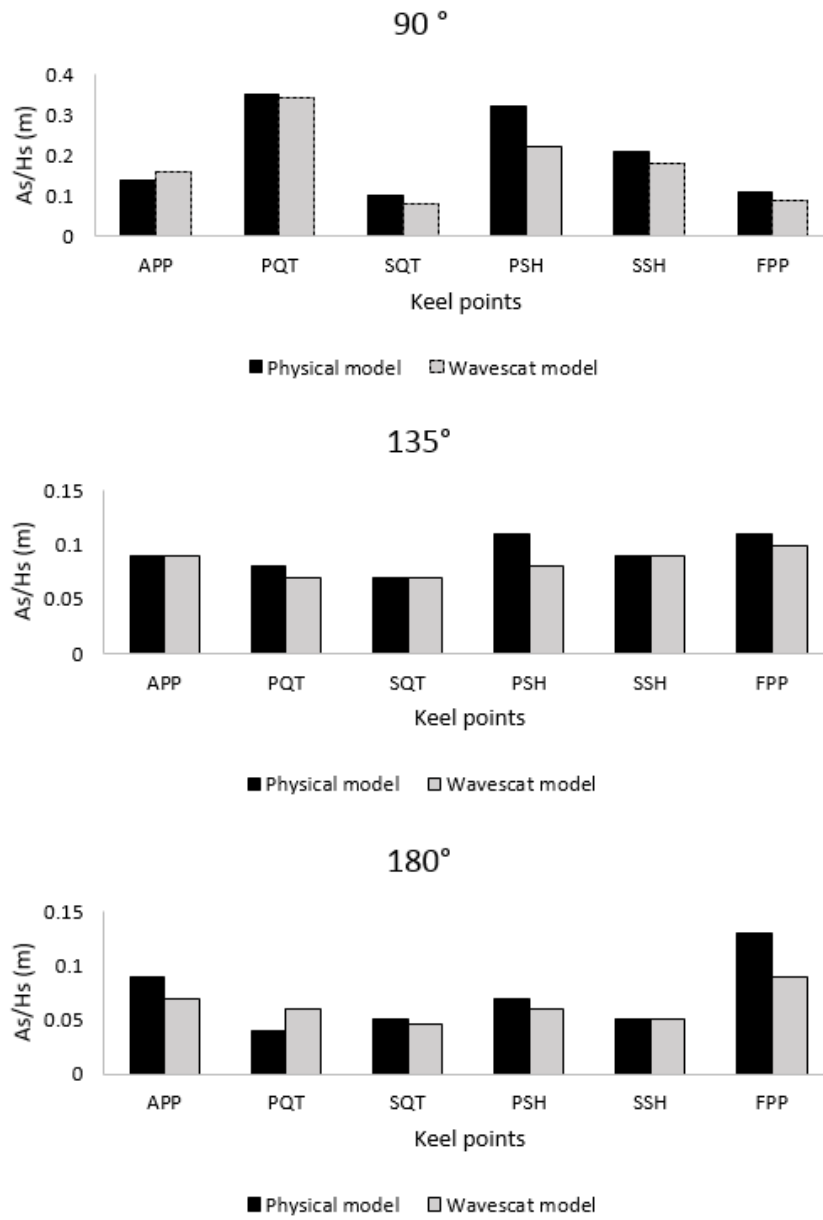


Figure 6.22: Comparison of physical model and Wavescat model for  $d/D = 1.1$

Figures 6.23 to 6.27 shows  $A_s/H_s$  plots for the physical model versus the Wavescat model for varying  $d/D$  ratios.

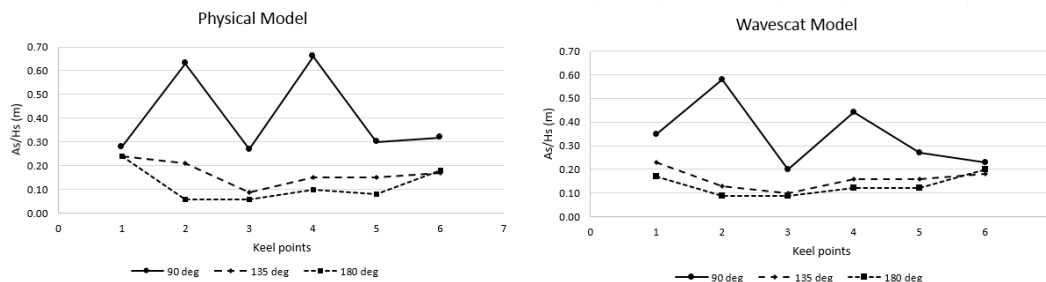


Figure 6.23: Physical model versus Wavescat model for  $d/D = 1.5$

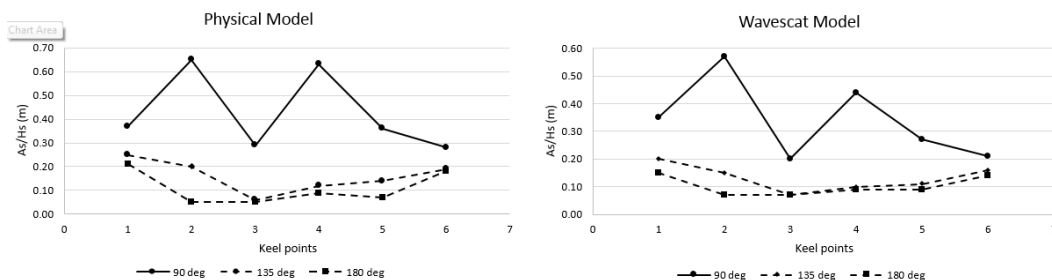


Figure 6.24: Physical model versus Wavescat model for  $d/D = 1.4$

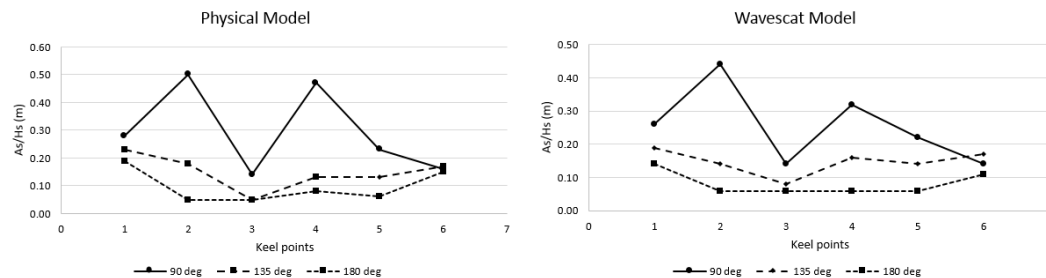


Figure 6.25: Physical model versus Wavescat model for  $d/D = 1.3$   
3.520

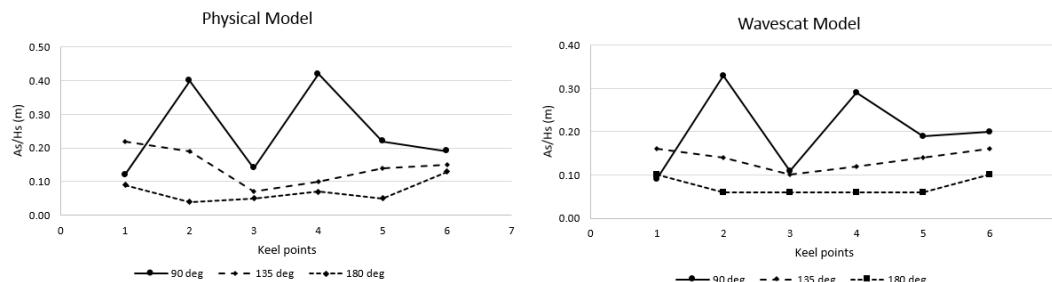


Figure 6.26: Physical model versus Wavescat model for  $d/D = 1.2$



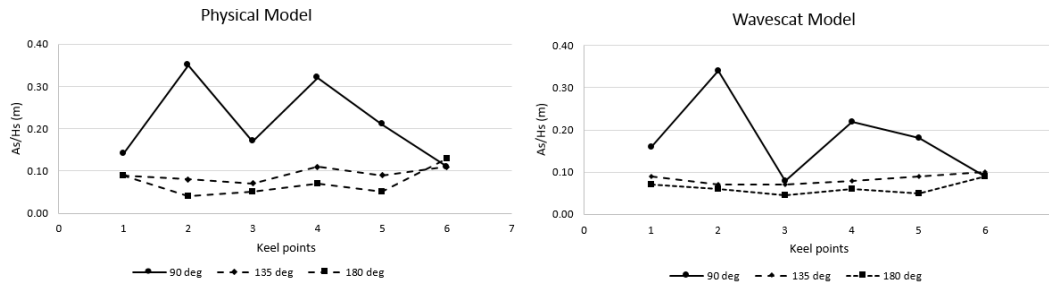


Figure 6.27: Physical model versus Wavescat model for  $d/D = 1.1$

It can be observed from all the  $d/D$  plots that the Wavescat under predicts all the six keel points when compared to physical model tests for wave incident angle  $90^\circ$ . The under predictions for  $A_s/H_s$  ratios for all the tested  $d/D$  is given by Table 6.22 for wave incident angle  $90^\circ$ .

$d/D$	APP (%)	PQT (%)	SQT (%)	PSH (%)	SSH (%)	FPP (%)
1.5	20,0	7,9	25,9	33,3	10,0	28,1
1.4	5,4	12,3	31,0	30,2	25,0	25,0
1.3	7,1	12,0	0,0	31,9	4,3	12,5
1.2	25,0	17,5	21,4	31,0	13,6	5,0
1.1	12,5	2,9	20,0	31,3	14,3	18,2

Table 6.22: Wavescat under prediction percentages for  $90^\circ$

It can also be observed that PSH and PQT have more magnitude than SSH and SQT. APP and FPP have almost the same magnitude as SSH and SQT. This means that when the ship model is exposed to beam waves at  $90^\circ$  incident wave angle, the lateral port side experiences more vertical ship motions.

All  $d/D$  plots reveal that APP and PQT have higher magnitude than the other keel points for incident wave angle of  $135^\circ$ . This means that waves that cause incident wave angle of  $135^\circ$ , causes more bow and port quarter vertical motions than the other keel points. Table 6.23 shows the over/under predictions between the physical and the Wavescat model for wave incident angle  $135^\circ$ .

d/D	APP (%)	PQT (%)	SQT (%)	PSH (%)	SSH (%)	FPP %
1.5	4,2	38,1	10,0	6,3	6,3	5,6
1.4	20,0	25,0	14,3	16,7	21,4	15,8
1.3	17,4	22,2	0,0	18,8	7,1	0,0
1.2	27,3	26,3	30,0	16,7	0,0	6,3
1.1	0,0	12,5	0,0	27,3	0,0	9,1

Table 6.23: Wavescat under prediction percentages for 135°

All d/D plots reveal that APP and FPP have higher magnitude than the other keel points for incident wave angle of 180°. This means that waves that cause incident wave angle of 180° causes more bow and stern vertical motions than the other keel points. This also means that the ship experiences more pitching. Table 6.24 shows the over/under predictions between the physical and the Wavescat model for wave incident angle 180°.

d/D	APP (%)	PQT (%)	SQT (%)	PSH (%)	SSH (%)	FPP %
1.5	29.2	33.3	33.3	16.7	33.3	10.0
1.4	28.6	28.6	28.6	0.0	22.2	22.2
1.3	26.3	16.7	16.7	25.0	0.0	26.7
1.2	10.0	33.3	16.7	14.3	16.7	23.1
1.1	22.2	33.3	8.3	14.3	0.0	30.8

Table 6.24: Wavescat under prediction percentages for 180°

Figure 6.28 shows the effect of water depth on significant hull motion response for incident waves of 90°, 135° and 180° by comparing port quarters (PQT) measured in the physical model tests and those produced by the Wavescat model.

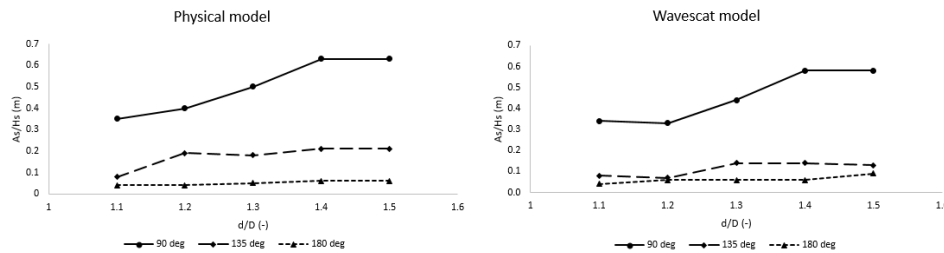


Figure 6.28: Effect of water depth on significant hull motion response

Figure 6.28 shows that both the physical and the Wavescat model follow similar patterns. Port quarters (PQT) in the physical and Wavescat model are of

the same magnitude for  $d/D = 1.5$  and  $1.4$  for wave incident angle  $90^\circ$  with an under-prediction of 10% for  $d/D = 1.5$  and 12% for  $d/D = 1.4$  in the Wavescat model. The  $A_s/H_s$  ratios in the Wavescat model decrease from  $d/D = 1.4$  to  $d/D = 1.2$ , then slightly increase for  $d/D = 1.1$  for incident wave angle  $90^\circ$ . The increase for  $d/D = 1.1$  is caused by the water depth difference of  $\pm 1.3$  m between the physical and Wavescat model where 18.7 m water depth was used in the physical model and 20 m was used in the Mike21BW and Wavescat model. This means that the Wavescat ship model was able to represent the decrease of motions with a decrease in water depth except for motions for  $d/D = 1.1$  which were not as well represented due to the difference in water depth.

Figure 6.28 also shows an almost similar pattern between the two models except for  $A_s/H_s$  ratios for  $d/D = 1.2$  which deviate from the physical model pattern for incident wave angle  $135^\circ$ . The figure shows that water depth does not have much of an effect on the port quarters' (PQT) vertical ship motions for wave incident angle  $135^\circ$ . The Wavescat model under predicts the port quarter motions by 12.5 % for  $d/D = 1.5$ , 26% for  $d/D = 1.4$ , 22% for  $d/D = 1.3$ , 25% for  $d/D = 1.2$  and 38% for  $d/D = 1.1$ . This means that the Wavescat model was able to represent similar patterns as the physical model with minor under-predictions of vertical ship motions for port quarters (PQT). The under-predictions can be solved by further testing different damping coefficient in the Wavescat model.

Figure 6.28 shows a similar pattern between the physical and the Wavescat model for wave incident angle  $180^\circ$ . The figure show that water depth does not have an effect on port quarters' (PQT) vertical ship motions for wave incident angle  $180^\circ$ . The Wavescat model over predicts the  $A_s/H_s$  ratios by 33% for  $d/D = 1.5$  and  $1.4$ , 17% for  $d/D = 1.3$ , 29% for  $d/D = 1.2$  and 33% for  $d/D = 1.1$ . This means that the Wavescat ship model's port quarter (PQT) experiences more vertical motions than those in the physical model. The over-prediction can also be solved by further testing different damping coefficients for wave incident angle  $180^\circ$ .

#### 6.2.4 Vessel response spectra

Vessel response spectra are calculated using equation 6.1.

$$S_\zeta(\omega) \cdot (RAO_z)^2 = S_z(\omega) \quad (6.1)$$

where  $S_\zeta(\omega)$  is the wave spectrum,  $RAO_z$  is the vessel amplitude operators and  $S_z(\omega)$  is the ship motion spectrum.

Figures 6.29 to 6.43 shows RAOs produced by Wavescat for the three rotational and three translation motions for water depths 25.2m, 23.4m, 21.6m 19.8m and 18.7m.

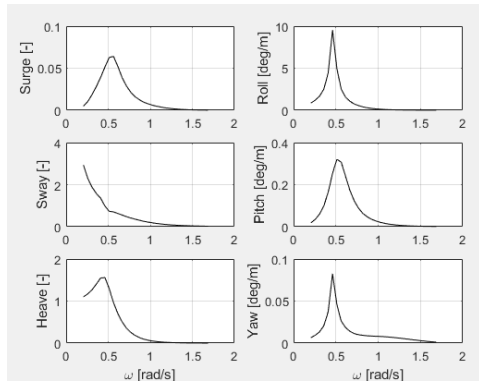


Figure 6.29: RAOs for 25.2m,  $90^\circ$

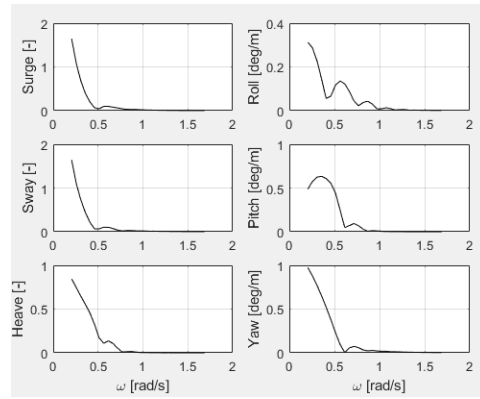


Figure 6.30: RAOs for 25.2m,  $135^\circ$

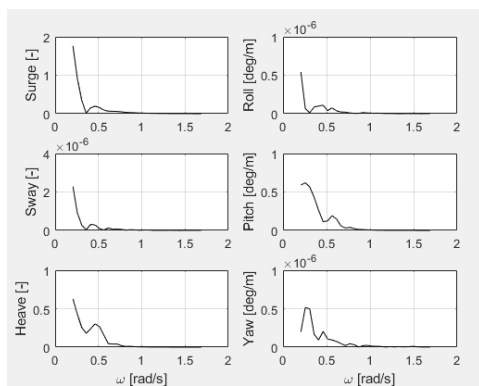


Figure 6.31: RAOs for 25.2m,  $180^\circ$

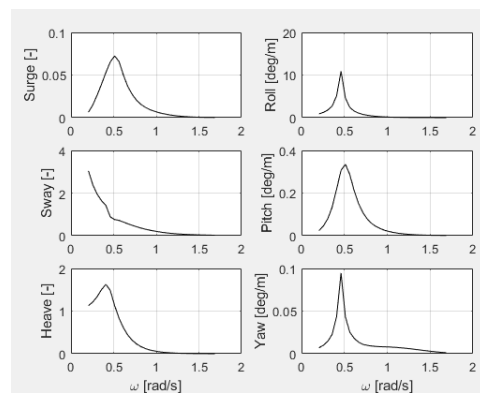


Figure 6.32: RAOs for 23.4m,  $90^\circ$

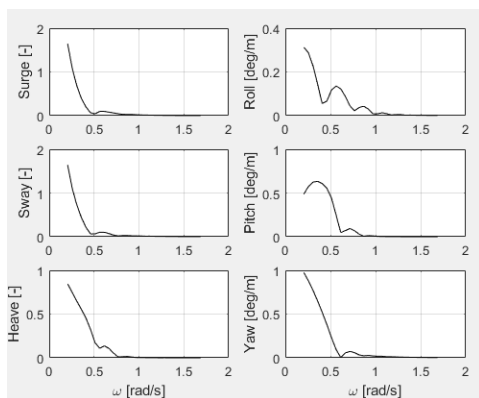


Figure 6.33: RAOs for 23.4m,  $135^\circ$

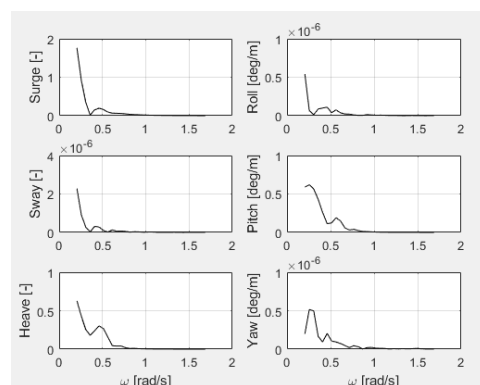


Figure 6.34: RAOs for 23.4m,  $180^\circ$

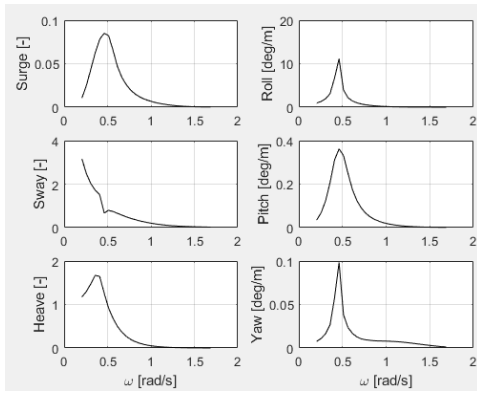


Figure 6.35: RAOs for 21.6m, 90°

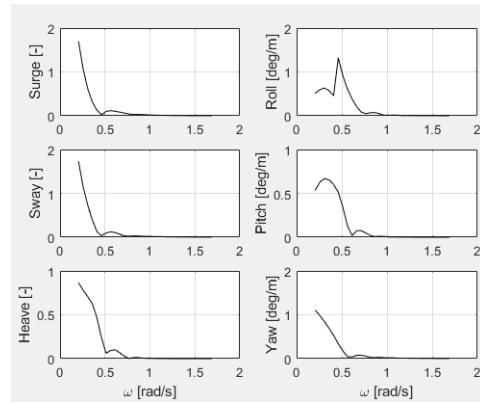


Figure 6.36: RAOs for 21.6m, 135°

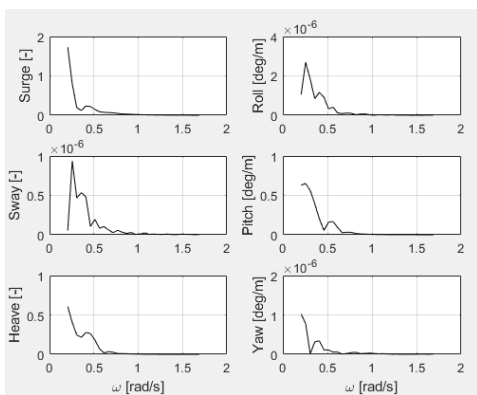


Figure 6.37: RAOs for 21.6m, 180°

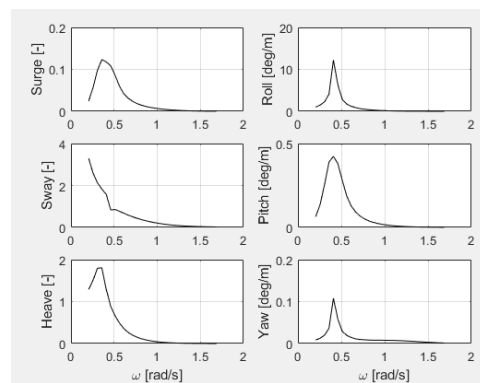


Figure 6.38: RAOs for 19.8m, 90°

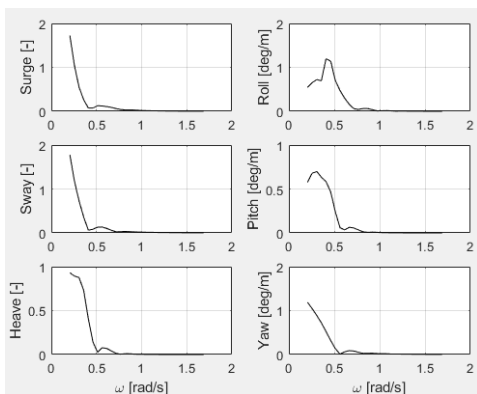


Figure 6.39: RAOs for 19.8m, 135°

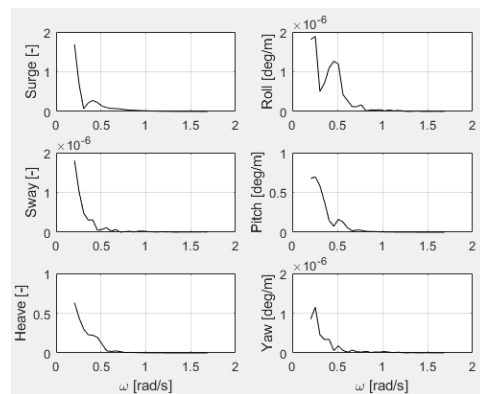


Figure 6.40: RAOs for 19.8m, 180°

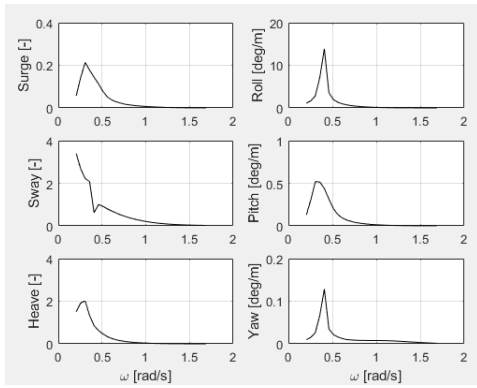


Figure 6.41: RAOs for 18.7m,  $90^\circ$

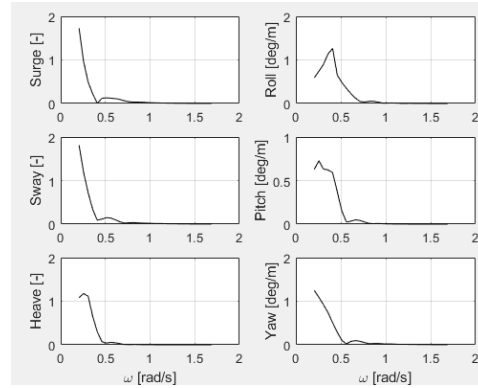


Figure 6.42: RAOs for 18.7m,  $135^\circ$

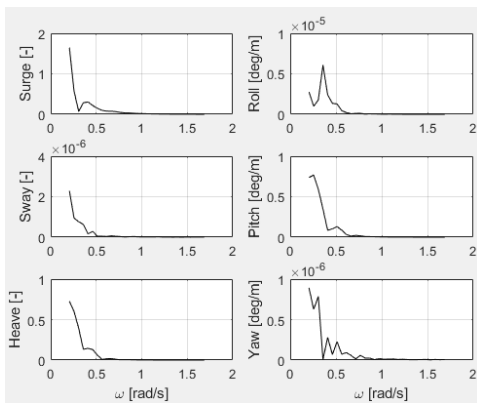


Figure 6.43: RAOs for 18.7m,  $180^\circ$

Figure 6.44 to 6.46 are vessel response spectrums for wave incidence  $90^\circ$ , water depth 25.2m.

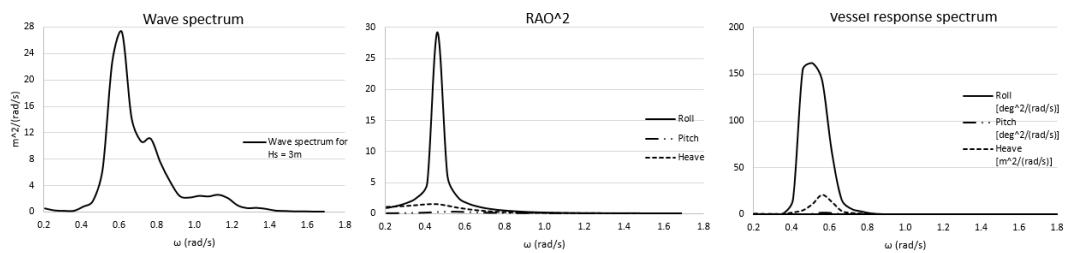


Figure 6.44: Vessel response spectrum for  $H_s = 3m$ , Direction =  $90^\circ$

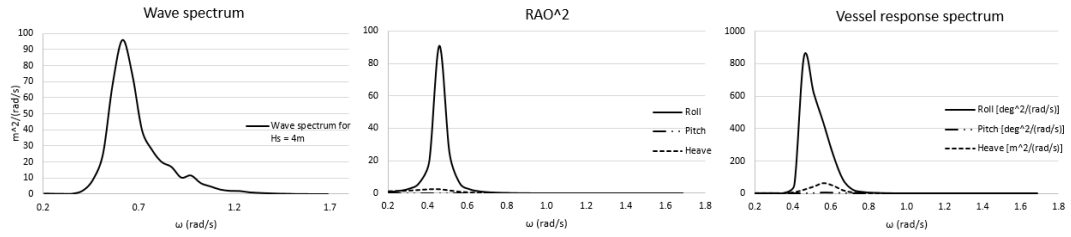


Figure 6.45: Vessel response spectrum for  $H_s = 4\text{m}$ , Direction =  $90^\circ$

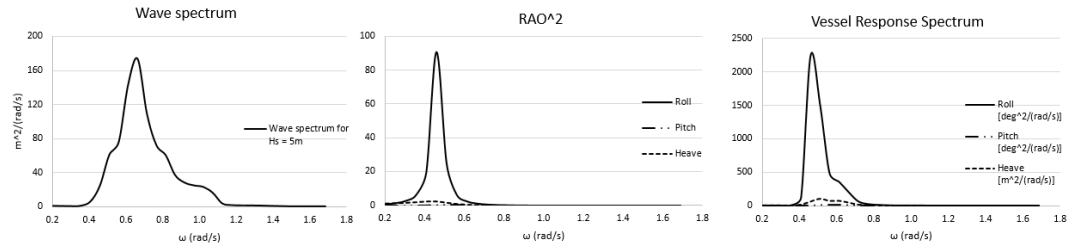


Figure 6.46: Vessel response spectrum for  $H_s = 5\text{m}$ , Direction =  $90^\circ$

Figure 6.47 to 6.49 are vessel response spectrums for wave incidence  $135^\circ$ , water depth 21.6m.

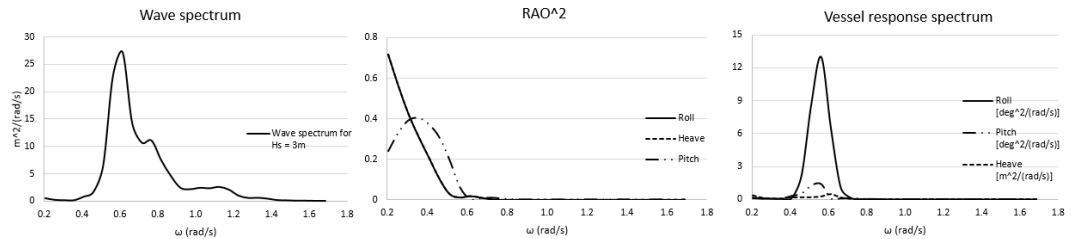


Figure 6.47: Vessel response spectrum for  $H_s = 3\text{m}$ , Direction =  $135^\circ$

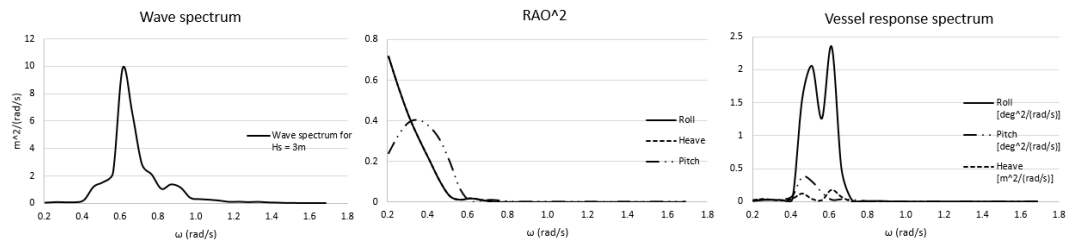


Figure 6.48: Vessel response spectrum for  $H_s = 4\text{m}$ , Direction =  $135^\circ$



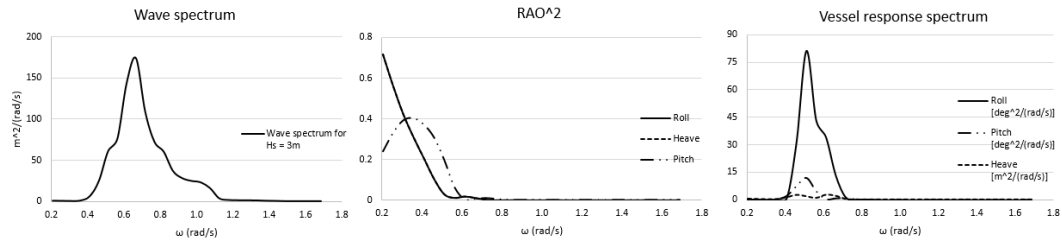


Figure 6.49: Vessel response spectrum for  $H_s = 5\text{m}$ , Direction =  $135^\circ$

Figure 6.50 to 6.52 are vessel response spectrums for wave incidence  $180^\circ$ , water depth 21.6m.

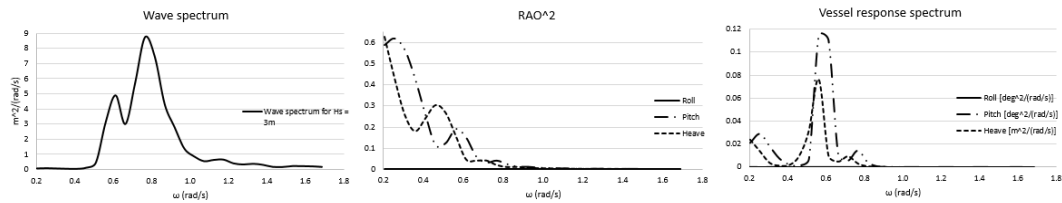


Figure 6.50: Vessel response spectrum for  $H_s = 3\text{m}$ , Direction =  $180^\circ$

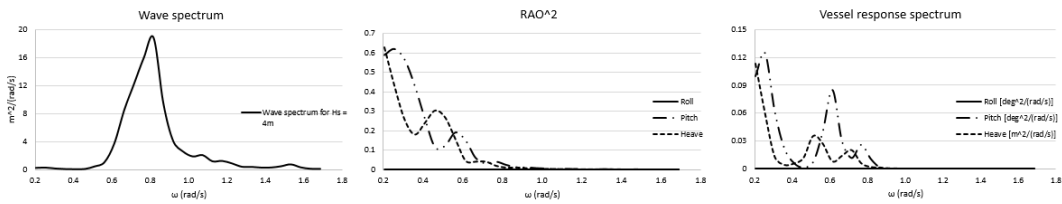


Figure 6.51: Vessel response spectrum for  $H_s = 4\text{m}$ , Direction =  $180^\circ$

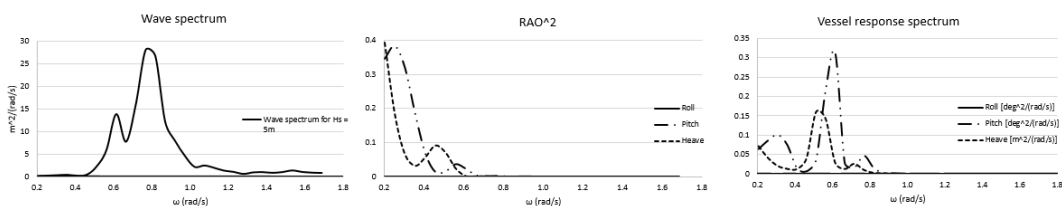


Figure 6.52: Vessel response spectrum for  $H_s = 5\text{m}$ , Direction =  $180^\circ$

It is observed from Figure 6.44 to 6.49 that, vessel response spectra increases with an increase in wave heights, with roll being the largest for wave incidence angles  $90^\circ$ . Incident wave angle  $135^\circ$  experiences more roll motions although they are a lot less than those of wave incident angle  $90^\circ$ . Small pitch and heave

motions occur for both incidence angles  $90^\circ$  and  $135^\circ$  with almost similar magnitude.

Figures 6.50 to 6.52 shows that large pitch motions and small heave motions are observed for wave incident angle  $180^\circ$  vessel response spectra. The ship's bow and stern experience a combination of large pitch and some heave motions and almost no roll motions when the incidence wave angle is either  $0^\circ$  or  $180^\circ$ .

Figures A.3 to A.10 in Appendix A show wave spectra for the other simulated wave conditions,  $RAO^2$  and vessel response spectra plots for roll, pitch and heave for  $H_s = 1$  m, 2 m, 3 m, 4 m and 5 m for wave incidence angle  $90^\circ$ ,  $T_p = 10$ s and  $d/D = 1.1$  to 1.5. Figures A.15 to A.29 show the results for wave incidence angle  $135^\circ$  and Figures A.30 to A.44 show the results for wave incidence angle  $180^\circ$ , all with  $T_p = 10$ s for  $H_s = 3$ m, 4m and 5m.

### 6.2.5 Underkeel clearance

Underkeel clearance sensitivity tests were conducted during the physical model studies, using only beam waves ( $90^\circ$ ), for  $d/D = 1.1$ . Ship's underkeel clearances were tested for  $T_p = 10$ s and 12s, with increased wave heights until bottom touching occurred. The sensitivity tests are undertaken to establish the maximum depth at which the 150 kt DWT bulk carrier can operate before exceeding safety limits, with respect to different wave heights and peak periods for beam waves. The same exercise undertaken in the physical model is repeated using the Wavescat model as part of the calibration process.

The net underkeel clearance is calculated using equation 6.2 (Gourlay, 2007):

$$\text{Net UKC} = [\text{Chart Datum depth}] + [\text{Tide}] - [\text{Static draft}] - [\text{Squat, heel and wave response}] \quad (6.2)$$

Two types of underkeel clearance can be distinguished namely the static and net underkeel clearance. Static underkeel clearance only takes into account the vertical distance between a non-moving ship's maximum draught and the channel bed. Net underkeel clearance takes into account squat, heel and wave response factors which further reduce the vertical distance between the ship hull and the sea bottom as shown in Figure 6.53.

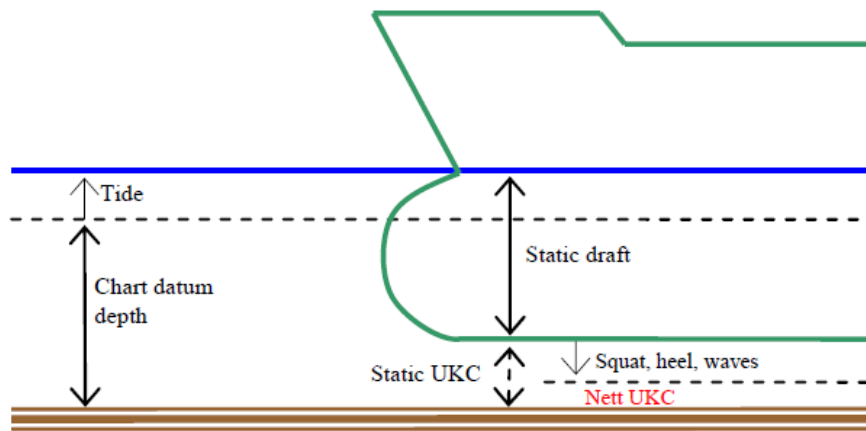


Figure 6.53: Factors affecting underkeel clearance

Since the 150kt deadweight bulk carrier ship model is tested for zero forward speed for calibration purposes, squat and turning heel become zero and only the draught and wave response of each tested wave condition are subtracted from the Chart datum depth plus tide. This results in equation 6.3, being used to calculate net underkeel clearance for the 150kt deadweight bulk carrier in the Wavescat model.

$$\text{Net UKC} = [\text{Chart Datum depth}] + [\text{Tide}] - [\text{Static draft}] - [\text{wave response}] \quad (6.3)$$

Average tide of 1m CD was added to the Mike 21BW depths, and will therefore, not be added to the computation of the underkeel clearance (including those in appendix C).

Beam waves for  $d/D = 1.1$  will be used for sensitivity tests as given in Table 6.25. Only beam waves are used to conduct underkeel clearance sensitivity tests because they cause the most vertical ship motions in these studies.  $H_s$  is increased for  $T_p = 10$  s and 12s, from 1m to 6m, to determine the effects of an increase in wave height on underkeel clearance.

Test no.	$H_s$ (m)	Depth (m)	$\alpha$ ( $^\circ$ )	$T_p$ (s)
1	1	20	90	10, 12
2	2	20	90	10, 12
3	3	20	90	10, 12
4	4	20	90	10, 12
5	5	20	90	10, 12
6	5.5	20	90	10, 12
7	6	20	90	10, 12

Table 6.25: Underkeel sensitivity test conditions

A depth of 20m is used instead of 18.7m as it is the shallowest measurement point in the Mike21BW grid. Table 6.26 shows how the keel points are calculated.

Axis	Midship	Bow shoulders	Port shoulders	Starboard quarter	Port quarter	Starboard	Stern
x	0	$0 \times L$	$0.33 \times L$	$0.33 \times L$	$-0.33 \times L$	$-0.33 \times L$	$-0.33 \times L$
y	0	0	$0.5 \times B$	$-0.33 \times B$	$0.33 \times B$	$-0.33 \times B$	0
z	0	-D	-D	-D	-D	-D	-D

Table 6.26: Hull keel points

B is breadth, D is draught, Keel1 = Midship, Keel2 = Bow, Keel3 = Starboard shoulder, Keel4 = Port Shoulder, Keel5 = Starboard quarter, Keel6 = Port shoulder and Keel7 = Stern. It is accepted that all 6 probe points along the channel (excluding the Waverider probe point) in Mike21BW have a depth of 20m. Figures 6.54 to 6.67 shows side by side, underkeel clearance for hull motion amplitudes ( $A_s$ ) of  $T_p = 10$ s and 12s, at 0 m/s speed. Equation 6.3 is used to compute the underkeel clearance figures.

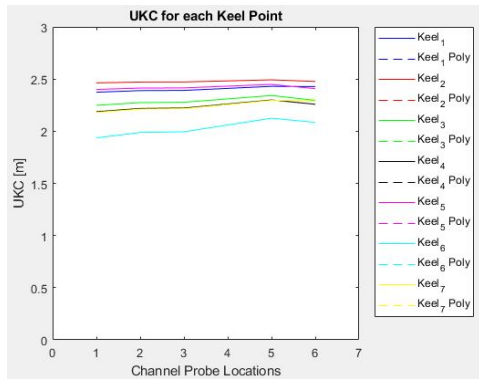


Figure 6.54: Underkeel clearance for  $H_s = 1\text{m}$ ,  $T_p = 10\text{s}$

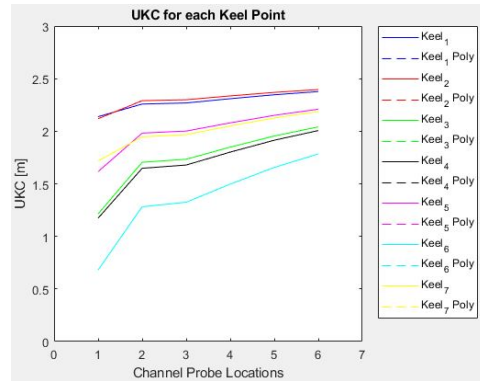


Figure 6.55: Underkeel clearance for  $H_s = 1\text{m}$ ,  $T_p = 12\text{s}$

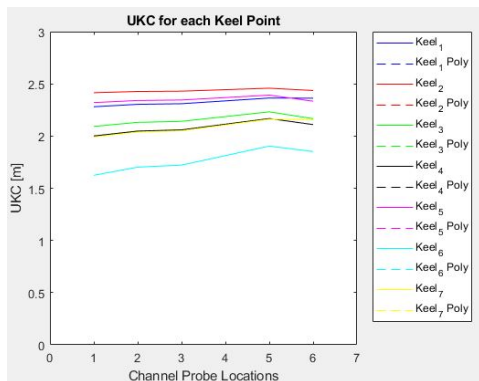


Figure 6.56: Underkeel clearance for  $H_s = 2\text{m}$ ,  $T_p = 10\text{s}$

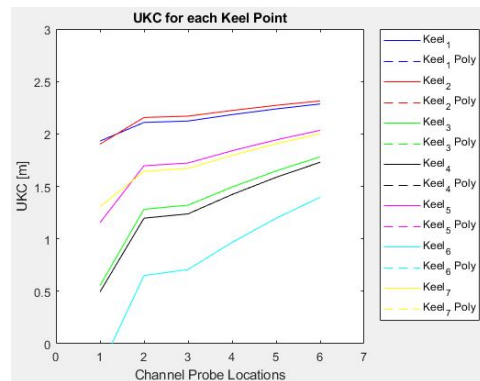


Figure 6.57: Underkeel clearance for  $H_s = 2\text{m}$ ,  $T_p = 12\text{s}$

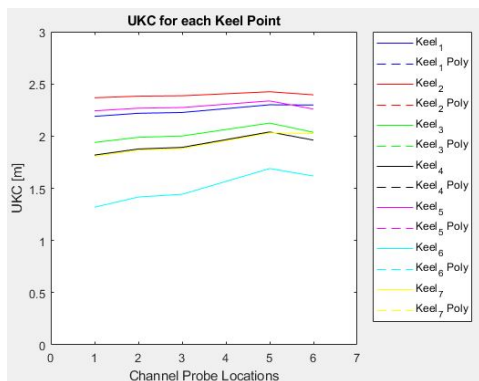


Figure 6.58: Underkeel clearance for  $H_s = 3\text{m}$ ,  $T_p = 10\text{s}$

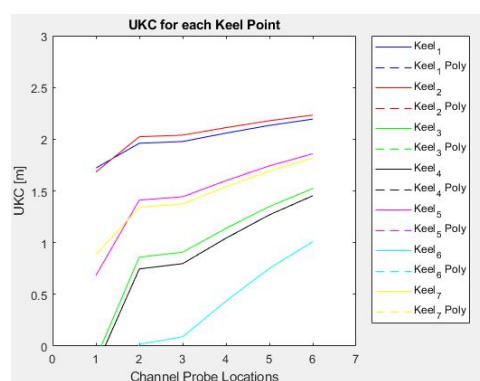


Figure 6.59: Underkeel clearance for  $H_s = 3\text{m}$ ,  $T_p = 12\text{s}$

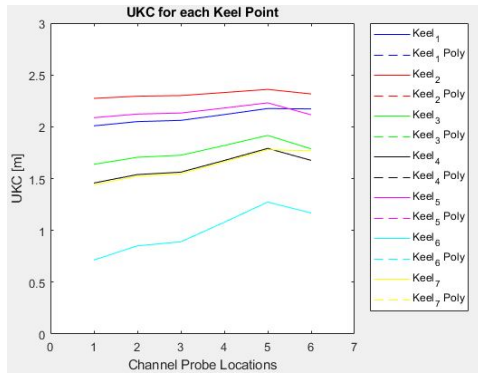


Figure 6.60: Underkeel clearance for  $H_s = 4\text{m}$ ,  $T_p = 10\text{s}$

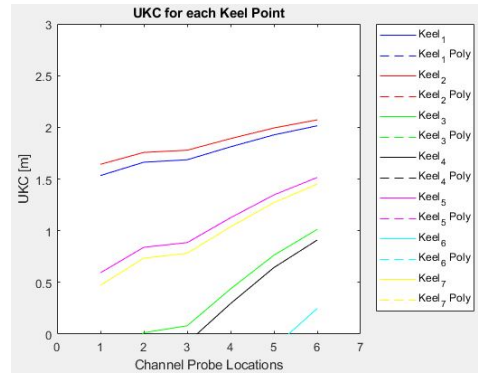


Figure 6.61: Underkeel clearance for  $H_s = 4\text{m}$ ,  $T_p = 12\text{s}$

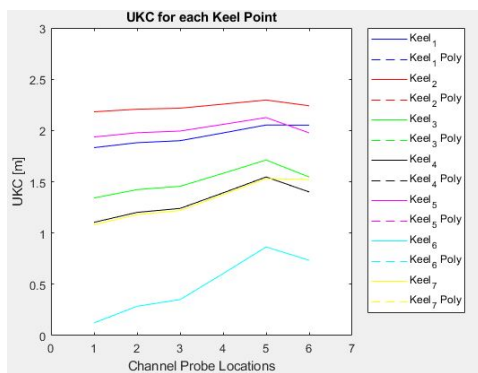


Figure 6.62: Underkeel clearance for  $H_s = 5\text{m}$ ,  $T_p = 10\text{s}$

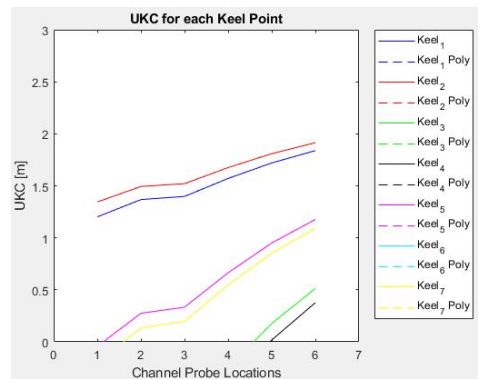


Figure 6.63: Underkeel clearance for  $H_s = 5\text{m}$ ,  $T_p = 12\text{s}$

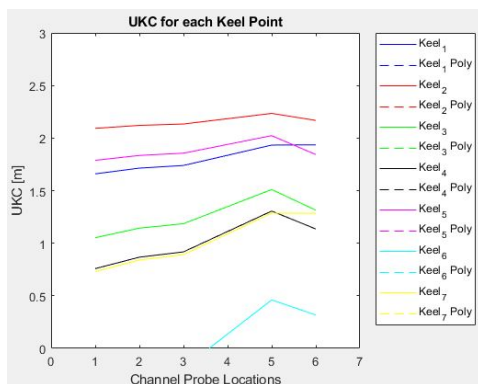


Figure 6.64: Underkeel clearance for  $H_s = 5.5\text{m}$ ,  $T_p = 10\text{s}$

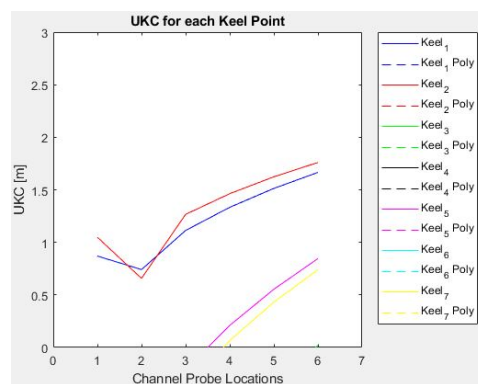


Figure 6.65: Underkeel clearance for  $H_s = 5.5\text{m}$ ,  $T_p = 12\text{s}$

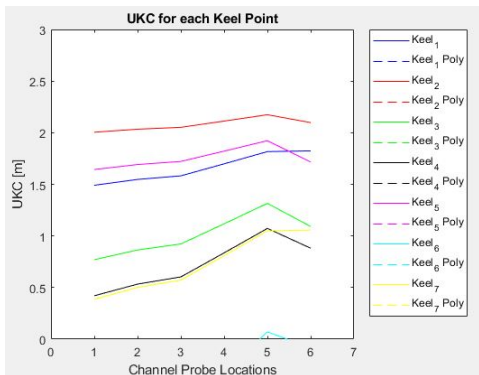


Figure 6.66: Underkeel clearance for  $H_s = 6\text{m}$ ,  $T_p = 10\text{s}$

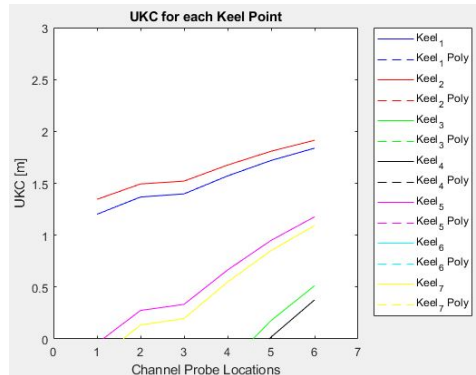


Figure 6.67: Underkeel clearance for  $H_s = 6\text{m}$ ,  $T_p = 12\text{s}$

It can be observed from Figure 6.54 to 6.67 that all the tested wave heights and peak periods for the sensitivity tests, exceed the underkeel clearance limit of 2 m. It can also be observed from all the  $T_p = 12\text{ s}$  figures that keel points decrease sharply between channel probe location 1 (water depth = 20 m) and 2 (water depth = 21 m) whereas a gradual decrease can be observed for channel probe location 3 (water depth = 22 m), 4 (water depth = 23 m), 5 (water depth = 24 m) and 6 (water depth = 25 m). Bottom touching for  $T_p = 10\text{ s}$  occurs from  $H_s = 5\text{ m}$  and occurs from  $H_s = 2\text{ m}$  for  $T_p = 12\text{ s}$ . The figures also show that keel 6 (SSH) experiences grounding first for both  $T_p = 10\text{ s}$  and  $12\text{ s}$ . This means that the port shoulder touches sea bottom first in the Wavescat model for all the tested wave heights except  $H_s = 1\text{ m}$  to  $4\text{ m}$  for  $T_p = 10\text{ s}$  and  $H_s = 1\text{ m}$  for  $T_p = 12\text{ s}$ .

Figures 6.68 and 6.69 show how the significant wave height ( $H_s$ ) influences the significant hull motion amplitudes ( $A_s$ ) of beam waves, for  $d/D = 1.1$  and  $T_p = 10\text{ s}$  and  $12\text{ s}$ .

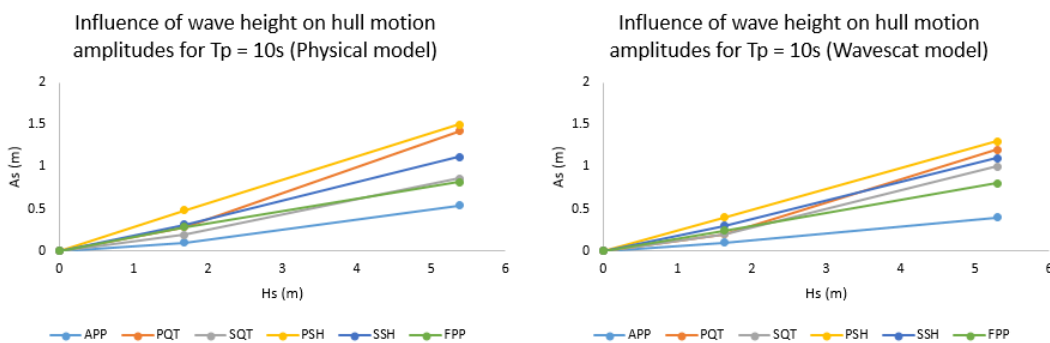


Figure 6.68: Influence of wave height on hull motion amplitudes for  $T_p = 10\text{s}$



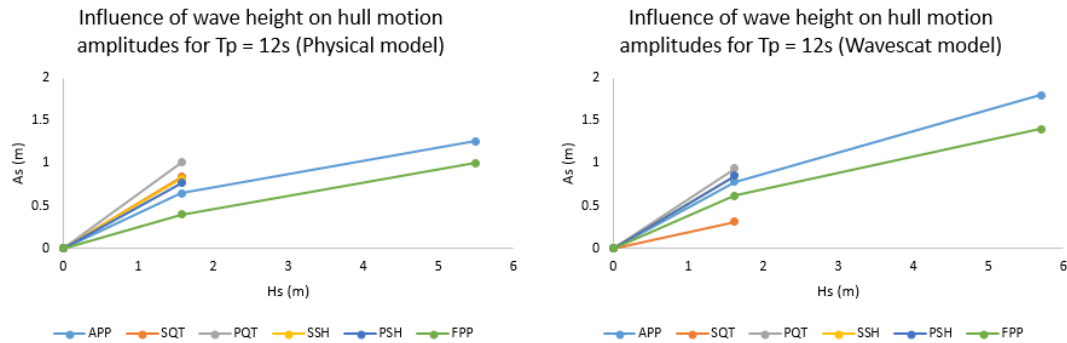


Figure 6.69: Influence of wave height on hull motion amplitudes for  $T_p = 12s$

A linear relationship between  $A_s$  and  $H_s$  can be observed from both the physical and the Wavescat models for  $T_p = 10 s$  which means an increase in wave height, leads to an increase in significant hull motion amplitudes. Figure 6.68 shows that the Wavescat model under-estimates the significant hull motion amplitudes when compared to physical model test results. This means that the Wavescat model over-predicts the influence of wave height on hull motion amplitudes for  $T_p = 10 s$  when compared to the physical model.

Figure 6.69 shows that the linear pattern changes slightly for  $T_p = 12s$ . This means that peak period of 12 s experiences an increase of significant hull motion amplitudes with an increase in wave heights, although the relationship is not linear in both the physical and Wavescat model. The more the wave height increases, the less linear  $A_s$  and  $H_s$  relationship becomes. The Wavescat model under-predicts the influence of wave height on hull motion amplitudes for  $T_p = 10 s$  when compared to the physical model.

### 6.3 Keel points probabilistic investigations

Ship motion time-series superposition of sinusoidal responses are created from ship motion spectra for heave, roll and pitch by using a phase compiling for each frequency. From the timeseries, the individual ship motion amplitudes are computed and fitted to extreme probability distributions. The ship motion amplitudes are fitted to the selected probability distributions to investigate the non-linearity patterns, but only for  $A_s$  greater than 1.5 m. The Weibull, Generalized Extreme Value and the Generalized Pareto distributions have been used historically to determine the non-linear trends of extreme events (Zhang *et al.*, 2019). Although the Generalized Extreme Value and the Generalized Pareto distributions are used to measure longer data with periods ranging from days to years, both the probability distributions are included in these studies, to find out if they can, to some extent, represent the non-linearity of significant hull motion amplitudes in this study.



### 6.3.1 Wave spectra

Fast Fourier Transformation (FFT) is used to generate wave spectra from Mike 21BW timeseries. The timeseries are computed for a period of 30 minutes. The first 5 minutes of each timeseries are considered a warm-up period which is the time it takes the waves to reach the Port. During post-processing of the Mike21BW timeseries, only waves that developed after 5 minutes are considered, reducing the record length to 25 minutes.

### 6.3.2 Generation of ship motion timeseries

It is from these wave spectra that ship motion timeseries for a combination of heave, roll and pitch are generated by following the Crossland (1990) and Branlard (2010) 's methods. Firstly, the wave spectrum frequency is changed to wave encounter frequencies through a process called warping given by equation 6.4

$$\omega_e = \omega - \frac{\omega^2 V \cos(\mu)}{g} \quad (6.4)$$

where  $V$  is the speed and  $\mu$  is the heading degrees. The spectral ordinate is given by:

$$S_\zeta(\omega_e) = \frac{S_\zeta(\omega)}{\left(1 - \frac{2\omega V \cos(\mu)}{g}\right)} \quad (6.5)$$

Discrete amplitudes of the vessel response spectrum are then calculated by using equation 6.6:

$$\zeta_{no} = \sqrt{2S_\zeta(\omega_e)\delta\omega_e} \quad (6.6)$$

where  $S_\zeta$  is the wave spectrum ( $m^2/(\text{rad/s})$ ). The angular frequency interval is given by:

$$\delta\omega_e = \left(1 - \frac{2\omega V \cos(\mu)}{g}\right)\delta\omega \quad (6.7)$$

Since in this study forward speed is zero, the encounter wave frequency becomes equivalent to the wave frequency given by equation 6.8:

$$\omega_e = \omega \quad (6.8)$$

The spectral ordinate equation reduces to:

$$S_\zeta(\omega_e) = S_\zeta(\omega) \quad (6.9)$$

and the encounter frequency interval becomes:

$$\delta\omega_e = \delta\omega \quad (6.10)$$

Due to the loss of phase data during the generation of the vessel response spectra, the original timeseries cannot be recreated. Instead, random phases

from  $-\pi$  to  $\pi$ , will be used to generate the timeseries. Equation 6.11 is used to generate the timeseries.

$$\zeta(t) = \sum_{n=1}^N \zeta_{no} \cos(\omega_e t + e_\zeta) \quad (6.11)$$

where  $t$  is time in seconds and  $e_\zeta$  is the random phase angle.

Two hour long ship motions timeseries, with 120 000 timesteps and an interval of 0.06s for each depth to draught ratio, are created from all the vessel response spectra. Since interest is in finding the probability distributions of ship motion oscillations, only individual amplitudes of the timeseries will be considered.

The zero-upcrossing method is used to determine all the amplitudes in the timeseries. From the two hours long timeseries only  $T_p = \pm 10s$  is considered. It is from these timeseries that ship motion wave amplitudes are generated. Equation 6.12 shows how the zero crossing period is calculated for each timeseries.

$$T_z = \frac{T_r}{N_z} = \frac{(120000 \times 0.06)}{(\pm 11915 \times 0.06)} = \frac{7200}{714.9} \approx 10.07s \quad (6.12)$$

where  $T_r$  is the length of the timeseries and  $N_z$  is the number of zero upcrossing crests in the timeseries with  $T_p \pm 10s$ .  $T_r$  and  $N_z$  values are computed using the Mike Zero Wave crossing analysis tool for each timeseries.

The completed ship motion amplitude timeseries are categorized by wave height and direction, before being fitted to the  $A_s$  distributions.

### 6.3.3 Rayleigh distribution

As mentioned in the CSIR 1991 report, a Rayleigh distribution was found to be the most suitable distribution to fit the linear relationship of  $A_s$  and  $A_{max}$  for  $A_s$  of no more than 1.5m.  $A_s$  of  $H_s = 3m, 4m$  and  $5m$  are computed to define the behaviour of the hull motion amplitudes ( $A_s$ ) of ships that interact with wave heights of more than 3m.

$A_s$  is calculated from the ship motion amplitude timeseries as the average of the highest one-third of the amplitude, as given by equation 6.13 (U.S. Army Corps of Engineers, 2002a)

$$A_s = \frac{1}{N/3} \sum_1^{N/3} A_i \quad (6.13)$$

where  $N$  is the number of individual ship motion amplitudes.

Using the Rayleigh distribution, the most probable extreme value ( $\mu(A_{max})$ ) is given by equation 6.14. The most probable extreme values for port quarter (PQT) or port shoulder (PSH) is given by Table 6.27, 6.28 and 6.29 for each wave heights and incident wave angle.

$$\mu(A_{max}) = \frac{1}{\sqrt{2}}(\ln N)^{0.5} \cdot A_s \quad (6.14)$$

where N is obtained by dividing 7200s by  $T_z$  10s, which makes  $N = 720$ .  $\mu(A_{max})/A_s = 2.3$ .

$H_s$ (m)	$A_s$ (m)	$\mu(A_{max})$ (m)
3	1.29	3.04
4	2.41	5.07
5	3.2	6.74

Table 6.27: Rayleigh distribution's estimated maximum value for PQT/PSH, incident wave angle  $90^\circ$

$H_s$ (m)	$A_s$ (m)	$\mu(A_{max})$ (m)
3	0.21	0.50
4	0.22	0.51
5	0.23	0.52

Table 6.28: Rayleigh distribution's estimated maximum value for PQT/PSH, incident wave angle  $135^\circ$

$H_s$ (m)	$A_s$ (m)	$\mu(A_{max})$ (m)
3	0.042	0.099
4	0.047	0.111
5	0.054	0.128

Table 6.29: Rayleigh distribution's estimated maximum value for PQT/PSH, incident wave angle  $180^\circ$

The Rayleigh probability density function is given by equation 6.15 (Archer, 1967)

$$f(x) = \frac{x}{\sigma^2} e^{-\frac{x^2}{2\sigma^2}} \quad (6.15)$$

where  $\sigma$  is a normalizing factor given by equation 6.2.11

$$\sigma = \frac{\bar{r}}{1.2533} \quad (6.16)$$

and  $\bar{r}$  is given by

$$\bar{r} = \frac{1}{n} \sum_{i=1}^n r_i \quad (6.17)$$

As represents ship motion amplitudes on the probability plots. Each wave height is ran individually for water depth 25.2 m, 23.4 m, 21.6 m, 19.8 m and 18.7 m which means five runs where computed for  $H_s = 3$  m, 4 m and 5 m. The ship motion amplitude runs are then categorized according to wave heights and merged, making the two hours run for each water depth, 10 hours long ship motion amplitude timeseries for incident wave angle of  $90^\circ$ . Theses 10 hours long ship motions amplitude are then fitted to Rayleigh, Weibull, Generalized Extreme Value and Generalized Pareto probability distributions.

Figure 6.70 to 6.72 shows the Rayleigh probability density function and probability plots for  $H_s = 3$  m, 4 m and 5 m, respectively for a wave incident direction  $90^\circ$  and  $T_p = 10$  s.

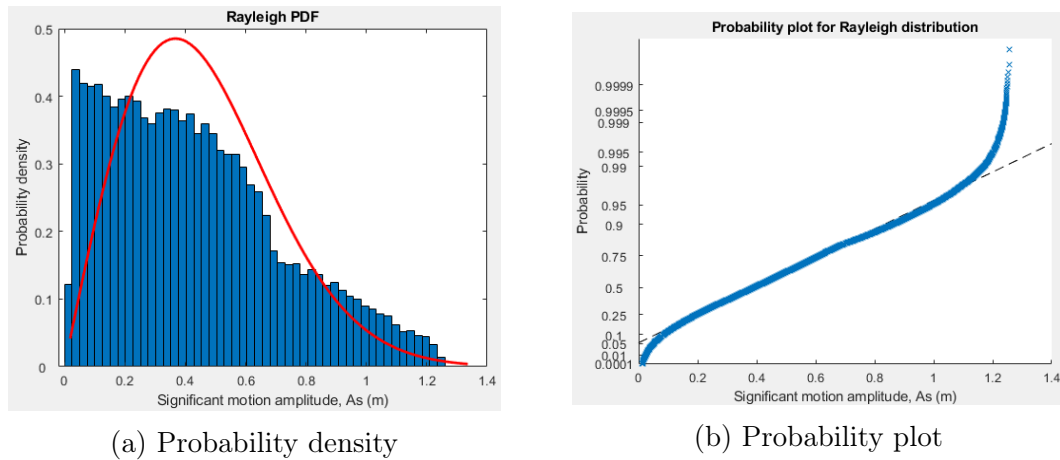


Figure 6.70: Rayleigh distribution density function and probability plot for ship motion amplitudes with  $H_s = 3$  m

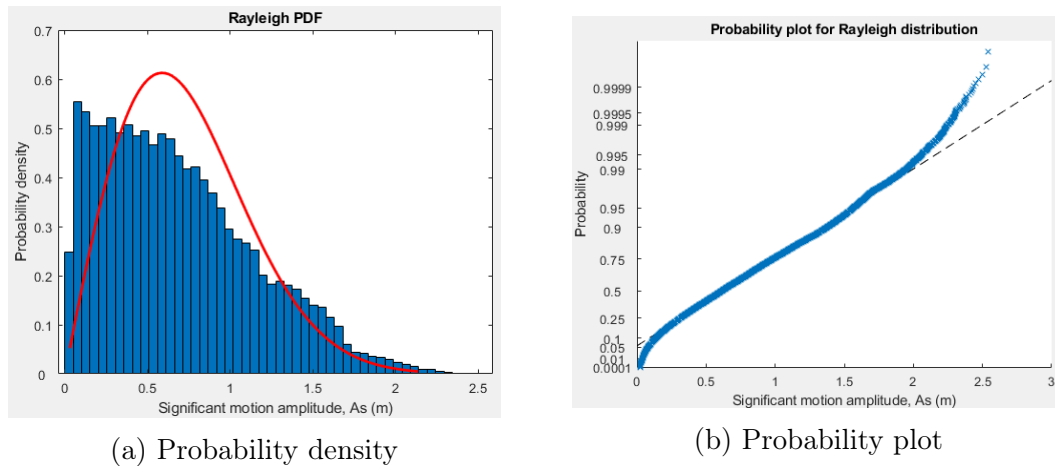


Figure 6.71: Rayleigh distribution density function and probability plot for ship motion amplitudes with  $H_s = 4\text{m}$

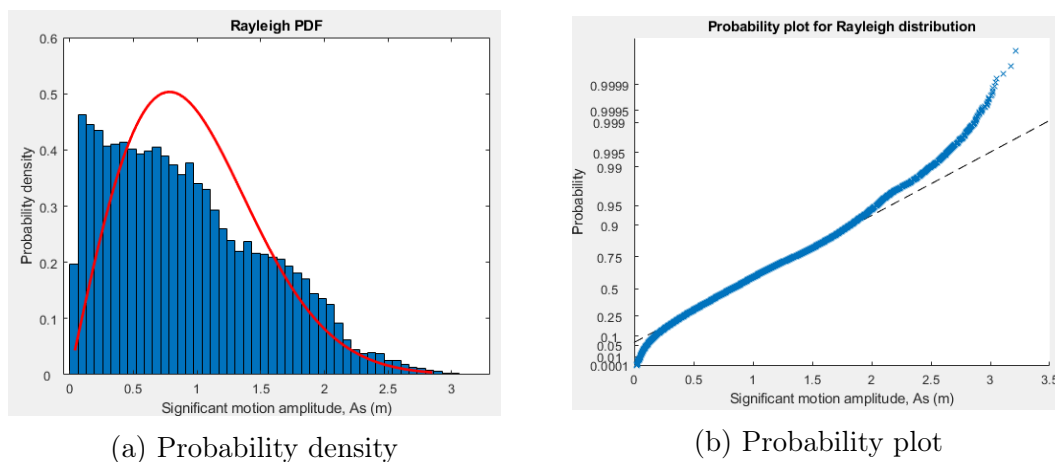


Figure 6.72: Rayleigh distribution density function and probability plot for ship motion amplitudes with  $H_s = 5\text{m}$

It can be observed from Figures 6.70 to 6.72 that the ship motions amplitude data fits the Rayleigh distribution to some extent. Ship motions amplitude for  $H_s = 3\text{m}$  deviates from  $A_s = 1\text{m}$  and ship motions amplitude for  $H_s = 4\text{m}$  and  $5\text{m}$  deviates from  $A_s = 2\text{m}$ . This means that the Rayleigh distribution is applicable to ship motion amplitudes for beam waves, to a certain extent depending on significant wave height.

### 6.3.4 Weibull distribution

As with the Rayleigh distribution, Weibull distribution belongs to the continuous probability distribution where the density function is given by equation

6.18 (Lai, 2006)

$$f(x) = e^{-(x/\lambda)^k} \quad (6.18)$$

where  $k$  is the shape parameter and  $\lambda$  is the scale parameter, given by

$$\lambda = \frac{\text{mean}(x)}{\Gamma(1 + (1/k))} \quad (6.19)$$

and  $k$  is given by equation

$$k = \left( \frac{\text{mean}(x)}{\text{std}(x)} \right)^{1.086} \quad (6.20)$$

Figures 6.73 to 6.75 presents Weibull probability density function and probability plots for  $H_s = 3\text{m}$  to  $5\text{m}$ , respectively for a wave incidence angle of  $90^\circ$  and  $T_p = 10\text{s}$ .

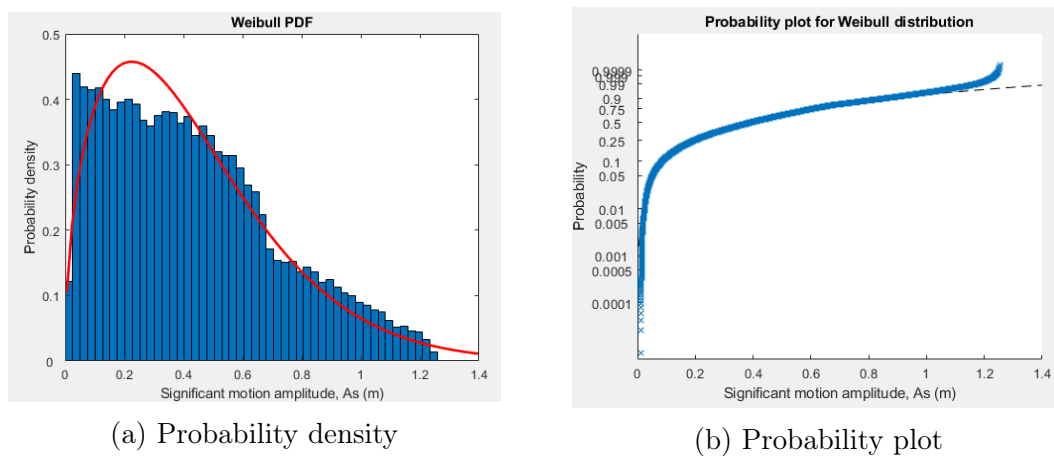


Figure 6.73: Weibull distribution density function and probability plot for ship motion amplitudes with  $H_s = 3\text{m}$

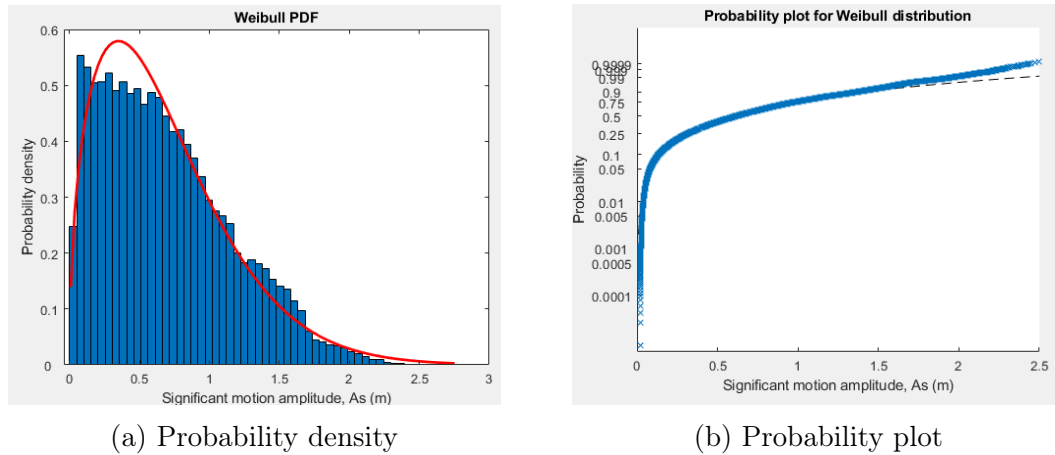


Figure 6.74: Weibull distribution density function and probability plot for ship motion amplitudes with  $H_s = 4\text{m}$

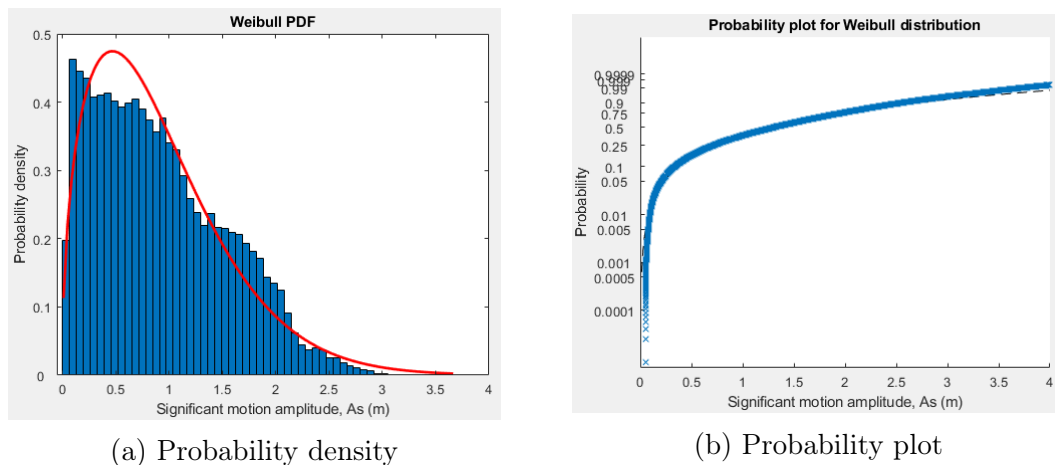


Figure 6.75: Weibull distribution density function and probability plot for ship motion amplitudes with  $H_s = 5\text{m}$

It can be observed from Figures 6.73 to 6.75 that the ship motion amplitudes for  $H_s = 3\text{m}$ ,  $4\text{m}$  and  $5\text{m}$  all fit the Weibull distribution very well, with deviation from  $A_s = 1.2\text{m}$  for  $H_s = 3\text{m}$  and deviation from  $A_s = 2\text{m}$  for  $H_s = 4\text{m}$  and  $5\text{m}$ . The probability results mean that the Weibull distribution is also applicable to beam waves to a certain extent.

### 6.3.5 Generalized Extreme Value distribution

Generalized extreme value distribution (GEV) belongs to a family of continuous probability distributions and can be described as a limiting distribution of the

maximum of series of independent, but identically distributed random variables. Its function is to help determine the tail of extremes of data that have been recorded. This theory of extreme values combines Gumbel, Fréchet and Weibull theorems (Martins and Stedinger, 2000; Shukla, 2010; Teena *et al.*, 2012).

The GEV density function ((Mathworks, 2018a)) is given by

$$F(x) = \frac{1}{\sigma} e^{-(1+k(\frac{x-\mu}{\sigma})^{-\frac{1}{k}})(1+k\frac{x-\mu}{\sigma})^{-1-\frac{1}{k}}} \quad (6.21)$$

for  $\kappa \neq 0$  and

$$F(x) = \frac{1}{\sigma} e^{-e^{-(\frac{x-\mu}{\sigma})} - (\frac{x-\mu}{\sigma})} \quad (6.22)$$

for  $\kappa = 0$

Figures 6.76 to 6.78 shows the Generalized Extreme Value (GEV) probability density function and probability plots for  $H_s = 3\text{m}$  to  $5\text{m}$ , respectively, for wave incident direction of  $90^\circ$  and  $T_p = 10\text{s}$ .

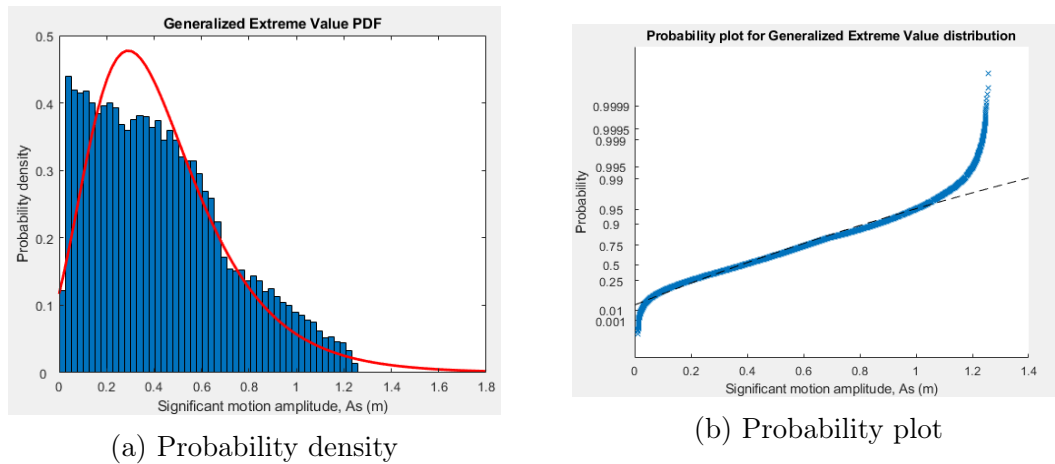


Figure 6.76: Generalized Extreme Value distribution density function and probability plot for ship motion amplitudes with  $H_s = 3\text{m}$



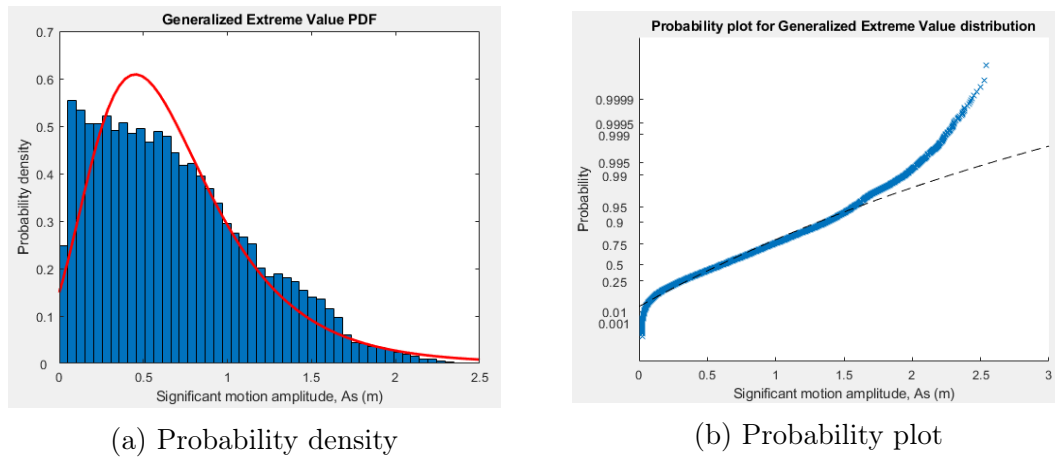


Figure 6.77: Generalized Extreme Value distribution density function and probability plot for ship motion amplitudes with  $H_s = 4\text{m}$

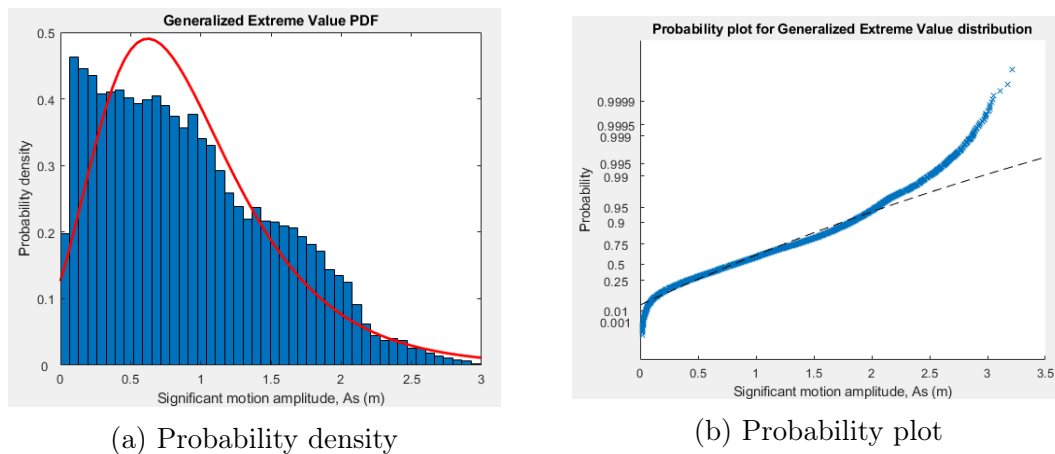


Figure 6.78: Generalized Extreme Value distribution density function and probability plot for ship motion amplitudes with  $H_s = 5\text{m}$

Figures 6.76 to 6.78 shows that the Generalized Extreme Value distribution (GEV) fits the ship motions amplitude to some extent. The probability deviation for  $H_s = 3\text{m}$  starts from  $A_s = 1\text{m}$ , the deviation for  $H_s = 4\text{m}$  starts from  $A_s = 1.5\text{m}$  and the deviation for  $H_s = 5\text{m}$  starts from  $A_s = 2\text{m}$ . Given that the Generalized Extreme Value distribution is used to fit the tails of extreme events, the ship motions amplitude data is not well represented as the tail deviates from the probability distribution. Since the significant motion amplitude timeseries is two hours long, the ship motion amplitude data might not be sufficient enough to fit to the GEV since the distribution is more applicable to longer timeseries.

### 6.3.6 Generalized Pareto distribution

Generalized Pareto (GP) is a logarithmic distribution which belongs to the continuous distribution family and is used to model tails of extreme distributions (Castillo and Daoudi, 2010).

The GP's density function (Mathworks, 2018b) is given by

$$f(x) = \frac{1}{\sigma} \left(1 + k \frac{x - \theta}{\sigma}\right)^{-1 - \frac{1}{k}} \quad (6.23)$$

for shape parameter  $k \neq 0$

and

$$f(x) = \frac{1}{\sigma} e^{-\left(\frac{x - \theta}{\sigma}\right)} \quad (6.24)$$

for shape parameter  $k = 0$

A shape parameter  $k = 0$  and a threshold parameter  $\theta$  of 0 is selected. The threshold parameter is used to define the minimum value in the significant motion amplitude data. Figures 6.79 to 6.81 show the Generalized Pareto distribution probability density function and probability plots for  $H_s = 3\text{m}$  to  $5\text{m}$ , wave incident direction of  $90^\circ$  and  $T_p = 10\text{s}$ .

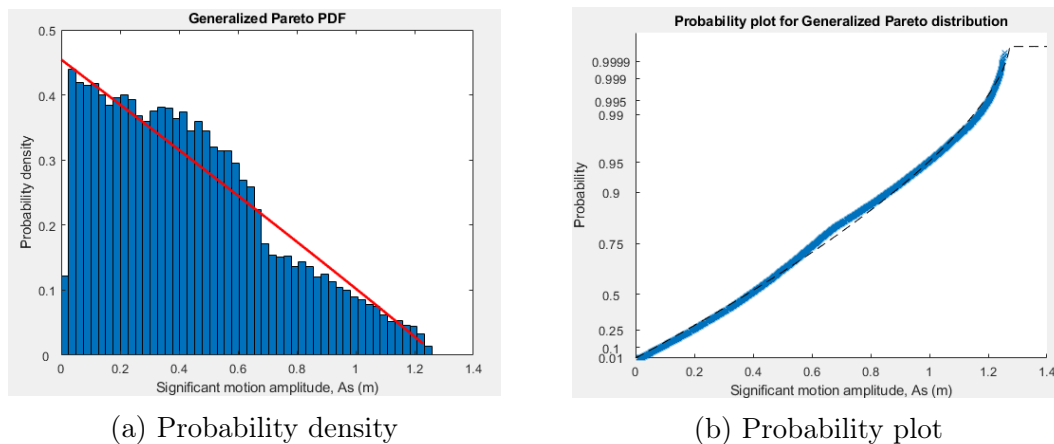


Figure 6.79: Generalized Pareto distribution density function and probability plot for ship motion amplitudes with  $H_s = 3\text{m}$

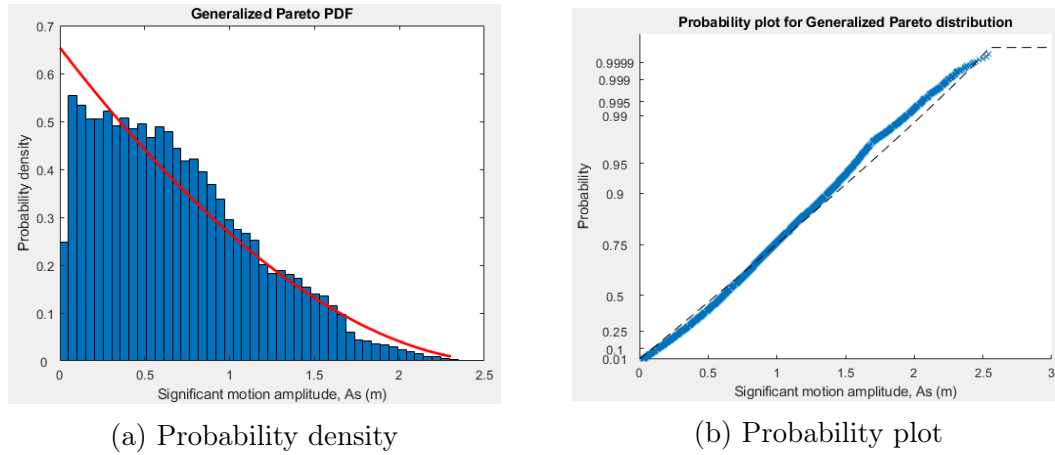


Figure 6.80: Generalized Pareto distribution density function and probability plot for ship motion amplitudes with  $H_s = 4\text{m}$

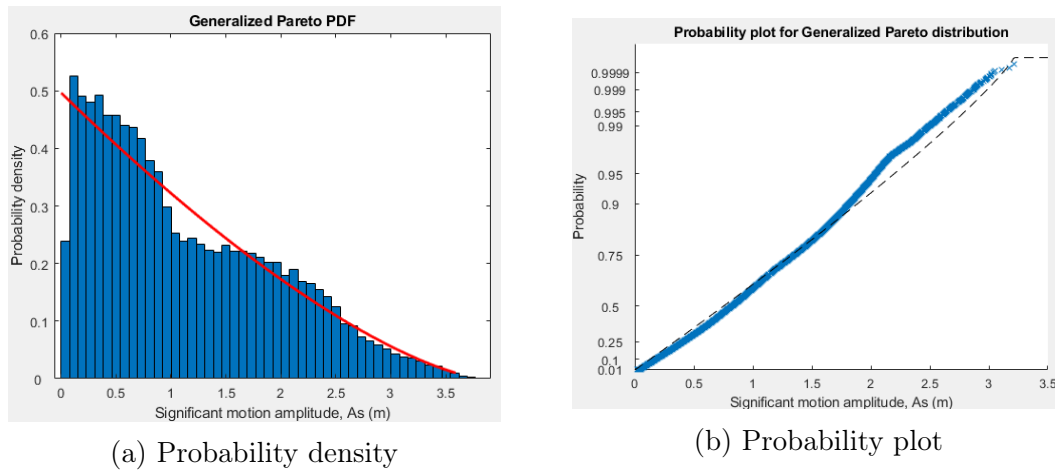


Figure 6.81: Generalized Pareto distribution density function and probability plot for ship motion amplitudes with  $H_s = 5\text{m}$

Figures 6.79 to 6.81 show that the significant motion amplitude data fits the Generalized Pareto probability distribution very well. This means that the probability distribution is a good fit and represents the non-linearity pattern of  $A_s$  above 1.5m much better than the other tested probability distributions.

## Chapter 7

# Modelling of Ship in Storm Conditions

The Wavescat is used to model a 150kt DWT fully laden bulk carrier moving at 4m/s speed along the Port of Richards Bay channel. Storm conditions with peak periods of  $T_p = 14s, 16s$  and  $18s$  and wave heights, 3m and 4m are selected and tested for wave incidence angles  $90^\circ$  and  $135^\circ$ .

### 7.1 Underkeel clearance for 4m/s ship speed

Equation 6.2 is used to calculate underkeel clearance. Squat and heel are calculated for different sections of the ship during vertical movement to determine the total sinkage or trim. Squat is given by equation 10.1 (Gourlay, 2007):

$$s = c_s \frac{\nabla}{L_{pp}^2} \frac{F_h^2}{\sqrt{1 - F_h^2}} \quad (7.1)$$

where  $s$  is the squat at the aft perpendicular,  $F_h = \frac{V}{\sqrt{gh}}$  which is the Froude number,  $V$  is speed,  $h$  is water depth,  $\nabla$  is ship displacement volume,  $g$  is gravity and  $c_s$  is bow or stern squat coefficient. Equation 10.1 is applicable to ships in open water or wide channels in shallow water. The International Commission for the Reception of Large Ships (ICORELS or I) recommends a squat coefficient  $c_s$  of 2.4 for ships with a block coefficient greater than 0.8 (PIANC, 2014). Since the 150kt DWT bulk carrier ship model's block coefficient is 0.828, squat values for different water depths is given in Table 7.1 and Figure 6.2.

Water depth (m)	Squat (m)
25	0.31
24	0.33
23	0.36
22	0.38
21	0.40
20	0.43

Table 7.1: Squat for ship speed of 4m/s

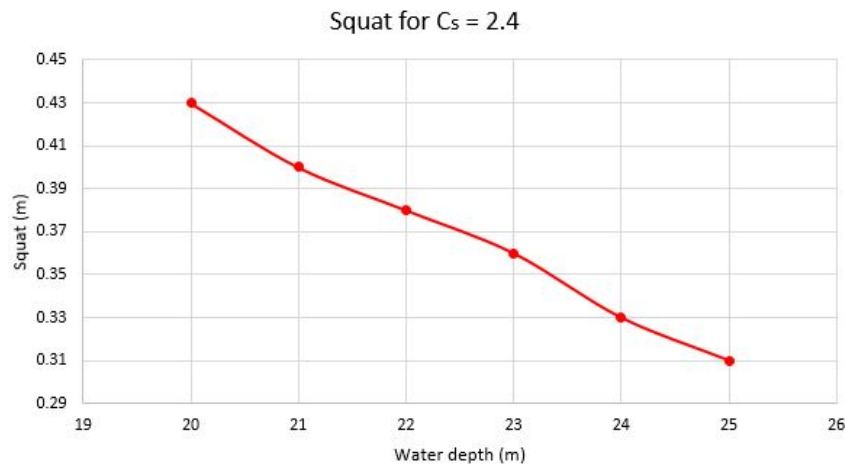


Figure 7.1: Squat for varying water depths

Heeling is given by equation 10.2 (Gourlay, 2007):

$$\phi = \frac{M}{mg\overline{GM}_T} \quad (7.2)$$

where  $\phi$  is the heel angle,  $M$  is the heeling moment,  $m$  is ship mass,  $g$  is gravity and  $\overline{GM}_T$  is the transverse metacentric height. Heeling can be caused by a ship turning or wind. The ship model sails straight into the Port of Richards Bay entrance channel where no turning of the 150 kt deadweight bulk carrier takes place therefore only wind heeling is taken into consideration. The wind heeling moment is given by equation 10.3 (DNV.GL, 2015):

$$M_w = 0.02 \frac{V_0^2}{L_{pp}} \cdot \Delta (KG - 0.05 \cdot D) \quad (7.3)$$

where  $M_w$  is the wind heeling moment,  $L_{pp}$  is length between perpendiculars (m),  $V$  is wind velocity (m/s),  $\Delta$  is ship displacement in ( $m^3$ ),  $KG$  is the centre of gravity above keel and  $D$  is draught (m). Using equation 10.3, wind heel

moment for 4m/s is  $M_w = 2358.76 \text{ Nm}$  and the heel angle from equation 10.2 becomes

$$\phi = \frac{25.5}{m} \tag{7.4}$$

where added mass  $m$  is also calculated in the Wavescat model. Added mass in roll is an important factor for a ship with forward speed since it accounts for 10 to 25% of mass moment of inertia (Kianejad *et al.*, 2017).

Figures 7.2 to 7.7 show how a ship moving at a speed of 4m/s affects the underkeel clearance for wave incidence  $90^\circ$  along the Port of Richards Bay channel for the varying water depths of 25m, 24m, 23m, 22m, 21m and 20m.

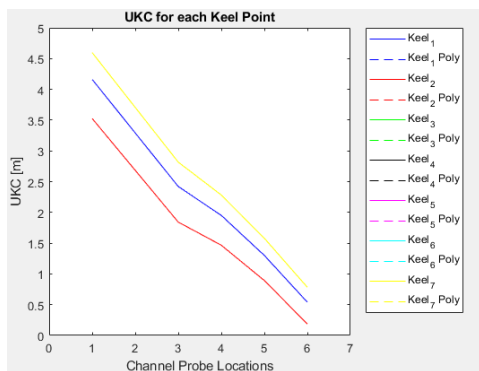


Figure 7.2: Underkeel clearance for  $H_s = 3\text{m}$ ,  $T_p = 14\text{s}$

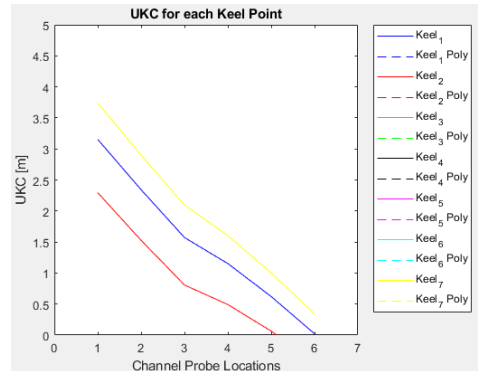


Figure 7.3: Underkeel clearance for  $H_s = 4\text{m}$ ,  $T_p = 14\text{s}$

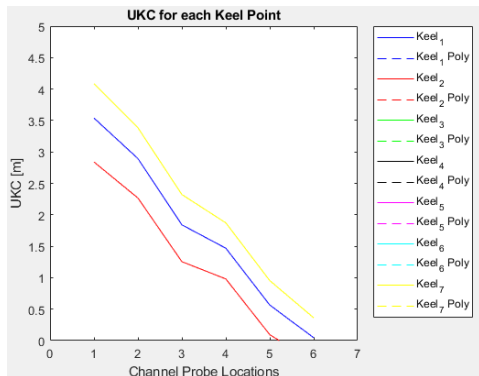


Figure 7.4: Underkeel clearance for  $H_s = 3\text{m}$ ,  $T_p = 16\text{s}$

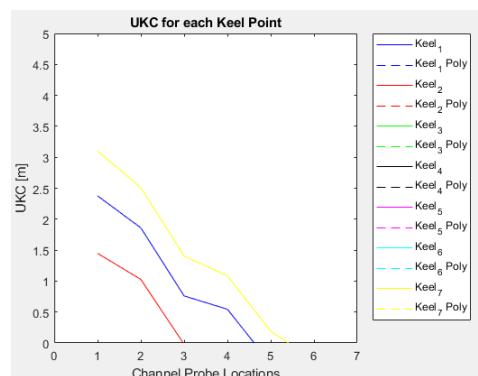


Figure 7.5: Underkeel clearance for  $H_s = 4\text{m}$ ,  $T_p = 16\text{s}$

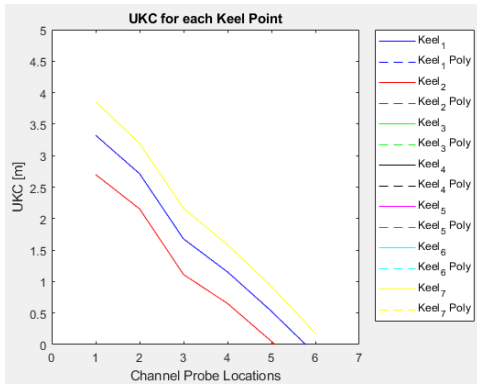


Figure 7.6: Underkeel clearance for  $H_s = 3\text{m}$ ,  $T_p = 18\text{s}$

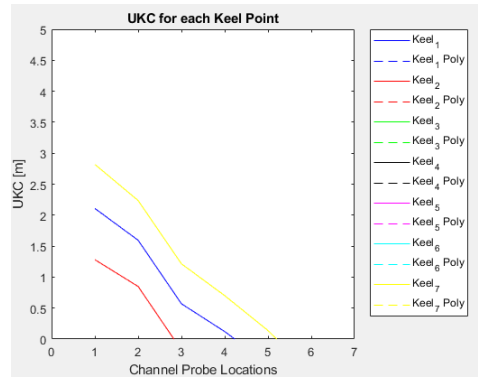


Figure 7.7: Underkeel clearance for  $H_s = 4\text{m}$ ,  $T_p = 18\text{s}$

Figures 7.8 to 7.13 show how the speed of 4m/s affects the underkeel clearance for wave incidence 135°.

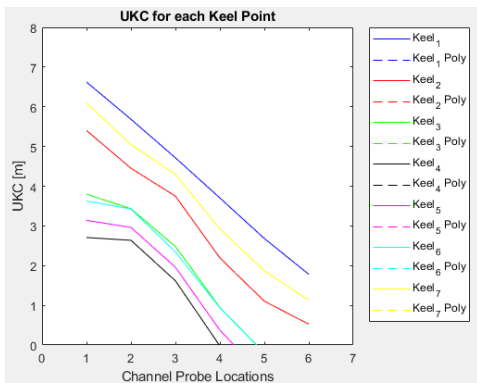


Figure 7.8: Underkeel clearance for  $H_s = 3\text{m}$ ,  $T_p = 14\text{s}$

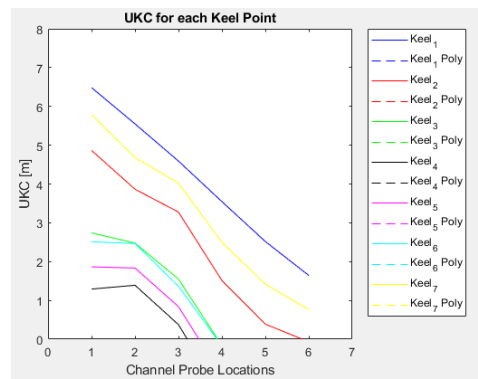


Figure 7.9: Underkeel clearance for  $H_s = 4\text{m}$ ,  $T_p = 14\text{s}$

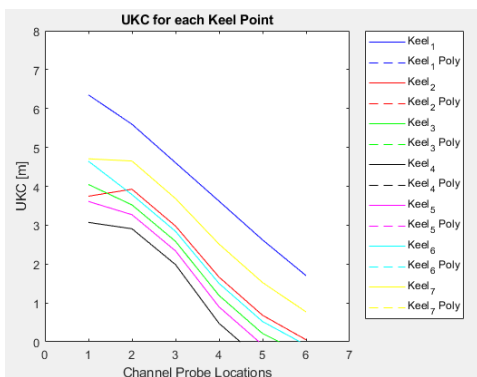


Figure 7.10: Underkeel clearance for  $H_s = 3\text{m}$ ,  $T_p = 16\text{s}$

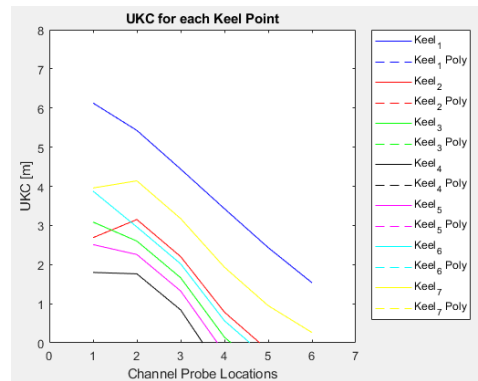


Figure 7.11: Underkeel clearance for  $H_s = 4\text{m}$ ,  $T_p = 16\text{s}$

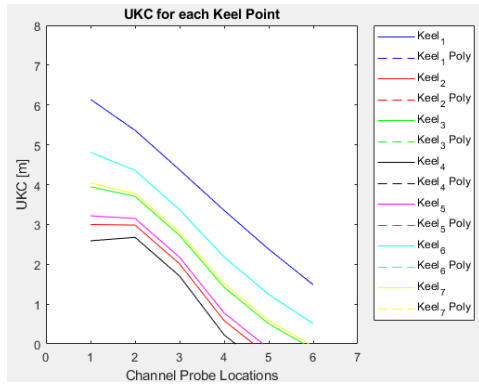


Figure 7.12: Underkeel clearance for  $H_s = 3m$ ,  $T_p = 18s$

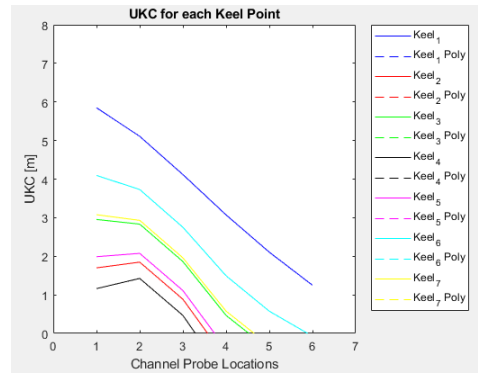


Figure 7.13: Underkeel clearance for  $H_s = 4m$ ,  $T_p = 18s$

Table 7.2 to 7.7 show the underkeel clearance keel point values for  $90^\circ$ .

Probe1	Probe2	Probe3	Probe4	Probe5	Probe6	Probe1	Probe2	Probe3	Probe4	Probe5	Probe6
4.575	3.783	2.916	2.582	1.840	1.024	3.671	2.948	2.188	1.956	1.288	0.600
2.811	1.917	1.183	0.939	0.504	-0.125	1.315	0.517	-0.054	-0.245	-0.497	-0.876
-1.630	-1.871	-2.320	-1.217	-1.301	-1.669	-4.799	-4.748	-4.791	-3.309	-3.134	-3.053
-4.955	-5.043	-5.291	-3.594	-3.275	-3.372	-9.296	-9.007	-8.717	-6.568	-5.861	-5.324
-2.628	-2.916	-3.298	-2.150	-2.065	-2.329	-6.130	-6.113	-6.058	-4.559	-4.153	-3.900
-3.910	-3.948	-4.289	-2.645	-2.506	-2.712	-7.892	-7.580	-7.422	-5.300	-4.840	-4.483
3.342	2.435	1.625	1.293	0.783	0.109	2.049	1.206	0.520	0.235	-0.119	-0.576

Table 7.2: Underkeel clearance for  $H_s = 3m$ ,  $T_p = 14s$

Table 7.3: Underkeel clearance for  $H_s = 3m$ ,  $T_p = 14s$

Probe1	Probe2	Probe3	Probe4	Probe5	Probe6	Probe1	Probe2	Probe3	Probe4	Probe5	Probe6
4.124	3.568	2.584	2.304	1.411	0.740	3.148	2.735	1.733	1.659	0.771	0.198
2.382	1.785	0.964	0.721	-0.070	-0.474	0.813	0.370	-0.426	-0.474	-1.207	-1.412
-1.849	-1.405	-1.353	-0.610	-1.193	-1.404	-4.785	-3.881	-3.537	-2.252	-2.768	-2.728
-4.676	-3.948	-3.330	-2.221	-2.836	-2.728	-8.543	-7.255	-6.178	-4.412	-4.990	-4.543
-2.441	-2.055	-1.874	-1.140	-1.883	-1.942	-5.572	-4.737	-4.228	-2.961	-3.694	-3.470
-3.815	-3.061	-2.517	-1.422	-1.930	-2.006	-7.394	-6.082	-5.096	-3.339	-3.778	-3.566
3.125	2.430	1.555	1.215	0.372	-0.109	1.805	1.229	0.365	0.190	-0.615	-0.926

Table 7.4: Underkeel clearance for  $H_s = 3m$ ,  $T_p = 16s$

Table 7.5: Underkeel clearance for  $H_s = 3m$ ,  $T_p = 16s$

Probe1	Probe2	Probe3	Probe4	Probe5	Probe6	Probe1	Probe2	Probe3	Probe4	Probe5	Probe6
4.016	3.464	2.482	2.095	1.371	0.634	3.021	2.590	1.640	1.374	0.705	0.039
2.520	1.900	0.871	0.389	-0.123	-0.673	1.013	0.483	-0.527	-0.922	-1.295	-1.728
-0.211	-0.104	-0.976	-0.657	-1.304	-1.277	-2.569	-2.166	-2.934	-2.325	-2.951	-2.593
-1.979	-1.685	-2.641	-2.107	-2.967	-2.511	-4.908	-4.266	-5.134	-4.270	-5.205	-4.294
-0.476	-0.398	-1.399	-1.123	-1.986	-1.846	-2.917	-2.548	-3.490	-2.947	-3.864	-3.375
-1.320	-1.011	-1.859	-1.275	-2.065	-1.688	-4.032	-3.370	-4.094	-3.154	-3.999	-3.171
3.190	2.507	1.460	0.926	0.326	-0.279	1.905	1.297	0.259	-0.200	-0.690	-1.194

Table 7.6: Underkeel clearance for  $H_s = 3m$ ,  $T_p = 18s$

Table 7.7: Underkeel clearance for  $H_s = 3m$ ,  $T_p = 18s$

Table 7.8 to 7.13 show underkeel clearance values for  $135^\circ$ .



Probe1	Probe2	Probe3	Probe4	Probe5	Probe6	Probe1	Probe2	Probe3	Probe4	Probe5	Probe6
5.979	4.961	4.000	2.814	1.912	0.942	5.609	4.542	3.607	2.332	1.459	0.494
3.659	3.227	2.325	0.724	-0.458	-1.060	2.533	2.165	1.319	-0.481	-1.743	-2.243
3.206	2.490	1.346	-0.218	-0.815	-1.325	1.926	1.177	0.009	-1.760	-2.223	-2.574
1.014	0.447	-0.428	-2.679	-3.415	-3.666	-0.981	-1.620	-2.404	-5.075	-5.738	-5.766
2.025	1.405	0.570	-1.512	-2.378	-2.653	0.364	-0.313	-1.050	-3.500	-4.336	-4.393
2.275	1.552	0.384	-1.350	-1.790	-2.386	0.687	-0.104	-1.297	-3.287	-3.545	-4.010
4.024	3.540	2.593	1.115	-0.038	-0.789	3.016	2.590	1.684	0.046	-1.178	-1.871

Table 7.8: Underkeel clearance for  $H_s = 3m$ ,  $T_p = 14s$ Table 7.9: Underkeel clearance for  $H_s = 3m$ ,  $T_p = 14s$ 

Probe1	Probe2	Probe3	Probe4	Probe5	Probe6	Probe1	Probe2	Probe3	Probe4	Probe5	Probe6
5.540	4.748	3.734	2.634	1.725	0.745	5.037	4.250	3.231	2.083	1.210	0.225
2.703	2.828	1.918	0.469	-0.528	-1.287	1.300	1.630	0.734	-0.844	-1.841	-2.542
3.382	2.557	1.452	-0.048	-0.703	-1.171	2.185	1.258	0.115	-1.553	-2.066	-2.404
1.177	0.482	-0.542	-2.328	-3.023	-3.564	-0.722	-1.579	-2.621	-4.634	-5.205	-5.649
1.878	1.294	0.304	-1.345	-2.140	-2.761	0.205	-0.469	-1.466	-3.301	-4.014	-4.556
3.377	1.925	0.772	-0.796	-1.332	-1.874	2.170	0.391	-0.810	-2.567	-2.913	-3.355
3.425	3.269	2.350	1.006	0.004	-0.902	2.252	2.231	1.327	-0.116	-1.121	-2.014

Table 7.10: Underkeel clearance for  $H_s = 3m$ ,  $T_p = 16s$ Table 7.11: Underkeel clearance for  $H_s = 3m$ ,  $T_p = 16s$ 

Probe1	Probe2	Probe3	Probe4	Probe5	Probe6	Probe1	Probe2	Probe3	Probe4	Probe5	Probe6
5.420	4.661	3.615	2.526	1.636	0.630	4.877	4.131	3.077	1.950	1.110	0.083
2.237	2.447	1.484	0.010	-0.899	-1.484	0.682	1.088	0.151	-1.449	-2.334	-2.771
3.256	2.885	1.786	0.346	-0.346	-0.943	2.017	1.715	0.580	-0.994	-1.548	-2.058
1.276	1.350	0.264	-1.308	-2.015	-2.741	-0.595	-0.399	-1.497	-3.215	-3.798	-4.472
1.920	1.910	0.849	-0.618	-1.400	-2.203	0.257	0.362	-0.701	-2.284	-2.976	-3.744
3.622	2.924	1.749	0.332	-0.246	-0.978	2.493	1.780	0.540	-1.008	-1.388	-2.106
3.061	3.033	2.056	0.696	-0.227	-0.957	1.769	1.891	0.936	-0.522	-1.423	-2.056

Table 7.12: Underkeel clearance for  $H_s = 3m$ ,  $T_p = 18s$ Table 7.13: Underkeel clearance for  $H_s = 3m$ ,  $T_p = 18s$ 

Figures 7.2 to 7.13 shows that a ship moving at a speed of 4m/s causes the ship to sink more with an increase of both wave heights and peak periods. The figures also show bottom touching for all tested wave heights, peak periods and wave incident angles. Tables 7.2 to 7.13 shows the keel point values for each tested peak period and wave height and the negative numbers indicate bottom touching. The figures show that all the tested storm peak periods and wave heights exceed the underkeel clearance limit of 2m.

Bottom touching also occurs for all tested storm conditions for wave incidence angle  $135^\circ$  where the ship also sinks with an increase in wave height and peak period although the magnitude is less than that of wave incident angle  $90^\circ$ .

# Chapter 8

## Discussion and Interpretation of Results

### 8.1 General discussion

The results presented in this thesis are based on and limited to the results produced by Mike 21BW and the Wavescat model tests, validated with results from the physical model, documented in the CSIR report (CSIR, 1991).

The numerical model results was used to address the following aspects:

- (i) The influence of depth to draught ratios for wave angles  $90^\circ$ ,  $135^\circ$  and  $180^\circ$ ,
- (ii) the influence of wave height on underkeel clearance for beam waves,
- (iii) significant and maximum hull motion amplitudes and fitting of distributions.
- (iv) effects of speed on ship in storm conditions.

#### 8.1.1 The influence of depth to draught ratios

Due to water depth and domain extend limitations found in the Richards Bay's Mike21BW model, wave spectrums for depth to draught ( $d/D$ ) ratios of 1.5, 1.4, 1.3, 1.2 and 1.1 with only wave incidence angles of  $90^\circ$ ,  $135^\circ$  and  $180^\circ$  relative to the earth bound coordinate system were investigated.  $d/D$  ratio of 1.1 is used for underkeel clearance sensitivity tests assuming that the depth off all six measurement points in Mike21BW is 20m. Wave incidence angles  $0^\circ$  and  $45^\circ$  could not be generated due to the orientation of the Mike 21BW model which did not allow for the placement of generation lines for waves from these directions. As much as the Wavescat can generate RAOs from these directions, there would not be any wave spectrums to calculate vessel response spectrums

for wave incident angles  $0^\circ$  and  $45^\circ$  therefore these incident wave angles will not be included in these studies. Figure 8.1 presents effects of water depth on significant hull motion response for wave incidents  $90^\circ$ ,  $135^\circ$  and  $180^\circ$ .

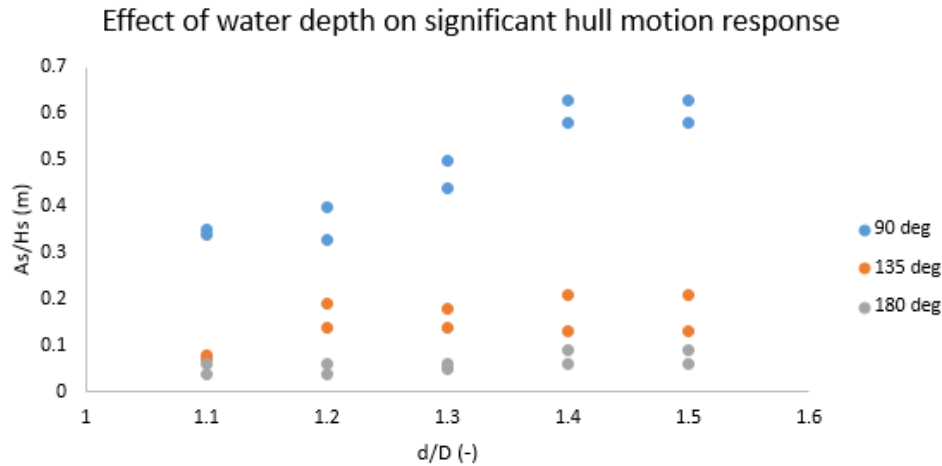


Figure 8.1: Comparison of effects of water depth on significant hull motion response between physical and Wavescat model

- (i) Figures 6.18 to 6.27 and Figure 8.1 compare  $d/D$  results of the physical model and the Wavescat model for all keel points. The results show that  $A_s/H_s$  ratios decrease with a decrease in water depth for wave incident angle  $90^\circ$ . The results also reveal that  $A_s/H_s$  ratios for  $90^\circ$  are higher in magnitude compared to the other incident wave angles.
- (ii)  $A_s/H_s$  ratios for wave incident angle  $135^\circ$  and  $180^\circ$  seem to be independent of a decrease in water depth.
- (iii) Table presents averaged differences between the physical model and the Wavescat model for each of the six keel points.

$\alpha(^{\circ})$	APP (%)	PQT (%)	SQT (%)	PSH (%)	SSH (%)	FPP (%)
90	14,01	10,52	19,68	31,52	13,45	17,76
135	13,77	24,83	10,86	17,12	6,96	7,34
180	23,26	29,05	20,71	14,05	14,44	22,55

Table 8.1: Averaged differences between the physical and the Wavescat model for  $90^\circ$ ,  $135^\circ$  and  $180^\circ$

Table 8.1 shows that the Wavescat model was able to produce almost similar results compared to the physical model test results with minor under-predictions. The port shoulder (PSH) has the highest averaged difference for wave incident angle  $90^\circ$  between the two models. The Wavescat model also under-predicted the port quarter (PQT) for wave incident angle  $135^\circ$  and under-predicted the bow (APP) for wave incident angle  $180^\circ$  the most. These under-predictions can be solved by further testing different damping coefficients, different gammas and testing for different frequencies.

### 8.1.2 Influence of wave height on underkeel clearance

Underkeel clearance sensitivity tests were conducted for  $H_s = 1\text{m}, 2\text{m}, 3\text{m}, 4\text{m}, 5, 5.5\text{m}$  and  $6\text{m}$ , for  $T_p = 10\text{s}$  and  $12\text{s}$ , and for beam waves ( $90^\circ$ ). Maximum hull motion amplitude ( $A_{\text{max}}$ ) values are used as part of the calculations, to obtain all the underkeel clearance values. The test results obtained from the Wavescat model are compared to those of the physical model. Results for  $d/D = 1.1$  where water depth in the physical model is  $18.7\text{m}$ , and  $20\text{m}$  in the Mike 21BW model, are compared and lead to the following conclusions.

- (i) Figures 6.54 to 6.67 show, side by side comparisons of the underkeel clearance sensitivity tests for all six keel points for  $T_p = 10\text{s}$  and  $12\text{s}$ . A linear relationship between  $A_s$  and  $H_s$  can be seen for  $T_p = 10\text{s}$  between the physical model and the Wavescat model.
- (ii) The linear relationship between  $A_s$  and  $H_s$  seems to change slightly for  $T_p = 12\text{s}$ . Significant hull motion amplitudes increase with an increase in wave height, although the relationship between the two seems to be non-linear.
- (iii) An increase in wave height leads higher significant hull motion amplitudes that lead to bottom touching that was experienced for wave heights higher than  $5\text{m}$  for  $T_p = 10\text{s}$  and wave heights higher than  $2\text{m}$  for  $T_p = 12\text{s}$ .

On the basis of Figure C.1 to C.6, underkeel clearance sensitivity tests with  $d/D = 1.1$  for wave incidence angle  $135^\circ$  and  $180^\circ$  are discussed and yield the following results:

- (i) All keel points for underkeel clearance sensitivity tests, with  $d/D = 1.1$ , for  $135^\circ$  and  $180^\circ$  exceed the clearance limit of about  $2\text{m}$  but no bottom touching occurs for both wave incidence angle  $135^\circ$  and  $180^\circ$  for  $H_s =$

3m, 4m and 5m,  $T_p = 10$ s.

The results for wave incidence  $135^\circ$  and  $180^\circ$  show that as much as no grounding occurs for both the wave incidence angles, exceedance of the underkeel clearance safety limits still poses as a potential risk.

### 8.1.3 Significant and maximum hull motion amplitudes and fitting of distributions

Significant hull motion amplitudes ( $A_s$ ) for all six keel points have been computed from the vessel response spectrum using the Wavescat model and maximum hull motion amplitudes were estimated to be  $2.3 \times A_s$  assuming about 720 wave cycles in the record. Timeseries created from the vessel response spectrums for  $H_s = 3$ m, 4m and 5m, for wave incidence angles  $\alpha = 90^\circ$ ,  $135^\circ$  and  $180^\circ$  are created and fitted to the Rayleigh distribution, the Weibull distribution, the Generalized Extreme Value Distribution and the Generalized Pareto distribution for amplitudes higher than 1.5m.

- (i) It can be observed from Figure 6.70 to 6.72 that the ship motion amplitudes fit reasonably well to the Rayleigh distribution with deviations of the significant motion hull amplitudes from  $A_s = 1$ m for  $H_s = 3$ m,  $A_s = 2$ m for  $H_s = 4$ m and  $A_s = 2$ m for  $H_s = 5$ m.
- (ii) Figures 6.73 to 6.75 show that the ship motion amplitudes fits the Weibull distribution quite well for all the  $A_s$  values with deviations from  $A_s = 1.2$ m for  $H_s = 3$ m and deviations of  $A_s = 2$ m for  $H_s = 3$ m and 4m.
- (iii) Figures 6.76 to 6.78 show that the ship motion amplitude data fit the Generalized Extreme Value distribution to a certain extent. The significant motion hull amplitudes deviates from  $A_s = 1$ m for  $H_s = 3$ m,  $A_s = 1.5$ m for  $H_s = 4$ m and  $A_s = 2$ m for  $H_s = 5$ m. The Generalized Extreme Value distribution is used to capture the extreme tails of events.
- (iv) Using a threshold of 0, Figures 6.79 to 6.81 show that the ship motion amplitude data fit the Generalized Pareto distribution. The non-linearity is captured well by the Generalized Pareto distribution.

Using a threshold of 0, Generalized Pareto is the best fitting probability distribution for the ship motion amplitudes tested for ships with 0 m/s speed.

### 8.1.4 Effects of speed on ship in storm conditions

Figures 7.2 to 7.13 and Tables 7.2 to 7.13 show how a ship moving at a speed of 4m/s affects the underkeel clearance. The figures show that a reduction in water depth leads to significant bottom touching that increases with an

increase in wave height and peak period. PIANC suggests that ships with a block coefficient  $C_b < 0.7$  squat at the bow while  $C_b > 0.7$  squat at the stern (PIANC, 2014). Using ICORELS's prediction methods, Tables 7.2 to 7.13 show that the ship modelled in the Wavescat sinks from the bow as a result of squat and wind heeling.

## 8.2 Reliability of calibration test results

Based on Figures 6.18 to 6.22, which compare the results of the depth to draught ratios arrived from the physical and Wavescat models, it appears that both models are in good agreement with each other with acceptable under/over predictions, particularly for APP, PQT, SQT and FPP keel points obtained from the Wavescat model. The differences might be due to several factors namely, the water depth difference of  $\pm 1.3\text{m}$  between the two models, the slightly different positioning of the probe points in the two models, Fast Fourier Transformation which is most likely to affect the peak period, the wave direction spreading and the spectra shape given by gamma of 3.3 in these studies.

## Chapter 9

# Conclusions and Recommendations

Based on the results obtained from Mike 21BW and Wavescat model, it can be concluded that:

- (i) The physical and the Wavescat model are in good agreement with some under-prediction of the PSH motions, particularly for  $\alpha = 90^\circ$ , under-predictions for PQT for  $\alpha = 135^\circ$  and under-predictions for APP for  $180^\circ$ . This observation indicates that the Wavescat model's port quarter, port shoulder and stern experiences less movement than those experienced in the physical model for wave incident angles  $90^\circ$ ,  $135^\circ$  and  $180^\circ$ .
- (ii) Wave induced hull motion's magnitude depends on wave incidence angles and wave heights. The results reveal that beam waves generate the largest hull motions due to a combination of roll, heave and pitch.  $A_s/H_s$  ratios for wave incident angles  $135^\circ$  and  $180^\circ$  compare very well with the Wavescat under-predicting bow and stern magnitude when compared to the physical model results.
- (iii) There is a reduction of ship motions response as the water depth reduces. This would indicate that there is increasing vertical ship motion cushioning for smaller underkeel clearance for beam waves. Vertical ship motions for wave incident angle  $135^\circ$  and  $180^\circ$  seem to however, be independent of a reduction in water depth.
- (iv) The underkeel clearance sensitivity tests for beam waves indicate that an underkeel clearance safety limit of 2m is exceeded for ship motions for  $H_s = 2\text{m}$ ,  $3\text{m}$ ,  $4\text{m}$ ,  $5\text{m}$ ,  $5.5\text{m}$  and  $6\text{m}$  for  $T_p = 10\text{s}$  and exceeded for  $T_p = 12\text{s}$  for ship motions for  $H_s = 1\text{m}$ ,  $2\text{m}$ ,  $3\text{m}$ ,  $4\text{m}$ ,  $5\text{m}$ ,  $5.5\text{m}$  and



6m. Bottom touching for  $T_p = 10$ s occurs for ship motions from  $H_s = 5$ m and bottom touching for  $T_p = 12$ s occurs from  $H_s = 2$ m for  $d/D = 1.1$ .

The underkeel clearance sensitivity tests for wave incidence angle  $\alpha = 135^\circ$  and  $\alpha = 180^\circ$  reveal that ship motions for  $H_s = 3$ m to 5m for  $d/D = 1.1$ , exceed the clearance limit of about 2m for  $T_p = 10$ s with no bottom touching occurrence.

The results mean that water depths of 20m and less, should be completely avoided by ships entering or leaving the Port with draughts of 17m and more, for wave of incidence angles  $90^\circ$ ,  $135^\circ$  and  $180^\circ$  to avoid the possibilities of grounding or bottom touching.

- (v) The overall underkeel clearance tests indicate that ship motions for  $H_s = 3$ m from wave incidence angle  $\alpha = 90^\circ$ ,  $T_p = 10$ s, seem to exceed the clearance limit of 2m for  $d/D = 1.2$  and 1.1, ship motions for  $H_s = 4$ m exceed the clearance limit for  $d/D = 1.3$ , 1.2 and 1.1 and ship motions for  $H_s = 5$ m exceed the clearance limits from  $d/D = 1.4$ , 1.3, 1.2 and 1.1. This means that the Port of Richards Bay should be cautious of allowing ships with draughts of more than 17m into the channel where water depth is 23m and less, unless the tide is more than 1m Chart Datum.
- (vi) Significant hull motions appear to increase almost linearly with wave heights.
- (vii) Significant hull motion amplitudes seem to have a linear relationship with the maximum hull motion amplitudes that does not seem to be dependent on depth to draught ratios. The average  $A_{max}/A_s$  Rayleigh distribution ratio for the Wavescat numerical model is 2.3 for all the tested wave incidence angles, for 2 hours long timeseries with a peak period of 10s.
- (viii) Out of all four distributions, it seems that the Generalized Pareto distribution captures the non-linearity of ship motion amplitude best, for all the tested wave incidence angles and depth to draught ratios.
- (ix) On the basis of the calibrated numerical model, Wavescat managed to compute the non-linear aspects namely the location of the centre of gravity of the vessel, assumed to be centre of roll rotation, the viscous roll damping, small-underkeel clearance damping and squat for the varying wave heights, peak periods and water depths. The results show that ships moving at a speed of 4m/s should stay clear of water depths shallower than 25m to avoid bottom touching or even grounding.

The aim of this research was to investigate whether maximum vertical keel point motions of coal carriers can be computed accurately on the basis of predicted wave and tide conditions. Their probability of exceedance needed to also, be determined so that acceptable risk factors can be chosen. This process



required calibrated numerical model and forecasting of environmental conditions. If this would be possible, the maximum safe draught of coal carriers should be able to be predicted for future departing conditions, as function of time, and the optimum time of departure can be established, through the use of a CSIR underkeel clearance program called the DMAX. This would form the basis for port operational procedures for the departure of laden deep-draught coal carriers.

It can be concluded that the research was able to compute maximum vertical keel point motions of coal carriers, quite well on the basis of predicted wave and tide conditions, in comparison to the physical model tests for  $T_p = 10$  s and 12 s.  $T_p = 14$  s to 18 s where not calibrated but used to study the effects of ships with forward speed in the Wavescat model. The quantile probability distribution that best describe the non-linearity of the computed maximum vertical keel point motions is the Generalized Pareto Distribution. Depending on the wave incidence angles as well as the wave height, acceptable risk factors can be chosen based on the Generalized Pareto distribution graphs. Maximum safe draught can also be estimated from the CSIR Underkeel Clearance software package (DMAX), which can be used as an assisting tool in the port's operation procedures for the departure of laden deep-draught coal carriers.

It would be recommended that ships that visit the Port with draughts of more than 17m, be very cautious of water depths less than 23m, with peak periods of  $T_p = 10$ s and more, to avoid exceeding the underkeel clearance limit, unless in the cases of high tide windows. It would also be recommended that ships moving at a certain speed stay clear of water depths less than 25m.

The findings of these studies can be applied to other Ports in the world, for numerical ship motions studies that focus on understanding the calibration of ships with zero forward speed. The studies can also be used to determine how ship speed affects the underkeel clearance of bulk carriers with draughts of 17m and more, for Port channels in open water.

## Chapter 10

# Application of the Wavescat model on storm conditions

The Wavescat is used to model a 150kt DWT fully laden bulk carrier moving at 4m/s speed along the Port of Richards Bay channel. Storm conditions with periods of  $T_p = 14s$ , 16s and 18s and wave heights, 3m, 4m and 5m are selected. Wave incidence angles  $90^\circ$  and  $135^\circ$  are tested.

### 10.1 Mike21BW test conditions

Table 10.1 shows Mike21BW input conditions.

Direction ( $^\circ$ )	Hmo (m)	$T_p = 14s$	$T_p = 16s$	$T_p = 18s$
90	3	x	x	x
	4	x	x	x
	5	x	x	x
135	3	x	x	x
	4	x	x	x
	5	x	x	x

Table 10.1: Mike 21BW input conditions

### 10.2 Underkeel clearance calculations

Squat, heel and wave response are calculated for different sections of the ship during vertical movement to determine the total sinkage or trim. Squat is

given by equation 10.1 (Gourlay, 2007):

$$s = c \frac{\nabla}{L_{pp}^2} \frac{F_h^2}{\sqrt{1 - F_h^2}} \quad (10.1)$$

where  $s$  is the squat at the aft perpendicular,  $F_h = \frac{V}{\sqrt{gh}}$  which is the Froude number,  $V$  is speed,  $h$  is water depth,  $\nabla$  is ship displacement volume,  $g$  is gravity and  $c$  is bow or stern squat coefficient. Equation 10.1 is applicable to ships in open water or wide channels in shallow water. Heeling is given by equation 10.2 (Gourlay, 2007):

$$\phi = \frac{M}{mg\overline{GM}} \quad (10.2)$$

where  $\phi$  is the heel angle,  $M$  is the heeling moment,  $m$  is ship mass,  $g$  is gravity and  $\overline{GM}$  is the transverse metacentric height. Heeling can be caused by a ship turning or wind. Since in the Port of Richards Bay entrance channel no turning of the 150 kt deadweight bulk carrier takes place, only wind heeling is taken into consideration. The wind heeling moment is given by equation 10.3 (DNV.GL, 2015):

$$M_w = 0.02 \frac{V_0^2}{L_{pp}} \cdot \Delta(KG - 0.05 \cdot D) \quad (10.3)$$

where  $M_w$  is the wind heeling moment,  $L_{pp}$  is length between perpendiculars (m),  $V$  is ship speed (m/s),  $\Delta$  is ship displacement in ( $m^3$ ),  $KG$  is the centre of gravity above keel and  $D$  is draught (m).

# Appendices

# Appendix A

## Computed Wave and Ship Motion Spectra

Wave spectrum,  $RAO^2$  and Vessel response spectrum figures for  $d/D = 1.5, 1.4, 1.3, 1.2$  and  $1.1$ .

Direction =  $90^\circ$ ,

Water depth = 23.4m,  $d/D$  1.5 to 1.1 and  $T_p = 10s$

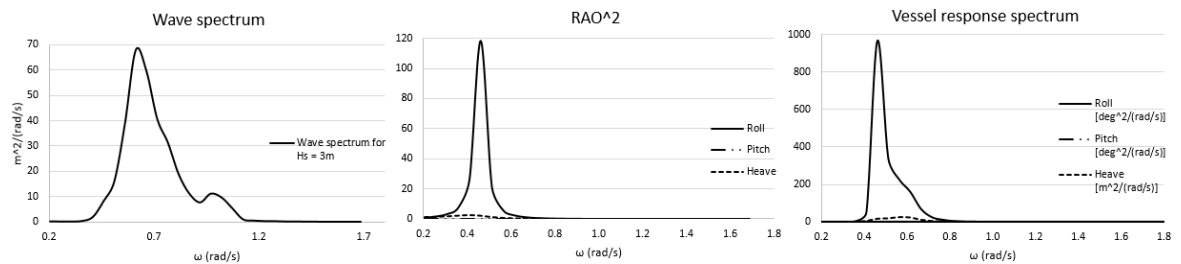


Figure A.1: Vessel response spectrum for  $H_s = 3m$ , Direction =  $90^\circ$

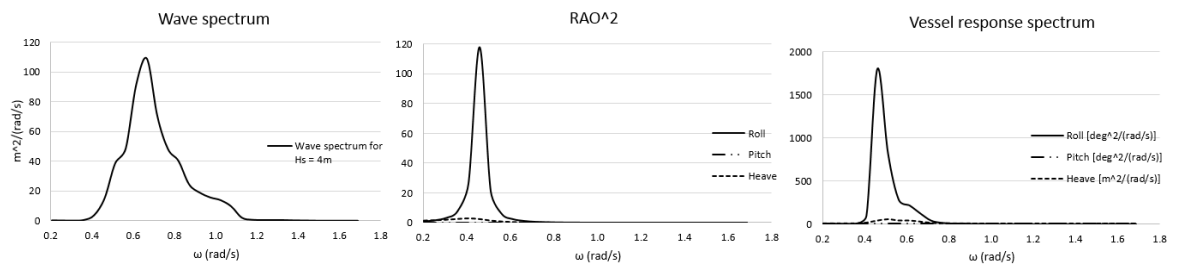


Figure A.2: Vessel response spectrum for  $H_s = 4m$ , Direction =  $90^\circ$

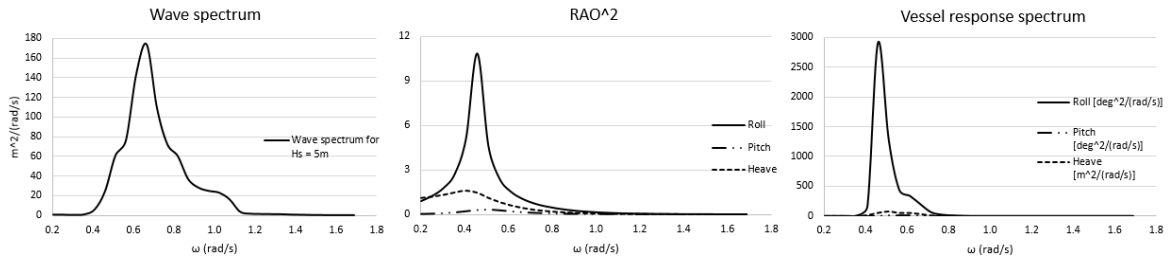


Figure A.3: Vessel response spectrum for  $H_s = 5\text{m}$ , Direction =  $90^\circ$

Water depth = 21.6m,  $d/D$  1.5 to 1.1 and  $T_p = 10\text{s}$

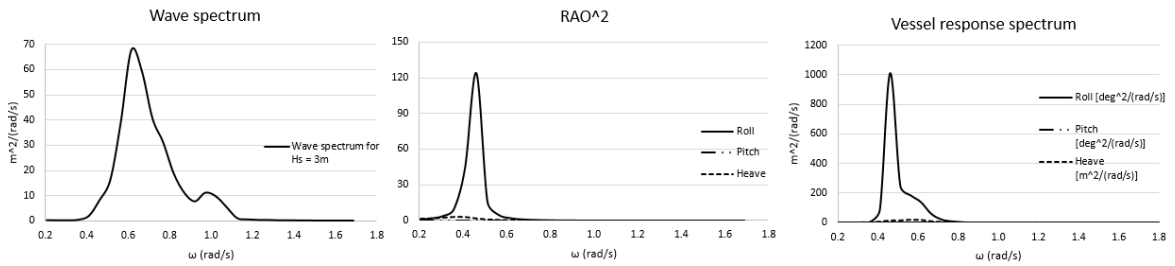


Figure A.4: Vessel response spectrum for  $H_s = 3\text{m}$ , Direction =  $90^\circ$

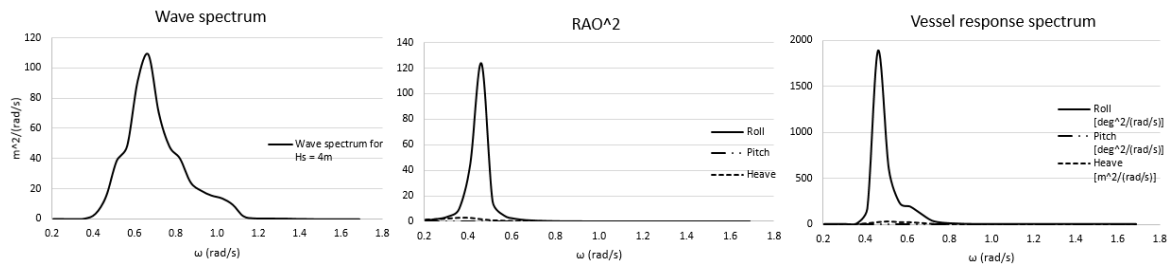


Figure A.5: Vessel response spectrum for  $H_s = 4\text{m}$ , Direction =  $90^\circ$

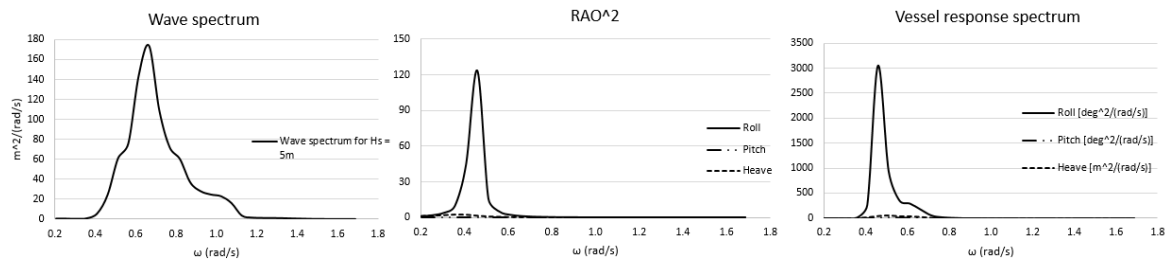


Figure A.6: Vessel response spectrum for  $H_s = 5\text{m}$ , Direction =  $90^\circ$

Water depth = 19.8m,  $d/D$  1.5 to 1.1 and  $T_p = 10\text{s}$

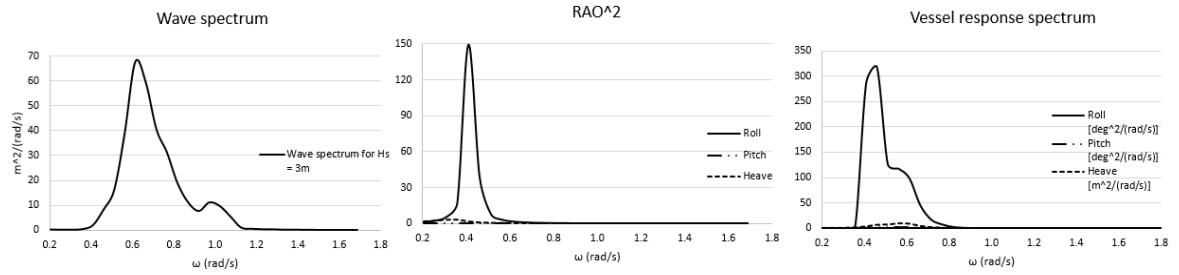


Figure A.7: Vessel response spectrum for  $H_s = 3\text{m}$ , Direction =  $90^\circ$

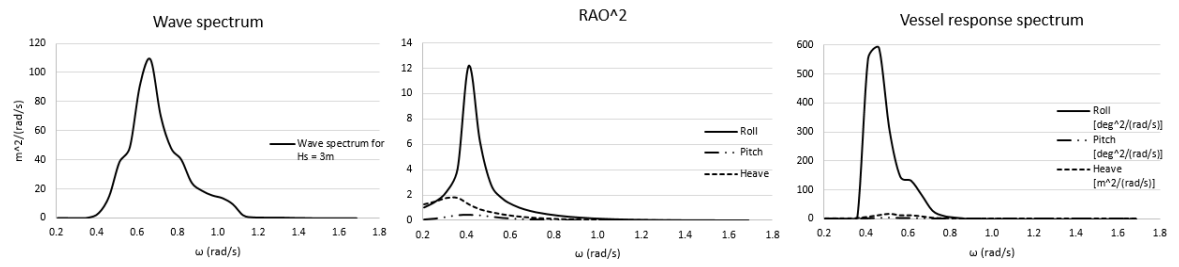


Figure A.8: Vessel response spectrum for  $H_s = 4\text{m}$ , Direction =  $90^\circ$

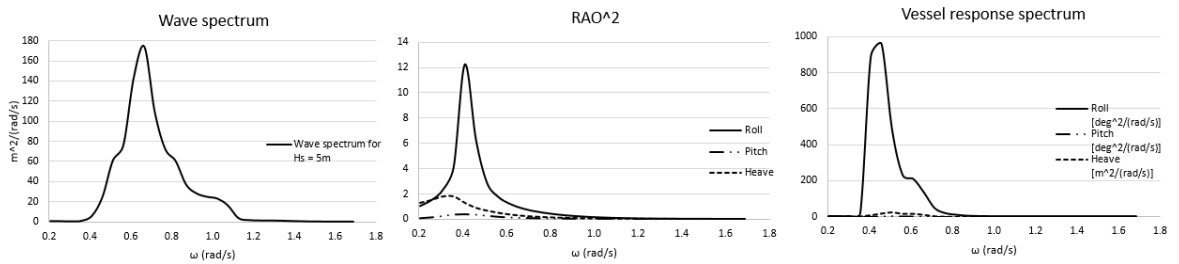


Figure A.9: Vessel response spectrum for  $H_s = 5\text{m}$ , Direction =  $90^\circ$

Water depth = 18.7m,  $d/D$  1.5 to 1.1 and  $T_p = 10\text{s}$

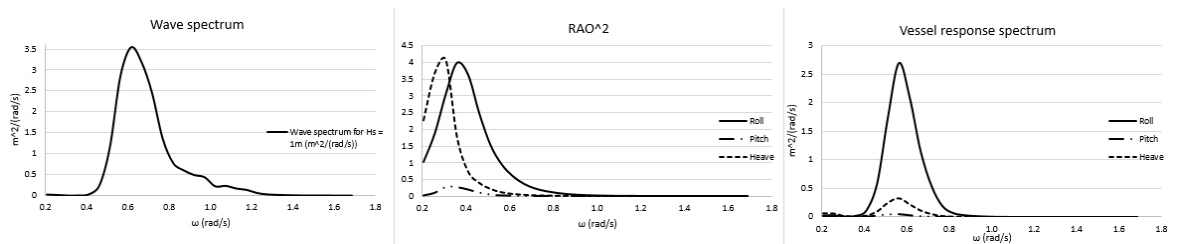


Figure A.10: Vessel response spectrum for  $H_s = 1\text{m}$ , Direction =  $90^\circ$

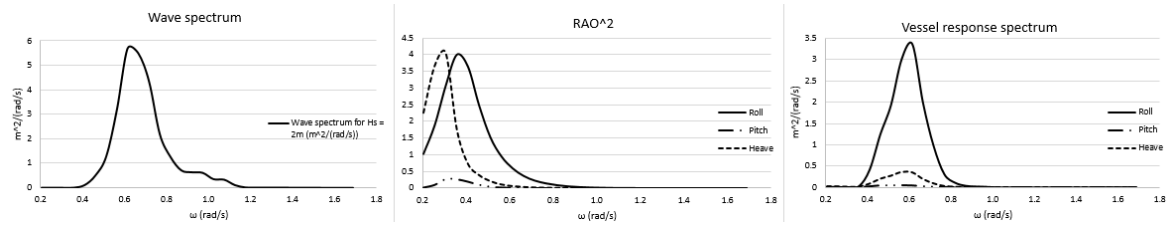


Figure A.11: Vessel response spectrum for  $H_s = 2\text{m}$ , Direction =  $90^\circ$

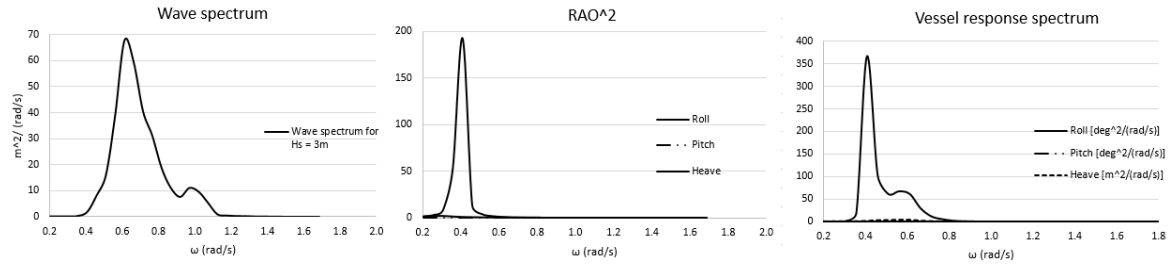


Figure A.12: Vessel response spectrum for  $H_s = 3\text{m}$ , Direction =  $90^\circ$

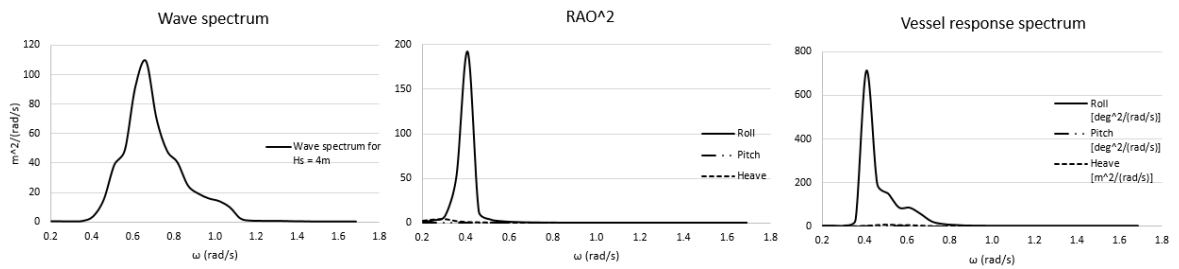


Figure A.13: Vessel response spectrum for  $H_s = 4\text{m}$ , Direction =  $90^\circ$

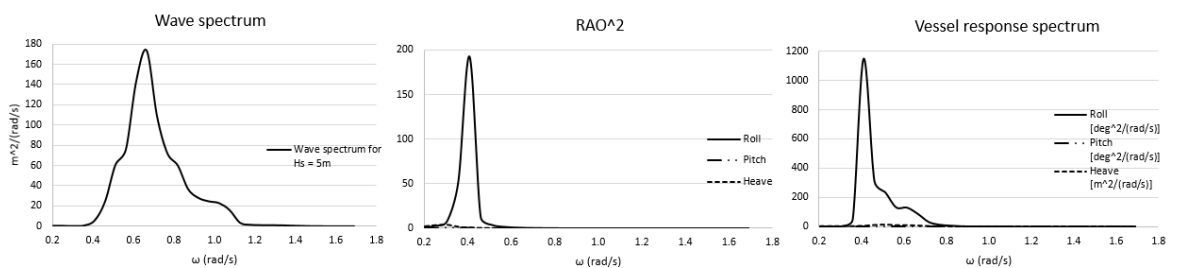


Figure A.14: Vessel response spectrum for  $H_s = 5\text{m}$ , Direction =  $90^\circ$

Direction =  $135^\circ$  Water depth = 25.2m,  $d/D$  1.5 to 1.1 and  $T_p = 10\text{s}$



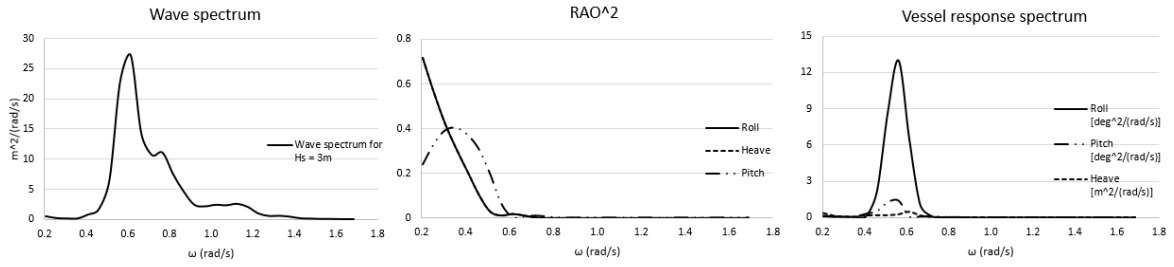


Figure A.15: Vessel response spectrum for  $H_s = 3\text{m}$ , Direction =  $135^\circ$

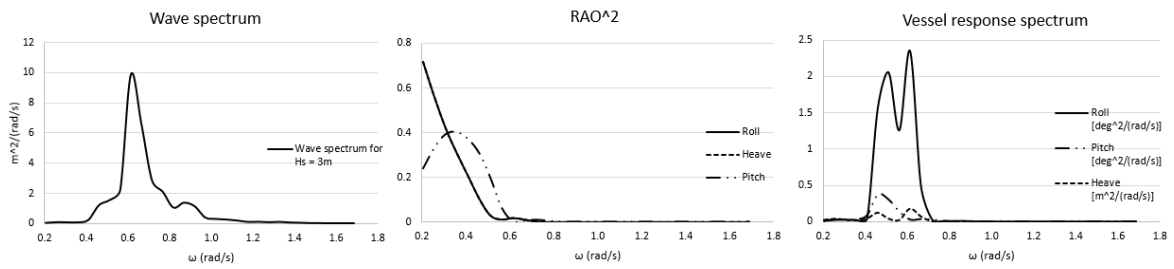


Figure A.16: Vessel response spectrum for  $H_s = 4\text{m}$ , Direction =  $135^\circ$

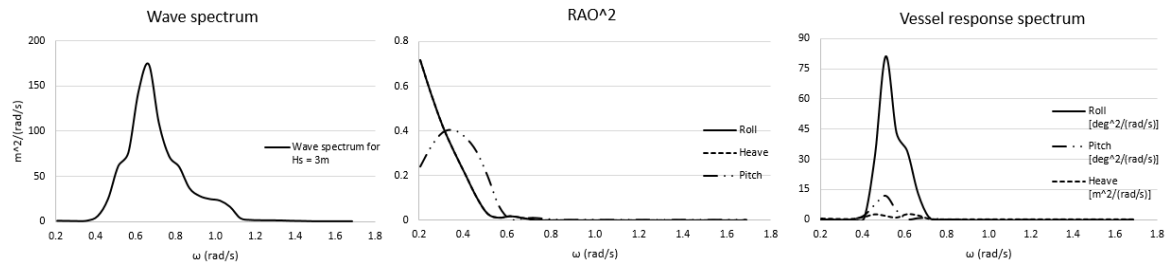


Figure A.17: Vessel response spectrum for  $H_s = 5\text{m}$ , Direction =  $135^\circ$

Water depth = 23.4m,  $d/D$  1.5 to 1.1 and  $T_p = 10\text{s}$

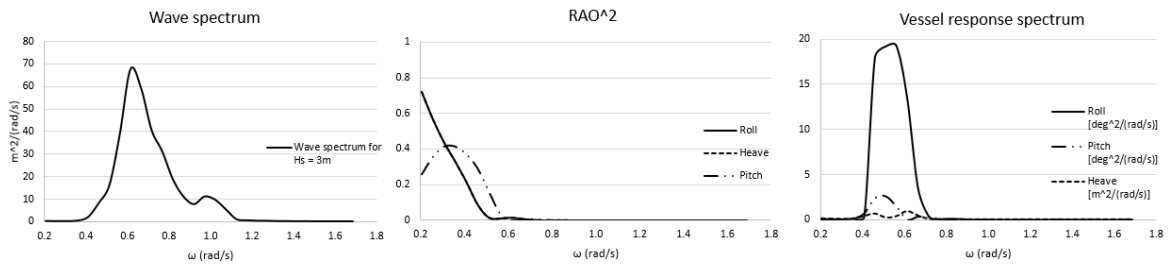


Figure A.18: Vessel response spectrum for  $H_s = 3\text{m}$ , Direction =  $135^\circ$

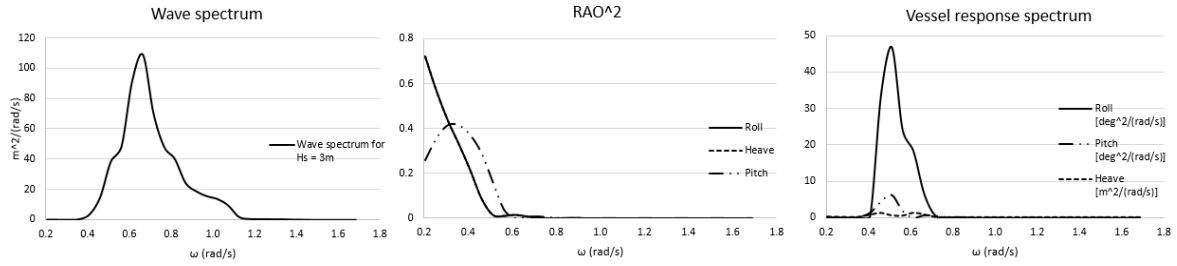


Figure A.19: Vessel response spectrum for  $H_s = 4\text{m}$ , Direction =  $135^\circ$

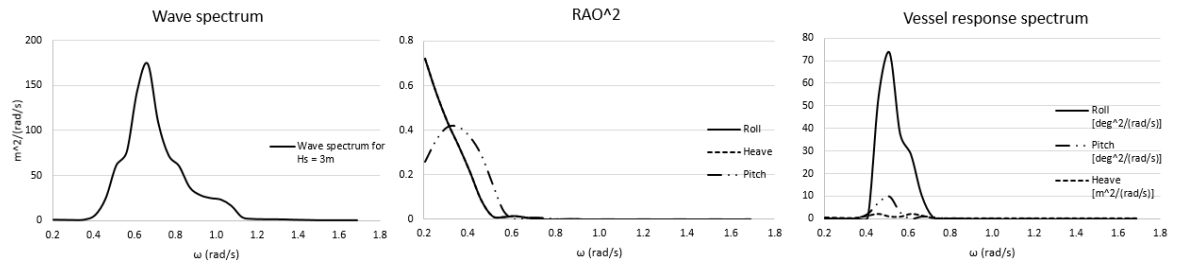


Figure A.20: Vessel response spectrum for  $H_s = 5\text{m}$ , Direction =  $135^\circ$

Water depth = 21.6m,  $d/D$  1.5 to 1.1 and  $T_p = 10\text{s}$

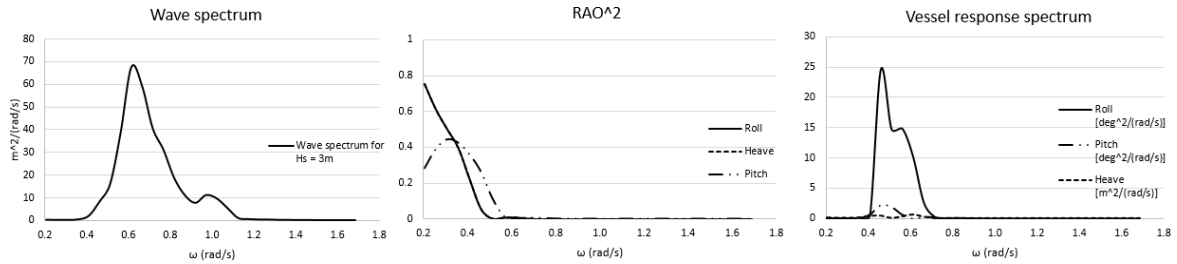


Figure A.21: Vessel response spectrum for  $H_s = 3\text{m}$ , Direction =  $135^\circ$

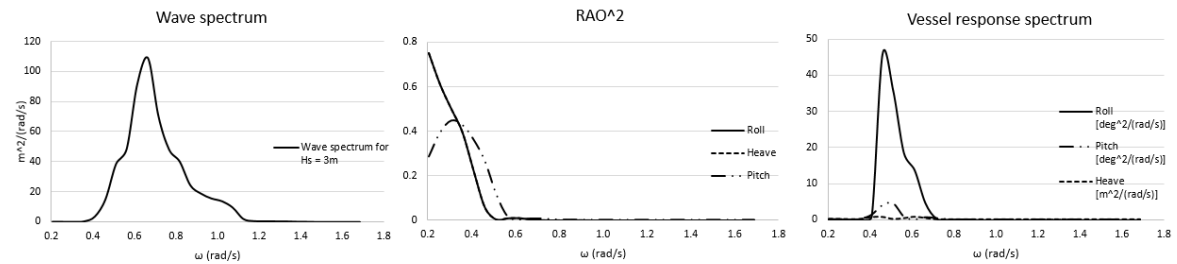


Figure A.22: Vessel response spectrum for  $H_s = 4\text{m}$ , Direction =  $135^\circ$

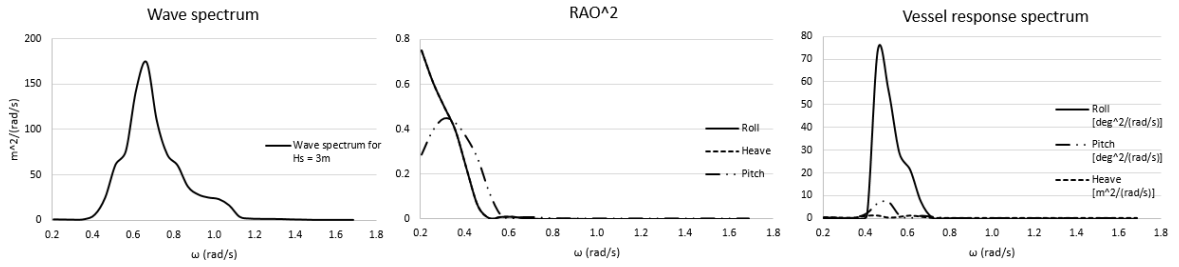


Figure A.23: Vessel response spectrum for  $H_s = 5\text{m}$ , Direction =  $135^\circ$

Water depth = 19.8m,  $d/D$  1.5 to 1.1 and  $T_p = 10\text{s}$

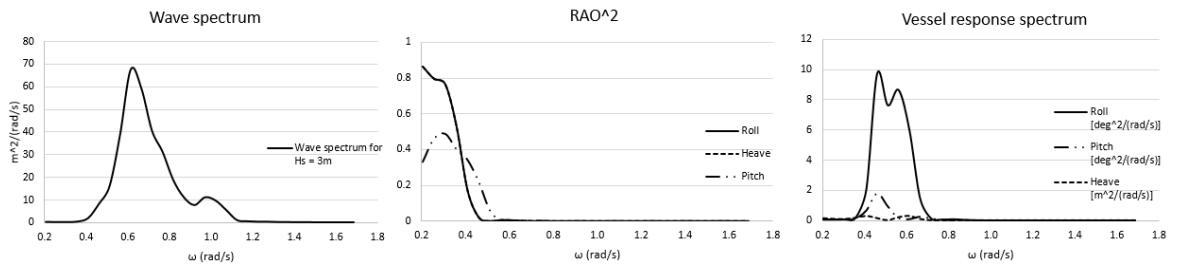


Figure A.24: Vessel response spectrum for  $H_s = 3\text{m}$ , Direction =  $135^\circ$

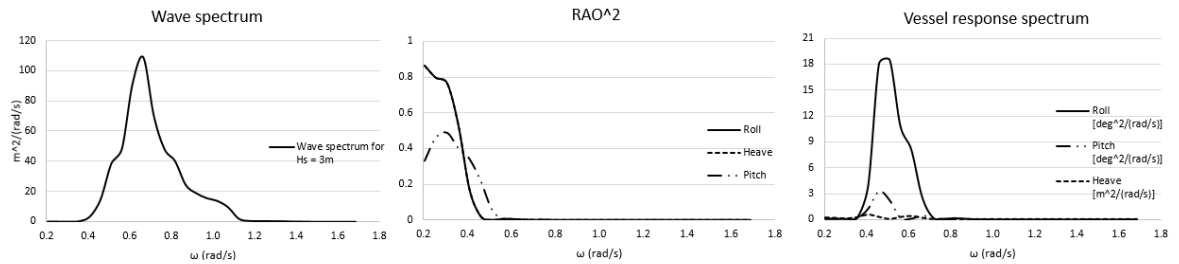


Figure A.25: Vessel response spectrum for  $H_s = 4\text{m}$ , Direction =  $135^\circ$

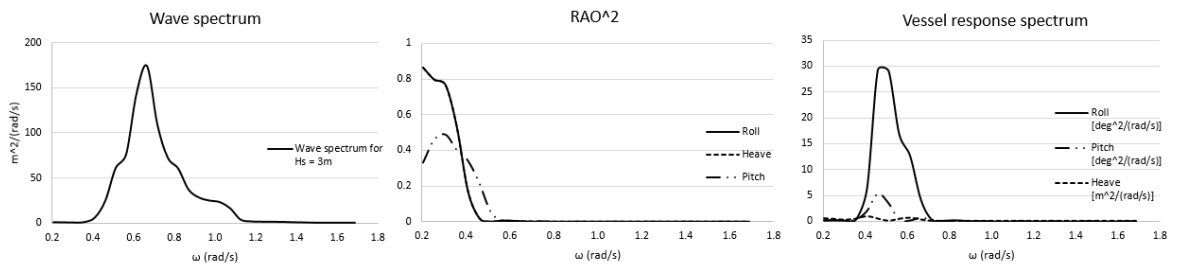
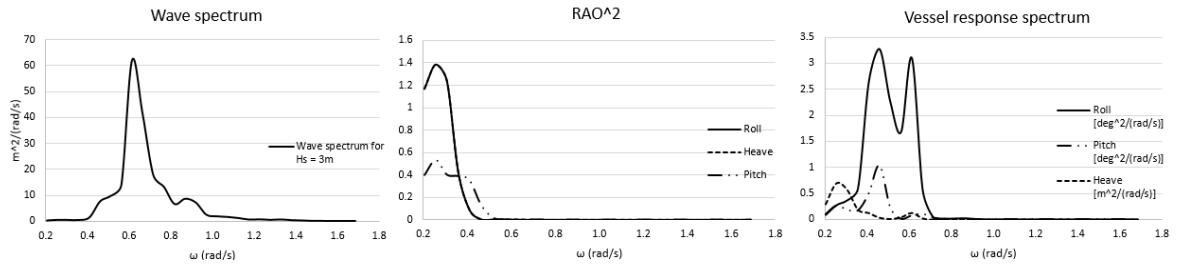
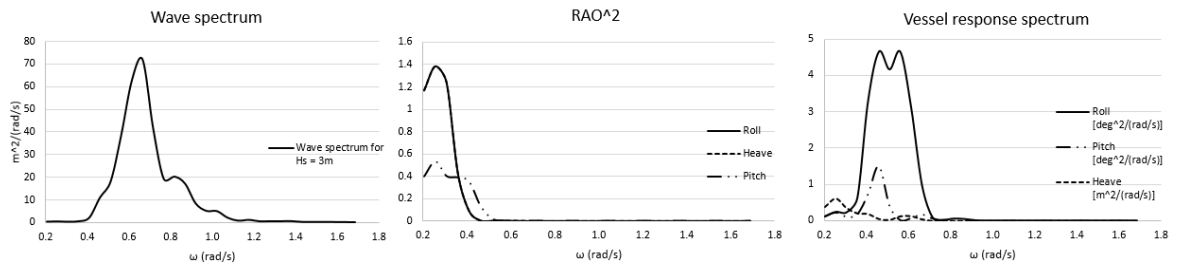
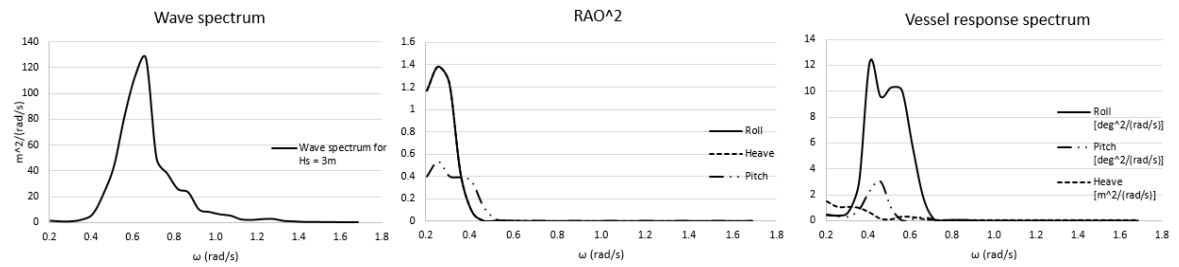
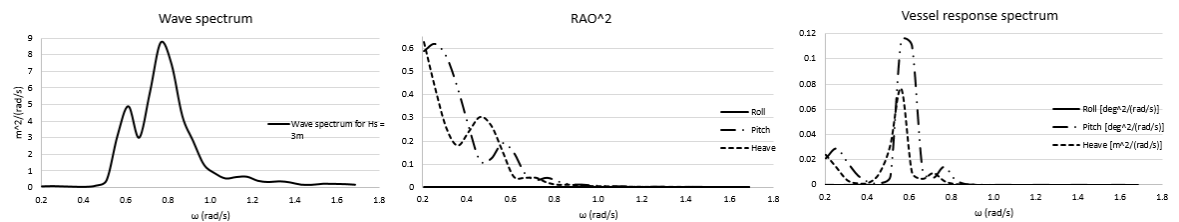


Figure A.26: Vessel response spectrum for  $H_s = 5\text{m}$ , Direction =  $135^\circ$

Water depth = 18.7m,  $d/D$  1.5 to 1.1 and  $T_p = 10\text{s}$

Figure A.27: Vessel response spectrum for  $H_s = 3\text{m}$ , Direction =  $135^\circ$ Figure A.28: Vessel response spectrum for  $H_s = 4\text{m}$ , Direction =  $135^\circ$ Figure A.29: Vessel response spectrum for  $H_s = 5\text{m}$ , Direction =  $135^\circ$ 

Direction =  $180^\circ$  Water depth = 25.2m,  $d/D$  1.5 to 1.1 and  $T_p = 10\text{s}$

Figure A.30: Vessel response spectrum for  $H_s = 3\text{m}$ , Direction =  $180^\circ$

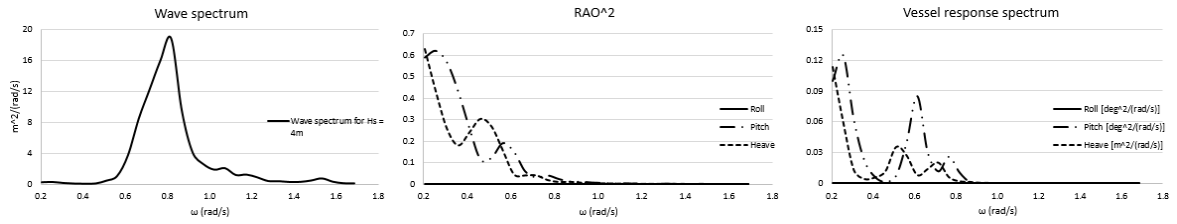


Figure A.31: Vessel response spectrum for  $H_s = 4\text{m}$ , Direction =  $180^\circ$

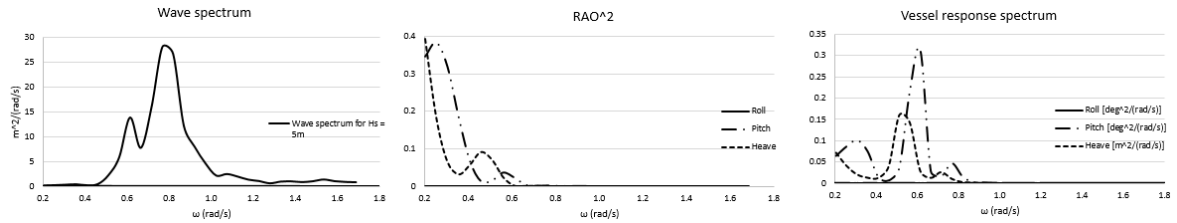


Figure A.32: Vessel response spectrum for  $H_s = 5\text{m}$ , Direction =  $180^\circ$

Water depth = 23.4m,  $d/D$  1.5 to 1.1 and  $T_p = 10\text{s}$

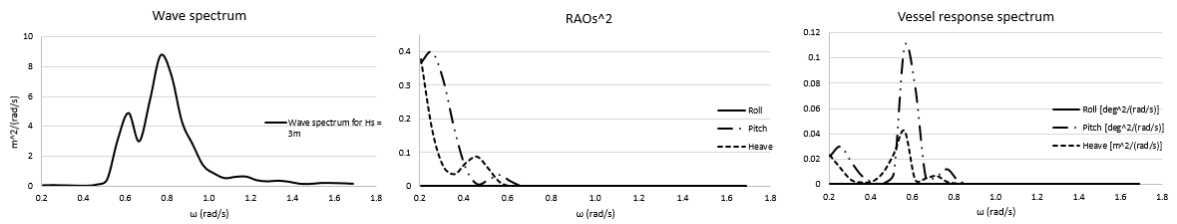


Figure A.33: Vessel response spectrum for  $H_s = 3\text{m}$ , Direction =  $180^\circ$

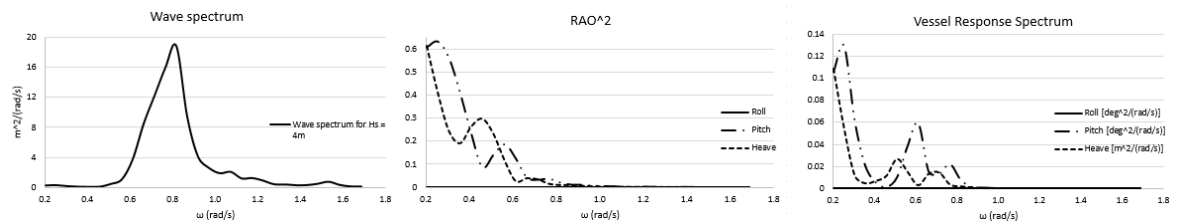


Figure A.34: Vessel response spectrum for  $H_s = 4\text{m}$ , Direction =  $180^\circ$

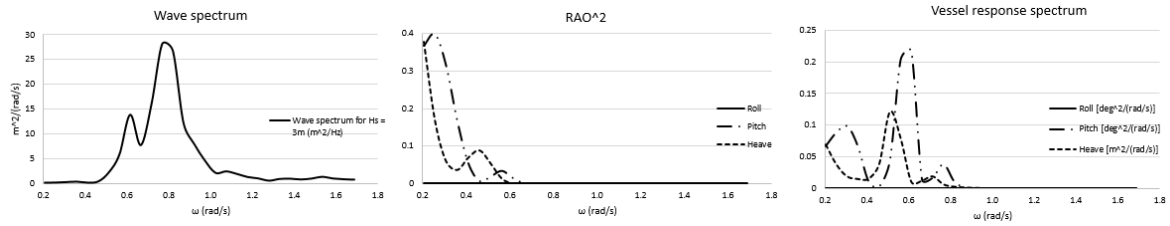


Figure A.35: Vessel response spectrum for  $H_s = 5\text{m}$ , Direction =  $180^\circ$

Water depth = 21.6m,  $d/D$  1.5 to 1.1 and  $T_p = 10\text{s}$

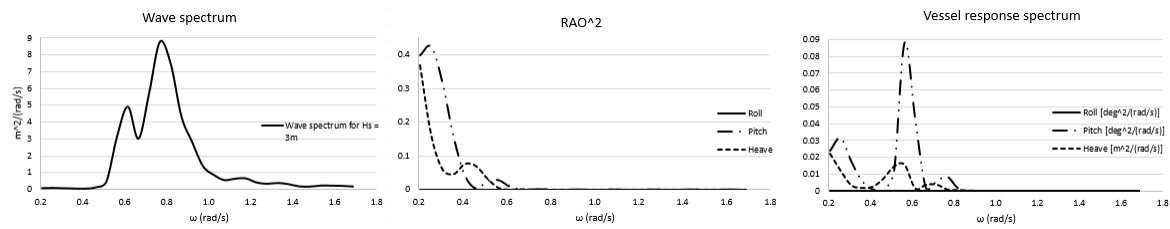


Figure A.36: Vessel response spectrum for  $H_s = 3\text{m}$ , Direction =  $180^\circ$

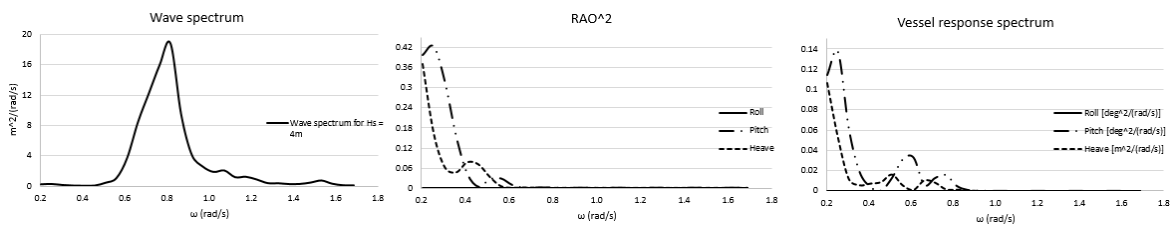


Figure A.37: Vessel response spectrum for  $H_s = 4\text{m}$ , Direction =  $180^\circ$

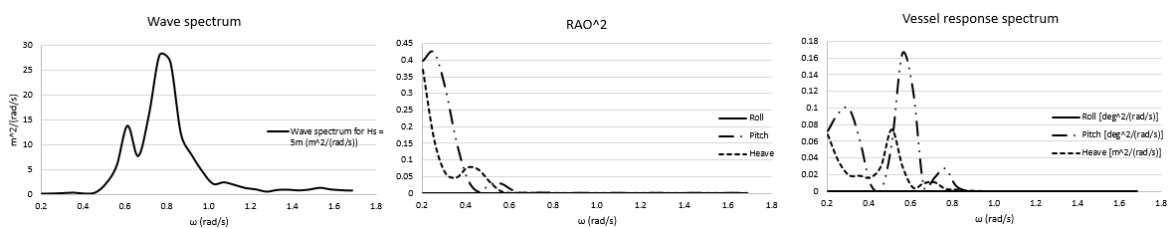


Figure A.38: Vessel response spectrum for  $H_s = 5\text{m}$ , Direction =  $180^\circ$

Water depth = 19.8m,  $d/D$  1.5 to 1.1 and  $T_p = 10\text{s}$

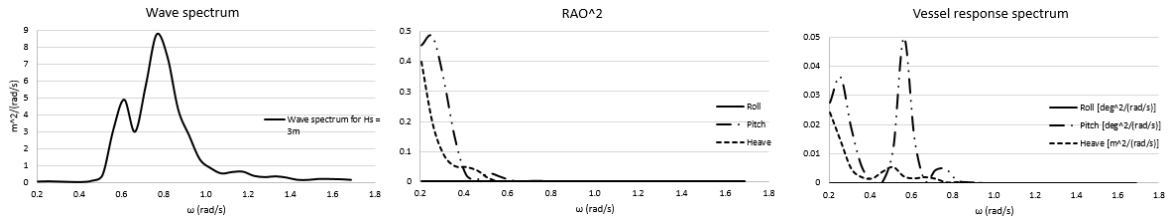


Figure A.39: Vessel response spectrum for  $H_s = 3\text{m}$ , Direction =  $180^\circ$

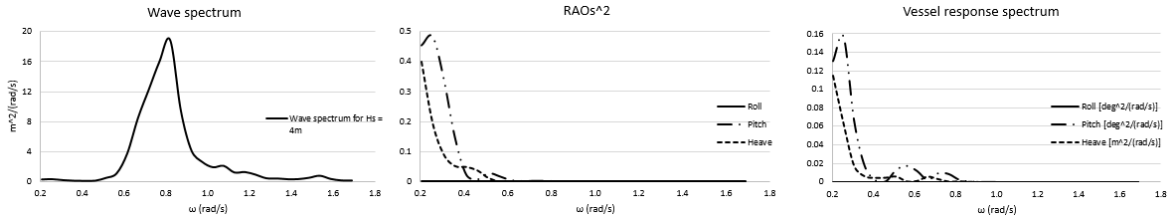


Figure A.40: Vessel response spectrum for  $H_s = 4\text{m}$ , Direction =  $180^\circ$

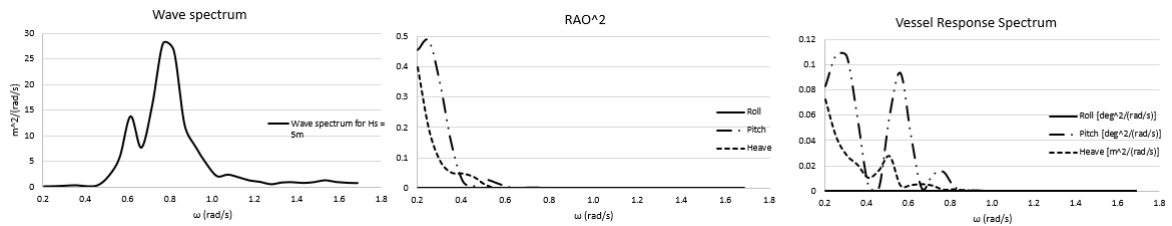


Figure A.41: Vessel response spectrum for  $H_s = 5\text{m}$ , Direction =  $180^\circ$

Water depth = 18.7m,  $d/D$  1.5 to 1.1 and  $T_p = 10\text{s}$

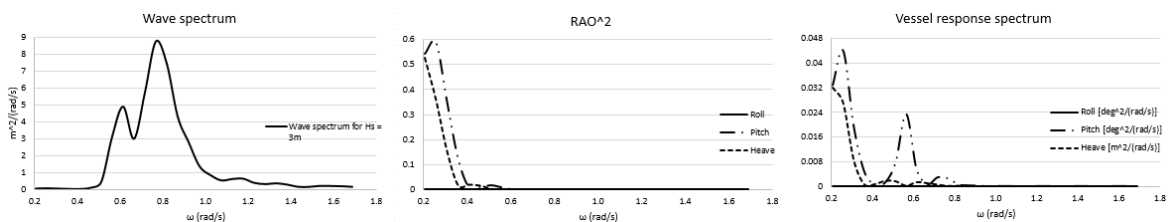
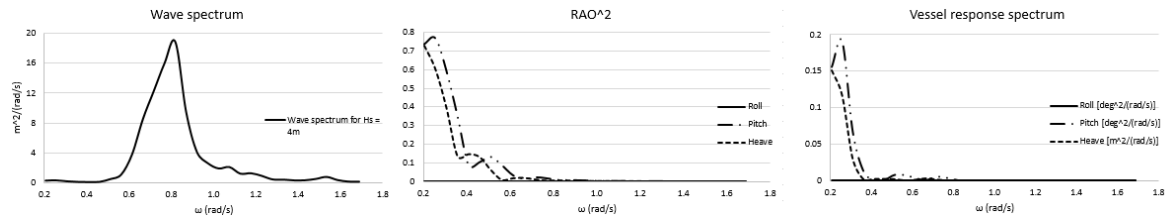
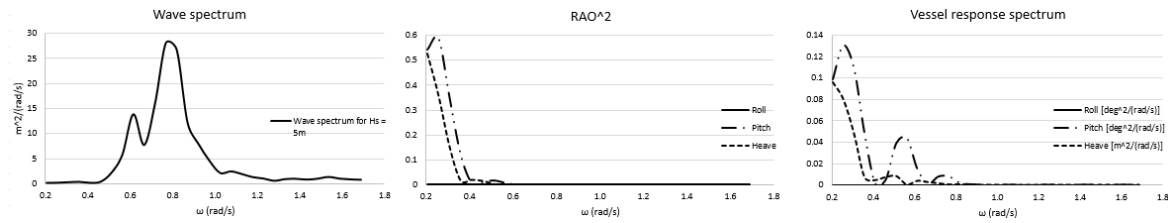


Figure A.42: Vessel response spectrum for  $H_s = 3\text{m}$ , Direction =  $180^\circ$

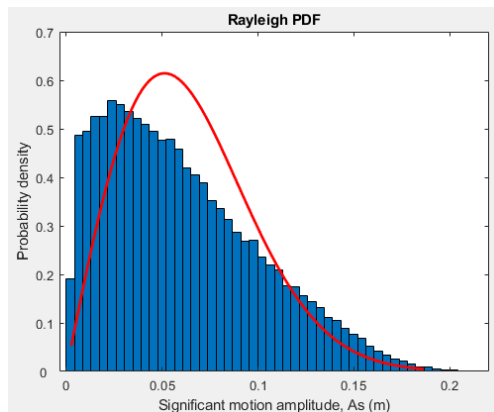
Figure A.43: Vessel response spectrum for  $H_s = 4\text{m}$ , Direction =  $180^\circ$ Figure A.44: Vessel response spectrum for  $H_s = 5\text{m}$ , Direction =  $180^\circ$



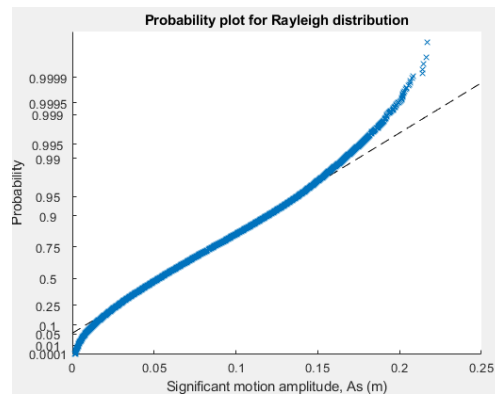
## Appendix B

# LIST OF PROBABILITY DISTRIBUTIONS

Rayleigh Distribution, Direction 135°

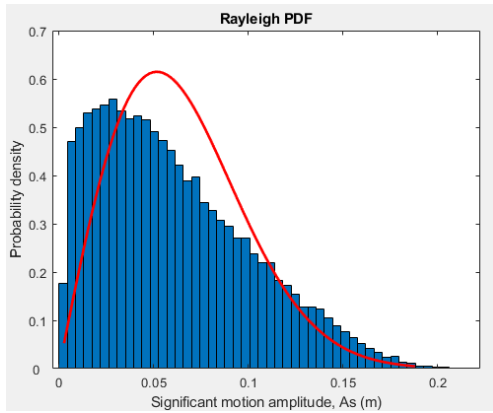


(a) Probability density

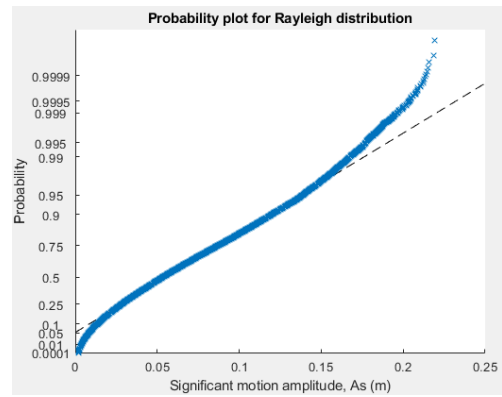


(b) Probability plot

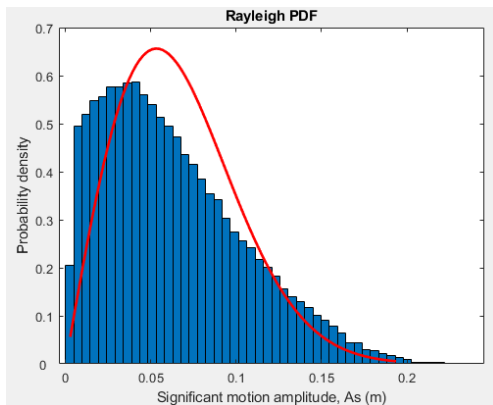
Figure B.1: Rayleigh distribution density function and probability plot for ship motion amplitudes with  $H_s = 3\text{m}$



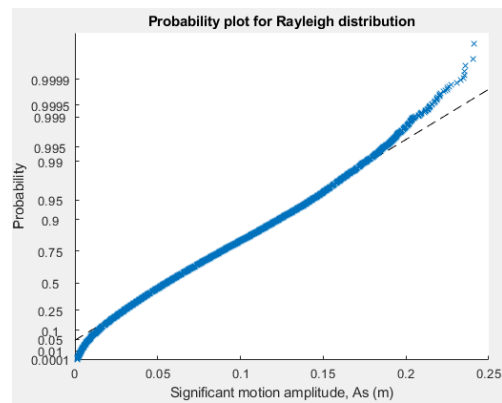
(a) Probability density



(b) Probability plot

Figure B.2: Rayleigh distribution density function and probability plot for ship motion amplitudes with  $H_s = 4$  m

(a) Probability density



(b) Probability plot

Figure B.3: Rayleigh distribution density function and probability plot for ship motion amplitudes with  $H_s = 5$  m

**Rayleigh Distribution, Direction 180°**

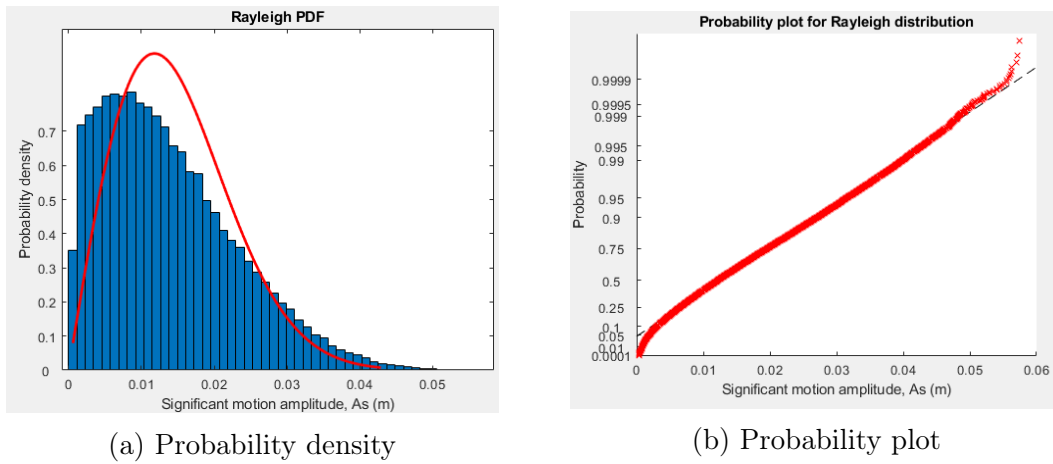


Figure B.4: Rayleigh distribution density function and probability plot for ship motion amplitudes with  $H_s = 3\text{m}$

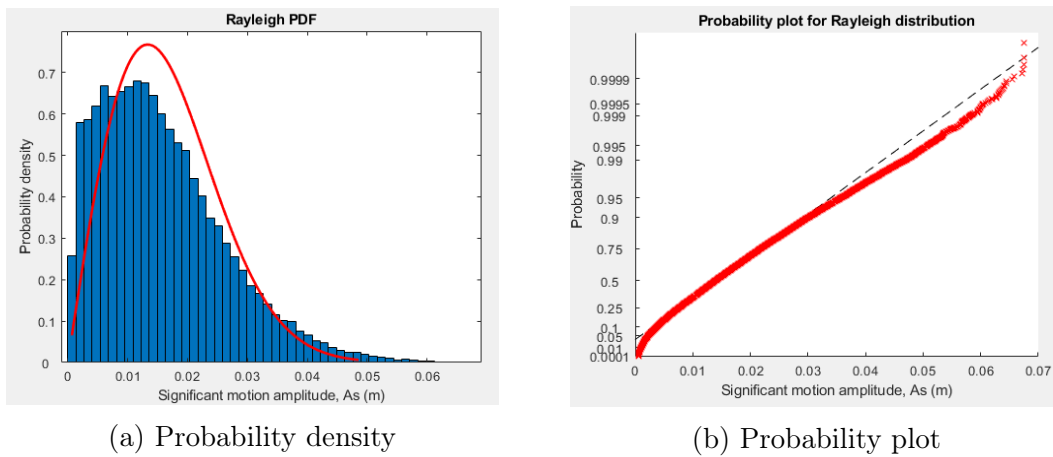


Figure B.5: Rayleigh distribution density function and probability plot for ship motion amplitudes with  $H_s = 4\text{m}$

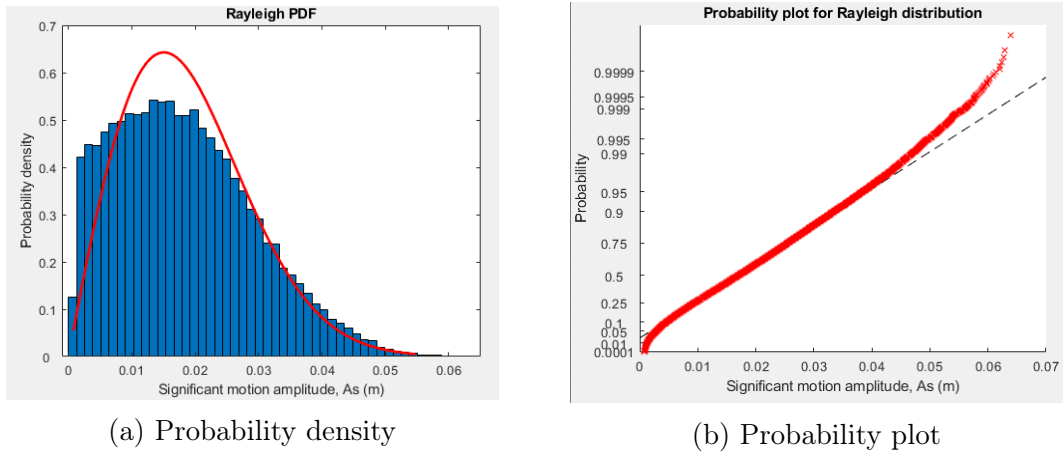


Figure B.6: Rayleigh distribution density function and probability plot for ship motion amplitudes with  $H_s = 5\text{m}$

### Weibull Distribution, Direction $135^\circ$

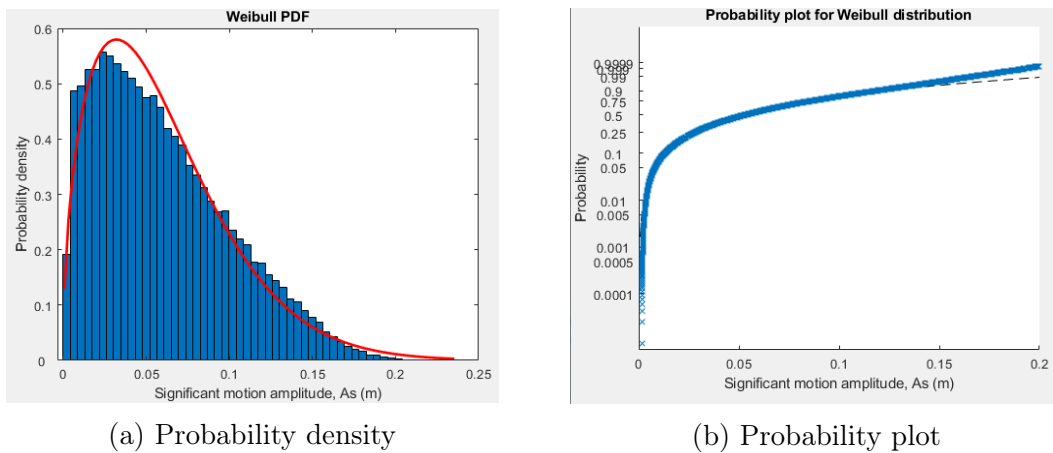


Figure B.7: Weibull distribution density function and probability plot for ship motion amplitudes with  $H_s = 3\text{m}$

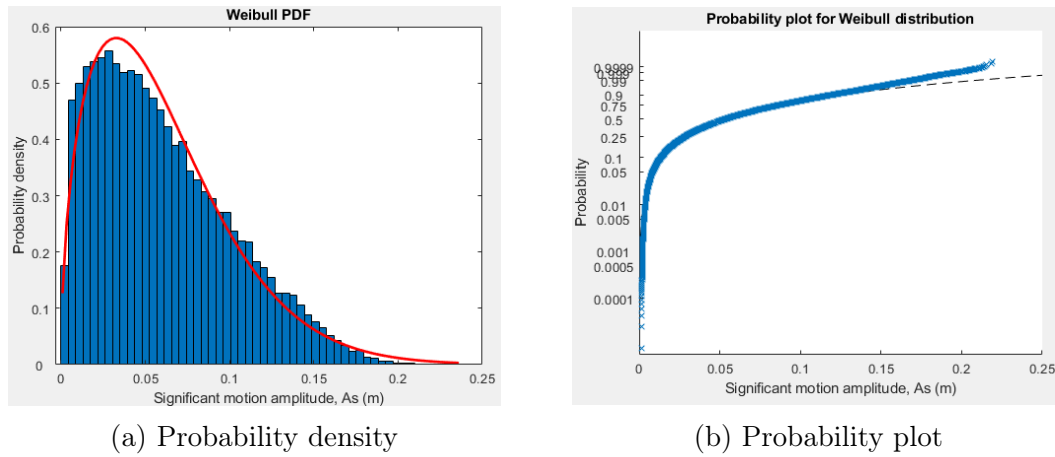


Figure B.8: Weibull distribution density function and probability plot for ship motion amplitudes with  $H_s = 4\text{m}$

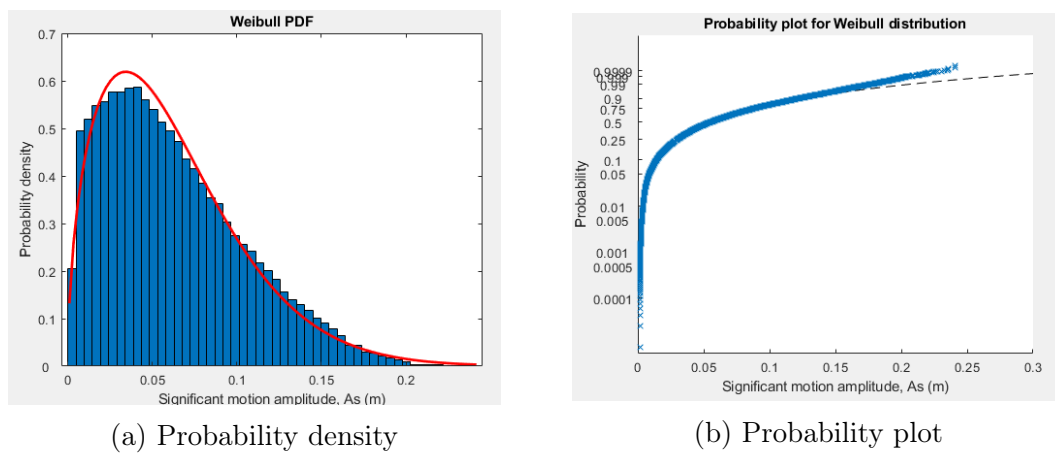
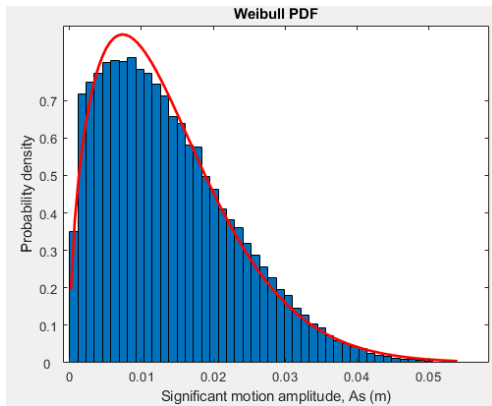
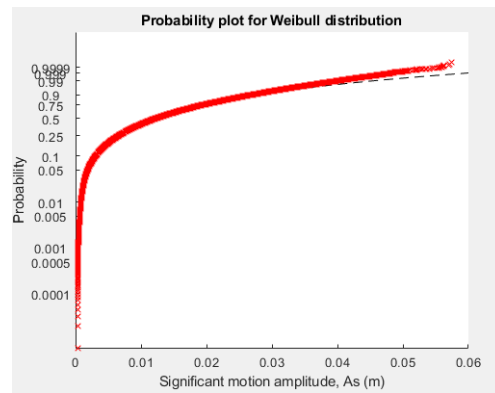


Figure B.9: Weibull distribution density function and probability plot for ship motion amplitudes with  $H_s = 5\text{m}$

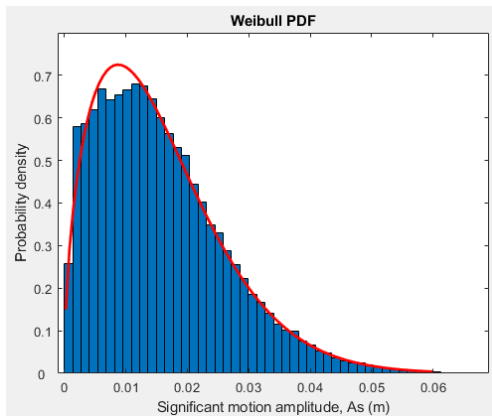
**Weibull Distribution, Direction 180°**



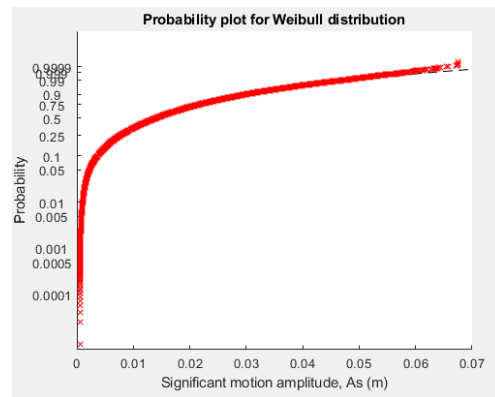
(a) Probability density



(b) Probability plot

Figure B.10: Weibull distribution density function and probability plot for ship motion amplitudes with  $H_s = 3$  m

(a) Probability density



(b) Probability plot

Figure B.11: Weibull distribution density function and probability plot for ship motion amplitudes with  $H_s = 4$  m

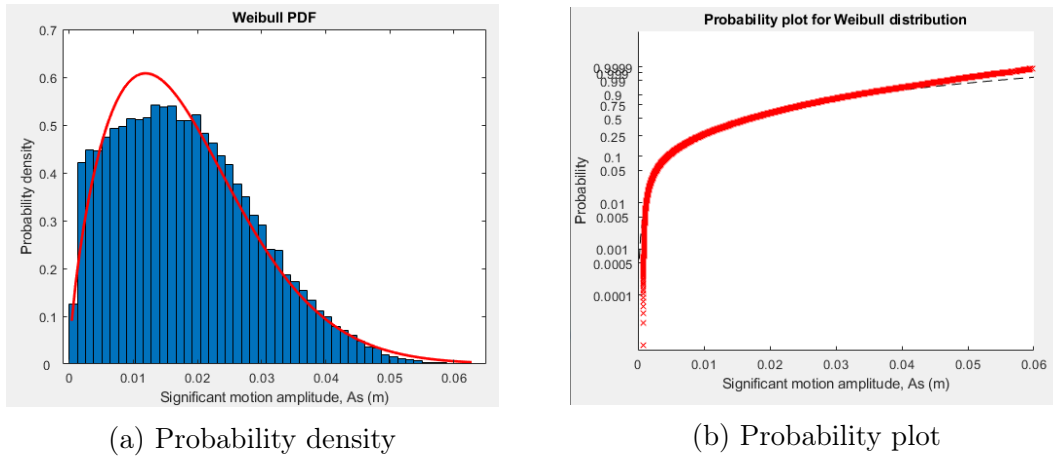


Figure B.12: Weibull distribution density function and probability plot for ship motion amplitudes with  $H_s = 5\text{m}$

### Generalized Extreme Value (GEV) Distribution, Direction $135^\circ$

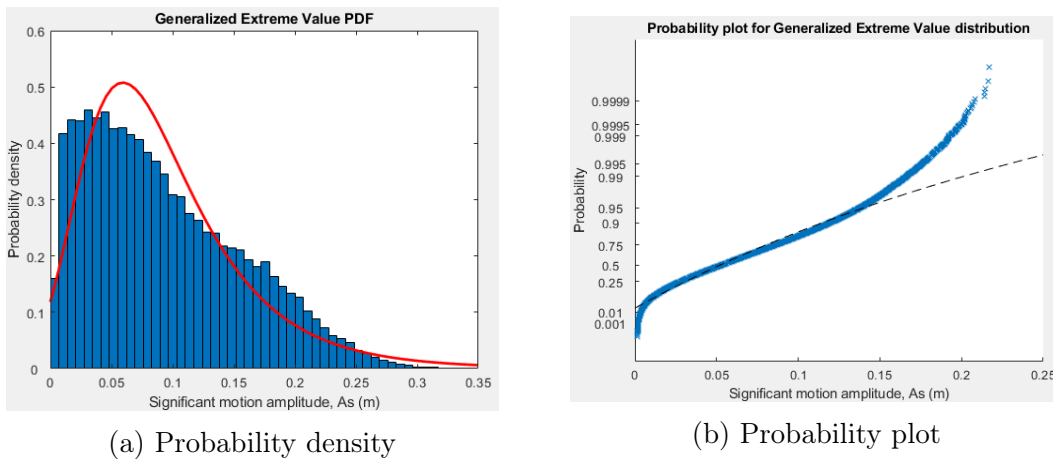
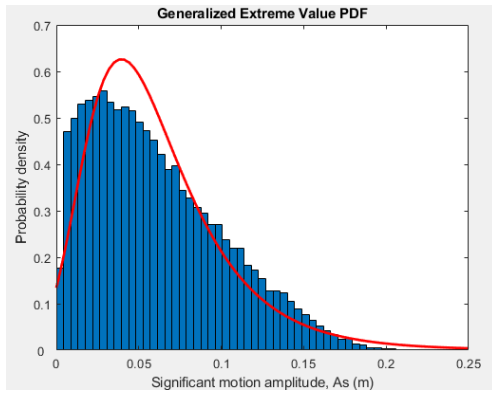
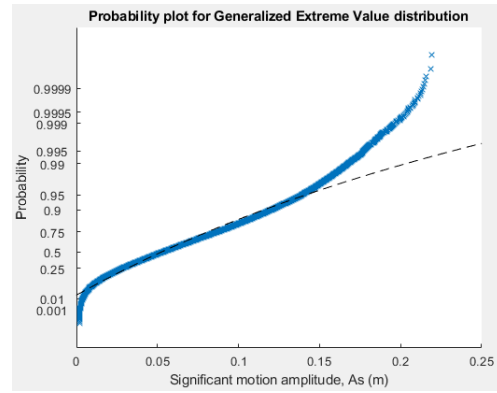


Figure B.13: Generalized Extreme Value distribution density function and probability plot for ship motion amplitudes with  $H_s = 3\text{m}$

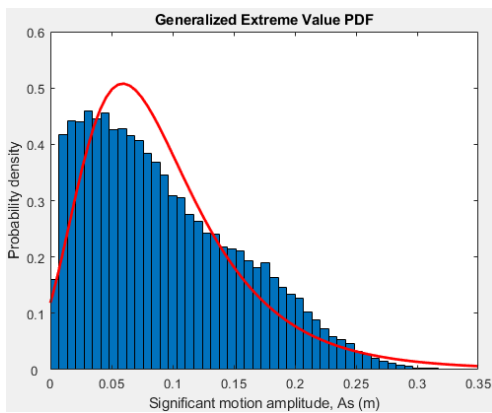


(a) Probability density

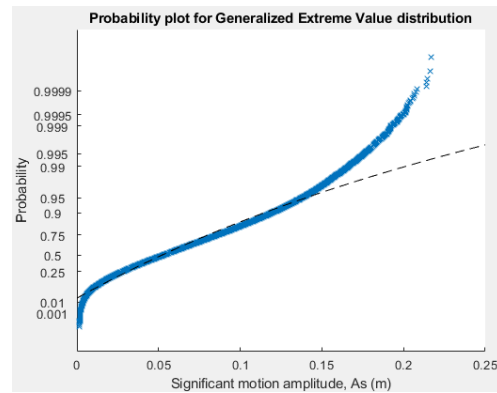


(b) Probability plot

Figure B.14: Generalized Extreme Value distribution density function and probability plot for ship motion amplitudes with  $H_s = 4m$



(a) Probability density

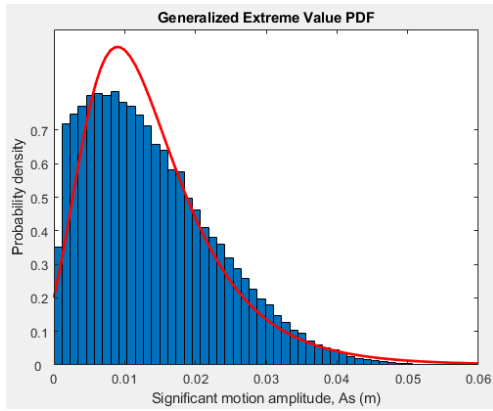


(b) Probability plot

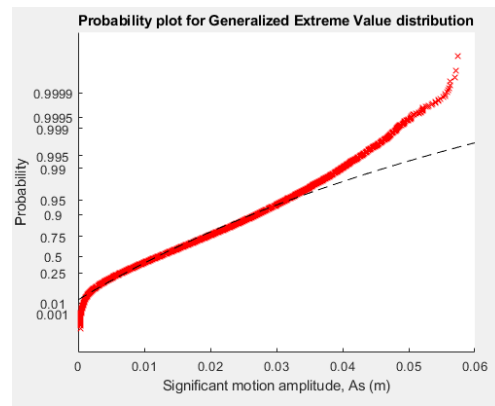
Figure B.15: Generalized Extreme Value distribution density function and probability plot for ship motion amplitudes with  $H_s = 5m$

### Generalized Extreme Value (GEV) Distribution, Direction $180^\circ$



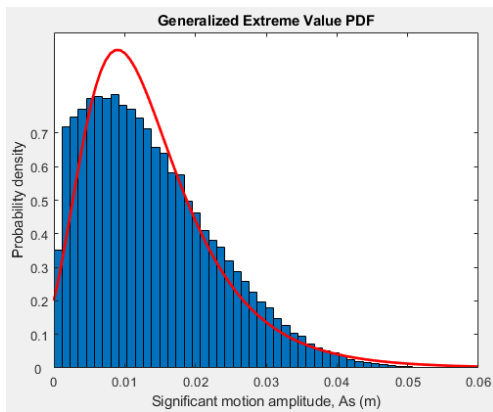


(a) Probability density

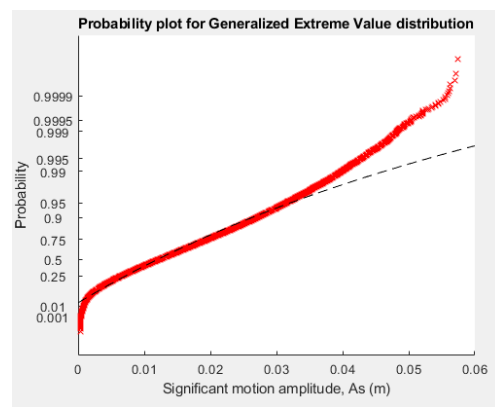


(b) Probability plot

Figure B.16: Generalized Extreme Value distribution density function and probability plot for ship motion amplitudes with  $H_s = 3\text{m}$



(a) Probability density



(b) Probability plot

Figure B.17: Generalized Extreme Value distribution density function and probability plot for ship motion amplitudes with  $H_s = 5\text{m}$

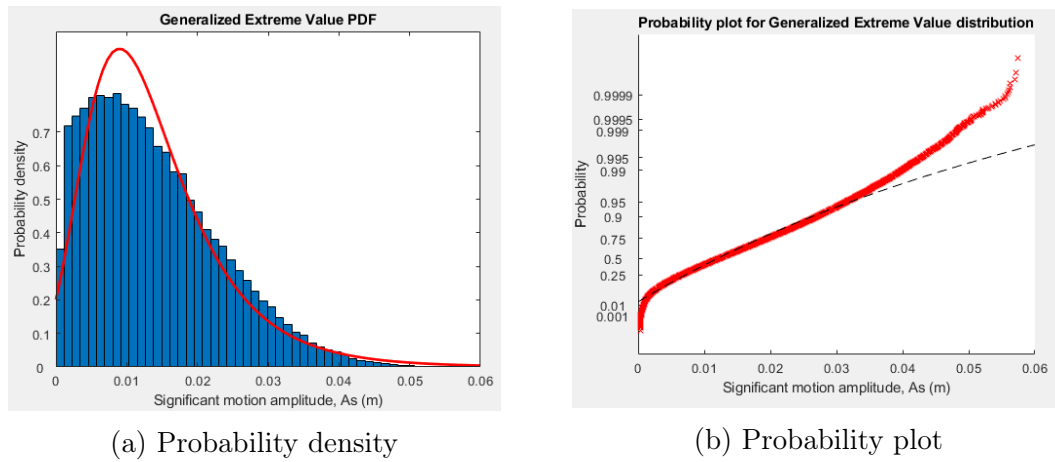


Figure B.18: Generalized Extreme Value distribution density function and probability plot for ship motion amplitudes with  $H_s = 4\text{m}$

### Generalized Pareto (GP) Distribution, Direction $135^\circ$

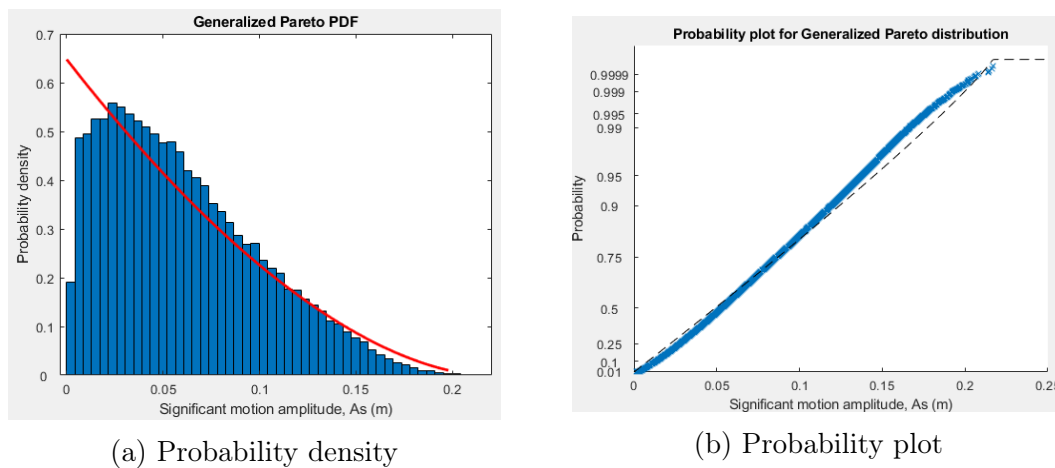


Figure B.19: Generalized Pareto distribution density function and probability plot for ship motion amplitudes with  $H_s = 3\text{m}$

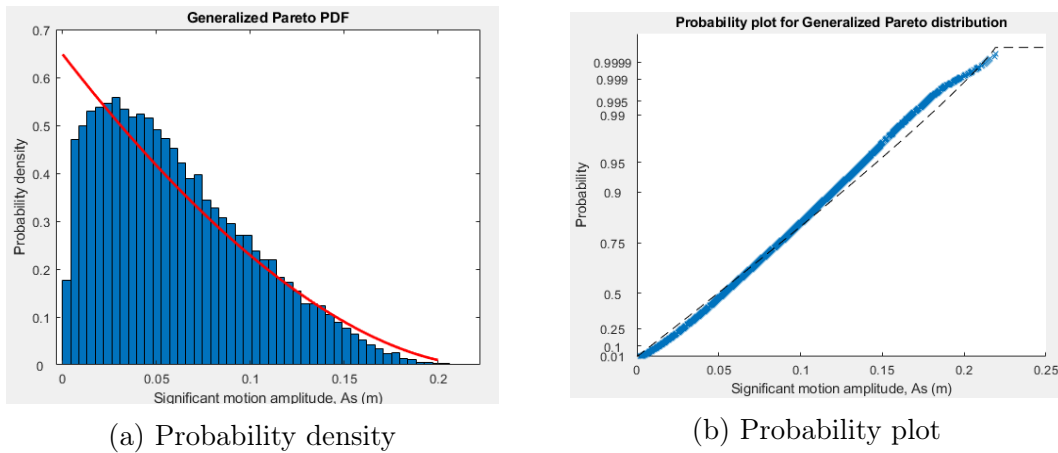


Figure B.20: Generalized Pareto distribution density function and probability plot for ship motion amplitudes with  $H_s = 4\text{m}$

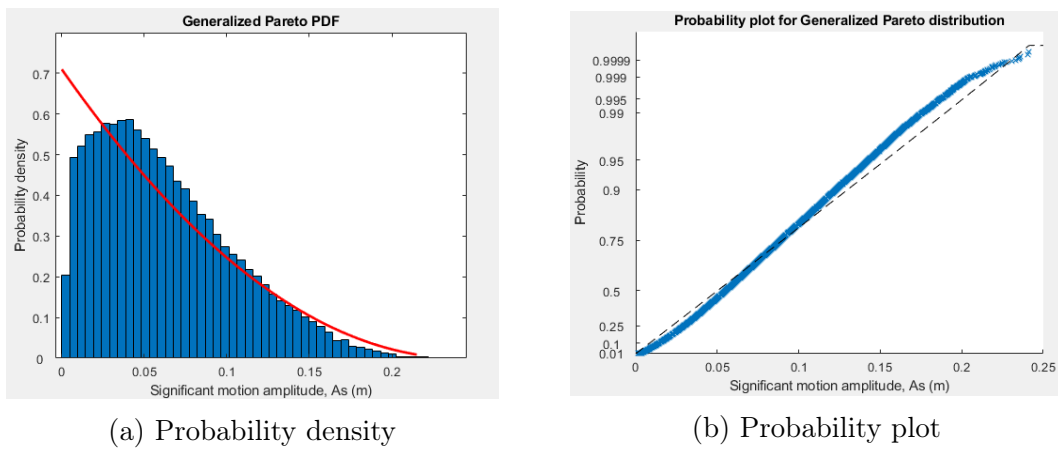


Figure B.21: Generalized Pareto distribution density function and probability plot for ship motion amplitudes with  $H_s = 5\text{m}$

**Generalized Pareto (GP) Distribution, Direction  $180^\circ$**

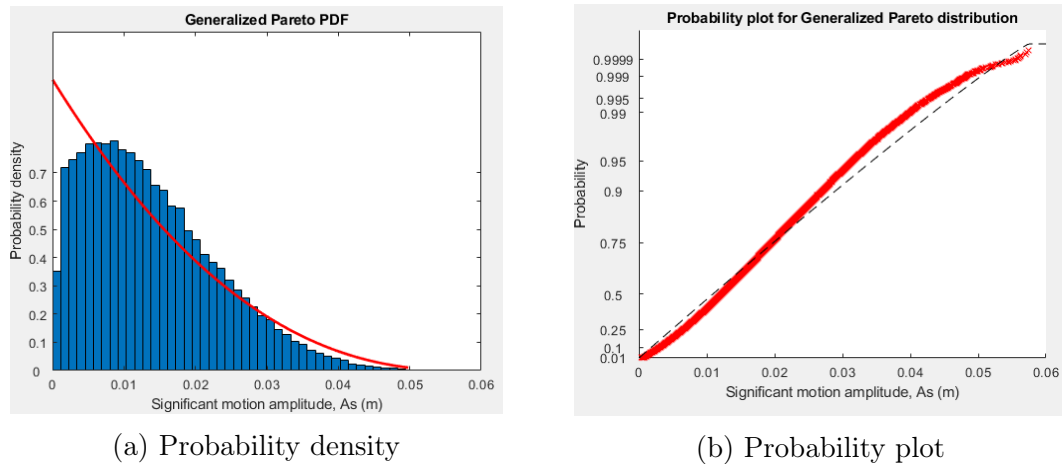


Figure B.22: Generalized Pareto distribution density function and probability plot for ship motion amplitudes with  $H_s = 3\text{m}$

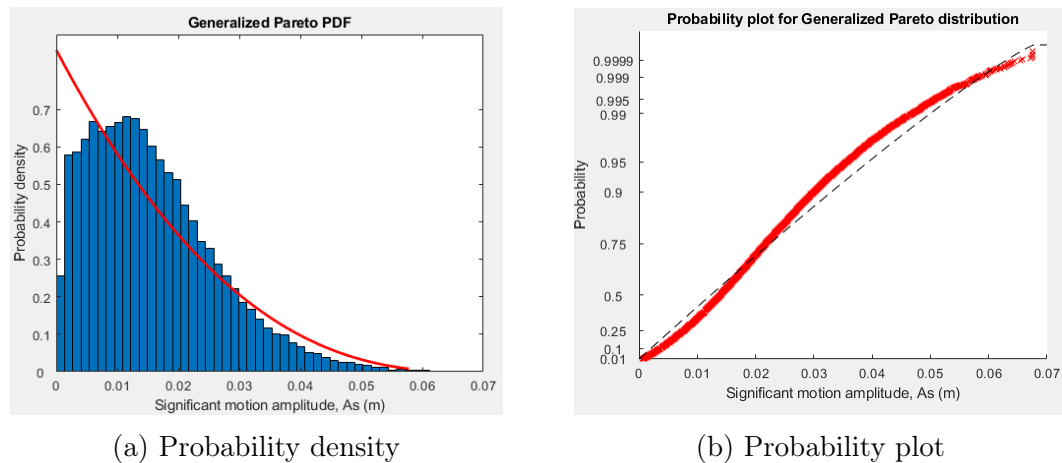


Figure B.23: Generalized Pareto distribution density function and probability plot for ship motion amplitudes with  $H_s = 4\text{m}$

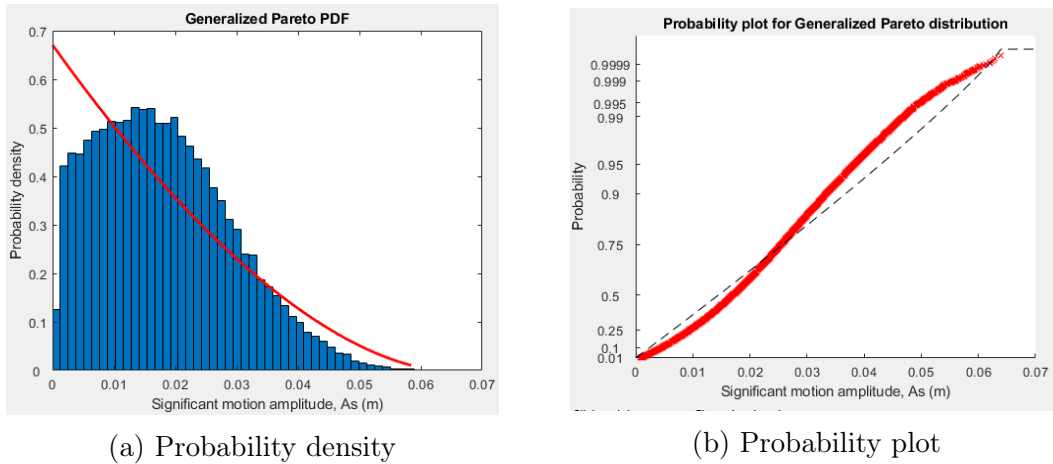


Figure B.24: Generalized Pareto distribution density function and probability plot for ship motion amplitudes with  $H_s = 5\text{m}$

# Appendix C

## List of Figures

### Underkeel clearance figures for $d/D = 1.5, 1.4, 1.3, 1.2$ and $1.1$

Channel Probe Location no(-)	Mike21BW depth (m)	depth/Draught ratio (-)
1	25	1.5
2	24	1.4
3	23	1.4
4	22	1.3
5	21	1.2
6	20	1.1

Table C.1: Channel probe locations, water depths and  $d/D$  ratios

## C.1 Underkeel clearance sensitivity tests

### C.1.1 $\alpha = 135^\circ$

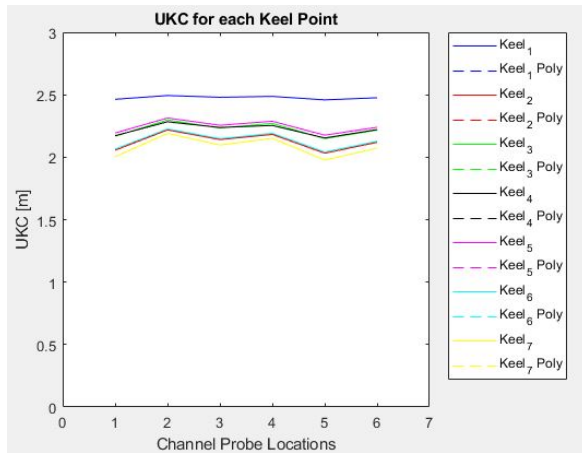


Figure C.1: Underkeel clearance for  $H_s = 3\text{m}$ ,  $T_p = 10\text{s}$

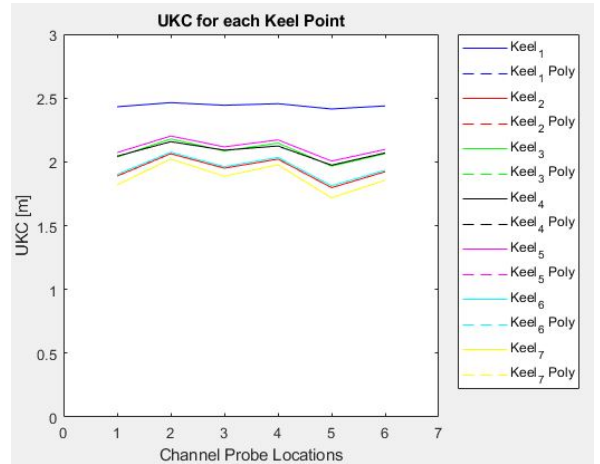


Figure C.2: Underkeel clearance for  $H_s = 4\text{m}$ ,  $T_p = 10\text{s}$

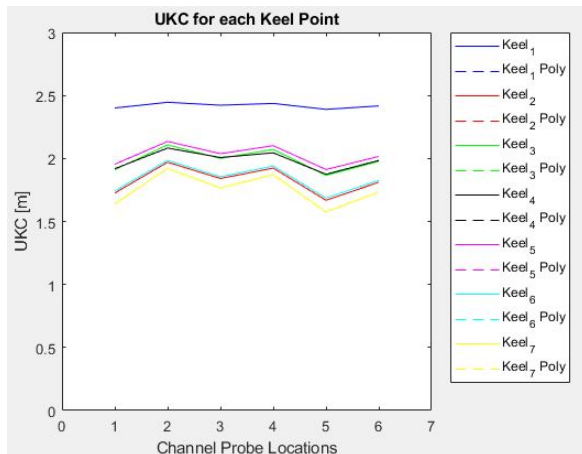
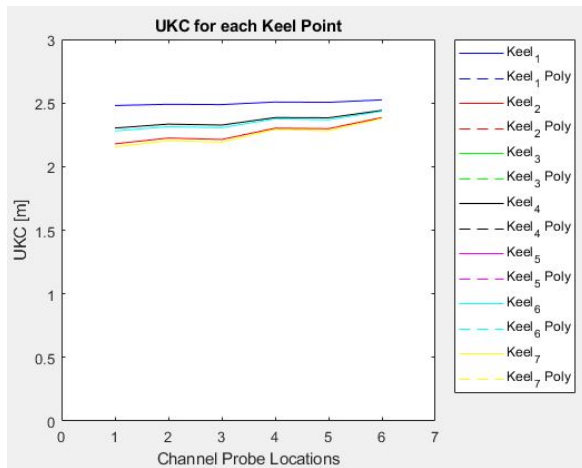
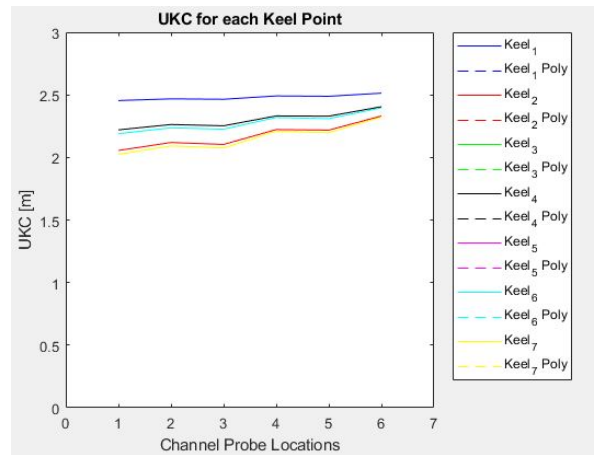
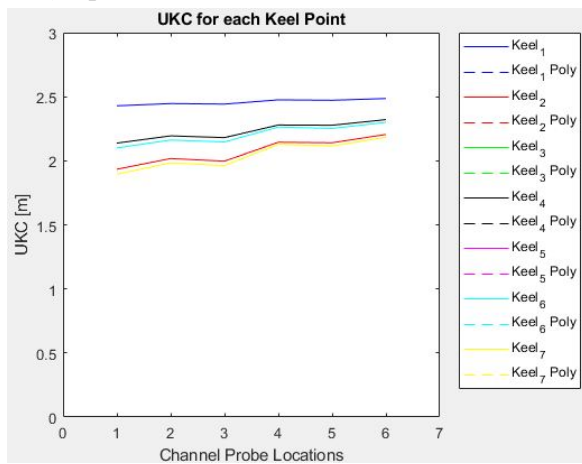


Figure C.3: Underkeel clearance for  $H_s = 5\text{m}$ ,  $T_p = 10\text{s}$

C.1.2  $\alpha = 180^\circ$ Figure C.4: Underkeel clearance for  $H_s = 3\text{m}$ ,  $T_p = 10\text{s}$ Figure C.5: Underkeel clearance for  $H_s = 4\text{m}$ ,  $T_p = 10\text{s}$ Figure C.6: Underkeel clearance for  $H_s = 5\text{m}$ ,  $T_p = 10\text{s}$



## C.2 Underkeel clearance for $d/D = 1.5$ to $1.1$ , depth = 25m, 23m, 21m, 19m and 18m

### C.2.1 $\alpha = 90^\circ$

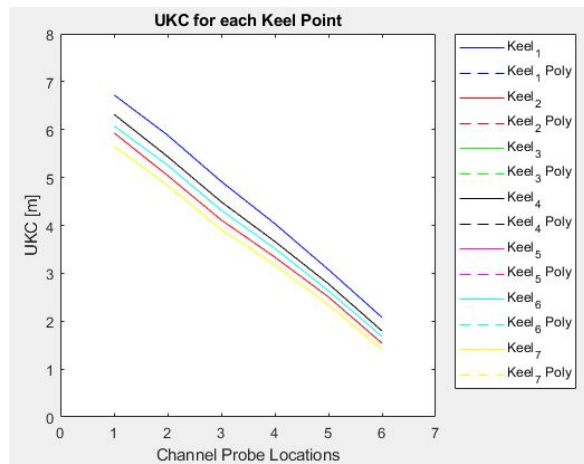


Figure C.7: Underkeel clearance for  $H_s = 3\text{m}$ ,  $T_p = 10\text{s}$

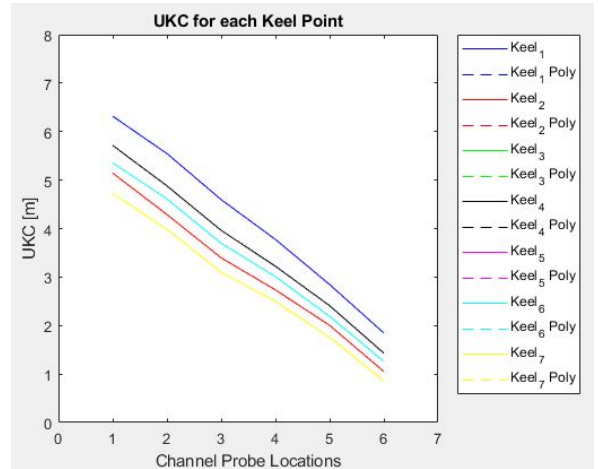


Figure C.8: Underkeel clearance for  $H_s = 4\text{m}$ ,  $T_p = 10\text{s}$

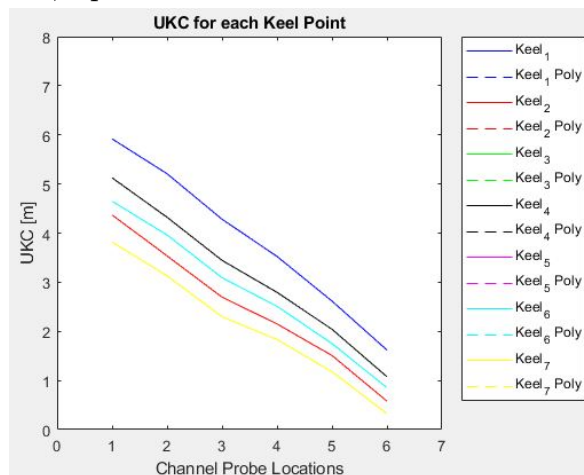
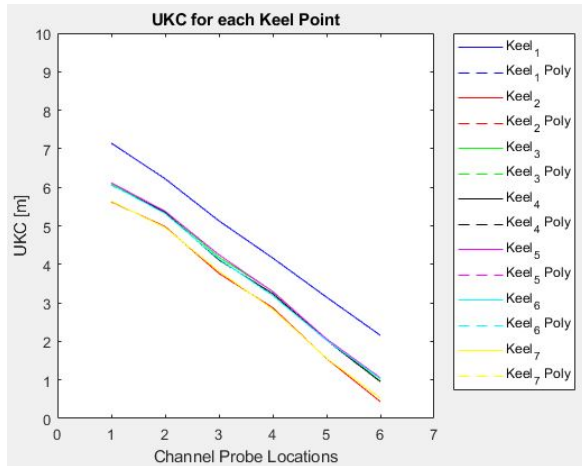
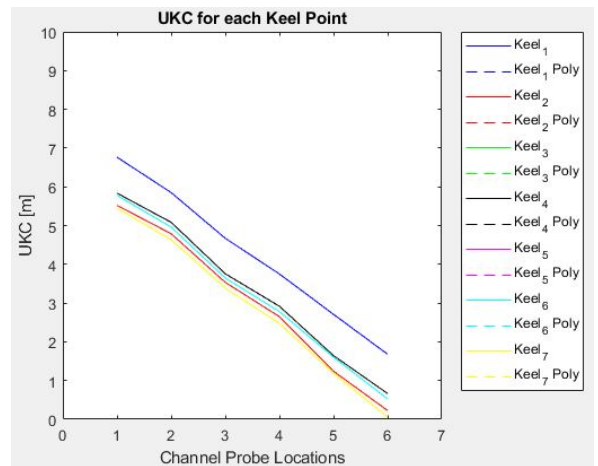
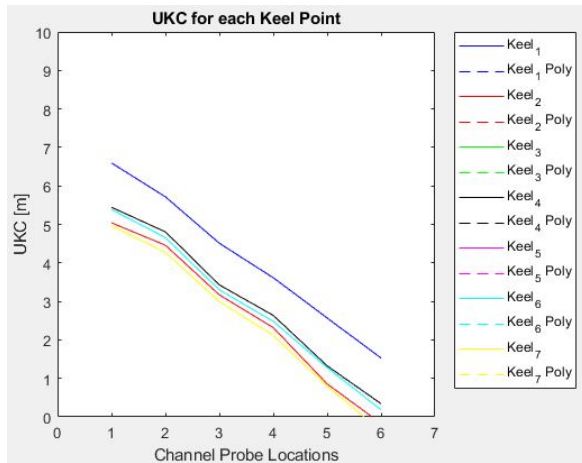


Figure C.9: Underkeel clearance for  $H_s = 5\text{m}$ ,  $T_p = 10\text{s}$

C.2.2  $\alpha = 135^\circ$ Figure C.10: Underkeel clearance for  $H_s = 3\text{m}$ ,  $T_p = 10\text{s}$ Figure C.11: Underkeel clearance for  $H_s = 4\text{m}$ ,  $T_p = 10\text{s}$ Figure C.12: Underkeel clearance for  $H_s = 5\text{m}$ ,  $T_p = 10\text{s}$

**C.2.3  $\alpha = 180^\circ$**

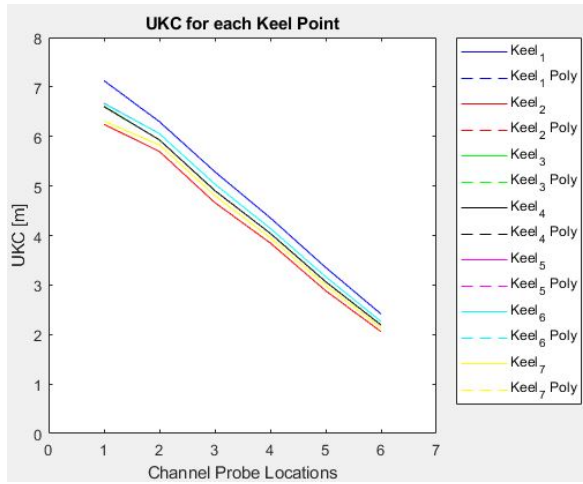


Figure C.13: Underkeel clearance for  $H_s = 3\text{m}$ ,  $T_p = 10\text{s}$

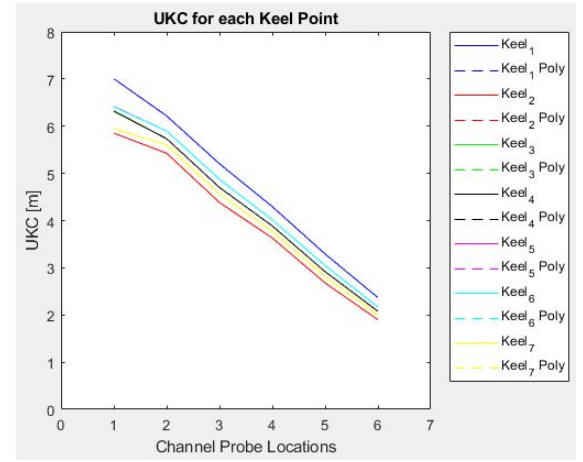


Figure C.14: Underkeel clearance for  $H_s = 4\text{m}$ ,  $T_p = 10\text{s}$

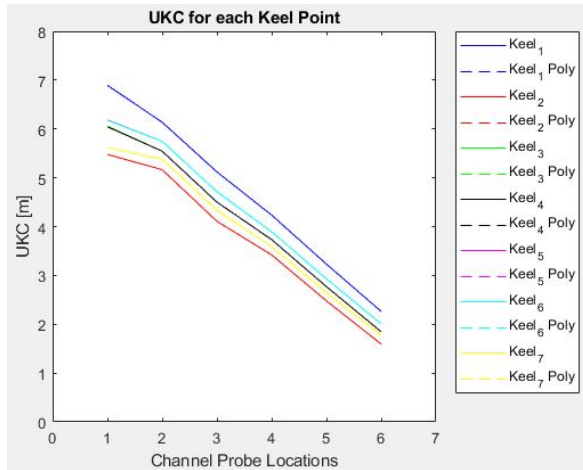


Figure C.15: Underkeel clearance for  $H_s = 5\text{m}$ ,  $T_p = 10\text{s}$

# Appendix D

## List of Tables

### D.1 Depth to draught ( $d/D$ ) test tables

P = Physical Model W = Wavescat model

$\alpha$ ( $^{\circ}$ )	Model	Hs (m)	APP(m)	PQT (m)	SQT (m)	PSH (m)	SSH (m)	FPP (m)
90	P	2.9	0.28	0.63	0.27	0.66	0.30	0.32
	W	3.0	0.35	0.58	0.20	0.44	0.27	0.23
135	P	3.97	0.24	0.21	0.09	0.15	0.15	0.17
	W	4.0	0.23	0.13	0.10	0.16	0.16	0.18
180	P	4.14	0.24	0.06	0.06	0.1	0.08	0.18
	W	4.18	0.17	0.09	0.09	0.12	0.12	0.20

Table D.1: Physical and Wavescat model results for depth to draught ratio ( $d/D$ ) = 1.5

$\alpha(\circ)$	Model	Hs (m)	APP(m)	PQT (m)	SQT (m)	PSH (m)	SSH (m)	FPP (m)
90	P	3.04	0.37	0.65	0.29	0.63	0.36	0.28
	W	3	0.35	0.57	0.2	0.44	0.27	0.21
135	P	4.02	0.25	0.2	0.06	0.12	0.14	0.19
	W	4	0.2	0.15	0.07	0.1	0.11	0.16
180	P	4.11	0.21	0.05	0.05	0.09	0.07	0.18
	W	4	0.15	0.07	0.07	0.09	0.09	0.14

Table D.2: Physical and Wavescat model results for depth to draught ratio  $(d/D) = 1.4$

$\alpha(\circ)$	Model	Hs (m)	APP(m)	PQT (m)	SQT (m)	PSH (m)	SSH (m)	FPP (m)
90	P	3.11	0.28	0.5	0.14	0.47	0.23	0.16
	W	3	0.26	0.44	0.14	0.32	0.22	0.14
135	P	3.99	0.23	0.18	0.05	0.13	0.13	0.17
	W	4	0.19	0.14	0.05	0.16	0.14	0.17
180	P	3.93	0.19	0.05	0.05	0.08	0.06	0.15
	W	4	0.14	0.06	0.06	0.06	0.06	0.11

Table D.3: Physical and Wavescat model results for depth to draught ratio  $(d/D) = 1.3$

$\alpha(\circ)$	Model	Hs (m)	APP(m)	PQT (m)	SQT (m)	PSH (m)	SSH (m)	FPP (m)
90	P	2.89	0.12	0.4	0.14	0.42	0.22	0.19
	W	3	0.09	0.33	0.11	0.29	0.19	0.20
135	P	4.12	0.22	0.19	0.07	0.1	0.14	0.15
	W	4	0.16	0.14	0.10	0.12	0.14	0.16
180	P	3.73	0.09	0.04	0.05	0.07	0.05	0.13
	W	4	0.10	0.06	0.06	0.06	0.06	0.10

Table D.4: Physical and Wavescat model results for depth to draught ratio  $(d/D) = 1.2$

$\alpha$ ( $^{\circ}$ )	Model	Hs (m)	APP(m)	PQT (m)	SQT (m)	PSH (m)	SSH (m)	FPP (m)
90	P	2.62	0.14	0.35	0.1	0.32	0.21	0.11
90	W	3	0.16	0.34	0.08	0.22	0.18	0.09
135	P	2.55	0.09	0.08	0.07	0.11	0.09	0.11
135	W	3	0.09	0.07	0.07	0.08	0.09	0.10
180	P	3.49	0.09	0.04	0.05	0.07	0.05	0.13
180	W	4	0.07	0.06	0.05	0.06	0.05	0.09

Table D.5: Physical and Wavescat model results for depth to draught ratio ( $d/D$ ) = 1.1

## D.2 Underkeel clearance sensitivity test tables for $d/D = 1.1$ , $\alpha = 90^{\circ}$

### D.2.1 As versus Hs test results for the physical and the Wavescat Model

Model	Hs (m)	APP(m)	PQT (m)	SQT (m)	PSH (m)	SSH (m)	FPP (m)
P	1.68	0.19	0.28	0.19	0.48	0.31	0.28
W	1.63	0.10	0.20	0.20	0.41	0.30	0.24
P	5.38	0.54	1.42	0.86	1.5	1.12	0.82
W	5.3	0.40	1.22	1.00	1.30	1.10	1.80

Table D.6: As versus Hs results for  $T_p = 10s$

Model	Hs (m)	APP(m)	PQT (m)	SQT (m)	PSH (m)	SSH (m)	FPP (m)
P	1.58	0.65	0.84	1.01	0.82	0.77	0.4
W	1.62	0.78	0.31	0.94	0.85	0.85	0.62
P	5.5	1.26					1
W	5.7	1.80					1.40

Table D.7: As versus Hs results for  $T_p = 12s$

### D.3 Significant hull motion amplitudes for the underkeel clearance sensitivity tests ( $d/D = 1.1$ ), depth = 20m

Keel points	As P1(m)	As P2(m)	As P3(m)	As P4(m)	As P5(m)	As P6(m)
APP	0.174	0.164	0.159	0.135	0.117	0.118
SQT	0.181	0.156	0.149	0.123	0.109	0.120
PQT	0.181	0.156	0.149	0.123	0.109	0.120
SSH	0.234	0.200	0.192	0.158	0.140	0.150
PSH	0.234	0.200	0.192	0.158	0.140	0.150
FPP	0.252	0.225	0.218	0.181	0.160	0.162

Table D.8: As for  $H_s = 1\text{m}$ ,  $T_p = 10\text{s}$  and  $\alpha = 90^\circ$ 

Keel points	As P1(m)	As P2(m)	As P3(m)	As P4(m)	As P5(m)	As P6(m)
APP	0.417	0.308	0.294	0.242	0.199	0.167
SQT	0.656	0.406	0.384	0.296	0.247	0.207
PQT	0.656	0.406	0.384	0.296	0.247	0.207
SSH	0.729	0.466	0.443	0.345	0.289	0.244
PSH	0.729	0.466	0.443	0.345	0.289	0.244
FPP	0.572	0.417	0.399	0.324	0.271	0.229

Table D.9: As for  $H_s = 1\text{m}$ ,  $T_p = 12\text{s}$  and  $\alpha = 90^\circ$ 

Keel points	As P1(m)	As P2(m)	As P3(m)	As P4(m)	As P5(m)	As P6(m)
APP	0.261	0.246	0.236	0.201	0.176	0.176
SQT	0.272	0.233	0.222	0.184	0.164	0.179
PQT	0.272	0.233	0.222	0.184	0.164	0.179
SSH	0.352	0.300	0.285	0.237	0.212	0.224
PSH	0.352	0.300	0.285	0.237	0.212	0.224
FPP	0.378	0.338	0.323	0.271	0.241	0.242

Table D.10: As for  $H_s = 2\text{m}$ ,  $T_p = 10\text{s}$  and  $\alpha = 90^\circ$

Keel points	As P1(m)	As P2(m)	As P3(m)	As P4(m)	As P5(m)	As P6(m)
APP	0.620	0.461	0.440	0.363	0.300	0.250
SQT	0.978	0.607	0.577	0.445	0.372	0.310
PQT	0.978	0.607	0.577	0.445	0.372	0.310
SSH	1.088	0.696	0.665	0.517	0.436	0.366
PSH	1.088	0.696	0.665	0.517	0.436	0.366
FPP	0.852	0.623	0.599	0.486	0.409	0.344

Table D.11: As for  $H_s = 2\text{m}$ ,  $T_p = 12\text{s}$  and  $\alpha = 90^\circ$ 

Keel points	As P1(m)	As P2(m)	As P3(m)	As P4(m)	As P5(m)	As P6(m)
APP	0.346	0.329	0.315	0.268	0.233	0.234
SQT	0.360	0.312	0.296	0.245	0.218	0.238
PQT	0.360	0.312	0.296	0.245	0.218	0.238
SSH	0.466	0.400	0.381	0.315	0.281	0.298
PSH	0.466	0.400	0.381	0.315	0.281	0.298
FPP	0.501	0.450	0.430	0.361	0.319	0.322

Table D.12: As for  $H_s = 3\text{m}$ ,  $T_p = 10\text{s}$  and  $\alpha = 90^\circ$ 

Keel points	As P1(m)	As P2(m)	As P3(m)	As P4(m)	As P5(m)	As P6(m)
APP	0.828	0.614	0.587	0.484	0.397	0.333
SQT	1.306	0.808	0.769	0.592	0.493	0.414
PQT	1.306	0.808	0.769	0.592	0.493	0.414
SSH	1.453	0.927	0.887	0.689	0.578	0.488
PSH	1.453	0.927	0.887	0.689	0.578	0.488
FPP	1.138	0.829	0.798	0.648	0.542	0.459

Table D.13: As for  $H_s = 3\text{m}$ ,  $T_p = 12\text{s}$  and  $\alpha = 90^\circ$



Keel points	As P1(m)	As P2(m)	As P3(m)	As P4(m)	As P5(m)	As P6(m)
APP	0.513	0.491	0.471	0.400	0.345	0.347
SQT	0.536	0.466	0.443	0.366	0.322	0.352
PQT	0.536	0.466	0.443	0.366	0.322	0.352
SSH	0.694	0.599	0.569	0.470	0.416	0.442
PSH	0.694	0.599	0.569	0.470	0.416	0.442
FPP	0.745	0.673	0.644	0.539	0.472	0.476

Table D.14: As for  $H_s = 4\text{m}$ ,  $T_p = 10\text{s}$  and  $\alpha = 90^\circ$ 

Keel points	As P1(m)	As P2(m)	As P3(m)	As P4(m)	As P5(m)	As P6(m)
APP	1.002	0.919	0.881	0.722	0.589	0.498
SQT	1.463	1.209	1.153	0.883	0.730	0.619
PQT	1.463	1.209	1.153	0.883	0.730	0.619
SSH	1.673	1.387	1.330	1.028	0.855	0.729
PSH	1.673	1.387	1.330	1.028	0.855	0.729
FPP	1.411	1.241	1.198	0.967	0.804	0.685

Table D.15: As for  $H_s = 4\text{m}$ ,  $T_p = 12\text{s}$  and  $\alpha = 90^\circ$ 

Keel points	As P1(m)	As P2(m)	As P3(m)	As P4(m)	As P5(m)	As P6(m)
APP	0.677	0.654	0.624	0.528	0.455	0.455
SQT	0.708	0.622	0.587	0.484	0.425	0.463
PQT	0.708	0.622	0.587	0.484	0.425	0.463
SSH	0.917	0.799	0.755	0.621	0.549	0.581
PSH	0.917	0.799	0.755	0.621	0.549	0.581
FPP	0.983	0.898	0.853	0.712	0.623	0.626

Table D.16: As for  $H_s = 5\text{m}$ ,  $T_p = 10\text{s}$  and  $\alpha = 90^\circ$

Keel points	As P1(m)	As P2(m)	As P3(m)	As P4(m)	As P5(m)	As P6(m)
APP	1.322	1.221	1.171	0.954	0.782	0.659
SQT	1.937	1.606	1.531	1.165	0.968	0.821
PQT	1.937	1.606	1.531	1.165	0.968	0.821
SSH	2.216	1.843	1.766	1.355	1.134	0.966
PSH	2.216	1.843	1.766	1.355	1.134	0.966
FPP	1.866	1.649	1.592	1.276	1.066	0.908

Table D.17: As for  $H_s = 5\text{m}$ ,  $T_p = 12\text{s}$  and  $\alpha = 90^\circ$ 

Keel points	As P1(m)	As P2(m)	As P3(m)	As P4(m)	As P5(m)	As P6(m)
APP	0.839	0.815	0.777	0.655	0.563	0.560
SQT	0.877	0.777	0.732	0.601	0.527	0.570
PQT	0.877	0.777	0.732	0.601	0.527	0.570
SSH	1.134	0.999	0.942	0.772	0.681	0.716
PSH	1.134	0.999	0.942	0.772	0.681	0.716
FPP	1.217	1.121	1.063	0.884	0.772	0.771

Table D.18: As for  $H_s = 5.5\text{m}$ ,  $T_p = 10\text{s}$  and  $\alpha = 90^\circ$ 

Keel points	As P1(m)	As P2(m)	As P3(m)	As P4(m)	As P5(m)	As P6(m)
APP	1.645	1.889	1.458	1.182	0.976	0.817
SQT	2.411	2.674	1.906	1.441	1.210	1.020
PQT	2.411	2.674	1.906	1.441	1.210	1.020
SSH	2.757	2.989	2.199	1.677	1.418	1.202
PSH	2.757	2.989	2.199	1.677	1.418	1.202
FPP	2.322	2.499	1.981	1.580	1.332	1.129

Table D.19: As for  $H_s = 5.5\text{m}$ ,  $T_p = 12\text{s}$  and  $\alpha = 90^\circ$

Keel points	As P1(m)	As P2(m)	As P3(m)	As P4(m)	As P5(m)	As P6(m)
APP	0.998	0.977	0.927	0.781	0.668	0.660
SQT	1.040	0.934	0.875	0.717	0.626	0.673
PQT	1.040	0.934	0.875	0.717	0.626	0.673
SSH	1.346	1.200	1.126	0.920	0.810	0.845
PSH	1.346	1.200	1.126	0.920	0.810	0.845
FPP	1.446	1.345	1.270	1.054	0.918	0.909

Table D.20: As for  $H_s = 6\text{m}$ ,  $T_p = 10\text{s}$  and  $\alpha = 90^\circ$ 

Keel points	As P1(m)	As P2(m)	As P3(m)	As P4(m)	As P5(m)	As P6(m)
APP	1.322	1.221	1.171	0.954	0.782	0.659
SQT	1.937	1.606	1.531	1.165	0.968	0.821
PQT	1.937	1.606	1.531	1.165	0.968	0.821
SSH	2.216	1.843	1.766	1.355	1.134	0.966
PSH	2.216	1.843	1.766	1.355	1.134	0.966
FPP	1.866	1.649	1.592	1.276	1.066	0.908

Table D.21: As for  $H_s = 6\text{m}$ ,  $T_p = 12\text{s}$  and  $\alpha = 90^\circ$ 

## D.4 Significant hull motion amplitudes for MIKE21BW measurement points

### D.4.1 $T_p = 10\text{s}$ and $\alpha = 90^\circ$

Keel points	d/D = 1.5	d/D = 1.4	d/D = 1.3	d/D = 1.2	d/D = 1.1
APP	1.098	0.967	0.716	0.548	0.686
SQT	1.571	1.486	1.414	1.714	2.388
SSH	1.883	1.788	1.59	1.809	2.451
PQT	2.051	1.879	1.637	1.796	2.459
PSH	1.599	1.572	1.488	1.78	2.409
FPP	1.332	1.176	0.886	0.661	1.101

Table D.22: As for  $H_s = 3\text{m}$ ,  $T_p = 10\text{s}$  and  $\alpha = 90^\circ$

Keel points	$d/D = 1.5$	$d/D = 1.4$	$d/D = 1.3$	$d/D = 1.2$	$d/D = 1.1$
APP	1.45	1.286	0.945	0.719	0.906
SQT	2.074	1.982	1.87	2.254	3.141
SSH	2.486	2.386	2.101	2.38	3.223
PQT	2.709	2.508	2.163	2.362	3.234
PSH	2.112	2.097	1.967	2.341	3.169
FPP	1.758	1.566	1.171	0.868	1.454

Table D.23: As for  $H_s = 4\text{m}$ ,  $T_p = 10\text{s}$  and  $\alpha = 90^\circ$ 

Keel points	$d/D = 1.5$	$d/D = 1.4$	$d/D = 1.3$	$d/D = 1.2$	$d/D = 1.1$
APP	1.797	1.602	1.172	0.885	1.12
SQT	2.565	2.478	2.323	2.782	3.874
SSH	3.079	2.985	2.61	2.935	3.975
PQT	3.355	3.138	2.688	2.912	3.988
PSH	2.611	2.62	2.443	2.889	3.908
FPP	2.177	1.953	1.453	1.067	1.801

Table D.24: As for  $H_s = 5\text{m}$ ,  $T_p = 10\text{s}$  and  $\alpha = 90^\circ$ 

Keel points	$d/D = 1.5$	$d/D = 1.4$	$d/D = 1.3$	$d/D = 1.2$	$d/D = 1.1$
APP	1.046	0.744	0.683	0.686	0.592
SQT	0.813	0.62	0.725	1.064	1.974
SSH	1.217	0.936	1.033	1.208	1.881
PQT	1.28	1.022	1.13	1.313	1.912
PSH	0.904	0.7	0.819	1.184	2.039
FPP	1.153	0.872	0.856	0.934	0.795

Table D.25: As for  $H_s = 3\text{m}$ ,  $T_p = 10\text{s}$  and  $\alpha = 135^\circ$

Keel points	$d/D = 1.5$	$d/D = 1.4$	$d/D = 1.3$	$d/D = 1.2$	$d/D = 1.1$
APP	1.193	0.934	0.89	1.08	1.054
SQT	1.331	1.257	1.613	2.336	2.911
SSH	1.444	1.241	1.62	2.294	3.02
PQT	1.337	1.196	1.593	2.203	3.012
PSH	1.471	1.368	1.699	2.408	2.913
FPP	1.222	1.004	0.97	1.056	1.042

Table D.26: As for  $H_s = 4\text{m}$ ,  $T_p = 10\text{s}$  and  $\alpha = 135^\circ$ 

Keel points	$d/D = 1.5$	$d/D = 1.4$	$d/D = 1.3$	$d/D = 1.2$	$d/D = 1.1$
APP	1.48	1.107	1.045	1.264	1.233
SQT	1.635	1.493	1.889	2.731	3.406
SSH	1.776	1.476	1.897	2.685	3.536
PQT	1.638	1.423	1.865	2.58	3.527
PSH	1.808	1.624	1.989	2.814	3.41
FPP	1.511	1.191	1.138	1.237	1.221

Table D.27: As for  $H_s = 5\text{m}$ ,  $T_p = 10\text{s}$  and  $\alpha = 135^\circ$ 

Keel points	$d/D = 1.5$	$d/D = 1.4$	$d/D = 1.3$	$d/D = 1.2$	$d/D = 1.1$
APP	0.777	0.45	0.349	0.218	0.218
SQT	0.813	0.578	0.506	0.425	0.846
SSH	0.978	0.674	0.578	0.503	0.86
PQT	0.861	0.579	0.545	0.517	0.861
PSH	0.882	0.619	0.522	0.442	0.862
FPP	0.728	0.388	0.325	0.262	0.264

Table D.28: As for  $H_s = 3\text{m}$ ,  $T_p = 10\text{s}$  and  $\alpha = 180^\circ$

Keel points	d/D = 1.5	d/D = 1.4	d/D = 1.3	d/D = 1.2	d/D = 1.1
APP	1.014	0.591	0.456	0.285	0.285
SQT	1.057	0.76	0.662	0.557	1.108
SSH	1.274	0.885	0.755	0.658	1.126
PQT	1.12	0.759	0.711	0.676	1.127
PSH	1.142	0.814	0.682	0.579	1.129
FPP	0.944	0.509	0.423	0.343	0.345

Table D.29: As for  $H_s = 4\text{m}$ ,  $T_p = 10\text{s}$  and  $\alpha = 180^\circ$ 

Keel points	d/D = 1.5	d/D = 1.4	d/D = 1.3	d/D = 1.2	d/D = 1.1
APP	1.239	0.727	0.559	0.432	0.44
SQT	1.288	0.934	0.812	0.851	1.591
SSH	1.558	1.087	0.926	1.038	1.633
PQT	1.367	0.931	0.87	1.062	1.631
PSH	1.388	1.002	0.837	0.882	1.621
FPP	1.147	0.626	0.518	0.514	0.511

Table D.30: As for  $H_s = 5\text{m}$ ,  $T_p = 10\text{s}$  and  $\alpha = 180^\circ$ 

## D.5 Significant hull motion amplitudes for values for Mike21BW measurement points

### D.5.1 $T_p = 14\text{s}$ , $16\text{s}$ and $18\text{s}$ and $\alpha = 90^\circ$

Probe1	Probe2	Probe3	Probe4	Probe5	Probe6
1.359	1.248	1.176	0.867	0.728	0.630
2.308	2.251	2.108	1.751	1.447	1.247
4.696	4.287	3.991	2.909	2.417	2.077
6.483	5.993	5.589	4.187	3.478	2.993
5.232	4.849	4.517	3.411	2.828	2.432
5.921	5.404	5.050	3.677	3.065	2.638
2.022	1.972	1.870	1.560	1.297	1.121

Table D.31: As for  $H_s = 3\text{m}$ ,  $T_p = 14\text{s}$

Probe1	Probe2	Probe3	Probe4	Probe5	Probe6
1.846	1.697	1.568	1.204	1.025	0.857
3.112	3.003	2.773	2.387	1.985	1.651
6.399	5.834	5.319	4.035	3.403	2.821
8.817	8.124	7.431	5.786	4.869	4.042
7.115	6.568	6.001	4.706	3.950	3.277
8.062	7.357	6.734	5.105	4.320	3.590
2.717	2.633	2.464	2.129	1.781	1.490

Table D.32: As for  $H_s = 4m$ ,  $T_p = 14s$ 

Probe1	Probe2	Probe3	Probe4	Probe5	Probe6
1.602	1.363	1.355	1.017	0.959	0.782
2.538	2.322	2.226	1.868	1.755	1.435
4.813	4.037	3.471	2.583	2.359	1.935
6.333	5.404	4.534	3.449	3.242	2.647
5.131	4.386	3.752	2.868	2.730	2.224
5.870	4.927	4.097	3.020	2.755	2.259
2.139	1.975	1.908	1.602	1.518	1.239

Table D.33: As for  $H_s = 3m$ ,  $T_p = 16s$ 

Probe1	Probe2	Probe3	Probe4	Probe5	Probe6
2.127	1.811	1.812	1.363	1.303	1.074
3.382	3.082	2.973	2.510	2.366	1.939
6.392	5.368	4.646	3.466	3.206	2.647
8.412	7.182	6.065	4.627	4.401	3.622
6.815	5.828	5.017	3.847	3.704	3.045
7.794	6.552	5.484	4.051	3.749	3.097
2.849	2.621	2.548	2.153	2.048	1.678

Table D.34: As for  $H_s = 4m$ ,  $T_p = 16s$ 

Probe1	Probe2	Probe3	Probe4	Probe5	Probe6
1.660	1.419	1.409	1.129	0.981	0.839
2.464	2.260	2.275	2.046	1.784	1.542
3.932	3.337	3.269	2.609	2.419	1.867
4.883	4.187	4.164	3.388	3.313	2.530
4.075	3.495	3.496	2.859	2.786	2.172
4.529	3.825	3.743	2.941	2.828	2.088
2.104	1.934	1.959	1.758	1.542	1.330

Table D.35: As for  $H_s = 3m$ ,  $T_p = 18s$

Probe1	Probe2	Probe3	Probe4	Probe5	Probe6
2.195	1.889	1.862	1.516	1.339	1.159
3.275	3.022	3.027	2.751	2.414	2.109
5.201	4.446	4.321	3.505	3.304	2.574
6.458	5.575	5.504	4.551	4.516	3.488
5.387	4.652	4.620	3.840	3.795	2.995
5.987	5.093	4.945	3.951	3.868	2.885
2.795	2.584	2.605	2.363	2.089	1.822

Table D.36: As for Hs = 4m, Tp = 18s

**D.5.2 Tp = 14s, 16s and 18s and  $\alpha = 135^\circ$** 

Probe1	Probe2	Probe3	Probe4	Probe5	Probe6
0.604	0.614	0.593	0.743	0.690	0.674
1.852	1.547	1.494	1.866	1.964	1.750
2.096	1.943	2.020	2.372	2.156	1.892
3.274	3.041	2.974	3.696	3.553	3.151
2.730	2.526	2.437	3.068	2.996	2.606
2.596	2.447	2.538	2.981	2.680	2.463
1.656	1.378	1.350	1.656	1.738	1.604

Table D.37: As for Hs = 3m, Tp = 14s

Probe1	Probe2	Probe3	Probe4	Probe5	Probe6
0.804	0.840	0.805	1.002	0.933	0.914
2.458	2.118	2.035	2.514	2.655	2.386
2.784	2.649	2.739	3.201	2.913	2.564
4.347	4.153	4.036	4.984	4.803	4.280
3.624	3.450	3.308	4.137	4.049	3.542
3.450	3.337	3.441	4.023	3.623	3.336
2.198	1.889	1.839	2.231	2.351	2.186

Table D.38: As for Hs = 4m, Tp = 14s

Probe1	Probe2	Probe3	Probe4	Probe5	Probe6
0.841	0.729	0.736	0.839	0.790	0.780
2.366	1.761	1.713	2.003	2.002	1.872
2.001	1.907	1.963	2.281	2.096	1.810
3.186	3.023	3.036	3.507	3.343	3.096
2.809	2.586	2.580	2.979	2.868	2.665
2.004	2.247	2.329	2.683	2.434	2.188
1.978	1.524	1.481	1.714	1.715	1.665

Table D.39: As for Hs = 3m, Tp = 16s



Probe1	Probe2	Probe3	Probe4	Probe5	Probe6
1.111	0.997	1.007	1.135	1.067	1.059
3.120	2.405	2.349	2.709	2.708	2.547
2.644	2.605	2.682	3.090	2.828	2.472
4.207	4.131	4.153	4.747	4.516	4.217
3.709	3.534	3.532	4.030	3.876	3.630
2.652	3.071	3.179	3.635	3.284	2.984
2.608	2.082	2.031	2.318	2.320	2.263

Table D.40: As for  $H_s = 4\text{m}$ ,  $T_p = 16\text{s}$ 

Probe1	Probe2	Probe3	Probe4	Probe5	Probe6
0.905	0.776	0.800	0.897	0.838	0.842
2.616	1.966	1.946	2.250	2.201	1.978
2.069	1.730	1.784	2.070	1.904	1.687
3.133	2.555	2.602	2.959	2.801	2.654
2.787	2.255	2.288	2.587	2.470	2.365
1.872	1.709	1.803	2.077	1.850	1.706
2.173	1.651	1.639	1.881	1.840	1.694

Table D.41: As for  $H_s = 3\text{m}$ ,  $T_p = 18\text{s}$ 

Probe1	Probe2	Probe3	Probe4	Probe5	Probe6
1.197	1.061	1.090	1.207	1.121	1.135
3.452	2.697	2.662	3.034	2.973	2.670
2.735	2.360	2.432	2.790	2.550	2.286
4.139	3.496	3.549	3.984	3.760	3.584
3.681	3.087	3.121	3.483	3.317	3.193
2.479	2.325	2.453	2.797	2.464	2.312
2.868	2.265	2.241	2.536	2.483	2.286

Table D.42: As for  $H_s = 4\text{m}$ ,  $T_p = 18\text{s}$ 

## D.6 Underkeel clearance values for Mike21BW measurement points

### D.6.1 $T_p = 10\text{s}$ and $\alpha = 90^\circ$ , $135^\circ$ and $180^\circ$

Keel points	$d/D = 1.5$	$d/D = 1.4$	$d/D = 1.3$	$d/D = 1.2$	$d/D = 1.1$
APP	5.06	4.306	2.864	1.176	1.57
SQT	4.182	3.34	1.564	-0.992	-1.882
SSH	3.602	2.778	1.238	-1.171	-1.998
PQT	3.288	2.608	1.151	-1.145	-2.014
PSH	4.129	3.18	1.428	-1.116	-1.922
FPP	4.627	3.916	2.546	0.965	1.399

Table D.43: UKC for  $H_s = 3\text{m}$ ,  $T_p = 10\text{s}$  and  $\alpha = 90^\circ$

Keel points	d/D = 1.5	d/D = 1.4	d/D = 1.3	d/D = 1.2	d/D = 1.1
APP	4.406	3.712	2.437	0.857	-3.283
SQT	3.246	2.416	0.717	-1.998	-3.436
SSH	2.48	1.666	0.287	-2.231	-3.455
PQT	2.065	1.439	0.172	-2.198	-3.334
PSH	3.176	2.203	0.537	-2.16	1.036
FPP	3.833	3.191	2.017	0.58	

Table D.44: UKC for  $H_s = 4\text{m}$ ,  $T_p = 10\text{s}$  and  $\alpha = 90^\circ$ 

Keel points	d/D = 1.5	d/D = 1.4	d/D = 1.3	d/D = 1.2	d/D = 1.1
APP	3.761	3.124	2.014	0.55	0.959
SQT	2.332	1.494	-0.126	-2.979	-4.646
SSH	1.377	0.552	-0.66	-3.264	-4.834
PQT	0.863	0.267	-0.804	-3.221	-4.858
PSH	2.247	1.23	-0.349	-3.178	-4.708
FPP	3.054	2.471	1.492	0.21	0.686

Table D.45: UKC for  $H_s = 5\text{m}$ ,  $T_p = 10\text{s}$  and  $\alpha = 90^\circ$ 

Keel points	d/D = 1.5	d/D = 1.4	d/D = 1.3	d/D = 1.2	d/D = 1.1
APP	5.158	4.72	2.925	0.919	1.459
SQT	5.591	4.95	2.846	0.215	-1.112
SSH	4.84	4.363	2.274	-0.052	-0.939
PQT	4.723	4.203	2.094	-0.247	-0.997
PSH	5.423	4.802	2.672	-0.008	-1.232
FPP	4.959	4.482	2.603	0.458	1.081

Table D.46: UKC for  $H_s = 3\text{m}$ ,  $T_p = 10\text{s}$  and  $\alpha = 135^\circ$

Keel points	d/D = 1.5	d/D = 1.4	d/D = 1.3	d/D = 1.2	d/D = 1.1
APP	4.886	4.367	2.539	0.186	0.6
SQT	4.627	3.765	1.194	-2.151	-2.854
SSH	4.417	3.796	1.182	-2.072	-3.057
PQT	4.617	3.88	1.232	-1.903	-3.043
PSH	4.367	3.56	1.034	-2.284	-2.859
FPP	4.831	4.236	2.39	0.232	0.622

Table D.47: UKC for  $H_s = 4\text{m}$ ,  $T_p = 10\text{s}$  and  $\alpha = 135^\circ$ 

Keel points	d/D = 1.5	d/D = 1.4	d/D = 1.3	d/D = 1.2	d/D = 1.1
APP	4.35	4.044	2.25	-0.156	0.266
SQT	4.062	3.326	0.682	-2.885	-3.776
SSH	3.8	3.359	0.666	-2.799	-4.016
PQT	4.058	3.456	0.726	-2.604	-4
PSH	3.741	3.083	0.495	-3.04	-3.782
FPP	4.293	3.888	2.079	-0.105	0.288

Table D.48: UKC for  $H_s = 5\text{m}$ ,  $T_p = 10\text{s}$  and  $\alpha = 135^\circ$ 

Keel points	d/D = 1.5	d/D = 1.4	d/D = 1.3	d/D = 1.2	d/D = 1.1
APP	5.658	5.266	3.546	1.79	2.155
SQT	5.591	5.028	3.253	1.405	0.986
SSH	5.285	4.85	3.12	1.259	0.96
PQT	5.503	5.027	3.182	1.234	0.958
PSH	5.463	4.951	3.225	1.374	0.956
FPP	5.75	5.383	3.591	1.707	2.069

Table D.49: UKC for  $H_s = 3\text{m}$ ,  $T_p = 10\text{s}$  and  $\alpha = 180^\circ$

Keel points	$d/D = 1.5$	$d/D = 1.4$	$d/D = 1.3$	$d/D = 1.2$	$d/D = 1.1$
APP	5.218	5.004	3.347	1.665	2.03
SQT	5.138	4.691	2.964	1.16	0.499
SSH	4.734	4.458	2.79	0.97	0.465
PQT	5.021	4.692	2.873	0.938	0.463
PSH	4.979	4.589	2.927	1.118	0.459
FPP	5.348	5.157	3.407	1.557	1.919

Table D.50: UKC for  $H_s = 4\text{m}$ ,  $T_p = 10\text{s}$  and  $\alpha = 180^\circ$ 

Keel points	$d/D = 1.5$	$d/D = 1.4$	$d/D = 1.3$	$d/D = 1.2$	$d/D = 1.1$
APP	4.798	4.751	3.156	1.391	1.741
SQT	4.708	4.366	2.684	0.611	-0.399
SSH	4.206	4.082	2.473	0.263	-0.477
PQT	4.562	4.371	2.576	0.219	-0.474
PSH	4.523	4.24	2.638	0.555	-0.454
FPP	4.969	4.94	3.231	1.239	1.609

Table D.51: UKC for  $H_s = 5\text{m}$ ,  $T_p = 10\text{s}$  and  $\alpha = 180^\circ$

# List of References

- Archer, C. (1967). Some properties of rayleigh distributed random variables and of their sums and products. Tech. Rep. AD650090, Naval Missile Centre.
- BMT (2011). Extreme wave height estimation. <http://www.globalwavestatisticsonline.com/Help/estimation.htm>.
- Branlard, E. (2010). *Generation of Time Series from a Spectrum*. Ph.D. thesis, Technical University of Denmark.
- Bretschneider, C. (1965). On the probability distribution of wave force and an introduction to the correlation drag coefficient and the correlation inertial coefficient. Technical Reoprt TLJ700150, TUDelft.
- BYJU'S The Learning App (2019). Snells law formula. <https://byjus.com/snells-law-formula>.
- Castillo, J. and Daoudi, J. (2010). Estimation of generalized pareto distribution. *Statistics and Probability Letters, Elsevier*, vol. 79, no. 5, p. 684.
- Chadwick, A. (2017). Shallow water wave theory. [http://www.coastalwiki.org/wiki/Shallow-water\\_wave\\_theory](http://www.coastalwiki.org/wiki/Shallow-water_wave_theory).
- Chu, P., Galanis, G. and Kuo, Y.-H. (2010). Statistical structure of global significant wave heights. In: *Conference on Probability and Statistics in Atmospheric Sciences*.
- Corbella, C. and Stretch, D. (2012). The wave climate on the kwazulu-natal coast of south africa. *Journal of the South African Institute of Civil Engineering*, vol. 54, no. 2, pp. 45–54.
- Crossland, P. (1990). Generating ship time histories. Report ARE TM(UHR) 90313, DTIC.
- CSIR (2017). Port of richards bay wavenet iposs annual summary report.
- DHI (2017). *Mike21BW User Guide*. DHI Group, Argen Alle 5, 2970, Horsholm, Denmark.
- DNV.GL (2015). *Rules for Classification, Inland navigation vessels*, vol. 6. DNV GLAS.  
Available at: <https://rules.dnvgl.com/docs/pdf/DNVGL/RU-INV/2015-12/DNVGL-RU-INV-Pt6Ch5.pdf>

- Dr Wim van der Molen (2011). *Boundary Element Model Wavescat*. CSIR.
- Google (2019). Richards bay, south africa. Google Earth Pro V 7.1.2.2041.
- Gourlay, T. (2007). Ship underkeel clearance in waves. In: *Coasts and Ports*. Curtin University of Technology, Centre for Marine Science and Technology, Western Australia.
- Hosch, W.L. (2006). Damping. <https://www.britannica.com/science/dampingref1808>.
- International Maritime Organization (2008). *International Code on Intact Stability*. 13-19. International Maritime Organization.
- Islam, M.N., Islam2, M.R. and Baree, M.S. (2004). Statistical analysis on extreme wave height. *Naval Architecture and Marine Engineering*, pp. 1813–8535.
- Jonker, M., Wyk, A.V., Lackay, D. and A.M.Leith (1991). Physical modelling of wave-induced vertical hull motions of 150kt deadweight model bulk carrier. Report D9101/3, CSIR.
- Journee, J. and Massie, W. (2001a). *Offshore Hydromechanics*, vol. 1. TU Delft.
- Journee, J. and Massie, W. (2001b). *Offshore Hydromechanics*, vol. 1. TU Delft.
- Katz, R., Parlange, M. and Naveau, P. (2002). Statistics of extremes in hydrology. *Advances in Water Resources, Elsevier*, vol. 27, pp. 1287–1304.
- Kawahara, Y., Maekawa, K. and Ikeda, Y. (2011). A simple prediction formula of roll damping of conventional cargo ships on the basis of ikeda method and its limitation. In: *Fluid Mechanics and Its Applications*, vol. 97, pp. 465–486. Springer.
- Kianejad, S., Enshaei, H. and Ranmuthugala, D. (2017). Estimation of added mass moment of inertia in roll motion through numerical simulation. Pacific2017 International Maritime Conference.
- Kumar, V.S., Kotteppad, S. and Sajeev, R. (2012). Statistical analysis on extreme wave height. *Spinger Science*, vol. 64, pp. 223–236.
- Lai, C.D. (2006). *Weibull Distributions and Their Applications*, chap. Basic Statistical Concepts, pp. 63–78. Springer.
- Marine Traffic (2018a). Cape america.  
Available at: [https://www.marinetraffic.com/en/ais/details/ships/shipid:727844/mmsi:564190000/imo:9654751/vessel:CAPE\\_AMERICA](https://www.marinetraffic.com/en/ais/details/ships/shipid:727844/mmsi:564190000/imo:9654751/vessel:CAPE_AMERICA)
- Marine Traffic (2018b). Clipper quiteo.  
Available at: [https://www.marinetraffic.com/en/ais/details/ships/shipid:309390/mmsi:257928000/imo:9630755/vessel:CLIPPER\\_QUITO%7D](https://www.marinetraffic.com/en/ais/details/ships/shipid:309390/mmsi:257928000/imo:9630755/vessel:CLIPPER_QUITO%7D)
- Marine Traffic (2018c). Leading glory.  
Available at: [https://www.marinetraffic.com/en/ais/details/ships/shipid:685832/mmsi:477135800/imo:9536454/vessel:LEADING\\_GLORY](https://www.marinetraffic.com/en/ais/details/ships/shipid:685832/mmsi:477135800/imo:9536454/vessel:LEADING_GLORY)

- Marine Traffic (2018d). Ocean prometheus.  
Available at: [https://www.marinetraffic.com/en/ais/details/ships/shipid:754000/mmsi:636013318/imo:9336957/vessel:OCEAN\\_PROMETHEUS](https://www.marinetraffic.com/en/ais/details/ships/shipid:754000/mmsi:636013318/imo:9336957/vessel:OCEAN_PROMETHEUS)
- Martins, E. and Stedinger, J. (2000). Generalized maximum-likelihood generalized extreme-value quantile estimators for hydrologic data. *Water Resources Research*, vol. 36, no. 3, pp. 737–744.
- Mathworks (2018a). Generalized extreme value distribution. <https://www.mathworks.com/help/stats/generalized-extreme-value-distribution.html>.
- Mathworks (2018b). Generalized pareto distribution. <https://www.mathworks.com/help/stats/generalized-pareto-distribution.html>.
- Moes, J. (2007). Measurement of vertical motions of bulk carriers navigating in port entrance channels. In: *Measurement of Vertical Motions of Bulk Carriers Navigating in Port Entrance Channels*, pp. 1–8. Hydroraphic Conference, Technical Awareness Seminar.
- Molen, W. and Ligteringen, H. (2005). Influence of loading condition on the behavior of a moored liquefied natural gas ship. Technical report 36, Journal of Waterway, Port, Coastal and Ocean Engineering.
- Naaijen, I.P. (2013). Introduction to ship motions. <https://ocw.tudelft.nl/course-lectures/introduction-ship-motions>.
- National Program on Technology Enhanced Learning (2011). Seakeeping. <https://nptel.ac.in/courses/114105006/assignments/Q&ASet-3.pdf>.
- PIANC (2014). Harbour approach channels design guidelines. Tech. Rep. 121, The World Association for Waterborne Transport Infrastructure.
- Piehl, H.P. (2016). *Ship Roll Damping Analysis*. Ph.D. thesis, Technical University of Denmark.
- Pike, J. (2018). *The Principles of Stability*. Federation of American Scientists. Code 70, 4-1.  
Available at: <https://fas.org/dod-101/navy/docs/swos/dca/stg4-01.html>
- Prat, M.C. (2010). *Overview of Ocean Wave Statistics*. Ph.D. thesis, Department of Mechanical and Process Engineering, the University of Duisburg-Essen.
- Rautenbach, C., Wessels, G., Shabangu, P. and Ramjukadh, C. (2015). Reconfiguration of the richards bay sand-trap and related dredging issues. Tech. Rep., CSIR, Transnet.
- SANHO (2019). South african tide tables.
- Shukla, R.K. (2010). On the proficient use of gev distribution: a case study of sub-tropical monsoon region in india. *Annals. Computer Science Series*, vol. 7.

- Taylan, M. (2000). The effect of nonlinear damping and restoring in ship rolling. *Ocean Engineering*, Pergamon, vol. 27, p. 921–932.
- Teena, N.V., Kumar, V.S., Sudheesh, K. and Sajeev, R. (2012). Statistical analysis on extreme wave height. *Natural Hazards*, vol. 64, pp. 223–236.
- The University of British Columbia (2003). *Single Slit Diffraction Pattern of Light*. The University of British Columbia, New York.  
Available at: <http://www.math.ubc.ca/~cass/courses/m309-03a/m309-projects/krzak/>
- TNPA (2016). Port of richards ship berthing spreadsheet.
- Transnet National Ports Authority (2010). Port of richards bay. <https://www.transnetnationalportsauthority.net/OurPorts/RichardsBay/Pages/Overview.aspx>.
- United States Naval Academy (2018). *Seakeeping*, chap. 8, p. 31. EN400. <https://www.mathworks.com/help/stats/generalized-pareto-distribution.html>.
- U.S. Army Corps of Engineers (2002a). *Coastal Engineering Manual (CEM)*. EM 1110-2-1100. U.S. Army Corps of Engineers, Washington, D.C.
- U.S. Army Corps of Engineers (2002b). *Coastal Engineering Manual (CEM)*. EM 1110-2-1100. U.S. Army Corps of Engineers, Washington, D.C.
- U.S. Army Corps of Engineers (2002c). *Coastal Engineering Manual (CEM)*. EM 1110-2-1100. U.S. Army Corps of Engineers, Washington, D.C.
- U.S. Army Corps of Engineers (2002d). *Coastal Engineering Manual (CEM)*. EM 1110-2-1100. U.S. Army Corps of Engineers, Washington, D.C.
- U.S. Army Corps of Engineers (2002e). *Coastal Engineering Manual (CEM)*. EM 1110-2-1100. U.S. Army Corps of Engineers, Washington, D.C.
- Wavewatch3DG (2019). Noaa wavewatch 3. <http://polar.ncep.noaa.gov/waves/>.
- Wikimedia (2012). Water wave mechanics. [https://commons.wikimedia.org/wiki/File:Water\\_wave\\_theories.svg](https://commons.wikimedia.org/wiki/File:Water_wave_theories.svg).
- WorldWinds Inc (2019). Wavewatch iii. <http://www.worldwindsinc.com/services/oceanographic-modeling/wavewatch-iii-2.htm>.
- Zhang, J., Benoit, M., Kimmoun, O., Chabchoub, A. and Hsu, H. (2019). Statistics of extreme waves in coastal waters: Large scale experiments and advanced numerical simulations. *Fluids*, vol. 4, p. 99.